National Conference on Materials at Extreme Conditions (MAX 2025)

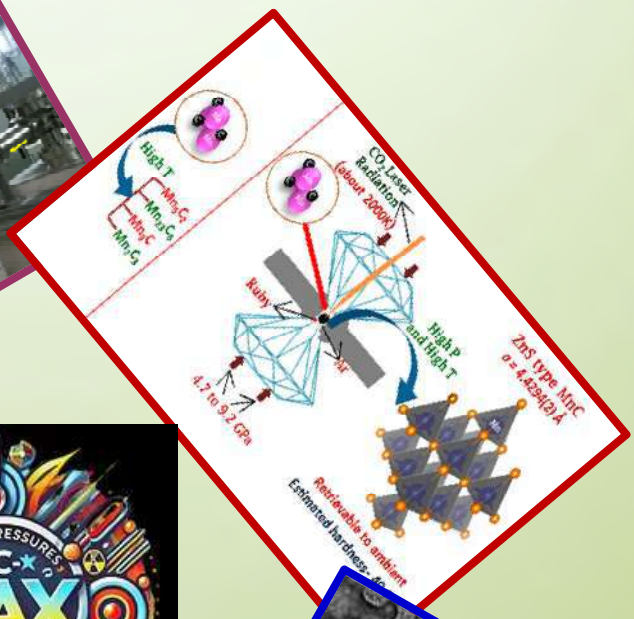

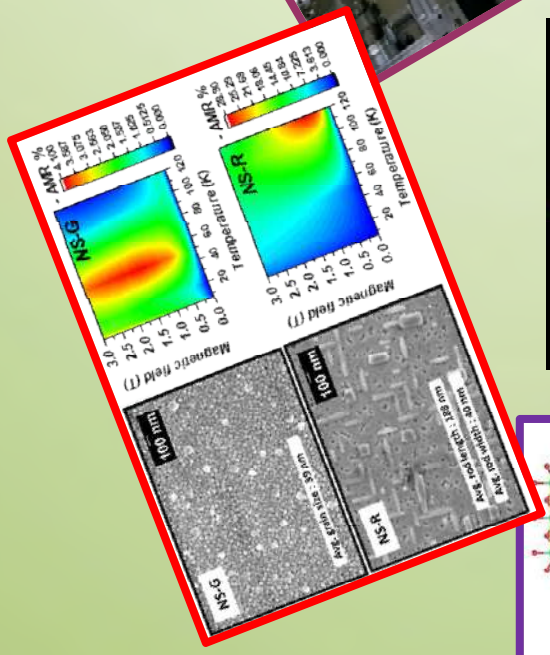

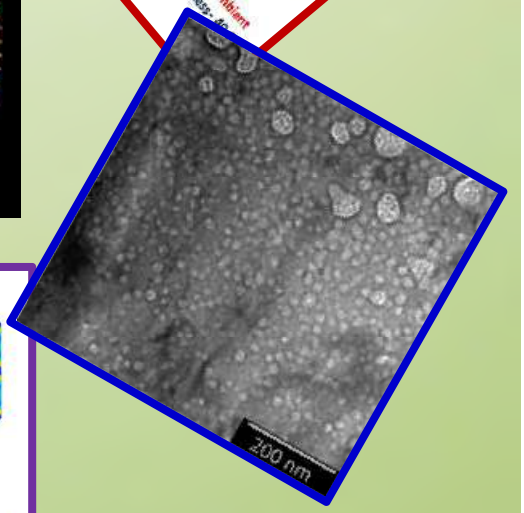

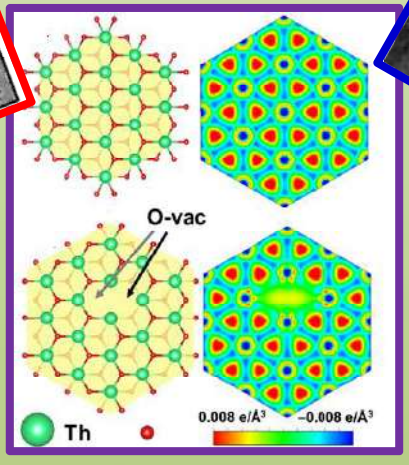

27 - 29 March 2025

Indira Gandhi Centre for Atomic research, Kalpakkam

डॉ. अजित कुमार मोहान्ती
Dr. Ajit Kumar Mohanty

भारत सरकार
Government of India

अध्यक्ष, परमाणु ऊर्जा आयोग
व
सचिव, परमाणु ऊर्जा विभाग
Chairman, Atomic Energy Commission
&
Secretary, Department of Atomic Energy

MESSAGE

I am very pleased to note that a National Conference on Materials at Extreme Conditions (MAX 2025) is being organized at Indira Gandhi centre for Atomic Research, Kalpakkam, Tamil Nadu during 27-29 March 2025.

Materials exposed to extreme temperatures, pressures, radiation, and corrosive environments demand innovative research to ensure safety, reliability, and efficiency. The role of innovative materials in advancing energy security and national technological progress cannot be overstated. Through insightful discussions and collaborations fostered by this conference, I am confident that we will witness significant contributions that shape the future of materials science and its applications in high-performance domains.

I commend the organizers for bringing together esteemed experts and young researchers, providing them with an excellent forum to present their findings and foster collaborations. I extend my best wishes for a highly productive and successful conference.

Ajit Kumar Mohanty
(Ajit Kumar Mohanty)

राष्ट्र की सेवा में परमाणु
प ऊ वि
DAE
ATOMS IN THE SERVICE OF THE NATION

अणुशक्तिभवन, छत्रपति शिवाजी महाराज मार्ग, मुंबई - 400 001, भारत • Anushakti Bhavan, Chhatrapati Shivaji Maharaj Marg, Mumbai - 400 001, India
दूरभाष/Phone:+(91) (22) 2202 2543 • फैक्स/Fax: +(91) (22) 2204 8476 / 2284 3888
ई-मेल/E-mail: chairman@dae.gov.in

सी. जी. कऱ्हाडकर
प्रतिष्ठित वैज्ञानिक एवं निदेशक

C.G. KARHADKAR
Distinguished Scientist & DIRECTOR

सत्यमेव जयते

भारत सरकार
परमाणु ऊर्जा विभाग
इन्दिरा गाँधी परमाणु अनुसंधान केन्द्र
कल्पाक्कम 603 102, तमिलनाडु, भारत

GOVERNMENT OF INDIA
DEPARTMENT OF ATOMIC ENERGY
INDIRA GANDHI CENTRE FOR ATOMIC RESEARCH
KALPAKKAM 603 102, TAMIL NADU, INDIA

March 18, 2025

MESSAGE

I am pleased that the National Conference on Materials at Extreme Conditions (MAX 2025) is being held from March 27-29, 2025, at our Centre i.e. Indira Gandhi Centre for Atomic Research, Kalpakkam. This conference provides a crucial platform to discuss the latest advancements in materials science, with a special emphasis on understanding and utilizing materials under extreme conditions such as high pressure, extreme temperatures, strong magnetic fields, and radiation. These materials play a vital role in nuclear energy and advanced manufacturing, making research in this area more important.

The conference will feature a diverse range of presentations covering advanced structural materials, high-entropy alloys, radiation-resistant materials, novel composites, superconductors, pressure-temperature phase diagrams, transition mechanisms and advanced characterization techniques. The exchange of knowledge and ideas will undoubtedly contribute to the ongoing pursuit of resilient and high-performance materials for next-generation applications.

I extend my best wishes for academically enriching discussions and a successful conference. To all outstation participants, I hope you have a pleasant stay on campus and enjoy the serene surroundings.

18.3.25

(C.G. Karhadkar)

दूरभाष/Phone: +91- 44 - 2748 0240 / 2748 0267 (O), फैक्स/Fax: +91 - 44 - 274 80060
मोबाइल / Mobile: 94985 99840 ई-मेल / E-mail: director@igcar.gov.in

Dr. (Prof.) Sandip Dhara, FRSC, FinstP, SMOptica
Director, Materials Science Group
Sr. Professor, Homi Bhabha National Institute
Indira Gandhi Centre for Atomic Research,
Kalpakkam 603 102,Tamil Nadu, INDIA

सत्यमेव जयते
Government of India

Message

It gives us immense pleasure to extend a warm welcome to all delegates of National Conference on Materials at Extreme Conditions (MAX-2025). At Materials Science Group, IGCAR, we pursue basic research in front line areas of Materials Studies at Extreme Conditions. The research areas include studies on radiation induced defects and their influence on physical properties, structural and electronic phase transitions at high pressures and low temperatures, as well as theoretical studies. At center level, Materials and Metallurgy Group with whom we complement our materials research, study structural materials at high temperature and also for post-irradiation characterization. Hence, it is very apt that the conference devoted to Materials Studies at Extreme Conditions is being held in this centre.

I am particularly happy that it is the first national conference on studying material at extreme conditions is being held at our Centre. The conference theme, being specialized, has drawn the attention of expert professionals from National Institutes, Premier Academic Institutes and Universities.

I wish that all participants, especially the students, will appreciate the essence of this field and benefit from the scientific deliberations during the conference, leading to inter-institutional collaborations.

With my best wishes and personal regards,

With best regards,

(SANDIP DHARA)
Chairman, Organization Committee, MAX-2025

डॉ. अवधेश मणि , वैज्ञानिक अधिकारी-H
प्रधान, संघनित पदार्थ भौतिकी प्रभाग
प्रोफ़ेसर एवं डीन, भौतिक विज्ञान, (शैक्षिक)
होमी भाभा राष्ट्रीय संस्थान
Dr. Awadhesh Mani, Scientific Officer – H
Head, Condensed Matter Physics Division,
Professor & Dean,(Academic), Physical Sciences, Homi Bhabha National Institute

भारत सरकार
परमाणु ऊर्जा विभाग
इन्दिरा गाँधी परमाणु अनुसंधान केन्द्र
कल्पाक्कम 603 102, तमिलनाडु, भारत

GOVERNMENT OF INDIA
DEPARTMENT OF ATOMIC ENERGY
INDIRA GANDHI CENTRE FOR ATOMIC RESEARCH
KALPAKKAM 603 102, TAMIL NADU, INDIA

MESSAGE

Dear Participants

It is with immense pleasure I welcome you to the National conference on Materials at Extreme conditions (MAX-2025) being held at Indira Gandhi Centre for Atomic Research, Kalpakkam. I thank IGCAR management for the valuable support that led to this conference.

This conference aims to bring the expert scientists, academicians and young researchers all together to exchange knowledge on how various materials behave under high temperatures, pressures, radiation, and magnetic field. We foster a discussion on enhancement of experimental techniques and computational models, refining our ability to predict and develop next-generation materials. I look forward to scintillating technical sessions on material resilience, quantum materials, multifunctional materials and much more. I believe, this conference will help advancing scientific understanding and technological innovations.

We are really grateful to BRNS, IIM and MRSI for the financial and all-round support. I thank all the authors and participants for their contributions and wish the delegates a scientifically satisfying experience.

Awadhesh Mani

(Awadhesh Mani)
Convener, Organization Committee, MAX-2025

National Advisory Committee

Patrons

Shri Vivek Bhasin	Director, BARC, Mumbai
Shri C G Karhadkar	Director, IGCAR, Kalpakkam

Advisory Committee

Prof. U. Kamachi Mudali	Vice Chancellor, HBNI
Dr. (Prof.) A K Tyagi	Dean HBNI, Mumbai
Prof. Chandrabhash Narayana	Director , RGCB, Thiruvananthapuram
Prof. Avinash Chandra Pandey	Director, IUAC, New Delhi
Dr. (Prof.) Sumit Som	Director, VECC, Kolkata
Dr. Amlan J. Pal	Director, UGC-DAE Consortium, Indore
Dr. (Prof.) R. Divakar	Director, MMG, IGCAR, Kalpakkam
Dr. (Prof.) Sandip Dhara	Director, MSG, IGCAR, Kalpakkam
Prof . K N Uttam	University of Allahabad, Prayagraj
Dr. (Prof.) Sudhir Kumar Dixit	Director, Laser Group, RRCAT, Indore

Organizing Committee

Chairman	Dr. (Prof.) Sandip Dhara
Convener	Dr. (Prof.) Awadhesh Mani
Co-Convener	Dr. Sanjay Kumar N R
Co-Convener	Dr. (Prof.) C David
Secretary	Dr. Balmukund Shukla
Treasurer	Dr. S Polaki Rao DR. V Ganesan

Program Schedule: MAX-2025

Time	Hall-1 (Sarabhai Auditorium, Ground Floor Homi Bhabha Building)	Time	Hall-2 (Blue Room, Ground Floor Homi Bhabha Building)
Day 1 (27 March 2025, Thursday): Materials at HP, HT, Related Computation			
10:00 - 10:30	**Inaugural Function**		
10:30-11:15 (IT-01)	**Keynote Address: Prof. Chandrabhas Narayana, RGCB, Thiruvananthapuram** *Finding New Topological Insulators Using Pressure*		
11:15-11:45	**High Tea**		
	Technical Session - I		
11:45-12:30 (IT-02)	**Plenary Talk: Dr. R Divakar, IGCAR, Kalpakkam** *Materials Behaviour under Irradiation at High-temperatures*		
12:30-12:50 (ET-1)	**Dr. Sanjay Kumar N R, IGCAR, Kalpakkam** *Polymorphic structural transition in $Cd_{0.9}Zn_{0.1}Te$ at high pressure*		
12:50-13:00 (O-1)	**Dr. M. O. Ajeesh** *Pressure-induced superconducting and magnetic phases in UTe_2*		
13:00-14:00	**Lunch**	**Lunch**	
	Technical Session-II	**Parallel Technical Session-III (Radiation resistant materials)**	
14:00-14:30 (IT-03)	**Prof. G D Mukherjee, IISER, Kolkata** *Halide Perovskites at Extreme Condition*	**14:00-14:30 (IT-07)**	**Dr. C David, IGCAR, Kalpakkam** *Studying radiation damage in nuclear materials by using ion accelerators*
14:30-15:00 (IT-04)	**Dr. Aditi Ray/BARC, Mumbai** *Dynamic Compression and Phase Change: The Fascinating Realm of Solids Under Extreme Conditions*	**14:30-14:50 (ET-3)**	**Dr. Gurpreet Kaur, IGCAR, Kalpakkam** *Effect of Pressure on Symmetry Breaking Transition in Uranium and Uranium Intermetallics*
15:00-15:20 (ET-2)	**Dr. Balmukund Shukla, IGCAR, Kalpakkam** *High Pressure Structural Investigation on Uranium Oxide Compounds*	**14:50-15:00 (O-7)**	**M. Muthuganesh** *Capsule and sample holder for irradiation of a-tig and tig weld joint specimens of wrapper (D9) to foot (SS316LN) of PFBR fuel sub-assembly in FBTR*
15:20 –15:30 (O-2)	**Suvashree Mukherjee** *Pressure induced emission enhancement in vacancy ordered halide double perovskite Cs_2TeCl_6*	**15:00-15:10 (O-8)**	**Argha Dutta** *Study of Depth-Dependent Microstructural Changes in Oxygen Irradiated Nb-1Zr-0.1C Alloy*
15:30-15:40 (O-3)	**Dr. Anand Kumar P** *High Pressure XRD studies on $Ho_{0.4}Eu_{0.6}MnO_3$*	**15:10-15:20 (O-9)**	**Dr. Sujoy Sen** *Investigations on phase transformation and ion induced luminescence in Eu doped ZrO_2*
15:40-15:50 (O-4)	**Dr. Arpita Aparajita A N** *Behaviour of molybdenum diphosphide at high pressure*	**15:20-15:30 (O-10)**	**Dr. Sagar Sen** *Tailoring Structural, Electronic, and Magnetic Properties of $CoFe_2O_4$ Thin Films using Swift Heavy Ions Irradiation*
		15:30-15:40 (O-26)	**Dr. Saurabh Mukherjee** *Positron maker: Intense positron facility at Dhruva Reactor*
16:00-16:15	**Coffee/Tea Break**	**16:00-16:15**	**Coffee/Tea Break**
	Technical Session-IV	**Parallel Technical Session-V (Radiation resistant materials)**	
16:15-16:45 (IT-05):	**Dr. Ashok K. Arya, BARC, Mumbai** *Ab-initio Characterization of High Pressure Phase Transformations in $CaTiSiO_5$ and $U_{1-x}Th_xSiO_4$*	**16:15-16:45 (IT-08)**	**Dr. Vinita Grover Gupta, BARC Mumbai** *Understanding radiation response of ceramics for nuclear applications*
16:45-17:15 (IT-06):	**Dr. Sharat Chandra, IGCAR, Kalpakkam** *Search for Superhard Carbides using DFT*	**16:45-16:55 (O-11)**	**Dr. K Suresh** *Indigenous Development of electronics and control instrumentation for Ion accelerator based radiation damage studies and materials research*
17:15-17:25 (O-5)	**Dr. Sunil kumar D** *Characterization and fabrication of metal matrix composites from machinery shop waste metal chips via friction stir processing*	**16:55-17:05 (O-12)**	**Dr. Ramcharan Meena** *Structural and microscopic studies of ion-irradiated NASICON($Na_3Zr_2Si_2PO_{12}$) ceramics*
17:25-17:35 (O-6)	**Dr. Ramesh Kumar** *First Principle Study of Topological Phase in YPdBi Material*	**17:05-17:15 (O-13)**	**Rishvana Parveen** *Investigation of radiation tolerance in ceramic composite and non-composite materials*
		17:15-17:25 (O-14)	**Dr. Dipak Kumar Baisnab** *Design and Development of a High-Heat-Load Target Holder for the Medical Cyclotron Facility at VECC*

20:00-21:00	**Dinner**	**Dinner**	
	Day 2 (28 March 2025, Friday) **(LT, HT, Magnetic Field, Related computation)**		
	Technical Session-VI		
10:00-10:45 **(IT-09)**	**Plenary Talk Dr. Awadhesh Mani, IGCAR, Kalpakkam** *Investigation on the evolution of ground states of selected novel systems under high pressure and high magnetic field at low temperatures*		
10:45-11:05 **(ET-4)**	**Dr. Edward Prabu, IGCAR, Kalpakkam** *Quantum transport signatures of Topological insulators (TI) at low temperatures and magnetic fields*		
11:05-11:15 **(O-15)**	**Dr. Narender Budhiraja** *Unveiling the low-temperature properties of CuO nanosheets: Modulating morphology, and crystallography for enhanced optoelectronic performance*		
11:15-11:30	**Coffee/Tea Break**	**Coffee/Tea Break**	
	Technical Session-VII	**Parallel Technical Session-VIII**	
11:30-12:00 **(IT-10)**	**Prof. A Sundaresan, JNCASR, Bengaluru** *High-Pressure and High-Temperature Synthesis of Quantum Materials*	**11:30-12:00** **(IT-12)**	**Dr. K N Uttam, Univ. of Allahabad, Prayagraj**
12:00-12:20 **(ET-5)**	**Dr. Mukhtiyar Singh, DTU, Delhi** *Existence of dual topological phases in Sn-based ternary chalcogenides*	**12:00-12:20** **(ET-7)**	**Dr. Gayathri N Banerjee, VECC, Kolkata** *Tailoring ion irradiation for radiation damage studies of nuclear structural materials*
12:20-12:30 **(O-16)**	**Dr. Rajesh Arun Joshi** *Effect of Annealing on Physicochemical and Optoelectronic Properties of Polyaniline Thin Films*	**12:20-12.30** **(O-21)**	**Ran Vijay Kumar** *X-Ray Absorption Spectroscopy of Neutron Irradiated SS 316L and SS316LN*
12:30-12:40 **(O-17)**	**Dr. Reshma P R** *Temperature dependence of Fano effect in optical phonon mode of V_2O_5 nanoparticles*	**12:30-12:40** **(O-22)**	**Dr. Sanatan Nath** *Structural, Optical and Temperature Dependent Ionic Conductivity Study of Green Chemical Synthesized Copper Sulphide Nanostructures in PVA Matrix*
13:00-14:00	**Lunch**	**Lunch**	
	Technical Session-IX	**Parallel Technical Session-X**	
14:00-14:30 **(IT-11)**	**Prof. A. Thamizhavel, TIFR, Mumbai** *Anisotropic Magnetotransport and Quantum Hall Effect in Bulk Semimetallic Single Crystals*	**14:00-14:30** **(IT-13)**	**Dr. Debdulal Kabiraj, IUAC, New Delhi** *Nano-scale evolution under swift heavy ion induced thermal spike*
14:30-14:50 **(ET-6)**	**Dr. Vinod K /IGCAR, Kalpakkam** *Magnetic/magneto-caloric studies on La_2NiMnO_6 based double perovskites*	**14:30-14:50** **(ET-8)**	**Dr. Amirthapandian S, IGCAR, Kalpakkam** *First experimental results from In-situ Ion Irradiation and Imaging with SEM (i^4 SEM) Facility*
14:50-15:00 **(O-18)**	**Dr. Pallati Naresh** *Thermal, Anti-bacterial and Structural analysis of bioactive glassy materials and their applications*	**14:50-15:00** **(O-23)**	**Abhilash Dwivedi** *Increase in Hydrostatic Limit of Pressure Transmitting Medium Methanol -Ethanol with Temperature*
15:00-15:10 **(O-19)**	**S Sureshbabu** *Experimental Investigation on Hot Tensile Properties of Melt-in Mode Plasma Arc Welded Inconel 625 Alloy Sheets*	**15:00-15:10** **(O-24)**	**Dr. Manan Dholakia** *A hybrid MC-MD Approach to study the irradiation behavior of Iron Phosphate Glasses*
15:10-15:20 **(O-20)**	**Bidisha Mukherjee** *Soft mode induced structural phase transition in Ba_2ZnTeO_6 at high pressures*	**15:10-15:20** **(O-25)**	**Dr. Pardhu Yella** *Nanoindentation studies on ordered and disordered iron aluminides*
15:30-15:45	**Coffee/Tea Break**	**Coffee/Tea Break**	
15:45-17:45	**Poster (P:1-30)**		
17:45-19:00	**Cultural Program**		
20:00-21:00	**Dinner**		

Day 3 (29 March 2025, Saturday)
(Radiation,Defects &Related computation)

10:00-10:50	**Technical Session-XI**
10:00-10:30 (IT-14)	**Dr. R Govindaraj, IGCAR, Kalpakkam** *Defects studies in reactor structural materials and Novel oxides using Advanced Nuclear Techniques*
10:30-10:50 (ET-09)	**Dr. Sinu Mathew, M. G. Univ, Kerala** *Focused Helium ion beam tailoring of luminescence in hexagonal boron nitride (h-BN)*
10:50-11:00	**Coffee/Tea Break**
11:00-13:00	**Poster(P:31-60)**
13:00-14:00	**Lunch**
14:00-15:00	**Valedictory function and award distribution**

Invited Talks

Expert Talks

List of Oral Presentations

Sl. No.	Title/ Authors	Affiliation of the presenter	Page. No.
O-1.	Pressure-induced superconducting and magnetic phases in UTe_2 **M. O. Ajeesh,** J. D. Thompson, E. D. Bauer, F. Ronning, S. M. Thomas, and P. F. S. Rosa	Indian Institute of Technology Palakkad, India	25
O-2.	Pressure induced emission enhancement in vacancy ordered halide double perovskite Cs_2TeCl_6 **Suvashree Mukherjee,** DebabrataSamanta, and Goutam Dev Mukherjee	Indian Institute of Science Education and Research Kolkata, West Bengal	26
O-3.	High Pressure XRD studies on $Ho_{0.4}Eu_{0.6}MnO_3$ **P Anand Kumar,** R. M. Sarguna, V. Srihari and N R Sanjay Kumar	Indira Gandhi Centre for Atomic Research, Kalpakkam	27
O-4.	Behaviour of molybdenum diphosphide at high pressure **Arpita Aparajita A N** , G. Shwetha, N. R. Sanjay Kumar, V. Srihari, Awadhesh Mani	Indira Gandhi Centre for Atomic Research, Kalpakkam	28
O-5.	Characterization and fabrication of metal matrix composites from machinery shop waste metal chips via friction stir processing Krishnalal M S, **Sunilkumar D**	National Institute of Technology Silchar, Assam,	29
O-6.	First Principle Study of Topological Phase in YPdBi Material Sanjeev, Mukhtiyar Singh and **Ramesh Kumar**	Guru Jambheshwar University of Science & Technology, Hisar	30
O-7.	Capsule and sample holder for irradiation of a-tig and tig weld joint specimens of wrapper (D9) to foot (SS316LN) of pfbr fuel sub-assembly in FBTR **M. Muthuganesh,** P. Vasantharaja, Ashish Kolhatkar, Rajesh Saxena, Ran Vijay Kumar, M. S. Rao, P. K. Chaurasia, V. Karthik, S. Joseph Winston and M. Vasudevan	Indira Gandhi Centre for Atomic Research, Kalpakkam	31
O-8.	Study of Depth-Dependent Microstructural Changes in Oxygen Irradiated Nb-1Zr-0.1C Alloy **Argha Dutta,** N. Gayathri, P. Mukherjee, P. Karmakar, V. Naik	Variable Energy Cyclotron Centre, Kolkata	32
O-9.	Investigations on phase transformation and ion induced luminescence in Eu doped ZrO_2 **Sujoy Sen,** Vikas Singh Gahlot, S.K. Srivastava, P.Jegadeesan, B. Sundaravel, S. Amirthapandian	Indira Gandhi Centre for Atomic Research, Kalpakkam	33
O-10.	Tailoring Structural, Electronic, and Magnetic Properties of $CoFe_2O_4$ Thin Films Using Swift Heavy Ions Irradiation	Maharaja Bhoj Govt. P.G. College Dhar, Madhya Pradesh	34

	Sagar Sen, Ambrish Dwivedi, Yksh Gupta, Sourav Chowdhury, Jayjit Kumar Dey, Moritz Hoesch, Sanjay Kumar Upadhyay, Keval Gadani, Anil Gome, V.R. Reddy, Ratnesh Gupta		
O-11.	Indigenous Development of electronics and control instrumentation for Ion accelerator based radiation damage studies and materials research **K. Suresh,** J.Navas, R.Govindaraj, C.David, S.K.Dhara,	Indira Gandhi Centre for Atomic Research, Kalpakkam	36
O-12.	Structural and microscopic studies of ion-irradiated NASICON ($Na_3Zr_2Si_2PO_{12}$) ceramics **Ramcharan Meena,** Rajendra Singh Dhaka	Inter-University Accelerator Center, New Delhi	37
O-13.	Investigation of radiation tolerance in ceramic composite and non-composite materials **Rishvana Parveen,** Parswajit Kalita, Rakesh Shukla, Vinita Grover, Sanjay Kedia, D.K. Avasthi	University of Petroleum and Energy Studies (UPES), Dehradun	38
O-14.	Design and Development of a High-Heat-Load Target Holder for the Medical Cyclotron Facility at VECC **Dipak Kumar Baisnab,** Binoy Kumar Maji, B. Sundaravel, C. David, P. Lijukrishnan, Indranil Banerjee and Vinod V, N. Gayathri and Paramita Mukherjee	Indira Gandhi Centre for Atomic Research, Kalpakkam	39
O-15.	Unveiling the low-temperature properties of CuO nanosheets: Modulating morphology, and crystallography for enhanced optoelectronic performance **Narender Budhiraja,** Krishna Begari, Rakesh K. Sonker	Satish Chander Dhawan Government College, Ludhiana, Punjab	40
O-16.	Effect of Annealing on Physicochemical and Optoelectronic Properties of Polyaniline Thin Films Karan K. Rathod, Jayesh R. Pawar, Munjaji E. Dudhmal, **Rajesh A. Joshi**	Toshniwal Arts, Commerce and Science College, Sengaon Dist. Hingoli, Maharashtra	41
O-17.	Temperature dependence of Fano effect in optical phonon mode of V_2O_5 nanoparticles **Reshma P R,** Arun K Prasad, Sandip Dhara	Indira Gandhi Centre for Atomic Research, Kalpakkam	42
O-18.	Thermal, Anti-bacterial and Structural analysis of bioactive glassy materials and their applications **Pallati Naresh,** D.Sreenivasu, K. Siva Kumar, Aravind Seema, Gangadhar Thalari, Sanjeev Kumar	Osmania University, Hyderabad, Telangana	44
O-19.	Experimental Investigation on Hot Tensile Properties of Melt-in Mode Plasma Arc Welded Inconel 625 Alloy Sheets **S Sureshbabu**, S Rajakumar	Annamalai University, Annamalai Nagar, Chidambaram	45
O-20.	Soft mode induced structural phase transition in Ba_2ZnTeO_6 at high pressures **Bidisha Mukherjee**, MrinmaySahu, Asish Kumar Mishra, Goutam Dev Mukherjee	Indian Institute of Science Education and Research Kolkata, West Bengal	46

O-21.	X-Ray Absorption Spectroscopy of Neutron Irradiated SS 316L and SS316LN **Ran Vijay Kumar**, K. Ashish, V. Karthik, R. Divakar	Indira Gandhi Centre for Atomic Research, Kalpakkam	47
O-22.	Structural, Optical and Temperature Dependent Ionic Conductivity Study of Green Chemical Synthesized Copper Sulphide Nanostructures in PVA Matrix **Sanatan Kr. Nath,** P. K. Kalita	B. H.College, Howly, Gauhati University	48
O-23.	Increase in Hydrostatic Limit of Pressure Transmitting Medium Methanol -Ethanol with Temperature **Abhilash Dwivedi**, Rahul Kaiwart, T. Balaganapathi and Himanshu Kumar Poswal	Bhabha Atomic Research Centre, Mumbai	49
O-24.	A hybrid MC-MD Approach to study the irradiation behavior of Iron Phosphate Glasses **Manan Dholakia,** Shakti Singh and Sharat Chandra	Indira Gandhi Centre for Atomic Research, HBNI, Kalpakkam	50
O-25.	Nanoindentation studies on ordered and disordered iron aluminides **Pardhu Yella**, Javed S. Ibrahim, Shivkumar Khaple, M.J.N.V. Prasad, M. Phani Raj	Mahatma Gandhi Institute of Technology, Gandipet, Hyderabad	51
O-26.	Positron maker: Intense positron facility at Dhruva Reactor **S. Mukherjee,** D. Dutta, H. Chatterjee, M. Dev, S. Shrotriya, M. Pande, J. Kumar, T. Singh, P. K. Pujari, K. Sudarshan	Bhabha Atomic Research Center, Trombay, Mumbai	52

List of Poster Presentations

Sl. No.	Title/Authors	Affiliation of the presenting author	Page No.
P-1.	Pressure and temperature-induced electron-phonon and spin-phonon coupling in $Cr_{3.04}Te_4$ **Asish Kumar Mishra**, Bidisha Mukherjee, S. Thirupathaiah, Goutam Dev Mukherjee	Indian Institute of Science Education and Research Kolkata, Nadia	54
P-2.	Exploring the Pressure-Dependent Structural Transitions of $RE_3TM_4Sn_{13}$ (RE=Sr, Ca and La; TM=Rh) CompoundsThrough Synchrotron X-Ray Diffraction **Muthukumaran Sundaramoorthy,** Arumugam Sonachalam, Boby Joseph	Bharathidasan University, Tiruchirappalli, TamilNadu	55
P-3.	Unusual pressure-volume behaviour of Hf-Nb-Ta-Ti-V high entropy alloy **Nirmal Sharma,** K. K. Pandey, H. K. Poswal, Nilabja K. Sarkar and Nandini Garg	Bhabha Atomic Research Centre, Mumbai	56
P-4.	Effect of plastic straining on *bcc-hcp* phase transition on pure iron: an in situ study **Suraj Kumar**, K. K. Pandey, Valery I. Levitas	Bhabha Atomic Research Centre, HBNI, Mumbai	57
P-5.	Spinel to perovskite transition in the Earth's lower mantle: Implication in Slab Dynamics **Rabindranath Mondal,** Swastika Chatterjee	Indian Institute of Science Education and Research Kolkata, Nadia	58
P-6.	Structural stability and compressibility behaviour of $CeTe_2$ under pressure **K. Sanitha**, P. Anand Kumar, S. Shyam Kumar, N. R. Sanjay Kumar, Anuj Upadhyay, R. Sudha and Rajesh Ganesan	Indira Gandhi Centre for Atomic Research, HBNI, Kalpakkam, Tamil Nadu	59
P-7.	Structural Stability of Gd^{3+} and Ce^{4+} co-doped Lanthanum ZirconatesUnder High Pressure:Insights intoActinide Host Matrices **Saideep Shirish Bhat,** Irshad K. A, Boby Joseph, Gurumurthy S C, Raghavendra K G	Manipal Institute of Technology, MAHE, Manipal, Karnataka	60
P-8.	Pressure induced topological phase in intermetallic Zintl compound $RbZn_4As_3$ **Ramesh Kumar,** Mukhtiyar Singh	Delhi Technological University, New Delhi	61
P-9.	Prediction of High Pressure Phase Transition of ThO_2 using USPEX code **D. Sornadurai**	Indira Gandhi Centre for Atomic Research, HBNI, Kalpakkam, Tamil Nadu	62
P-10.	Structural Transition of Perovskite type $LaVO_3$ at High-pressures **A. K. Sivadasan,** K. A. Irshad, I. Packia Selvam, Boby Joseph, S. N. Potty	Centre for Materials for Electronics Technology (C-MET), Thrissur, Kerala,	63

P-11.	Structural properties and phase transition of U_3Si under pressure: A DFT study **Prasanta Kumar Maharana**, Gurpreet Kaur, Sharat Chandra, R Govindaraj	Indira Gandhi Centre for Atomic Research, HBNI, Kalpakkam, Tamil Nadu	64
P-12.	High pressure density functional theory studies on $CaCu_2O_3$ compound **Aiswarya S M,** Somesh Chandra, Gurpreet Kaur, G M Bhalerao and R Govindaraj	UGC-DAE CSR Kalpakkam Centre, Kokilamedu, Tamil Nadu	65
P-13.	Modification of Physicochemical and Optoelectronic Properties of CZTS Thin Films Using Post Deposition Treatments **Munjaji E. Dudhmal,** Jayesh R. Pawar, Rajesh A. Joshi	Toshniwal Arts, Commerce and Science College, Sengaon-Hingoli, Maharashtra	66
P-14.	Experimental Investigation of Aluminium Oxide (Al_2O_3) Doped Yttria Stabilized Zirconia (YSZ) Thermal Barrier Coatings **Deva Priya P,** Suresh Kumar J	College of Engineering, Anna University, Chennai	67
P-15.	Development Of Titanium Honeycomb Sandwich Structure for Thermal Protection Systems in Hypersonic Vehicles **Suresh Kumar J ,** Kalaichelvan K	College of Engineering, Anna University Chennai	68
P-16.	Developing Empirical Relationship to Predict Hot-Wire TIG Welded Inconel 625 Alloy Using RSM and Machine Learning Approach **M. Reddeiah,** S.Rajakumar,, P.Hema, S.Kavitha, K. Devakumaran	Annamalai University, Annamalai Nagar, Chidambaram	69
P-17.	Experimental Characterization Diffusion Bonded Light Weight Blade-Rings for Aero engine Application using Ti_6Al_4V Sheets with Ti_6Al_4V Wire Reinforcement **S Prakashkumar,** S Rajakumar, S Sureshbabu	Annamalai University, Annamalai Nagar, Chidambaram	71
P-18.	Ab-initio study of SiC, Ti and V-doped SiC nanotubes for gas sensing application **Nikhil M. Solanki,** Suresh V. Chaudhari, Sanjeev K. Gupta, P. N. Gajjar	University School of Sciences, Gujarat University, Ahmedabad	72
P-19.	Exploring thermal effects on dynamic uniaxial compression of single-crystal tungsten using molecular dynamics **A. Abhijith,** K. Basavaraj, Anuradha S. Dwivedi, Apu Sarkar, Aditi Ray	Bhabha Atomic Research Centre, Mumbai	73
P-20.	Optical properties of the NiB_6 monolayer*: In silico* study **Suresh V. Chaudhari,** Nikhil M. Solanki, Sanjeev K. Gupta, P. N. Gajjar	University School of Sciences, Gujarat University, Ahmedabad	74

P-21.	Electrical and Thermoelectric properties of Bi_2Te_3 and Sb_2Te_3 single crystal **NabarunBera**, Ayush Ramchandra Mokashi, Anoop M. D., Sachin Sharma, Nisha Yadav, Deepika Kanwar, Balram Tripathi, D. K. Shukla and Manoj Kumar	Malaviya National Institute of Technology, Jaipur	75
P-22.	Analysis of AC Losses in High-Temperature Superconducting Tapes Using a Magnetic Formulation Based on the Thin Shell Model **Garkki B** and Revathi S	National Institute of Technology Puducherry	76
P-23.	Atomic scale study of defects in Fe_2CrAl Heusler compounds **Ravi Kumar Yadav,** R.Govindaraj, K Vinod and V.Srihari	Indira Gandhi Centre for Atomic Research, HBNI,Kalpakkam	77
P-24.	Evolution of transport regimes from classical to quantum in $Bi_{1.95}Sb_{0.05}Se_3$ thin film by substrate Temperature **Shivani Soni**, Edward Prabu Amaladass, Jegadeesan P, S. Amirthapandian, Kishore Kumar Madupu, Ramanathaswamy Pandian, Awadhesh Mani	Indira Gandhi Centre for Atomic Research, HBNI,Kalpakkam	78
P-25.	Compositional Dependence of Magnetic Transition in Double Perovskite $Ho_2MnNi_{1-x}Cu_xO_6$ Systems **V R Pooja,** A T Sathyanarayana, K Vinod and Awadhesh Mani	Indira Gandhi Centre for Atomic Research, A CI of Homi Bhabha National Institute, Kalpakkam	79
P-26.	Superconducting and Non-Superconducting States in $Nd_{1.85}Ce_{0.15}CuO_{4\pm\delta}$: Impact of Argon Annealing **Vinita Kumawat**, Riya Sindhwani, K.Vinod, Kishore Kumar Madupu, T. Geetha Kumary, Awadhesh Mani	Indira Gandhi Centre for Atomic Research, Kalpakkam	80
P-27.	Cryogenic Testing of Niobium Material for Superconducting RF Cavity Applications using the RRR measurement Technique **Anand Yadav**, Vinesh K. Verma, Ajay Yedle, Suresh Maloth, Vikas K. Jain, Sanjay Chouksey & Mahendra Lad.	Raja Ramanna Centre for Advanced Technology, Indore	81
P-28.	Effect of Substrate Temperature on the Structural and Magnetic Properties of Cobalt Ferrite ($CoFe_2O_4$) Thin Films Grown by Pulsed Laser Deposition **Vinay Shrivastava**, Ambrish Dwivedi, Yksh Gupta, Keval Gadani, Sanjay Kumar Upadhyay, Sourav Chowdhury, Anil Gome, Ratnesh Gupta, Sagar Sen	Maharaja Bhoj Govt. P.G. College, Dhar, Madhya Pradesh	82
P-29.	Exploring the magnetic properties of La_2MMnO_6 (M = Cr, Zn) double perovskites **K. Jeevanandham,** K. Vinod, A. T. Sathyanarayana and Sujoy Sen	Indira Gandhi Centre for Atomic Research, HBNI, Kalpakkam, Tamil Nadu	84

P-30.	Structural Investigations in Gd^{3+} and Ce^{4+}co-doped Lanthanum Zirconate Pyrochlores **Vidya M,** Raghavendra K G	Manipal Institute of Technology Manipal Academy of Higher Education (MAHE), Manipal	85
P-31.	Study on structural and dye degradation property of Mn doped MoO_3/SiO_2nanocomposites Boobesh S, **Abuthahir J**, Janardhanan P, Elango M	Government College of Technology, Coimbatore, Tamilnadu, India	86
P-32.	Assessing the Corrosion Resistance, Structural, and Energy Consumption Properties of TiO_2-based PEO coatings for photo catalysis on pre-anodized AA2024-Al **Sanjeev Kumar Singh**, Dr. P Naresh	Avanthi Degree & PG College, Hyderabad, Telangana	87
P-33.	Ballooning Behavior in End Plug Repaired Welds of Fuel Clad Tubes at Extreme Conditions **Rosy Sarkar,** R. Suresh Kumar, R. Manu, K. Mohan, K.Natesan	Indira Gandhi Centre for Atomic Research, Kalpakkam, Tamil Nadu	89
P-34.	Mechanical characterization of multi-directional C_f-SiC_m composites **Saurav Kumar Sahoo,** Arjun Mahato, Samar Mandal, M. Thangarasua, Shibayan Roy	Indian Institute of Technology Kharagpur, Kharagpur, India,	90
P-35.	Altercations in Physicochemical Properties of Soft Chemical Route Synthesized ZnO Thin Film **Jayesh R. Pawar,** Munjaji E. Dudhmal, Rajesh A. Joshi	Toshniwal Arts, Commerce and Science College, Sengaon-Hingoli, Maharashtra	91
P-36.	Reducing low thermal conductivity of GeTe compounds via nanostructure modulation by spark plasma sintering method **A. Sampathu,** Chellakumar. R, Narendran. D and M. Balakrishnan	Kalaignar Karunanidhi Government Arts College, Tiruvannamalai, Tamil Nadu, India	92
P-37.	Effect of Vacuum Annealing on the Cationic Distribution and Magnetic Properties of $NiFe_2O_4$ Thin Films **Ambrish Dwivedi,** Vinay Shrivastava , Yksh Gupta ,Keval Gadani , Sanjay Kumar Upadhyay, Sourav Chowdhury, Jayjit Kumar Dey, MoritzHoesch, Anil Gome, Ratnesh Gupta, Sagar Sen	Maharaja Bhoj Govt. P.G. College, Dhar, Madhya Pradesh	93
P-38.	Gamma-ray effects on Gd^{3+} doped Borophosphate Glass for radiation shielding and TL-Dosimetry Applications **Paul Dhinakaran**, P. Vinothkumar	Saveetha Engineering College, Thandalam, Chennai	95
P-39.	Morphological evolution of MBE grown Antimony nanocrystals under ion irradiation **Jinu Job,** Vikas Singh Gahlot, P. Jegadeesan, Sujoy Sen, S. Amirthapandian, B. Sundaravel	Indira Gandhi Centre for Atomic Research, HBNI,Kalpakkam	96

P-40.	Comparative analysis of the radiation hardness of PM6 and PTB7-th for space application in organic solar cell **Anuradha**	Malaviya National Institute of Technology, Malviya Nagar ,Jaipur	97
P-41.	Energy Storage study on gamma irradiated PANI – CuO nano Composites S. Ramakrishnan and **S. Rajakarthihan**	Thiagarajar College, Madurai	98
P-42.	Nanostructuring of Germanium surface using low energy Ga ion implantation **Hrudya Radhakrishnan,** Kamalesh N, Ramanathaswamy Pandian	Indira Gandhi Centre for Atomic Research, HBNI,Kalpakkam	99
P-43.	Insights into the Behaviour of Shape Memory Alloys under Extreme Conditions: A Candidate Material for the Passive Systems in Future FBR **Salil Verma,** Rosy Sarkar, Bhuwan Chandra Sati, R. Suresh Kumar, K. Natesan	Indira Gandhi Centre for Atomic Research, HBNI,Kalpakkam	100
P-44.	Real-time reliability analysis of 8051 microcontroller in gamma and proton environments **Charu Sharma**, R. P. Behera, Saif A. Khan, Puspalata Rajesh, S.Amirthapandian	Indira Gandhi Centre for Atomic Research, HBNI,Kalpakkam	101
P-45.	Defect Evolution in Sequential He and Ni Ion Implanted FeCrMnNi High Entropy Alloy **S. Vinitha**, S. Abhaya, C. David	Indira Gandhi Centre for Atomic Research, HBNI,Kalpakkam	102
P-46.	Study of ion beam-induced luminescence in β-$Ga_2O_3$by 100 keV He^+ions **Monu Kataria**, Fouran Singh, Sujoy Sen, Christopher David and Debdulal Kabiraj	Inter-University Accelerator Centre, New Delhi	103
P-47.	Proton irradiation studies on pristine & 20 % cold work D9 samples using Medical Cyclotron Facility **Binoy Kumar Maji**, Dipak Kumar Baisnab, B. Sundervel, Gayathri N. Banerjee, C. David and Paramita Mukherjee	Indira Gandhi Centre for Atomic Research, Kalpakkam	104
P-48.	Ion Beam-Induced Modification in the Microstructural and Mechanical Properties of 15-5PH Steel Fabricated by Selective Laser Melting **Pritam Patra**, Ambuj Tripathi, Sagar Sarkar	Indian Institute of Technology Delhi, New Delhi, India	105
P-49.	Irradiation studies on mechanical properties of silicon rubber compound **Suba. M,** Prakash. S, Falix Lawrence D, Kodandaraman. J, Venkatesan. K. A and Rajan. K	Indira Gandhi Centre for Atomic Research, ,Kalpakkam	106
P-50.	Unveiling the structural, radiation shielding properties of $BiVO_4$ - epoxy resin nanocomposites Vikram T, Abuthahir J, Sanjeevi P, Saravanakumar A, **Elango M**	PSG College of Arts and Science, Coimbatore, Tamilnadu, India	107

P-51.	Molecular dynamics study of self diffusion in Iron Phosphate glass **Aishwarya K,** Manan Dholakia, Sharat Chandra	Indira Gandhi Centre for Atomic Research, HBNI,Kalpakkam	108
P-52.	Investigation of Vacancy Formation Energy and Mechanical Properties in FeCrMnNi Alloy **Vallinathan K,** Gurpreet Kaur, Sharat Chandra	Indira Gandhi Centre for Atomic Research, HBNI,Kalpakkam	109
P-53.	Irradiation induced dissolution of precipitates in P91 steel – in-situ SEM investigation **Vikas Singh Gahlot**, P. Jegadeesan, V. D. Vijayanand, S. Amirthapandian	Indira Gandhi Centre for Atomic Research, HBNI,Kalpakkam	110
P-54.	Microstructural Characterization of carbide fuel elements of FBTR at linear heat rating of 400W/cm **Bhabani Shankar Dash,** K. G. Chaithanyaa, M. Padalakshmi,V. V. Jayaraj, C. Padmaprabu, V. Karthik & R. Divakar	Indira Gandhi Centre for Atomic Research, HBNI,Kalpakkam	111
P-55.	Studies on Fatigue Behavior of neutron irradiated SS316 using small specimens **Aishwary Vardhan Pandey,** V. Karthik, Ashish Kolhatkar, Divakar R.	Indira Gandhi Centre for Atomic Research, HBNI,Kalpakkam	112
P-56.	Fabrication of Components with Integrated Cladding for Harsh Environments through Casting Tumula Tirumala and **Ajay Kumar**	Indian Institute of Technology Tirupati (A.P.)	113
P-57.	Development of an experimental setup for low-temperature ion irradiations **S. Chinnathambi**	Indira Gandhi Centre for Atomic Research, Kalpakkam	114

Invited Talks

Finding New Topological Insulators Using Pressure

Prof. Chandrabhas Narayana

JNCASR, Bangalore & RGCB, Thiruvanthapuram

Email: cbhas@jncasr.ac.in & cbhas@rgcb.res.in

The talk will highlight the new topological quantum phase transitions in binary and ternary chalcogenides and high z materials under pressures. These include the presence of Strong/Weak Topological Insulators, Topological Crystaline Insulators, Electronic Topological Transition materials etc. Pressure tunes the volume of a material and in turn provides an ideal simulation of chemical pressure, hence these would lead to newer materials under ambient pressures. To detect these under pressure in presence of a hydrostatic liquid, we have used Raman spectroscopy and x-ray diffraction under pressure and supported by theoretical calculations to elucidate the electronic transitions instead off the Angle Resolved Photo Emission Spectroscopy (ARPES) commonly used as ARPES is not possible to do under pressure. These materials find applications in spintronic as well as thermoelectric applications.

Halide Perovskites at Extreme Conditions

Prof. Goutam Dev Mukherjee

IISER Kolkata

Email: goutamdev@iiserkol.ac.in

It is well known that hydrostatic compression reduces the inter-atomic distances resulting in distortions in the structural units of a lattice, which induces interesting changes in the physical properties including novel phase transitions. Sometimes these structural distortions are beneficial for enhancements of certain physical properties. In recent times the exploration of energy-harvesting materials for photovoltaic and optoelectronic applications has inspired intense research interest in the scientific community. In this search, halide-Perovskites have shown excellent photovoltaic properties. In this talk I shall take examples of a few lead-free model halide Perovskites and double Perovskites and show that structural distortions enhance the photoluminescence (PL) in these systems.

Dynamic Compression and Phase Change: The Fascinating Realm of Solids Under Extreme Conditions

Dr. Aditi Ray

BARC, Mumbai

Email: aray@barc.gov.in

The behavior of solids under extreme dynamic conditions offers an interesting glimpse into the complex world of phase transformations in response to rapid change in temperature and pressure. This talk aims to explore how shock loading, or dynamic compression, alters the structure of solids, inducing new phases not observed under ambient conditions. Highlighting the limitations of shock waves, the lecture will also discuss the advantages of isentropic compression for studying structural phase transitions in solids. From the formation of new crystalline structures to the onset of amorphization and melting, these phase transitions are not only intriguing from physics point of view, but also crucial for understanding material performance under extreme thermodynamic conditions as encountered in many high energy density systems. Using insights of molecular dynamics simulations and recent experimental results, the talk will delve into unveiling the intricate relationship between dynamic stress, strain rate and phase transformation dynamics. Emphasizing the importance of studying dynamic compression induced phase transitions, the talk will revolve around introducing various high energy density systems, including hypervelocity impacts, direct irradiation of ultra short laser pulse and extreme thermal radiations, all of which are integral to advancing material design and progress in contemporary research.

Ab-initio Characterization of High Pressure Phase Transformations in $CaTiSiO_5$ and $U_{1-x}Th_xSiO_4$

Dr. Ashok Kumar Arya

Formerly with BARC, Mumbai

Email: ashokarya@gmail.com

The most significant components of the Earth's crust and mantle are silicates. Mineralogists and crystallographers have long been interested in conducting systematic studies on these minerals. The behavior of silicates under high pressures (HP) and high temperatures (HT) has received particular interest, since it is crucial to our comprehension of crystalline materials in deep-earth geospheres. This talk will focus on Ab-initio Characterization of high pressure phase transformations in two important silicate materials, viz., titanite-based $CaTiSiO_5$ and zircon based $U_{1-x}Th_xSiO_4$, In terms of their topological, mechanical, dynamical and thermodynamic features.

Search for Superhard Carbides using DFT

Dr. Sharat Chandra

IGCAR, Kalpakkam

Email: sharat@igcar.gov.in

Transition metal (TM) carbides and nitrides have many industrial applications due to their high hardness, high melting point, excellent thermal conductivity, good wear and corrosion resistance. The exploration of novel phases of TM carbides and nitrides is an alternative route in the quest for super hard materials as compared to systems formed with low atomic number elements like cubic boron nitride. The essence of this approach is to have maximum valence electron charge density, basically contributed by the TM, and forming a p–d hybridized covalent bond between C and TM respectively. This talk will focus on a review of the density functional theoretic approaches for understanding the properties of superhard materials, taking transition metal carbides as the case study.

Studying radiation damage in nuclear materials by using ion accelerators

Dr. C. David

IGCAR, Kalpakkam

david@igcar.gov.in

The power of ion accelerators in the investigation of radiation damage is attributed to their ability to assess fundamental processes, achieved through exceptional management of experimental parameters.The third stage of Indian nuclear power programmefocuses on advancing the Indian molten salt breeder reactor (IMSBR) as a means to utilize thorium.One of the major obstacles in the development of molten salt reactors (MSRs) is the corrosion of primary and structural materials that come into contact with molten salts such as FLiNaK. Applying a nickel coating to the inner surfaces of primary structural components has emerged as a method to enhance resistance to corrosion. These nickel coatings in MSRs will also be subjected to fission neutrons and fission fragments, which can lead to alterations in texture, changes in surface morphology, and the formation of voids. This presentation covers the findings from our recent research that provides new perspectives on irradiation-induced texture changes, as well as void nucleation and growth in nanocrystalline nickel.

Understanding radiation response of ceramics for nuclear applications

Dr. Vinita Grover Gupta

Chemistry Division, BARC, Mumbai

Email: vinita@barc.gov.in

Understanding irradiation behaviour of materials is important for designing superior radiation stable materials for applications in industries such as space and nuclear. The radiation tolerance depends on radiation characteristics, intrinsic properties of material and external conditions such as irradiation temperature. The materials-specific factors that control the radiation response include composition, crystal structure, particle size, morphology, presence of defects/disorder, nature of boding etc. Our group has been involved in research on radiation response of ceramics such fluorites, pyrochlores, garnets by employing different ion beams of both high energy (to mimic fission fragments) and low energy (to simulate alpha recoils). The structures which are either open (fluorites) or have the scope of absorbing/mitigating the damage by virtue of defect creation and undergoing phase transition (borderline pyrochlores) exhibit enhanced radiation stability. Enhancing disorder at local crystal level imparts superior radiation tolerance, exemplified using $Nd_2Zr_2O_7$. Increase in average bond ionicity improves radiation tolerance as well. The effect of particle size, morphology on ceria and stabilized zirconia (YSZ) has been investigated and the results in both high and low energy regime have been compared. Detailed radiation response of garnet, $Y_3Al_5O_{12}$ has been compared with fluorite-type structure, and significant guidelines for ceramics to exhibit radiation tolerance have been established. The talk shall discuss the effect of radiation energy and crystal structure, microstructure and bonding characteristics of a materials on its response towards radiation with relevant examples.

Investigation on evolution of ground states of selected novel systems under high pressure and high magnetic field at low temperatures

Prof. Awadhesh Mani

Head CMPD, MSG, IGCAR, Kalpakkam

Email: mani@igcar.gov.in

Condensed matter systems are adorned with varieties fascinating ground states. The thermodynamic parameters such as external pressure (P), temperature (T), and magnetic field (H) have profound effect on the evolution/transformation/modification of the ground state properties of these systems. In this talk, I will present our studies on a few selected grounds (such as FeAs-based superconductors, Bi_2Se_3-based 3-D topological insulators (TI) and d-electron based Kondo insulators (KI)) subjected under high pressure & high magnetic field at low temperatures. The FeAs-system, namely, $BaFe_2As_2$, exhibits pressure/chemical substitution induced superconductivity which emerges at the cost of spin density wave. Intersecting quantum phenomena and pressure induced superconductivity in Bi_2Se_3 topological insulators will also be discussed.

High-Pressure and High-Temperature Synthesis of Quantum Materials

Prof. A. Sundaresan

JNCASR, Bangalore

Email: sundaresan@jncasr.ac.in

High-pressure and high-temperature (HPHT) synthesis is a powerful tool for discovering novel materials by stabilizing exotic phases that do not form under ambient conditions. This method is crucial in realizing strongly correlated electron systems, topological phases, and unconventional superconductors, providing a deeper understanding of emergent quantum phenomena. Moreover, HPHT synthesis develops next-generation electronic, spintronic, and quantum information technologies. In this talk, I will illustrate the effectiveness of HPHT techniques in uncovering new phases and their unique properties through select examples.

Anisotropic Magnetotransport and Quantum Hall Effect in Bulk Semimetallic Single Crystals

Prof. A. Thamizhavel

Chairperson, Condensed Matter Physics & Materials Science, TIFR, Mumbai

Email: thamizh@tifr.res.in

In the quest for new material systems, we have identified two interesting systems viz., CaCuSb and $CaCu_4As_2$ both exhibiting a hexagonal and rhombohedral crystal structure respectively. One of the unique features of this crystal structure is that it possesses Cu-Sb and Cu-As conduction layers, respectively. Both these compounds exhibit highly anisotropic magnetotransport properties thus establishing the quasi-2D character. The angular dependence of magnetoconductivity and Shubnikov-de Haas (SdH) also confirmed the 2D nature of the charge carriers. High field transport measurements measured up to 45 T revealed quantized Hall plateaus in the $1/\rho_{xy}$ *vs.* 1/B plot.

Nano-scale evolution under swift heavy ion induced thermal spike

Dr. Debdulal Kabiraj

IUAC, New Delhi

Email: d.kabiraj@gmail.com

While travelling through a material energetic ions lose energy by nuclear (Sn) and electronic (Se) energy loss. Swift heavy ions (SHI) lose their energy predominantly through Se where inelastic interactions with electrons takes place on femtosecond time scales. The high density of energy transfer to the electrons along the ion path leads to local states of intense electronic excitation. Through electron-phonon coupling, the excited electrons transfer their energy to atoms, which are rapidly heated, resulting in thermal spike. Beyond a material-dependent threshold, a collective atomic movement is possible leading to an ion track that is a few nanometers in diameter and tens of micrometers in length. The ultra-fast thermal spike within this narrow region creates an extreme condition within a time scale of pico- to nanosecond. Here we present how nanoscale voids are formed within individual tracks in amorphous Ge and their size and shape evolve in subsequent ion impacts. And size and shape change of alloy nano-particles embedded in the silica matrix.

A few highlights on some Defects studies in Reactor stuctural materials and Novel oxides using Advanced Nuclear Techniques

Prof. R. Govindaraj
Defects and Damage Studies Division, Materials Science Group
Homi Bhabha National Institute , Kalpakkam - 603102
(govind@igcar.gov.in)

Asbstract

In addition to positron annihilation spectroscopy (PAS) , which has been established as a powerful tool to study open volume defects from monovacancy onwards up to voids , other nuclear techniques such as time differential perturbed angular correlation (TDPAC) and Mossbauer spectroscopy have also been extensively being utilized in Defects and Damage studies division of Materials Science Group for the last decades. These techniques have been employed for in depth studies of defects, defects-solute interactions in reactor structural materials and for also comprehending defects associated phenomenon in a number of novel condensed matter systems. In this talk some of the recent representative results on defects studies in Indian RAFM steel obtained using PAS [1,2] will be highlighted in addition to the discussion on the representative results on the nucleation and growth of helium bubbles in Zr and Ni obtained using TDPAC and PAS [3,4]. Importance of defects in affecting magnetic and hence spin polarization properties in Heusler compounds would be elucidated based on MS results [5,6] . Atomic scale understanding of negative thermal expansion in zirconium tungstate [7,8] and correlation between charge , spin, orbital ordering in $La_{0.7}Sr_{0.3}MnO_3$ would also be highlighted based on the results of TDPAC studies [9,10,11].

References

1. Renjith et al, JNM 544 (2021) 152697
2. Renjith et al , Phil Mag 99 (2019) 38
3. R. Govindaraj et al, Nuclear Instrumentation and Methods B179 (2001) 200
4. R. Govindaraj et al, JNM 265 (1999) 139
5. Ravi Kumar Yadav et al, RSC Advances 13 (2023) 19106
6. Ravi Kumar Yadav et al, Phys Chem Chem Phys 22 (2020) 26876
7. R. Govindaraj et al , Phys. Rev B76 (2007) 012104
8. R. Govindaraj et al, Jour Physics Cond Matter 21 (2009) 235402
9. R Govindaraj et al, Chem Phys. 302 (2004) 185
10. R. Govindaraj JPCM 18 (2006) 7651
11. R. Govindaraj et al, Phys Rev B70 , 220405 (R) , (2004)

Expert Talks

Polymorphic structural transition in $Cd_{0.9}Zn_{0.1}Te$ at high pressure

N. R. Sanjay Kumar
Materials Science Group, Indira Gandhi Centre for Atomic Research, A CI of Homi Bhabha National Institute, Kalpakkam, 603 102, Tamil Nadu, India
sanju@igcar.gov.in

Abstract: $Cd_{0.9}Zn_{0.1}Te$ (CZT) has gained a lot of traction with its application in the field of radiation detectors. In this study, CZT has been investigated using *in-situ* X-ray diffraction(XRD) at high pressures up to 22 GPa, and both high pressure and high temperature (HP HT) up to 5 GPa and 400 °C. CZT adopts zincblende phase at ambient condition. We have observed the previously unreported cinnabar type phase in CZT at high pressure. Cinnabar type phase nucleated at 1.8 GPa because of the motion of Te atoms in the *ab*-plane of zinc blende CZT and coexisted with the parent phase. The onset of transition to rocksalt phase took place at 4.7 GPa with successive atomic displacement along *a* and *c* direction of the cinnabar type unit cell. The parent phase disappeared at 6.3 GPa, but cinnabar type phase as a distorted form of rocksalt phase coexisted with the rocksalt phase due to the comparable energy for both the structures. The mechanism of transitions to cinnabar type and rocksalt phase is of quasi-reconstructive nature. Further, the rocksalt phase underwent a displacive transition to an orthorhombic (*Cmcm*) phase at 10.7 GPa which is accompanied by expansion along one axis and compression along the other two axes. In the reverse pressure cycle, the transitions were reversible and sluggish in nature. In the *in-situ* high pressure and high temperature XRD studies, distinct structural hysteresis was observed and the transition to rocksalt phase was irreversible. At ambient pressure, the zinc blende structure remained stable up to 400°C. The thermal expansion coefficient of the zinc blende phase and the high pressure rocksalt phase were estimated to be 23(1) × 10^{-6}/°C and 10.2(1) × 10^{-6}/°C respectively.

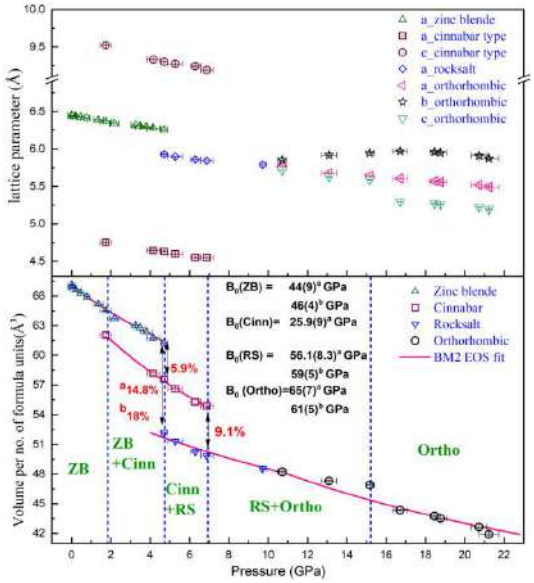

FIG. Evolution of lattice parameters and unit cell volume under pressure. ZB – zinc blende, Cinn- cinnabar type, RS – rocksalt and Ortho– orthorhombic structure.

Reference: Structural evolution of zinc doped cadmium telluride at high pressure and high temperature, *A. N. Arpita Aparajita, Balmukund Shukla, P Vijayakumar, N R Sanjay Kumar, S Ganesamoorthy, V. Srihari and N V Chandra Shekar, Physica Scripta 99 (2024) 105939*

High Pressure Structural Investigation on Uranium Oxide Compounds

Balmukund Shukla*, N R Sanjay Kumar

[1]Materials Science Group, Indira Gandhi Centre for Atomic Research, HBNI, Kalpakkam, 603102, Tamil Nadu, India

bshukla@igcar.gov.in

Abstract

Ce-doped UO_2 is an important material in nuclear research because the structural properties of Ce are similar to those of Pu. This makes Ce-doped UO_2 a valuable surrogate for studying the behavior of Pu-doped UO_2, which is relevant in nuclear fuel applications and waste management. Cerium doped UO_2 samples $U_{1-x}Ce_xO_2$ (x=0.2, 0.4, 0.6, 0.8) were synthesized using sol-gel method. $U_{1-x}Ce_xO_2$ retains fluorite UO_2 structure with decreasing lattice parameter as Ce content is increased. The decrease in lattice parameter is due to the larger presence of tetravalent Ce cation than trivalent cations. In-situ high pressure x-ray diffraction studies were carried out to find out effect of doping Ce and study their compressibility behavior. These compounds remain in fluorite structure at least up to 25 GPa, beyond which phase transition to orthorhombic structure is seen. The ambient pressure bulk modulii for x = (0.2, 0.4, 0.8) in $U_{1-x}Ce_xO_2$ are 216 (6) GPa, 225 (9) GPa, and 247 (8) GPa, respectively that indicates consistent increase in the bulk modulus of the material when Ce content is increased. The behavior of bulk modulus with Ce doping follows lattice parameter i.e. smaller lattice shows lesser compressibility.

Topic Code: Computational Materials Science in Extreme Conditions

Effect of Pressure on Symmetry Breaking Transition in Uranium and Uranium Intermetallics

Gurpreet Kaur[a,b]

[a]**Materials Modeling Section, Defects and Damage Studies Division, MSG, IGCAR, Kalpakkam**

[b]**HBNI, Anushaktinagar, Mumbai**

Email: *gurpreet@igcar.gov.in*

Uranium compounds show a variety of interesting properties from a quantum theoretical point of view. The 5*f* electrons are on the verge of delocalization and thus the electron correlations play an important role in deciding the properties of these compounds ranging from Mott insulating behaviour, valence fluctuation, magnetism to heavy fermions [1]. When localized, they give rise to the Mott insulating behaviour or the magnetic behaviour and when delocalized, they lead to heavy fermions and charge and spin density waves. In uranium intermetallics the behaviour of 5f electrons is affected by bonding with atoms of other elements. Under an applied external pressure the bonding changes, which can lead to change in the nature of 5*f* electrons. Our density functional theory calculations have verified and predicted the existence of symmetry breaking transitions in α-Uranium, U_2Ti and U_2Mo which is observed as phonon instabilities [2,3]. This transition leads to dimerization of the U atoms, leading to doubling of the unit cell in one direction. For α-U it is along the *a*-axis, for U_2Ti along the *c*-axis and for U_2Mo along the *b*-axis. At ambient pressures the transition is known to occur at low temperatures. These instabilities are linked to the Fermi surface topology. It is found increasing the pressure leads to changes in the Fermi surface suppressing the symmetry breaking transition. There is also a correlation between the symmetry breaking and U-U bond length in these systems. In the direction of symmetry breaking, the U-U bond distances are 2.79 Å, 2.80 Å and 2.78 Å for α-U, U_2Ti and U_2Mo respectively. For α-U & U_2Ti, the prediction has been verified by experiments [4] and for U_2Mo future experiments may confirm these findings. The relationship between the U-U bond length & the dimerization of U atoms is summarized in table.

Compd.	**U-U (Å) (Original)**	**U-U (Å) (Distorted)**	**Facts**
α-U	2.79	2.61, 3.13	CDW known from experiments [2]
U_2Ti	2.80	2.58, 3.18	CDW Verified by experiments [4]
U_2Mo	2.78	2.70, 2.99, 2.67	No data available at low temperatures

Table 1: Summary of the symmetry breaking in α-U, U_2Ti and U_2Mo.

References

1. A.J. Arko, J.J. Joyce, and L. Havela, "5f-Electron Phenomena in the metallic state" in 'The Chemistry of the Actinide and Transactinide Elements' (Springer, 2011), chapter 21, 2307–2379.
2. R. Qiu, H. Lu, B. Ao, T. Tang and P. Chen, Modelling Simul. Mat Sci. Eng. **24 (**2016) 055011.
3. Gurpreet Kaur, S. Mathi Jaya and B.K. Panigrahi, J. Alloys and Compds. **730** (2018) 36.
4. C.R. Stevens, A. Hermann, A. Huxley and D. Wermeille, Phys. Rev. B **109** (2024) 125116

Quantum transport signatures of Topological insulators (TI) at low temperatures and magnetic fields

E.P Amaladass[1,2], Shivani Soni[1,2], Akhilesh Kumar[1,2], P.Anees[1,2], Jegadeesan P[1] , Kishore K. Madapu[1,2], Ramanathaswamy Pandian[1,2], S. Amirthapandian[1,2], Awadhesh Mani[1,2]

[1]Material Science Group, Indira Gandhi Centre For Atomic Research, Kalpakkam, 603102

[2]Homi Bhabha National Institute, Training School Complex, Anushaktinagar, Mumbai, 400094

Abstract

Three-dimensional (3D) topological insulators (TI) are a novel class of materials that host highly mobile and spin-polarized Dirac fermions in the two-dimensional (2D) conducting Dirac surface states (SS). Here in this talk, I will be presenting how the magnetotransport signatures, namely i) the Subnikov-de Haas (SdH) oscillation observed at low temperatures and high magnetic fields and ii) the Weak antilocalization (WAL) effect observed at low temperature and weak magnetic field are used to probe the Dirac states. The first part will discuss the effect of ion irradiation on TI single crystals. $Bi_{1.9}Sb_{0.1}Se_3$ single crystals were irrated with 140 KeV proton beam at different fluences. Lifshitz-Kosovich (LK) analysis of the Subnikov-de Haas (SdH) oscillationreveals SS characteristics with a Berry phase factor of ~0.6. The oscillation frequency systematically drops from 156 T for the pristine sample to 136 T for the irradiated sample. According to the Onsager relation, this shift in frequency shows the downward shift of Fermi energy toward the DP. Studies using Raman and TEM demonstrate irradiating induced compressive strain in the system.To corroborate the effect of the strain on the 2D Dirac states, we calculated the surface band structure using Wannier Hamiltonian formalism. A systematic upward shifting of Dirac states upon biaxial compressive strain is observed in line with the experimental findings. The second part will address the effect of charge compensation in TI thin films due to the phase-segregated Sb_2Se_3 phase. Here, the weak antilocalization (WAL) quantum phenomenon, analyzed using the Hikami–Larkin–Nagaoka equation, is used as aprobe for the SS. The sample with a higher phase fraction of segregated Sb_2Se_3exhibits better surface characteristics due to the compensation of Se-vacancies-induced excess electrons with the p-type Sb_2Se_3impurity phase.

Pressure Induced Topological Phase Transitions in Sn-based Ternary Chalcogenides

Dr. Mukhtiyar Singh

DTU, New Delhi

Email: mukhtiyarsingh@dtu.ac.in

It is quite intriguing to investigate the transition from a topological insulator (TI) phase to topological crystalline insulator (TCI) phase in a material as the latter has an advantage over the former in controlled device applications. Here, we demonstrated the existence of dual topological phase in ternary chalcogenide $PbSnX_2$ (X = S, Se, Te) using *first principles* calculations and the green function approach. This family have a topologically trivial ground state with direct band gaps 0.338 eV, 0.183 eV and 0.235 eV for $PbSnS_2$, $PbSnSe_2$ and $PbSnTe_2$, respectively. Under the effect of the applied hydrostatic pressure of 5 GPa, 2.5 GPa and 3.5 GPa these materials show a topological phase transition to the topological insulator. A further rise in pressure to 5.5 GPa, 3 GPa, and 4 GPa induces another band inversion at the *Γ-point*, rendering these materials topologically trivial again due to an even number of band inversions in the bulk band structure but the presence of a mirror symmetry around $(10\bar{1})$ plane provides symmetry protection to these Dirac cones existing along $(\bar{1}2\bar{1})$ surface which confirms the TCI phase in these materials.

Magnetic/magneto-caloric studies on La_2NiMnO_6 based double perovskites

Dr. Vinod K

Low Temperature Studies Section, Condensed Matter Physics Division, Materials Science Group, IGCAR, Kalpakkam-603102, Tamil Nadu, India

email: vinod@igcar.gov.in

Abstract: The talk will present the magnetic/magneto-caloric studies on La_2NiMnO_6 based double perovskites. An introduction to the magneto-caloric effect (MCE) will be given first. The La_2NiMnO_6 double perovskites were introduced, followed by the detailed discussion of the magnetic/magneto-caloric studies on the system. The results of Cu substitution at the Ni site in the form of $La_2Ni_{1-x}Cu_xMnO_6$ series will be discussed in detail.

Tailoring ion irradiation for radiation damage studies of nuclear structural materials

Dr. Gayathri N Banerjee

VECC, Kolkata

Email: gayathri@vecc.gov.in

Ion irradiation studies have proven to be an effective method for replicating neutron-induced damage in nuclear reactors. By precisely controlling factors such as dose, dose rate, and temperature, researchers can simulate the degradation experienced by core structural materials in reactor environments.

In this talk, we will present the facilities available at the Variable Energy Cyclotron Centre (VECC), and how we have employed a range of light and heavy ion beams over the past few decades to explore the structure-property relationships of key candidate alloys for core component application. Recent experimental results along with atomic scale support from MD and DFT calculation will be presented.

First experimental results from In-situ Ion Irradiation and Imaging with SEM (i^4 SEM) Facility

S. Amirthapandian[1,2*], P. Jegadeesan[1], Vikas Singh Gahlot[1,2], S. Chinnathambi[1],
[1]Materials Science Group, Indira Gandhi Centre for Atomic Research (IGCAR), Kalpakkam, 603102
[2]Homi Bhabha National Insitute, Indira Gandhi Centre for Atomic Research, Kalpakkam, 603102
*** Email: pandian@igcar.gov.in, pandiancmp@gmail.com**

Abstract: We have recently established a new in-situ ion irradiation and imaging with field emission scanning electron microscope (i^4-FESEM) facility at Indira Gandhi Centre for Atomic Research (IGCAR), Kalpakkam, the first of its kind in India and third of its kind in the world. This facility is established by integrating a high resolution FESEM (Model: Carl Zeiss CrossBeam 340) with the 10° beamline of 1.7 MV tandetron accelerator. Many steps were taken to effectively isolate mechanical vibrations from the beamlines to the FESEM. This in-situ setup makes it possible to monitor the evolution of individual features or structures with submicron dimensions as a function of ion fluence. We have demonstrated this by tracking the displacement of individual gold nanoparticles decorating the FIB pattern which was irradiated with 2MeV Si^+ ions. It allows us to track the displacement of individual gold particles in addition to examining the average displacement of particles overall, which would be nearly impossible in a typical ex situ experiment.

1. INTRODUCTION

Scanning Electron Microscopy (SEM) is the perfect tool for characterizing the surface modifications in materials. So an in-situ ion irradiation and SEM imaging facility would be an appropriate facility to study irradiation induced phenomena such as precipitate dissolution/growth, blistering of bubbles, irradiation induced grain growth, modification of nanostructures or islands on the surfaces, morphology of the thin film under ion irradiation and mechanical properties of nano pillars.There are two such in-situ ion irradiation and SEM imaging facilities in the world, one at materials science beamline (M-branch) of the universal linear accelerator (UNILAC) at Gesellschaft für Schwerionenforschung (GSI), Darmstadt[1] and another at the Sandia National Laboratory where the SEM was coupled with a 6 MV Tandem accelerator[2]. In the present work, we discuss about the developmental work and the preliminary results obtained from this facility.

2. EXPERIMENTAL SET-UP

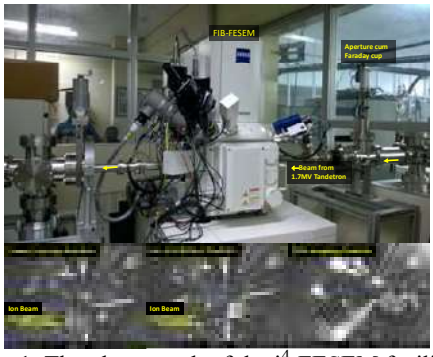

Fig.1. The photograph of the i^4-FESEM facility

A standard FESEM (model: cross beam 340, Carl Zeiss make, resolution:1.5nm@15kV) was installed in a vibration free platform (sand filled aluminium box). The height of the SEM was adjusted to match the beamline height and alignment of the beamline was completed. The SEM was connected with beamline via ion beam - SEM interface(refer Fig.1), which consists of pumping system, and aperture cum Faraday cup. Pneumatically operated aperture cum Faraday cup was fabricated and installed in the beamline. The Faraday cup (with aperture of 4mm and secondary electron suppressor) was installed to measure beam current during experiments.

3. RESULTS AND DISCUSSION

Figure 2 shows the sequence of SEM images of the Au clusters decorating FIB patterns in Si substrate under 2 MeV Si^+ ion irradiation. . The Au nanoparticles were displaced under ion irradiation from their original site by approximately 400nm in the beam direction and it is caused by thermal stress induced by ion irradiation.

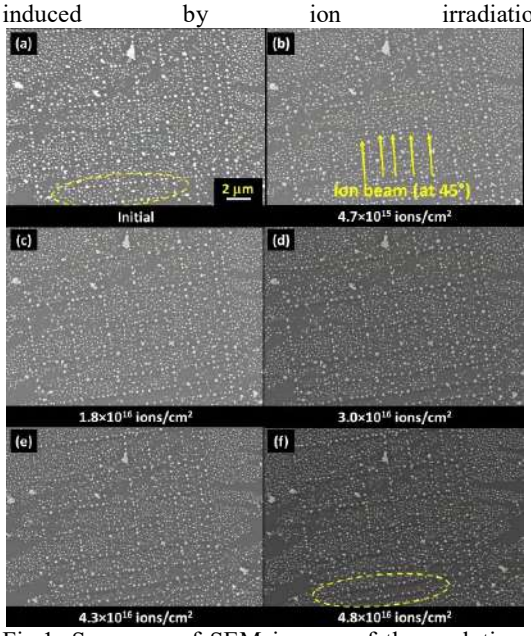

Fig.1. Sequence of SEM images of the evolution of Au clusters decorating FIB patterns in Si substrate under 2 MeV Si^+ ion irradiation.

REFERENCES

[1]. Amirthapandian S, et al. Rev. Sci. Instrum. 81 (2010) 033702.
[2]. Briggs S.A, et al, Microsc. Microanal. 25 (2019) 1596.

Focused Helium ion beam tailoring of luminescence in hexagonal boron nitride (h-BN)

Dr. Sinu Mathew

S. B. College, Mahatma Gandhi University, Kerala

Email: sinumathew@sbcollege.ac.in

- keV He^+ irradiation induced strong room temperature visible luminescence due to mid-gap states of h-BN
- The ion energy and fluence dependence is investigated
- Comparison with keV neon, argon ion irradiation
- Single step direct patterning of luminescence centers of h-BN is demonstrated.

Oral Presentations

Pressure-induced superconducting and magnetic phases in UTe_2

M. O. Ajeesh*, J. D. Thompson, E. D. Bauer, F. Ronning, S. M. Thomas, and P. F. S. Rosa
Los Alamos National Laboratory, Los Alamos, NM 87545, USA
(* presently at Indian Institute of Technology Palakkad, India, ajeesh@iitpkd.ac.in)

Abstract: UTe_2 has recently attracted enormous attention as a spin-triplet superconductor candidate, promising the realization of topological superconductivity in bulk materials. Several intriguing properties have been observed in UTe_2, such as multiple pressure-induced superconducting and magnetic phases as well as re-entrant superconductivity under applied magnetic field. Importantly, the superconducting properties of UTe_2 at ambient conditions crucially depend on the sample quality, arguably due to the presence of uranium vacancies. Here, we investigate UTe_2 samples of different qualities using electrical transport, magnetic, and thermodynamic measurements under hydrostatic pressure to investigate the intrinsic properties. Our results reveal that the pressure-induced superconducting and magnetic phases also crucially depend on the sample quality.

1. INTRODUCTION

Unconventional superconductor UTe_2 has been heavily investigated recently as a candidate for spin-triplet pairing, especially in realizing topological superconductivity in a bulk material. Several intriguing properties have been observed in UTe_2, such as multiple pressure-induced superconducting and magnetic phases as well as re-entrant superconductivity under applied magnetic field [1]. The superconducting (SC) properties of UTe_2 at ambient conditions crucially depend on the details of crystal growth. For instance, both the SC transition temperature (Tc) and the residual specific heat coefficient vary significantly among crystals grown in different conditions despite having very similar structural properties [2-4]. Samples grown via the chemical vapor transport (CVT) technique exhibit systematic changes in Tc as a function of the growth temperatures, and superconductivity abruptly disappears for samples grown beyond certain upper and lower growth-temperature limits [3]. Presence of uranium vacancies has been attributed to the lower Tc/absence of SC in low-quality samples [4]. Here, we investigated CVT-grown UTe_2 samples of high (Tc around 1.9 K) and low (no bulk SC) quality under pressure to understand the sample dependence of the pressure-induced SC and magnetic phases.

2. EXPERIMENTAL DETAILS

Single crystals of UTe_2 were grown using the CVT method [3]. Electrical resistivity (standard four probe method), heat capacity (ac calorimetry technique) and ac magnetic susceptibility measurements under hydrostatic pressure were performed in a single setup using a piston-clamp pressure cell with Daphne 7373 oil as the pressure medium. Pressure-dependent measurements at low temperatures were carried out in an adiabatic demagnetization refrigerator.

2. RSULTS AND DISCUSSION

Our measurements on the high-quality UTe_2 sample yielded a temperature-pressure phase diagram similar to that reported on earlier samples [5]. Importantly, our ac magnetic susceptibility data show diamagnetic behavior at both the pressure induced SC_2 and SC_3 phases. Additionally we observe features in the ac susceptibility corresponding to the pressure-induced magnetic phase transitions, providing further confirmation of their magnetic nature.

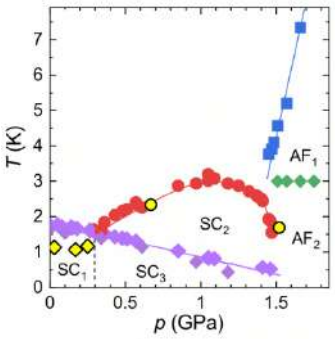

Fig. 1 Pressure-temperature phase diagram of UTe_2

The low-quality UTe_2 single crystal that we chose does not undergo a bulk SC transition, but shows filamentary superconductivity with a Tc of 1 K at ambient pressure. Remarkably, resistivity measurements reveal that the evolution of the filamentary SC state under pressure resembles the behavior observed in previous reports on bulk SC samples. However, ac calorimetry data do not show evidence for either bulk superconductivity or magnetism in the low-quality sample for pressures up to 1.6 GPa. These results suggest that the pressure-induced SC phases, as well as the magnetic phases are susceptible to uranium vacancies. Our results highlight the role of inhomogeneity in CVT-grown UTe_2 samples and serve as a cautionary tale when probing electrical resistivity alone to investigate superconductivity in such materials [6].

REFERENCES

[1]. D. Aoki et al., J. Phys.: Condens. Matter 34 243002 (2022).
[2]. Y. Haga et al. J. Phys. Condens. Matter 34, 175601 (2022).
[3] P. F. S. Rosa et al. Commun Mater 3, 33 (2022).
[4] A. Weiland et al. J. Phys. Mater. 5 044001 (2022).
[5] S. M. Thomas et al., Sci. Adv. 6, eabc8709 (2020).
[6]. M. O. Ajeesh et al., J. Phys. Soc. Jpn. 93, 055001 (2024)

Pressure induced emission enhancement in vacancy ordered halide double perovskite Cs_2TeCl_6

Suvashree Mukherjee, Debabrata Samanta, and Goutam Dev Mukherjee*
National Centre for High Pressure Studies, Department of Physical Sciences, Indian Institute of Science Education and Research Kolkata
***Email:** goutamdev@iiserkol.ac.in

Abstract: The effect of pressure on the enhancement of photoluminescence (PL) intensity, optical bandgap and structural evolution of a vacancy ordered double halide perovskite Cs_2TeCl_6 is investigated systematically up to 30.0 GPa. A significant increase in photoluminescence intensity and a rapid decrease in optical band gap are observed, which are related to the octahedral distortion and structural transition.

1. INTRODUCTION

Cs_2TeCl_6, a member of the lead-free vacancy ordered halide double perovskite, is a stable compound at ambient conditions and might be a potential candidate in nonlinear optoelectronics. However, the indirect nature of its optical band gap with a large value (≈2.54 eV) affects its performance as a photovoltaic material [1]. Because of the soft lattice of halide double perovskites, the application of external pressure could greatly impact the crystal structure of the material, allowing tuning of the optical band gap and improve its performance as a photovoltaic material.

2. EXPERIMENTAL SECTION

Crystalline powders of Cs_2TeCl_6 are prepared by acid precipitation method [2]. To generate the high pressure, we have used piston-cylinder type diamond anvil cell (DAC). Laser sources of 532 nm and 488 nm are used for Raman and PL spectra measurements respectively. XRD measurements are carried out at the P02.2 beamline at PETRA III, Germany with a wavelength 0.2907 Å.

3. RESULT AND DISCUSSION

3.1. Pressure dependent PL measurements

The Cs_2TeCl_6 exhibits a broad emission band at 599 nm with a full-width half maximum (FWHM) of 123 nm accompanied by a large Stokes shift 0.8 eV at ambient conditions, which correspond to the self-trapped excitonic (STE) emission [1]. The PL intensity increases with pressure up to 1.2 GPa followed by a continuous decrease up to 16.2 GPa, above which it vanishes. The PL intensity at 1.2 GPa pressure is almost 6 times that at ambient pressure.

3.2. Pressure dependent optical bandgap measurements

The optical bandgap of Cs_2TeCl_6 is found to be 2.51(4) eV in ambient condition. The band gap initially reduces under compression up to 2.9 GPa, above which it increases with pressure up to 4.8 GPa followed by a continuous reduction up to 32.0 GPa.

3.3. Pressure dependent XRD measurements

The crystal structure of Cs_2TeCl_6 is cubic (Fm-3m) in ambient conditions. The sample undergoes cubic to monoclinic ($P2_1/n$) structural transition at around 1.0 GPa. The distortion of $TeCl_6$ octahedra causes increase in the PL intensity. The monoclinic phase persists up to 2.6 Gpa. Interestingly, the sample regains the cubic (Fm-3m) structure at around 3.4 GPa and no other structural change is observed up to 30.0 Gpa. An iso-structural transition is observed at around 14.1 GPa with a slight decrease in compressibility. The Te-Cl bond length plays a crucial role in the variation of optical bandgap under pressure.

3.4. Pressure dependent Raman spectra

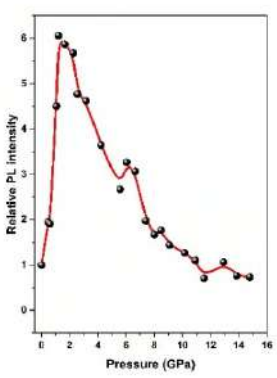

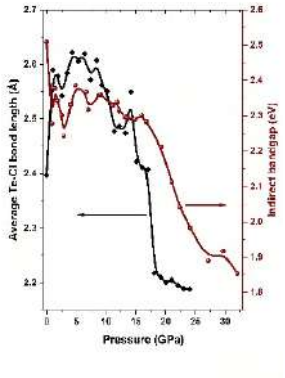

Fig-1: PL intensity under pressure, Fig-2: Variation of optical bandgap under pressure

measurements

The Cs_2TeCl_6 shows four Raman active modes P_1 (T_{2g}), P_2 (T_{2g}), P_3 (E_g) and P_4 (A_{1g}) at 47.2, 137.3, 242.6 and 286.0 cm^{-1}, respectively at ambient conditions. A new Raman mode P_5 at is observed at 119.0 cm^{-1} in the pressure range 0.1 GPa to 2.5 GPa, which is associated with the cubic to monoclinic structural transition, as suggested by the XRD analysis. The data are compatible with the pressure dependent XRD measurements.

4. CONCLUSION

Cs_2TeCl_6 undergoes a structural transition from cubic Fm-3m to monoclinic $P2_1/n$ at around 1.0 GPa. A significant increase in photoluminescence intensity and a rapid decrease in optical band gap are observed, which are related to the octahedral distortion and structural transition.

ACKNOWLEDGEMENT

The authors acknowledge the DST, Government of India and IISER Kolkata. S.M. also acknowledge CSIR, Government of India.

REFERENCES

[1] J. Jiang et al, Advanced Optical Materials. **11**, (2202634) 2022
[2]. D. Samanta et al J. Phys. Chem. C. **125**, (3432) 2021.

Topic Code: High-Pressure Materials Science

High Pressure XRD studies on $Ho_{0.4}Eu_{0.6}MnO_3$

P Anand Kumar[1]*, R. M. sarguna[1], V. Srihari[2] and N R Sanjay Kumar[1]
[1]Indira Gandhi Centre for Atomic Research, A CI of Homi Bhabha National Institute, Kalpakkam
[2]High Pressure & Synchrotron Radiation Physics Division, Bhabha Atomic Research Centre, Mumbai

Email: (*ak_police@igcar.gov.in)

Abstract: $EuMnO_3$ was doped with Holmium (40 atom% of RE) adopting an orthorhombic structure (SG: Pnma) with composition $Ho_{0.4}Eu_{0.6}MnO_3$. High pressure XRD studies on $Ho_{0.4}Eu_{0.6}MnO_3$ were carried out up to 30 GPa at BL-11 beamline of Indus-2, RRCAT. The orthorhombic structure was found to be stable up to the highest pressure studied. The bulk modulus obtained from the HPXRD experiments is 170±18 GPa. The volume of the MnO_6 octahedra decreases with pressure. The octahedra gets distorted with increasing pressure and quadratic elongation increases from 1.01 to 1.20 at the highest pressure. The Mn-O bonds oriented along the c-axis slightly increase. However, in the ab plane, two types of Mn-O bonds behave differently. One of the bonds contracts while another one expands.

1. INTRODUCTION

The rare-earth manganites, $RMnO_3$ (R = La–Lu), host a wide range of novel structural and physical properties that are highly dependent on the choice of R [1]. At ambient conditions the compounds with larger rare-earth cations (R = La–Dy) adopt the orthorhombic $GdFeO_3$ perovskite structure type (*o* −$RMnO_3$, space group Pnma, No. 62), whereas for the smaller R cations (R = Ho–Lu, Y, In, Sc) the system crystallizes in a hexagonal structure (*h* −$RMnO_3$, space group $P6_3/mmc$, No. 185). While both polymorphs exhibit multiferroic behavior with the coexistence of antiferromagnetism and improper ferroelectricity.

2. EXPERIMENTAL TECHNIQUES

Mao-Bell type diamond anvil cell (DAC) was used to collect HPXRD data in angle dispersive X-ray mode. A mixture of methanol, ethanol, and water (MEW) in the volume ratio of 16:3:1 was used as a pressure transmitting medium (PTM). Along with the sample and PTM, Ag powder was loaded for in-situ measurement of pressure seen by the sample. High pressure XRD patterns were collected in BL-11 beamline of the INDUS-2 synchrotron facility. The X-ray wavelength of λ= 0.552 Å was selected from synchrotron radiation for X-ray diffraction. The two-dimensional X-ray diffraction images obtained from the mar345 image plate detector were integrated using the FIT2D [2] program.

3. RESULTS AND DISCUSSION

The unit cell volume of $EuMnO_3$ reduces from 232.05 $Å^3$ to 231.65 $Å^3$ up on Holmium substitution of 0.4. High pressure XRD patterns of $Ho_{0.4}Eu_{0.6}MnO_3$ up to the pressure of ~30 GPa are displayed as a stacked plot in **Error! Reference source not found.**. 1. Ag is used for estimating pressure inside DAC and $2\theta_{111}$ reflection of Ag is indicated in the multiplot. The XRD fingerprint remains the same with pressure, indicating that the orthorhombic structure of $Ho_{0.4}Eu_{0.6}MnO_3$ remains stable up to the highest pressure studied. The P-V data obtained from HPXRD data is fitted with 2nd order Birch-Murnaghan EOS which yields a bulk modulus of 208±7 GPa, whereas the undoped $EuMnO_3$ has a bulk modulus of 185 GPa. Quadratic elongation quantifies the amount of distortion in the octahedra of MnO_6. The Quadratic elongation changes from 1.01 at amb to 1.20 at the highest pressure. This indicates that with pressure the distortion of octahedra increases resulting in a significant change in the multiferroic property.

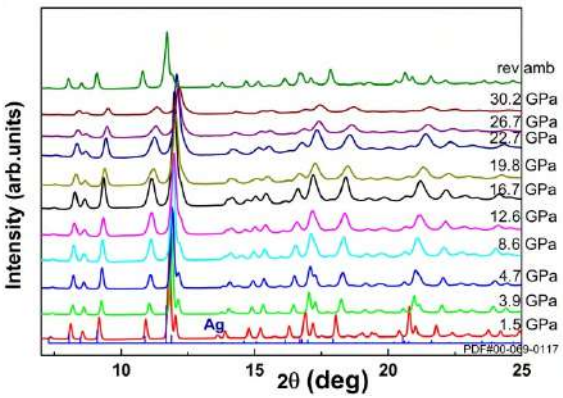

Fig.1. HPXRD patterns collected at various pressures.

ACKNOWLEDGEMENT

The authors thank HPSS members and the management of IGCAR for their support.

REFERENCES

[1] M. Ottesen, E. Ehrenreich-Petersen, C.H. Kronbo, F. Baudelet, L. Nataf, I. Kantor, M.R.V. Jørgensen, M. Bremholm, PhRvB, 107 (2023) 134115.
[2] A.P. Hammersley, S.O. Svensson, M. Hanfland, A.N. Fitch, D. Hausermann, HPR, 14 (1996) 235-248.

Topic Code: 01-High Pressure Material Science

Behaviour of molybdenum diphosphide at high pressure

Arpita Aparajita A. N [1], G. Shwetha[2], N. R. Sanjay Kumar[1], V. Srihari[3], Awadhesh Mani[1]
[1] Indira Gandhi Centre for Atomic Research, Kalpakkam, Tamil Nadu, a CI of HBNI, India
[2] Department of physics, Anurag University, Hyderabad, Telangana, India
[3] High Pressure & Synchrotron Radiation Physics Division, Bhabha Atomic Research Centre, Mumbai, India

Abstract: Molybdenum diphosphide which is a recently identified Weyl semimetal is structurally stable up to 55 GPa. The previously predicted decomposition at high pressure was not observed. The changes observed in the band structure and slope change in axial ratio *c/a* at ~36 GPa suggest that the predicted instability could be because of electronic transition instead of structural transition. Lattice compressibility was observed to be anisotropic. The least compressibility of unit cell along *b* axis is contributed by two covalent P-P bonds along this direction as compared to one bond along *c* and no covalent bond along *a* direction. Presence of close packed polyhedra along *a* axis and one covalent bond along *c* axis resulted in comparable incompressibility along them.

1. INTRODUCTION

Molybdenum phosphides exhibit diverse stoichiometries, structures and computed to exist in various stable and metastable phases at high pressure. Among them, particularly, MoP_2 is identified to host long-awaited Weyl quasiparticles as the low-energy excitation near the Fermi energy and Weyl cones are observed below the Fermi level using angle resolved photo electron spectroscopy [1]. It is being widely explored for its photo and electrocatalytic effect as well as exotic magneto-transport properties [2-4]. A recent computational study predicts a decomposition of MoP_2 to Mo_2P_3 + P at 38 GPa [5]. In this study, our objective is to investigate the effect of high pressure on the structure and electronic properties of MoP_2.

2. METHODOLOGY

MoP_2 was synthesized by the reaction between MoO_3 and stabilised red P, taken in atomic weight ratio of 2:7, at 800°C for 8 hour.High pressure X-ray diffraction experiments were performed up to 55 GPa using Mao-Bell type diamond anvil cell at the synchrotron facility at BL-11, Indus-2, RRCAT, India with λ = 0.6668 Å. Elastic constants and band structures were computed at high pressures using the density functional theory method as implemented in the CASTEP code. For structure optimization, a 12x4x18 k-point grid and an energy cut-off of 520eV with the GGA functional were utilized.

3. RESULTS AND DISCUSSION

The synthesized sample was phase pure. The crystal structure was obtained as orthorhombic with space group *Cmc2₁*, *a*=3.1459(4) Å, *b*=11.1842(3) Å, *c*=4.9846(1) Å. Mo and two types of P atoms designated as P1 and P2 are at Wyckoff positions 4*a* with coordinates (0, 0.093, 0), (0, 0.297, 0.809) and (0, 0.428, 0.115) respectively. The structure was found to be stable up to 55 GPa and the predicted decomposition was not observed [5]. To substantiate further, the elastic constants were computed up to 60 GPa. The constants satisfied Born's criteria implying mechanical stability of the orthorhombic structure. Anisotropic lattice compressibility is compatible with the bond alignment, bond nature and the polyhedral arrangement in the unit cell. The bulk modulus B_0 and was estimated to be 179.2(5.7) GPa. Interestingly, a slope change in axial ratio c/a (Fig. 1) was observed at ~36 GPa. To understand the origin, the band structures at various at ambient and 36 GPa were examined. They are presented in Fig. 2. At ambient pressure, the conduction and valence band cross the Fermi level at Γ and Y points. At 36 GPa, the conduction band is pushed below the Fermi level, and the gap between two valence bands close at the Γ point. Other prominent changes were also seen in both conduction and valence bands between Y and Γ as shown with red circles in Fig. 2.

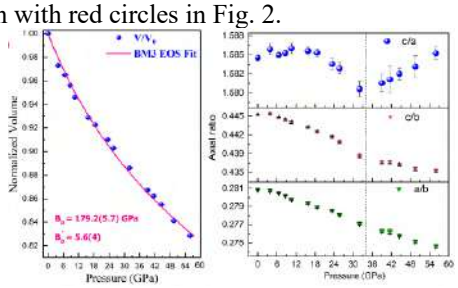

Fig.1. Evolution of volume and axial ratio of MoP_2 with high pressure.

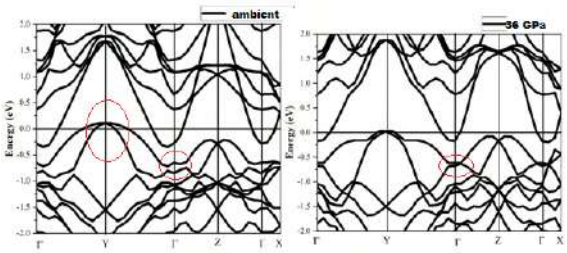

Fig. 2. Band structure of MoP_2 at ambient and 36 GPa.

4. SUMMARY

Structure of MoP_2 is stable up to 55 GPa. Predicted instability or decomposition might be having electronic origin and not of structural origin.

ACKNOWLEDGEMENT

Authors thank K. Sanitha for her help during experiment, and DAE, India for the financial support

REFERENCES

[1] Kumar, N., et al., Nature Communications, 2017. **8**(1): p. 1642.
[2] Jin, J. and U. Schwingenschlögl, npj 2D Materials and Applications, 2024. **8**(1): p. 31.
[3] Soluyanov, A.A., et al., Nature, 2015. **527**(7579): p. 495-498.
[4] Wang, A., et al., Physical Review B, 2017. **96**(19): p. 195107.
[5] Cao, K., et al., The Journal of Physical Chemistry C, 2019. **123**(50): p. 30187-30197.

CHARACTERIZATION AND FABRICATION OF METAL MATRIX COMPOSITES FROM MACHINERY SHOP WASTE METAL CHIPS VIA FRICTION STIR PROCESSING

Krishnalal M S [1], Sunilkumar D * [2]
Department of Mechanical Engineering, National Institute of Technology Silchar, Assam, India
***Email:** sunilkumar@mech.nits.ac.in

Abstract: This study investigates the fabrication of metal matrix composites by integrating mild steel (MS) and cast iron (CI) powders into a Nylon 66 matrix using friction stir processing (FSP). Mild steel and cast iron machining chips from lath machine shop were ball-milled into fine powders and embedded in the Nylon 66 plate. To achieve uniform dispersion, small punch holes were created in the Nylon 66 specimen prior to FSP. The hardness properties of the base material (BM) and the metal powder-incorporated composites were evaluated using Shore-D hardness and found the significant enhancement. This research highlights the potential of repurposing industrial waste to enhance the mechanical properties of composite materials.

1. INTRODUCTION

Metal matrix composites (MMCs) are advanced materials that consist of a metal matrix and reinforcing phases, such as ceramic particles or fibers. These materials are widely used in industries like aerospace, automotive, and defense due to their superior strength, wear resistance, and lightweight properties [1]. Traditionally, MMCs are fabricated using expensive and complex processes; however, waste metal chips from machining operations provide a low-cost, sustainable alternative. The increasing generation of metal chips from manufacturing processes presents both a challenge and an opportunity for the recycling industry [2]. This research explores the potential of using waste metal chips from a machinery shop to fabricate MMCs using FSP. By using this innovative technique, metal chips are integrated into a base metal, creating composite materials with enhanced mechanical properties. The study investigates the characterization and fabrication of these composites, focusing on their microstructure, hardness, tensile strength, and wear resistance.

2. EXPERIMENTAL

In this study, machining chips of mild steel and cast iron were collected, finely ground using ball milling, and incorporated into a Nylon 66 matrix to create a composite material [Fig. 1]. To ensure uniform dispersion of the metallic powders within the matrix, multiple small punch holes, each with a diameter of 1.98 mm, were introduced into the Nylon 66 specimen before applying Friction Stir Processing (FSP). The FSP was conducted using process parameters of 350 rpm for tool rotation speed and 30 mm/min for traverse speed. The processed metal matrix composites (MMCs) were then analyzed using optical microscopy and hardness testing (Shore).

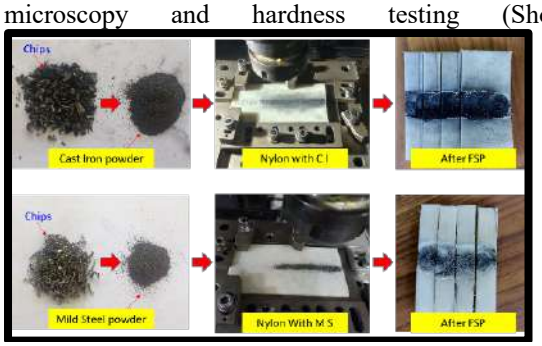

Fig.1. Experimental setup

2. RESULT AND DISCUSSION

The FSP-processed specimen was found to be free of defects and basin shaped MMCs. Shore-D hardness testing revealed that the cast iron-reinforced Nylon 66 composite exhibited a hardness value of 70, while the mild steel-reinforced Nylon 66 composite had a hardness value of 68. In contrast, the base Nylon 66 showed a hardness value of 63 [Fig. 2]. The variation in hardness can be attributed to the distinct mechanical properties of the metal powders incorporated into the Nylon 66 matrix. Cast iron, with its higher carbon content and brittleness, typically exhibits greater hardness compared to mild steel [2], which is more ductile due to its lower carbon content. The addition of these metal reinforcements enhances the overall hardness of the composite, as the hard metal particles resist deformation. Furthermore, the finer dispersion of the metal powders, achieved through FSP, further contributes to the improved hardness of the composite. Additional characterizations, including X-ray Diffraction (XRD), wear, and corrosion tests, are currently in progress in our laboratory.

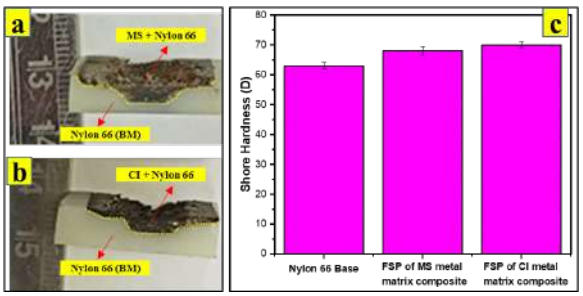

Fig.2(a) Macrograph (b) Hardness plot

3. CONCLUSION The study demonstrates that incorporating mild steel and cast iron into Nylon 66 via FSP enhances hardness, highlighting the potential of recycling industrial waste for improved composites.

REFERENCES

[1]. Singh, Lokesh, Bharat Singh, "Manufacturing techniques for metal matrix composites (MMC): an overview." Advances in Materials and Processing Technologies 6.2 (2020): 441-457.

[2]. Murray, James W., et al. "A review of principles and options for the re-use of machining chips by solid, semi-solid or melt-based processing." *Journal of Materials Processing Technology* (2024): 118514.

First Principle Study of Topological Phase in YPdBi Material

Sanjeev[a], Mukhtiyar Singh[b] , and Ramesh Kumar[a,*],

[a] *Department of Physics, Guru Jambheshwar University of Science & Technology, Hisar-125001, India*
[b]*Department of Applied Physics, Delhi Technological University, Delhi-110042, India*

* Email: ramesh85@gjust.org

Abstract

The topological phase tuning in Half-Heusler alloys could be hosted from trivial to non-trivial states and vice-versa, either with a small variation in the lattice parameter or by introducing the spin-orbit coupling. First principles simulations of the electronic bulk band structure of the YPdBi material exhibit the topologically non-trivial semimetal state without and with spin-orbit coupling at equilibrium lattice constant due to the single band-inversion at Γ-point. We observed the topological phase tuning from a non-trivial to a trivial state due to the second band-inversion at Γ-point, after applying the hydrostatic pressure of ~4 GPa. The semimetallic nature of these compounds is protected by the cubic symmetry of the crystal. Thus, by breaking cubic symmetry of the crystal with the application of uniaxial strain along the *c*-axis and biaxial strain in the *ab*-plane, we have noticed the topological phase transition from a non-trivial semimetal state to a topological insulator. The importance of half-Heusler compounds lies in their usage as a promising candidate in nanoelectronic applications.

Keywords: Semimetal, DFT, Spin-Orbit Coupling, Pressure, Strain, Topological Insulator.

CAPSULE AND SAMPLE HOLDER FOR IRRADIATION OF A-TIG AND TIG WELD JOINT SPECIMENS OF WRAPPER (D9) TO FOOT (SS316LN) OF PFBR FUEL SUB-ASSEMBLY IN FBTR

M. Muthuganesh[1], P. Vasantharaja[2], Ashish Kolhatkar[2], Rajesh Saxena[1], Ran Vijay Kumar[2], M. S. Rao[1], P. K. Chaurasia[1], V. Karthik[2], S. Joseph Winston[1] and M. Vasudevan[2]
[1]Fast Reactor Technology Group (FRTG) and [2]Materials & Metallurgy Group (MMG), IGCAR, Kalpakkam-603102
Email: mmganesh@igcar.go.in

Abstract:
An irradiation of sub size tensile and microscopy specimens made from weld location of wrapper (D9) to foot (SS316LN) of PFBR fuel sub-assembly (FSA) is currently in-progress in FBTR. Samples from both A–TIG (Activated Tungsten Inert Gas) and TIG (Tungsten Inert Gas) weld joints are chosen for irradiation. It has been found that A-TIG welding in stainless steel provides reduced residual stresses, distortion and significant reduction in manufacturing time and cost, therefore, it is planned to be utilized in the manufacturing of future FBR Sub-Assemblies (SA). In order to deploy A-TIG welding in mass production of PFBR SAs, an irradiation experiment to generate baseline irradiation performance data to determine the effects of fast neutron irradiation at low fluence (~ 2 dpa) on the tensile properties of weld and compare the results of both A-TIG &TIG welded joints has been initiated. Along with A-TIG specimens, TIG specimens are also included in the irradiation capsules as a reference, for which already wide range of data are available in the literature. Miniature tensile and microscopy specimens were prepared from qualified welds (A-TIG & TIG methods) made between D9 wrapper to SS316LN foot part of Fuel Sub-Assembly (FSA) are loaded in different partitions of an irradiation capsule. Special containers which can be remotely opened were made for holding microscopy specimens and loaded in the capsule partitions. The specimens were suitably labeled with laser markings and notches for easy identification in hot cells post irradiation. Assembled capsule was locked in a carrier steel sub-assembly of bore diameter: 22 mm. Carrier steel sub-assembly is loaded in the 5th ring of FBTR core, to irradiate the specimens and to achieve displacement damage in the range of 1.3 to 4.7dpa at the temperature of around 380-400 °C. After irradiation, carrier steel sub-assembly will be discharged to hot cell of Radio-Metallurgy Laboratory, PIED/MMG. Post irradiation examination (PIE) of the weld specimens will be carried out to determine the tensile properties & changes in microstructure. Additionally, to study the effect of nitrogen content on mechanical properties and microstructural changes of SS316LN irradiated to low neutron doses, disc specimens of four different nitrogen contents viz.: 0.07, 0.12, 0.14 and 0.22 wt% are also included in the same irradiation capsule for the irradiation in FBTR core and for the post irradiation examinations. This paper discusses in detail about the scope of irradiation, design of irradiation capsule and specimen holders, challenges in manufacturing the specimens, irradiation parameters, present status etc.

Study of Depth-Dependent Microstructural Changes in Oxygen Irradiated Nb-1Zr-0.1C Alloy

Argha Dutta[*#], N. Gayathri[#], P. Mukherjee[#], P. Karmakar[#], V. Naik[#]
Variable Energy Cyclotron Centre, Kolkata-700064
[#]Homi Bhabha National Institute, Mumbai 400094, India
Email: a.dutta@vecc.gov.in

Abstract: Niobium-based alloys, such as Nb-1Zr-0.1C, are promising for high-temperature nuclear reactors. This study examines the depth-wise microstructural variations in heavy ion irradiated Nb-1Zr-0.1C alloy. X-ray diffraction line profile analysis revealed variation in microstructural parameters as a function of ion penetration depth as well as irradiation dose. Electron backscatter diffraction showed an increase in geometrically necessary dislocations after irradiation by the formation of low-angle boundaries and saturates at highest dose. All these findings provide insights into the irradiation-induced microstructural evolution of Nb alloys.

1. INTRODUCTION

Niobium (Nb) and its alloys are promising candidates for structural materials in compact high-temperature nuclear reactors due to their excellent properties, including high-temperature strength, corrosion resistance against various coolants, and favourable thermal properties [1]. However, assessing radiation damage is crucial before using these materials in reactor environments. Radiation damage by ions are generally in-homogeneous in nature. Here approach has been made to understand the variation in microstructure depth-wise in a non-destructive manner.

2. EXPERIMENTAL

In this study, Nb-1Zr-0.1C alloy was irradiated with 1.6 MeV O^{5+} ions from Radioactive Ion Beam Facility, VECC at room temperature upto three different doses. The ion penetration depth was calculated to be 1.3 μm, with a maximum displacement per atom (dpa) of 7.7, as determined by SRIM-2013 for the highest dose [2]. X-ray diffraction (XRD) line profile analysis was employed to characterize the irradiated samples. The damage profile, in terms of dpa, was found to be inhomogeneous along the ion penetration depth (Fig. 1). To elucidate this profile, XRD data were collected at three different incidence angles (ω = 2.5°, 5.0° and 7.0°), allowing for the determination of various microstructural parameters, such as domain size and microstrain, along the ion penetration depth. Additionally, electron backscatter diffraction (EBSD) analysis was performed on the both the as-received and selected irradiated Nb-1Zr-0.1C alloys.

3. RESULTS AND DISCUSSION

XRD analysis indicated a reduction in domain size and an increase in microstrain after irradiation compared to the as-received sample in all three-incident angles. The large coherent domain present in as-received sample breaks down to smaller coherent regions by the irradiation induced defects. In the highest irradiated sample, domain size increased while microstrain decreased with depth, suggesting defect annihilation, possibly due to interactions between dense cascades during heavy ion irradiation. The kernel average misorientation (KAM) distribution calculated from EBSD revealed a shift in peak maxima towards lower misorientation angles after irradiation, indicating the formation of low-angle boundaries. The density of geometrically necessary dislocations (GNDs) showed an increase after irradiation (Table 1). However, it tends to saturate at highest dose. The formation of irradiation-induced clusters or loops, which introduce small misorientation within the matrix, likely contributes to the observed rise in GND density.

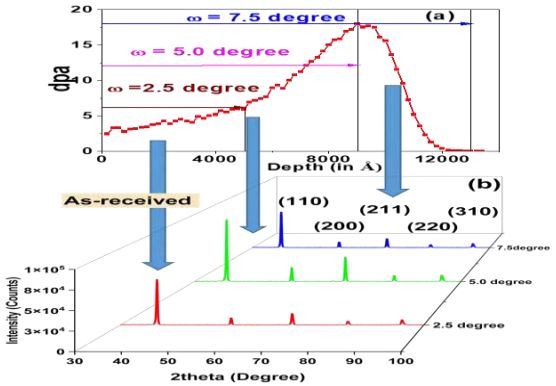

Fig.1. a) Displacement per atom (dpa) for as a function of ion penetration depth and b) XRD data collected from different depth by varying incident angles of XRD.

Table 1. GND density calculated from EBSD as a function of irradiation dose

Sample	GND density (m^{-2})
As-received	5.08E14
1.0E16	2.74E15
7.0E16	2.84E15

4. CONCLUSION

The XRD and EBSD analysis collectively shows defect annihilation at higher dose leading to saturation of dislocation density. This study indicates that Nb-1Zr-0.1C alloy may withstand very high dose as observed from the analysis.

REFERENCES

[1] K.J. Leonard et al, Compr. Nucl. Mater., Elsevier Science, UK, 2012: pp. 181–213.
[2] J.F. Ziegler et al, Nucl. Instruments Methods Phys. Res. Sect. B Beam Interact. with Mater. Atoms. **268** (2010) 1818–1823.

Topic Code: Radiation Resistant Materials and Radiation Induced Defects

Investigations on phase transformation and ion induced luminescence in Eu doped ZrO_2

Sujoy Sen[1,2*], Vikas Singh Gahlot[1,2], S.K. Srivastava[3], P. Jegadeesan[1], B. Sundaravel[1,2], S. Amirthapandian[1,2]
[1]Materials Science Group, Indira Gandhi Centre for Atomic Research, Kalpakkam- 603 102
[2]Homi Bhabha National Institute, Indira Gandhi Centre for Atomic Research, Kalpakkam - 603 102
[3]Accelerator Physics and Synchrotron Utilization Division, Raja Ramanna Centre for Advanced Technology Indore, 452013.
***Email: sujoy@igcar.gov.in, pandian@igcar.gov.in**

Abstract: Europium (Eu)-doped zirconium dioxide (ZrO_2) find its application in ion beam profiling monitor in particle accelerators. ZrO_2, highly radiation resistant material, is doped with 1–5% of Eu to enhance luminescence property by introducing Eu^{3+} emission bands. This doping also induces a phase transformation (monoclinic to a tetragonal phase) in ZrO_2, This phase transformation also influence the $^5D_0 \rightarrow {}^7F_2$ electric dipole transition in photoluminescence (PL) and ionoluminescence (IL) spectra. Our studies show that Eu-doped ZrO_2 maintains higher IL intensity and decays slowly even at high ion fluence, demonstrating its suitability for beam profiling applications.

1. INTRODUCTION

Scintillation screen with beam profiling monitors are important beam diagnostic component in ion accelerators [1]. These screen materials should be radiation resistant, cost- effective, mechanically stable, and minimal out-gassing in vacuum. In this context, Eu doped ZrO_2 is most favorable candidate material, and the present study show the effect of Eu doping on luminescence intensity, and phase stability of ZrO_2.

2. EXPERIMENTAL TECHNIQUES

The Eu doped ZrO_2 samples are synthesized via microwave assisted solvo-thermal method. The samples were characterized with synchrotron X-ray diffraction (XRD) with BL12 beamline at INDUS-2, PL measurements with FLS-980 spectrometer and IL measurements at 150 kV ion accelerator [2].

3. RESULTS AND DISCUSSION

The synchrotron XRD patterns of undoped and Eu doped ZrO_2 reveals that monoclinic to tetragonal phase transformation and it is evident from XRD pattern 12.5° to 15.5°(where wavelength of X-ray λ=0.724887Å). Up to 2% of Eu doping, we observed both monoclinic and tetragonal phase, however, beyond 3% Eu doping, we observed only tetragonal phase. This stress driven phase transformation is aided by oxygen vacancies which causes local stress in the material. Our PL observations shows the change in the $^5D_0 \rightarrow {}^7F_2$ electric dipole transition corresponding to Eu^{3+} ion which is signature of the phase transformation.

IL studies were conducted using 100 keV He^+ ions. In undoped ZrO_2, the decay IL intensity of O-vacancies (Fig 1(a)) show drastic reduction in the intensity even at fluence of 4×10^{15} ions/cm^2. However upon Eu doping of 1 and 2% (Fig 1(b) and 1(c)), Eu^{3+} emission bands show significant IL intensity, even after the ion fluence of 4×10^{16} ions/cm^2.The present work demonstrates that Eu doping enhances the IL property and it suits for ion beam viewing applications.

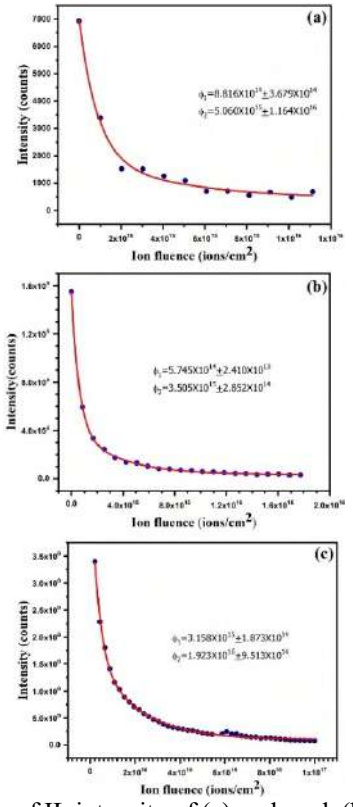

Fig 1. Decay of IL intensity of (a) undoped, (b) 1% Eu doped and (c) 2% Eu doped ZrO_2.

REFERENCES

[1]. Liberwirth.A, *et. al.* Nuclear Instruments and Methods B **365** (2015) 533.
[2]. Srivastava S.K, *et. al.* AIP Conf. Proc. **2265** (2020) 030225.

Tailoring Structural, Electronic, and Magnetic Properties of $CoFe_2O_4$ Thin Films Using Swift Heavy Ions Irradiation

Sagar Sen[1], Ambrish Dwivedi[1], Yksh Gupta[2], Sourav Chowdhury[3], Jayjit Kumar Dey[3] Moritz Hoesch[3], Sanjay Kumar Upadhyay[4], Keval Gadani[5], Anil Gome[6] V.R. Reddy[6], Ratnesh Gupta[2]*

[1]Department of Physics, Maharaja Bhoj Govt. P.G. College Dhar, India

[2]School of Instrumentation, Devi Ahilya Vishwavidyalaya Indore, Indore, India

[3]Deutsches Elektronen-Synchrotron DESY Notkestrasse 85, 22607, Hamburg, Germany.

[4]HNB Garhwal University Srinagar Garhwal, Uttarakhand -246174, India

[5]Center of Education, Indian Institute of Teacher Education (IITE), Gandhinagar – 382016

[6]UGC DAE CSR, Indore Campus, Indore, India

***Corresponding author sssagarsen@gmail.com**

Abstract: The study investigates the effects of 100 MeV Au^{7+} ion irradiation at fluences of 1×10^{13} and 6×10^{13} ions/cm² on the structural, electronic, and magnetic properties of $CoFe_2O_4$ thin films. Ion irradiation induces redistribution of Co^{2+} and Fe^{3+} ions, partial reduction to Co^0 and Fe^{2+}, and increases oxygen vacancies. These changes disrupt Co^{2+}–O–Fe^{3+} superexchange interactions, reducing magnetic order and net magnetization. Element-specific X-ray magnetic circular dichroism confirms reduced spin and orbital contributions to the magnetic moment post-irradiation.

1. INTRODUCTION

Bulk $CoFe_2O_4$, an inverse spinel ferrite, is known for its high coercivity, chemical stability, magneto-crystalline anisotropy, and magnetostriction, making it ideal for applications such as catalysis, data storage, drug delivery, ferrofluids, and magnetic refrigeration [1,2]. In these ferrites, cationic defects can disrupt the arrangement within the sublattices, significantly altering magnetic properties. Swift Heavy Ion (SHI) irradiation is an effective method for engineering thin films, allowing precise creation of defects, structural manipulation, and internal strain modification. Studies on high-energy irradiation reveal that material composition, cation distribution, crystallite size, and SHI energy influence the results [3]. However, the correlation between electronic structure and magnetic properties in ferrite thin films remains underexplored. Cation redistribution, a key factor in magnetic behavior, is known but requires further investigation. In this work, advanced synchrotron-based techniques such as X-ray absorption spectroscopy (XAS), X-ray Magnetic Circular Dichroism (XMCD), and X-ray Photoelectron Spectroscopy (XPS) have been utilized to gain deeper insights into the electronic properties and oxidation state changes in $CoFe_2O_4$ thin films.

2. EXPERIMENTAL DETAILS

A polycrystalline $CoFe_2O_4$ target was synthesized via the solid-state reaction method and used for pulsed laser deposition (PLD) of thin films on a Si substrate. The films were irradiated with 100 MeV Au^{7+} ions at room temperature using a 15 UD Tandem Accelerator at IUAC, New Delhi. Magnetic properties were analyzed using a 7 Tesla SQUID-VSM, and XPS measurements were performed with an Al-Kα source after Ar-ion sputtering. XAS and XMCD at Co & Fe $L_{3,2}$-edges and O K-edge were conducted at Petra III, DESY, Hamburg, at room temperature in TEY mode with a 0.5T magnetic field..

3. RESULTS AND DISCUSSIONS

Fig. 1(a) shows the magnetic hysteresis curves of pristine and SHI-modified $CoFe_2O_4$ thin films (1×10^{13} and 6×10^{13} ions/cm²) at room temperature, revealing a significant decrease in magnetic behavior after ion irradiation. The figure indicates that saturation magnetization (M_s) decreases from 1.63 μB for the pristine film to 1.25 μB at a fluence of 6×10^{13} ions/cm², while coercivity (H_C) increases with ion fluence.

X-ray photoelectron spectroscopy (XPS) analysis of $CoFe_2O_4$ thin films showed that Co^{2+} was the dominant species in the pristine film. After ion irradiation at fluences of 1×10^{13} and 6×10^{13} ions/cm², a reduction in Co^{3+} and Co^{2+} peaks occurred, with the emergence of a Co^0 peak. This suggests that ion irradiation reduced cobalt ions to their metallic state, driven by defect formation and oxygen vacancies.

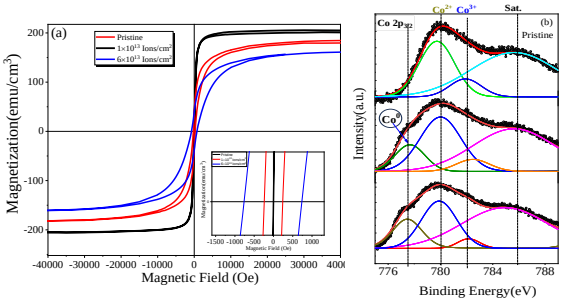

Fig 1: (a) M-H loops of pristine and ion-irradiated samples at different fluences,(b) Co $2p_{3/2}$ XPS spectra.

The study investigates ion irradiation effects on $CoFe_2O_4$ thin films using XAS and XMCD. Co L-edge XAS shows a shift from Co^{2+} to metallic Co, while Fe L-edge transitions from Fe^{3+} to a Fe^{2+}/Fe^{3+} mix. O K-edge XAS reveals hybridization changes, and the Bohr magneton values from M-H loops and XMCD confirm stable magnetic results.

4. CONCLUSION

Oxygen vacancies and partial reduction of Co and Fe oxidation states due to SHI are quantified by XPS and validated by SXAS. Magnetic property changes in CFO after ion irradiation are explored through macroscopic (SQUID-VSM) and microscopic (XMCD) measurements. The Bohr magneton values from M-H loops and XMCD sum rules are consistent, confirming the magnetic results. These findings highlight the

potential of ion-induced modifications for tailoring the structural, electronic, and magnetic properties of spinel ferrite thin films for spintronics applications.

ACKNOWLEDGEMENT

The financial support from Madhya Pradesh Science and Technology Council (MPCST), Bhopal (Project No. 3830/CST/R&D/Phy&Engg and Pharmacy/2023-24 dated 31/03/2024) and the Inter-University Accelerator Centre (IUAC), New Delhi (Ref: IUAC/XIII.3A/UFR-74320 dated 17-07-2023) is gratefully acknowledged.

REFERENCES

[1]. J. Dash, S. Prasad, N. Venkataramani, R. Krishnan, P. Kishan, N. Kumar, S.D. Kulkarni, S.K. J. Appl. Phys 86 (1999) 3303. https://doi.org/10.1063/1.371206.

[2] K.K. Kefeni, T.A.M. Msagati, B.B. Mamba, Materials Science and Engineering: B 215 (2017) 37–55.

[3] M. Balaji, M.M. Raja, K. Asokan, D. Kanjilal, T.R. Rajasekaran, D. Pathinettam Padiyan, , Nucl Instrum Methods Phys Res B 269 (2011) 1088–1093.

Topic category: Radiation Resistant Materials and Radiation Induced Defects

Indigenous Development of electronics and control instrumentation for Ion accelerator based radiation damage studies materials research

K.Suresh[1,2], J.Navas[1], R.Govindaraj[1,2], C.David[1,2], S.K.Dhara[1,2],
[1]Material Science Group, Indira Gandhi Centre for Atomic Research, Kalpakkam, Tamil Nadu, 603102, India
[2]Homi Bhabha National Institute, Mumbai, India
Email:ksuru@igcar.gov.in

Abstract: At the Particle Irradiation Facility (PIF) of Indira Gandhi Centre for Atomic Research(IGCAR), Kalpakkam, three accelerators - the 1.7 MV Tandetron Accelerator, indigenously developed 400 kV Ion Accelerator and the 150 kV Ion Accelerators, a state of art dual ion irradiation facility and a host of ion implantation and characterization facilities form the core of active experimental research being pursued on a variety of nuclear materials pertaining to present and future nuclear reactors. In this paper, we present an over view of our recent indigenous electronics and instrumentation design and developments done to achieve an efficient, enhanced and reliable exploitation of the accelerators and associated experimental facilities for conduct of advanced accelerator based materials research.

1. INTRODUCTION

Reproducing material microstructure and select property evolution resulting from neutron irradiation with three to four orders of magnitude reduction in time and cost, make ion irradiation an ideal candidate for accelerated irradiation testing of materials for current and future advanced nuclear reactors [1]. At the Particle Irradiation Facility (PIF) of Indira Gandhi Centre for Atomic Research (IGCAR), Kalpakkam, three accelerators - the 1.7 MV Tandetron Accelerator, indigenously developed 400 kV Ion Accelerator and the 150 kV Ion Accelerators, a state of art dual ion irradiation facility and a host of ion implantation and characterization facilities are used to pursue an active experimental research on a variety of nuclear materials. Various indigenous cost-effective electronics and instrumentation design and developments have been carried out to operate, maintain the accelerators and associated experimental facilities, ensure their high availability and enhance their capabilities for the materials research[2-3].

2. DESIGN AND DEVELOPMENTAL DETAILS

The important electronics and instrumentation systems developed include a) control and monitoring systems for 1.7MV, 400kV accelerators and the dual ion irradiation facility, b) automated conduct of single/dual ion irradiations and ion beam analysis experiments, measurement of indirect ion fluence measurement for ion irradiations, multichannel ion beam current cum dose measurement, c) setting up of automated experimental facilities for precise and fast in-situ/ex situ characterisation of the samples. Some of such systems developed are for in-situ measurement of resistivity, Hall-effect, field emission, high resolution RBS, deep level transient spectroscopy(DLTS), etc. The hardware of the systems are centred around COTS data acquisition cards, microcontroller based embedded systems, personal computer based interfaces, discrete logic based circuits, etc. The softwares developed are based on C/C++, LabVIEW,etc. As a whole, the systems are designed to be modular, scalable, cost-effective, reconfigurable and customised.

3. RESULTS AND DISCUSSION

Using the control and monitor systems for the accelerators, dual ion irradiation facility, a total of >200 analog signals are controlled and monitored with a resolution of better than 14 bit resolution at a rate varying from few Hz to 10s of kHz. Various digital signals(>150) representing the binary status of the accelerator systems such as Faraday cup, gate valves, and safety interlocks are monitored at a rate of 1 millisecond/signal. The ion beam current measurement systems developed can measure ion beam currents in the range of few pA to 100s of uA and the dose ranging from 1e8 to 1e18 ions/sqcm. These measurements can be done with a resolution of better than 10pA, precision of 0.5% and an accuracy of 2%. The ion implantations can be done in the range from 10K to 1200K with a precision of better than 0.1 deg C. With automated high-resolution RBS, an energy resolution better than 1.5keV was achieved[4]. Using the DLTS, electrically active deep level defects in semiconductors like Si, Ge, HpGe were studied using I-V,C-V and DLTS measurements in the temperature range of 20K to 300K. The capacitance transients are acquired over 1e-6 sec to few tens of seconds, processed with different correlation algorithms to obtain various types of defects, their concentration, activation energy, capture cross-section. The low cost indigenous developments enable and facilitated conduct of single/dual ion radiation damage studies on variety of materials for fission and fusion reactor applications. These developments help precise and fast in-situ/ex situ characterisation of the samples to get their ion irradiation responses.

REFERENCES

[1]. Stephen Taller, et al Journal of Nuclear materials,603,(2025),155385.
[2]. K.Suresh, et al., NIM B (2019), 92-99.
[3]. K.Suresh, et al., JINST (2018), P02033
[4]. K.Suresh, et al., JINST (2020), P05008

Structural and microscopic studies of ion-irradiated NASICON ($Na_3Zr_2Si_2PO_{12}$) ceramics

Ramcharan Meena[1,2], Rajendra Singh Dhaka[2]
1. Material Science Division, Inter-University Accelerator Center, New Delhi, India-110067
2. Department of Physics, Indian Institute of Technology (IIT), Delhi, India-110016.
Email: ramcharanmeena1992@gmail.com

Abstract: NASICON ($Na_3Zr_2Si_2PO_{12}$) ceramics are prepared using the solid-state reaction. The bulk samples are irradiated with Au (100 MeV), Ag (100 MeV), and O (90 MeV) ion beam. The structural analysis using the XRD shows the full amorphization for the Au-irradiated samples with lesser damage for Ag-irradiated samples. The crystal structure remains intact for the O-irradiated samples up to the maximum fluence of 5E13 ions/cm^2. A similar type of effect was also found during the microstructural analysis. The obtained experimental results were explained using the electronic energy loss mechanism.

1. INTRODUCTION

The NASICON samples having the chemical composition of $Na_{1+x}Zr_2Si_xP_{3-x}O_{12}$ ($0<x<3$) are of great interest due to their potential application as a solid-state electrolyte material in Na-ion-based solid-state batteries. The highest conductivity is observed for the $Na_3Zr_2Si_2PO_{12}$ ($x=2$) bulk ceramics [1]. Conductivity and other physical properties explained in the literature are mainly related to the structural arrangements. Hence, structural stability must be checked for all practical applications in different environments, including irradiation environments.

In this work, the ion-irradiation response of $Na_3Zr_2Si_2PO_{12}$ was checked using the high-energy ions of Au, Ag (100 MeV), and O (90 MeV) in the fluence range of 5E11 to 5E13 ions/cm^2. The crystal structure before and after irradiation was checked using the GIXRD (glancing angle X-ray diffraction) and electron diffraction (ED). The microscopic imaging was performed using a transmission electron microscope (TEM) in bright field mode.

2. EXPERIMENTAL

The bulk NAICON, which has a chemical composition of $Na_3Zr_2Si_2PO_{12}$, was prepared using the solid-state reaction method. For microstructural analysis, the colloidal suspension of NASICON is deposited onto the Cu grids covered with amorphous carbon of size 200 mesh by drop casting method. The ion irradiation work is performed at the Inter-University Accelerator Center (IUAC), New Delhi, using the 15 UD Pelletron accelerator in the material science beamline (Phase-1). The electronic (Se) and nuclear (Sn) energy loss were calculated using the SRIM-2013 software in full damage cascades mode [2]. It is found that for selected energies, the dominant energy loss mechanism is due to electronic excitation. The calculated electronic (Se) and nuclear energy loss (Sn) are shown in Table 1.

Table 1. Comparison of electronic (Se) and nuclear energy loss (Sn) for Au, Ag and O ions in NASICON.

Ion and energy	Se (keV/nm)	Sn (keV/nm)	Range (μm)
Au (100 MeV)	16.72	0.315	11.38
Ag (100 MeV)	14.41	0.075	11.93
O (90 MeV)	0.99	0.0005	63.50

3. RESULTS AND DISCUSSION

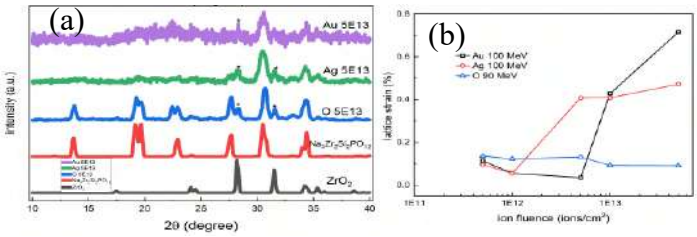

Fig.1. (a) Shows the XRD comparison of irradiated samples at the fluence 5E13 ions/cm^2. (b) Strain generated due to ion beam at various fluences.

The XRD analysis shows no additional peak formation with irradiation, which excludes the possibility of new phase formation due to irradiation. The intensity of peaks decreases with the broadening on increasing the ion fluence. It has been found that Au and Ag-irradiated samples show the amorphized type behavior with above 5E12 ions/cm^2 ion fluence, while crystal structure remains intact for the O-irradiation. The Coulomb explosion or thermal spike models explain the ion beam-induced damage in NASICON ceramics [3,4]. The strain calculated from XRD measurements is shown in Figure 1(b), which shows that the strain generated due to O-ion is nearly the same for all fluence. In contrast, strain generated due to Au and Ag irradiation shows an increase in strain on increasing ion fluence, leading to amorphization-type behavior on higher fluence. The XRD analysis shows the swelling-type effect for the Au and Ag ion irradiation [5].

Microstructural studies were performed on the irradiated samples using the transmission electron microscope (TEM). The experimental results confirm the damage by seeing the track formation along the ion path for the Au and Ag irradiation. At the same time, the crystal structure remains intact for O-irradiation, as confirmed by the electron diffraction.

REFERENCES

[1]. K. Singh et al Ionics **28** (2022) 5289.
[2]. J.F. Ziegler, et al., The Stopping and Range of Ions in Solids, Pergamon, New York, 1985. .
[3]. W.J. Weber et al. NIM B **166** (2000) 98.
[4]. M. Toulemonde et al. PRB **46** (1992) 14362.
[5] P. Kalita et al. J. Appl. Phy. **122** (2017) 025902.

Investigation of radiation tolerance in ceramic composite and non-composite materials

Rishvana Parveen[1], Parswajit Kalita[*1], Rakesh Shukla[2], Vinita Grover[2], Sanjay Kedia[3], D.K. Avasthi[4]
[1] Department of Physics, Applied Sciences Cluster, UPES, Dehradun, India
[2] Chemistry Division, Bhabha Atomic Research Centre, Mumbai, India
[3] Material Science Division, Inter University Accelerator Centre, New Delhi, India
[4] Centre for Interdisciplinary Research and Innovation, UPES, Dehradun, India
***Correspondence email: parswajitkalita90@gmail.com**

Abstract: Materials in extreme environments face challenges from high radiation and temperatures, degrading their properties and operational lifespan. YSZ, known for radiation tolerance, is limited by low thermal conductivity. To address this, YSZ-MgO composites, combining YSZ with a higher conductivity material, are explored to enhance radiation tolerance. GIXRD shows improved tolerance of YSZ-MgO composites under 80 MeV I^{6+} ion irradiation at room temperature and 700°C. Insights from Raman spectroscopy, EXAFS, and thermal spike simulations will explain the mechanisms behind the enhanced radiation resistance.

1. INTRODUCTION

Materials used in extreme environments, such as those encountered in nuclear reactors and space exploration, must withstand harsh conditions, including high radiation and extreme temperatures [1]. These conditions can severely degrade material properties, limiting their efficiency and in-service lifetime. Developing materials with enhanced radiation tolerance is therefore essential for ensuring their performance and safety in such applications.

Yttria-stabilized zirconia (YSZ) is widely recognized for its excellent radiation tolerance, making it a promising candidate for nuclear applications [1]. However, its low thermal conductivity poses a significant limitation, as efficient heat dissipation is critical for mitigating radiation-induced damage. To address this drawback, composite materials incorporating YSZ and MgO, a material with higher thermal conductivity, offer a promising way for improving radiation resistance.

This study examines the radiation tolerance of YSZ-MgO composites under 80 MeV I ion irradiation at room temperature (RT) and 700°C (HT). Initial results from GIXRD, Raman spectroscopy, EXAFS, and thermal spike simulations offer insights into the mechanisms enhancing their radiation tolerance.

2. EXPERIMENTAL DETAILS

2.1. Synthesis

YSZ powder were synthesized via the gel combustion method. Synthesized YSZ powder was mixed with preheated commercial MgO powder in 100-0, 75-25, and 50-50 wt.%, weight ratios. The mixture was ground, pelletized, and sintered at 1400°C for 36 hours.

2.2. Irradiation and Characterization

The pellets were irradiated by 80 MeV I^{6+} ions at IUAC, New Delhi. The irradiations were carried out at both RT and 700 °C (HT) and at the fluence of 1×10^{14} ions/cm^2. The structural investigation of pristine and irradiated pellets was conducted using GIXRD, Raman spectroscopy, and EXAFS.

3. RESULTS AND DISCUSSIONS

Figure 1 shows the GIXRD plots of both pristine and irradiated samples. The fluorite structure is retained in all samples after irradiation, indicating their high crystallographic stability. However, despite retaining crystallinity, the irradiated samples exhibit peak broadening, suggesting irradiation-induced damage. Notably, the change in the FWHM of the (220) peak is most pronounced in the YSZ followed by YSZ-MgO (72-25 wt.%) and least pronounced in the YSZ-MgO (50-50 wt.%). Additionally, samples irradiated at HT show reduced damage compared to those irradiated at RT. Similarly, Raman spectroscopy and EXAFS measurements were performed to further analyse the structural and local environment changes after irradiation. Detailed results and analyses will be presented during the conference.

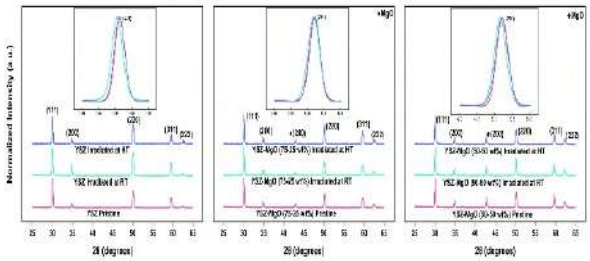

Figure 1: GIXRD plots of pristine & irradiated samples.

4. CONCLUSION

Composite samples show enhanced radiation tolerance compared to single-component samples. The radiation tolerance of the composites increases with the MgO concentration. Additionally, samples irradiated at 700 °C exhibit less damage than those irradiated at RT.

ACKNOWLEDGEMENT

We are thankful to DAE-BRNS (Project Sanction no.: 58/14/16/2022-BRNS) for financial assistance.

REFERENCE

[1] R. Parveen et al, Nuclear Inst. and Methods in Physics Research, B 551 (2024) 165344

Design and Development of a High-Heat-Load Target Holder for the Medical Cyclotron Facility at VECC

Dipak Kumar Baisnab*, Binoy Kumar Maji, B. Sundaravel, C. David
MSG, Indira Gandhi Centre for Atomic Research, Kalpakkam-603102
P. Lijukrishnan, Indranil Banerjee and Vinod V.
RDTG, Indira Gandhi Centre for Atomic Research, Kalpakkam-603102
N. Gayathri and Paramita Mukherjee
MS&MG, Variable Energy Cyclotron Centre, Kolkata-700064
** Email:dk.baisnab@vecc.gov.in*

Abstract: The Medical Cyclotron Facility (MCF) at VECC, Kolkata, supports radioisotope production and material science research with a proton beamline operating at currents up to 200 μA and energies up to 30 MeV. Managing the high thermal load (~1.5 kW/cm²) on target materials necessitated a specialized holder with efficient cooling. Designed using ANSYS simulations, it features a shower jet cooling system and a stainless steel plate for optimal heat dissipation. The assembly ensures vacuum compatibility using knife-edge joints and VITON O-rings. Fabrication is complete, enabling high-current experiments and advancing research at MCF.

The Medical Cyclotron Facility (MCF) at VECC, Chakgaria campus, Kolkata, has been established to produce radioisotopes and support research in material science and radiochemistry. The facility includes a specialized beamline with two sub-beamlines designed to handle proton beams of varying currents up to 50 μA for low-current applications and up to 200 μA for high-current experiments. The proton beam energy can reach a maximum of 30 MeV.

A key challenge in utilizing the high-current beamline lies in managing the intense heat generated on the target material. At full capacity, the proton beam deposits approximately 6 kW of power over an area of 4 cm² (1.5 kW/cm²), necessitating an advanced target holder capable of efficient cooling to prevent material degradation. To address this, as a first step, a target holder has been conceptualized and designed to dissipate up to 1.5 kW of thermal load effectively. The design incorporates results from dynamic heat load simulations performed using ANSYS software. The target holder features a trapezoidal outer casing with a front face measuring 105 mm x 75 mm, suitable for holding circular samples with a 30 mm diameter (see Fig.1.). These dimensions are tailored to fit the existing multipurpose chamber of the beamline. A forced cooling system employing a shower jet mechanism has been integrated to provide direct-contact cooling from the rear of the target. Thermal analysis indicates that optimal heat transfer can be achieved using a 1 mm thick stainless steel (SS) plate with a 25 mm cooling area and a convective heat transfer coefficient of 80,000 W/m²K. Under these conditions, the sample's front surface exposed to the proton beam maintains a max. temperature of 373°C, while the rear side stays at 79°C. Ensuring vacuum compatibility is another critical aspect of the design. The beam-facing side of the target operates under a high vacuum (~1×10^{-6} mbar), while the rear side interfaces with a water cooling system. Effective sealing is achieved through the use of knife-edge joints combined with VITON O-ring along with Aluminium flange, ensuring the assembly can endure high thermal and vacuum conditions.

Fig. 1. Target Holder Assembly

The fabrication of the target holder has been completed, paving the way for enhanced experimentation capabilities in high-current beamline research at the MCF.

References:

[1] J. Siikanen et al. , Applied Radiation and Isotopes 94 (2014) 294
[2] H. Takahashi et. al., J Radioanal Nucl Chem 305 (2015) 803

Unveiling the low-temperature properties of CuO nanosheets: Modulating morphology, and crystallography for enhanced optoelectronic performance

Narender Budhiraja[1,*], Krishna Begari[2], Rakesh K. Sonker[3]

[1,*]PG Department of Physics, Satish Chander Dhawan Government College, Ludhiana, Punjab-141007

[2]Mahindra Ecole Center, Mahindra University, Jeedimetla, Hyderabad-500043

[3]Department of Physics, Motilal Nehru College, University of Delhi, New Delhi-110021

Email: narenderarora1988@gmail.com

Abstract: Copper (II) Oxide (CuO), has garnered significant attention due to its exceptional electrical conductivity and natural abundance. CuO nanosheets have various applications which include energy storage, electronics, catalysis, and optics[1]. Its low-temperature synthesis, characteristics, and associated properties are not well understood, yet. Here, we provide a thorough analysis of CuO nanosheets synthesized by facile low-temperature solvothermal methodology. As such obtained nanosheets exhibit high surface area and enhanced catalytic activity along with tailored optical properties having a significant blue shift in absorption edge. This low-temperature synthesis approach unlocks new avenues for CuO nanosheets in electronics and quantum technologies. Furthermore, these nanosheets are investigated for dielectric properties at extremely low temperatures ranging from 100K to 350K and at broad frequency windows lying between 20Hz to 1MHz.

Keywords: Electronics, Solvothermal, Nanosheets, Low temperature, Quantum

Reference:

1. Budhiraja, N., Sapna, Kumar, V., Tomar, M., Gupta, V., Singh, S.K.: Multifunctional CuO Nanosheets for High-Performance Supercapacitor Electrodes with Enhanced Photocatalytic Activity. J. Inorg. Organomet. Polym. Mater. 29, 1067–1075 (2019). https://doi.org/10.1007/s10904-018-0995-4

Effect of Annealing on Physicochemical and Optoelectronic Properties of Polyaniline Thin Films

Karan K. Rathod, Jayesh R. Pawar, Munjaji E. Dudhmal, Rajesh A. Joshi*

Thin films and Nanotechnology Laboratory,

Department of Physics,

Toshniwal Arts, Commerce and Science College, Sengaon Dist. Hingoli 431542 MS

*Corresponding Author: urajoshi@gmail.com

Abstract:

The present article describes about synthesis of polyaniline thin films by soft chemical solution polymerization method at room temperature over glass substrate and effect of air annealing at 100, 200 and 300^{o}C on the physicochemical and optoelectronic properties intending to characterize as gas sensing materials. The as deposited and annealed thin films characterized for compositional, elemental, surface morphology and optical properties. Slight shift in peaks positions from 1167, 1372, 1506 and 1593 cm^{-1} and broadening of peak with increase in intensity obtained from Fourier transform infra red (FTIR) spectra confirm annealing induced elemental variations, while Raman spectrum represents chemical bond shifting upon annealing polyaniline thin films. Fatty granular appearing surface morphology obtained in atomic force microscopy (AFM) found to be coalesces into smaller granular shapes on post deposition treatments which can also be confirmed from the scanning electron microscopy (SEM) images. Optical absorbance shows shift of absorbance peaks from ~ 420nm and at ~837nm, these peaks can be interpreted as excitation to the polaron band which observed to be red shifted may be due to material modifications. These updations in the materials can be correlated to polygonization process i.e. absorbance of energy at the surface and utilizing in materials modifications.

Key words: Thin films, polymer, polaron, compositional modifications, sensor

Topic Code: Materials at high-temperature and thermal stability

Temperature dependence of Fano effect in optical phonon mode of V_2O_5 nanoparticles

Reshma P R, Arun K Prasad, Sandip Dhara
Materials Science Group, Indira Gandhi Centre for Atomic Research, A CI of Homi Bhabha National Institute, Kalpakkam 603102, Tamil Nadu, India
Email: reshmapattaniparambil@gmail.com

Abstract: The present study reports the observation of weakening of Fano resonance effect in the Raman spectrum of V_2O_5 nanoparticles along with the electronic phase transition. The high temperature semiconductor-to-metal transition observed in the materials induces phonon anharmonicity and a consequent destabilization of the lattice. The destabilization of the lattice further leads to the removal of out-of-plane O atom. The phonon anharmonicity also results in a weakening of electron-phonon bound state, which is envisaged in the current study as weakening of Fano type asymmetry in the Raman mode.

1. INTRODUCTION

Oxides of V metal are well known for the electronic, structural, and magnetic phase transitions exhibited by them. Among the vanadium oxides, the most stable one, V_2O_5 shows a temperature dependent semiconductor to metal transition at ~380°C[1]. This electronic phase transition is known to be associated with surface structural changes due to the loss of out-of-plane O atom. The onset of the phase transition is observed to occur at 100 to 150°C[1]. In the present study, we report a weakening of the Fano effect associated with the surface structural changes and the consequent electronic phase transition.

2. EXPERIMENTAL DETAILS

The V_2O_5 nanoparticles are synthesized via a hydrothermal route employing thermal decomposition of NH_4VO_3. The morphology of the synthesized nanoparticles (NPs) was studied using field emission scanning electron microscopy (FESEM, Zeiss). The crystal structure of the nanoparticles was confirmed to be V_2O_5 using X-ray diffraction (XRD, Inel, Equinox 2000). A temperature dependent (THMS600, Linkam scientific) Raman spectroscopic study (InVia, Renishaw, UK) was carried out using a 532 nm, Nd:YAG excitation laser.

3. RESULTS AND DISCUSSION

FESEM image of the synthesized np showed irregularly shaped nanoparticles with an average size of 49 ± 5 nm (inset of fig.1a). The XRD pattern showed the diffraction peaks corresponding to α-V_2O_5 (fig.1a). Raman spectrum of V_2O_5 NPs collected at room temperature is shown in Fig.1b. Raman spectra of the V_2O_5 NPs were collected at a temperature range of -175 to 340°C, to understand the temperature dependence of Fano type asymmetric broadening in the out-of-plane mode at 994 cm^{-1}(inset of Fig.1a). It is observed that the mode exhibited red shift with the increase in temperature, along with a thermally induced broadening. In addition, it is observed that the asymmetry in the Raman line shape is stronger at low temperatures, manifested as the lower value of Fano factor, q (Fig.1d). It is reported earlier that, at high temperatures, the optical phonon modes decay into multiple phonon modes resulting in peak broadening. This anharmonic effect also results in red shift in optical phonon modes[2,3]

In order to understand the onset temperature of phase transition, change in the ratio of in-plane-mode (@ 144 cm^{-1}) to out-of-plane (@ 994 cm^{-1}) is studied with temperature (Fig.1c). A considerable change in the intensity ratio is observed beyond 100°C indicating the removal of out-of-plane oxygen from the surface associated with the phase transition. In addition, the Fano parameter, q, also showed a noticeable increase above 100°C (Fig.1d), which is an indicative of the weakening of Fano effect. The observation indicates that the thermally induced anharmonicity in optical phonon mode results in the weakening of electron-phonon bound state. Consequently, Fano asymmetry also weakens with increasing temperature.

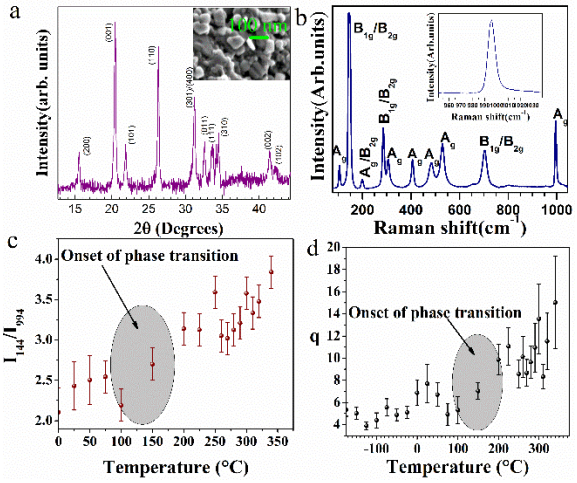

Fig.1. a) Raman spectrum of the V_2O_5 NP. The Mode at 994 cm^{-1}, with the asymmetric line shape is shown in the inset. b) XRD pattern of hydrothermally synthesized V_2O_5 nanoparticles. FESEM image is shown in the inset. Temperature dependence of c) the ratio of in-plane (B_{1g}) and out-of-plane (A_{1g}) vibrational modes and d) Fano parameter (q).

5. CONCLUSIONS

The present study reports the observation of a considerable change in the Fano parameter at the onset

of electronic phase transition. Irrespective of the increase in the number of free carriers in the material as a result of the removal out-of-plane O atoms, the anharmonicity in the optical modes results in a weakening of electron-phonon bound state, which is demonstrated in the current study as weakening of Fano effect.

ACKNOWLEDGEMENT

One of the authors, R.P.R. thanks DAE, Govt. of India for financial support.

REFERENCES

1. Basu, R., et al., Role of Vanadyl Oxygen in Understanding Metallic Behavior of V_2O_5(001) Nanorods. The Journal of Physical Chemistry C, 2016. 120(46): p. 26539-26543.
2. Balkanski, M., R.F. Wallis, and E. Haro, Anharmonic effects in light scattering due to optical phonons in silicon. Physical Review B, 1983. 28(4): p. 1928-1934.
3. Rath, D.K., et al., Resonant Electron–Phonon Interaction and Its Non-Fano-Type Wavelength and Power-Dependent Raman Manifestation. The Journal of Physical Chemistry C, 2024. 128(36): p. 15186-15193.

Topic Code: Materials at High Temperature and Thermal Stability

Thermal, Anti-bacterial and Structural analysis of bioactive glassy materials and their applications

Pallati Naresh[1], D.Sreenivasu[2], K. Siva Kumar[2], Aravind Seema[3], Gangadhar Thalari[3], Sanjeev Kumar[4]

[1]*Department of Physics, University College of Science, Saifabad, Osmania University, Hyderabad, Telangana, India -500004*

[2]*Department of Physics, Osmania University, Hyderabad, Telangana, India -500007*

[3]*Department of Chemistry, Osmania University, Hyderabad, Telangana, India -500007*

[4]*Avanthi Degree and PG College, Barkathpura, Hyderabad, Telangana, India -500027*

Email: nareshosmania13@gmail.com

Abstract: Newly developed bioactive glasses of chemical composition xAg_2O-20ZnO-10TeO_2-(60-x) B_2O_3 ($0 \leq x \leq 2$ mol%) were synthesized via conventional melt-quench route. The synthesized glassy materials were investigated for various applications including antibacterial efficiency. The antibacterial properties of the obtained glasses examined against two gram negative bacterial strains like Salmonella and Escherichia coli (E. coli) species. The anti-bacterial zone of inhibitions were shown increasing trends when the doping content (Ag_2O) increased. The thermal properties were analysed with TM-DSC measurement. The density **(ρ)** of the glasses increased from 3.54 to 3.82 g/cm^3 with the addition of Ag_2O. The UV-Vis. absorption spectrum of the glass system was recorded and estimated the cut-off wavelength (λ_c), the optical band gap energies (E_{opt}), the Urbach energy (ΔE), the refractive index etc. The cut-off increased whereas bandgap energies were decreased. The AC Conductivity measurements on the glassy materials revealed that the NBOs playing an important role in the increment of the ionic conductivity and also causing the enhancement of antibacterial efficiency.

1. INTRODUCTION

The present work deals with the newly developed bioactive glassy materials containing zinc oxide, boric acid, tellurium oxide doped with silver oxide. At high temperatures these materials were synthesized and thermally stable [**1**]. Various applications point of view the investigations were done on the materials and obtained good results. Especially, the antibacterial zones of inhibitions were enhanced with the dopant concentrations.

2. EXPERIMENTAL

The selected compositions were prepared by melt-derived method at high temperatures around 1250ºC.The antibacterial efficiency measured by Agar plate diffusion technique [**2-3**].

3. FIGURES AND IMAGES

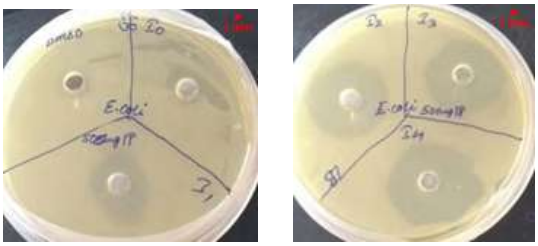

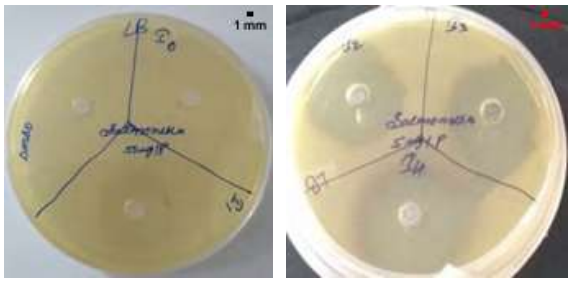

Fig.1. Trypticase Soy Agar (TSA) plate assay for bacterial strains E.Coli.and Salmonella bacterial strains

4. RESULTS

- The zone of inhibitions were increased upto 20mm and 21mm with the Ag_2O content against E.Coli and Salmonella.
- The ac conductivity enhanced upto $10^{-2}\Omega^{-1}cm^{-1}$ order for Ag-2 sample.

ACKNOWLEDGEMENT

The authors must thank **UGC DAE-Consortium for Scientific Research, Indore center** for continuous support in characterization of samples.

REFERENCES

[1]. Pallati Naresh et al, J.Non Crys.solids. **549** (2020) 120361.

[2]. Pallati Naresh,J.Mol.Struct,1213(2020)128184

[3]. Pallati Naresh et al, J.Non Crys.solids, 589 (2022) 121642

Topic Code: Materials at High Temperatures and Thermal

Experimental Investigation on Hot Tensile Properties of Melt-in Mode Plasma Arc Welded Inconel 625 Alloy Sheets

S Sureshbabu [1], S Rajakumar [2],
[1- 2,] Centre for Materials Joining and Research (CEMAJOR),
Department of Manufacturing Engineering, FEAT,
Annamalai University, Annamalai Nagar, Chidambaram, India-608002.
Email: srkcemajor@gmail.com

Abstract: Melt-in Mode Plasma Arc Welding has garnered special interest and is widely utilized to produce medium-thickness joints that demand high strength and durability. In this experiment, the hot tensile characteristics of 2.4 mm thick Inconel 625 butt joints welded using melt-in mode plasma arc welding are examined. The experiments exhibited increased service temperature from 200 ^{0} C to 600 ^{0} C leads to a reduction in hot tensile properties such as ultimate tensile strength of 820 MPa to 598 MPa. Elevated temperature fracture surface and EDS analysis also revealed and the detailed results and discussion are presented in this paper.

1. INTRODUCTION

Melt-in Mode Plasma Arc Welding (MIMPAW) is one of the welding techniques utilized in the sheet metal industry for joining sheets with thicknesses ranging from 1 to 2.4 mm. The austenitic nickel-based superalloy Inconel 625 is incredibly adaptable and has good ductility and strength at elevated temperatures. Typical uses include cryogenic temperature components for liquid rockets, various hardware, tooling, and aero-engine hot section components. Numerous welding techniques, including as gas tungsten arc welding, plasma arc welding, laser beam welding, and electron beam welding, can be used to join Inconel 625. Among these techniques, Melt-in Mode Plasma Arc Welding has garnered special interest and is widely utilized to produce medium-thickness joints that demand high strength and durability.

2. EXPERIMENTAL METHODOLOGY

Tensile tests were carried out using Instron Universal Testing Machine (UTM) under the constant crosshead speed with a nominal strain rate of $1 \times 10{-}3s^{-1}$. The tensile tests were carried out at test temperatures of RT, 200◦,400◦, and 600◦C. The UTM was equipped with a three zone resistance heating furnace for high temperature testing and a computer with data acquisition system for obtaining digital load elongation data. The photographs of hot tensile specimens before and after test are shown in Fig. 1.

2.1. Equations

The hardening capacity (Hc) of a material may be considered as a ratio of the ultimate tensile strength (σ_{UTS}), to the yield strength (σ_y)

$Hc = (\sigma_{UTS} - \sigma_y)/\sigma y = (\sigma_{UTS}/\sigma_y) - 1$ ……...(1)

3. FIGURES AND IMAGES

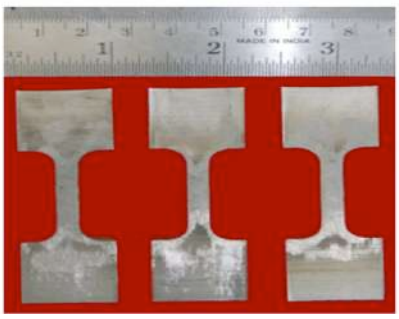

Tensile specimen before and after test

4. TABLES

Table 1. Hot Tensile properties of MIM PAW welded Inconel 625 butt joints at different test temperatures.

Test temperature (◦ C)	0.2% Yield strength (MPa)	Ultimate tensile strength (MPa)	Strain hardening capacity 'Hc'
RT	566	872	0.54
200	697	820	0.17
400	606	732	0.21
600	469	598	0.26

5. REFERENCING

[1]Chowdhury SM, Chen DL, Bhole SD, Cao X, Powidajko E,Weckman DC, et al. Tensile properties and strain-hardeningbehavior of double-sided arc welded and friction stir weldedAZ31B magnesium alloy. Mater Sci Eng A 2010;527:2951–61.

[2] Mecking H, Kocks UF. Kinetics of flow and strain hardening.Acta Metall Mater 1981;29:1865–75.

[3] Christopher J, Choudhary K, Isaac Samuel E, Srinivasan VS,Mathew MD. Tensile flow and work hardening behaviour of9Cr-1Mo ferritic steel in the frame work of Voce relationship.Mater Sci Eng A 2011;528:6589–95.

[4] Farabi N, Chen DL, Zhou Y. Microstructure and mechanicalproperties of laser welded dissimilar DP600/DP980 dualphase steel joints. Alloys Compd 2011;509:982–9.

Topic Code:

Soft mode induced structural phase transition in Ba_2ZnTeO_6 at high pressures

Bidisha Mukherjee, Mrinmay Sahu, Asish Kumar Mishra, Goutam Dev Mukherjee*
National Centre for High-Pressure Studies, Department of Physical Sciences, Indian Institute of Science Education and Research Kolkata, Mohanpur Campus, Mohanpur 741246, Nadia, West Bengal, India.
Email: goutamdev@iiserkol.ac.in

Abstract: We present a thorough investigation of vibrational, and structural properties of perovskite-type rhombohedral Ba_2ZnTeO_6 (BZTO) under systematic application of pressure. To carry out the analysis, we have performed pressure-dependent Raman spectroscopic measurements and synchrotron XRD. At ambient conditions, BZTO has $R\bar{3}m$ space group, which under pressure undergoes a structural transition to a monoclinic phase with space group C2/m at around 18~GPa. In-depth Raman analysis reveals softening of a phonon mode E_g (~28cm^{-1}) leads to the structural phase transition.

1. INTRODUCTION

Double perovskite oxides ($A_2BB'O_6$) possess a variety of desirable physical characteristics due to the different possible combinations of B and B′ cations. Especially the compounds $Ba_2M^{2+}Te^{6+}O_6$ (where M^{2+} =Co, Ni, Cu, or Zn) feature a unique layered structure of face-sharing TeO_6 and MO_6 octahedra, connected by corner-sharing TeO_6 octahedra. Low temperature induces lower symmetry in BZTO [1]. On the other hand, the high-pressure-high-temperature synthesis process stabilizes it to the cubic phase [1]. All these facts make the structural dynamics of BZTO very rich and interesting to study further.

2. EXPERIMENTAL DETAILS

Single-phase pure BZTO powder was synthesized using solid-state synthesis method [1]. The phase purity of the sample was confirmed by XRD and SEM measurements. High-pressure XRD measurements were carried out at the PETRA P02.2 beamline with a wavelength λ=0.2907 Å using piston-cylinder type DAC, Re gasket, neon gas as PTM. For high-pressure Raman measurements, a steel gasket and 4:1 methanol-ethanol mixture was used with an excitation wavelength of 532 nm.

3. RESULTS AND DISCUSSION

3.1. High-pressure Raman

$R\bar{3}m$ structure has 16 Raman active modes [1] among them we can detect 15. Peak positions of all the modes show slope change at ~8GPa with pressure. One of the E_g modes, which is coming due to rotation of TeO6 octahedra and translation of Ba and Zn does not follow normal linear dependence above 8GPa; instead, it follows Cochran-type relation [2]. Though the mode becomes faint after 13 GPa but extrapolating the fitting we get the critical pressure (P_c) around 18GPa. Also, the nature of FWHM of all the Raman modes indicates the structure is becoming distorted in the pressure region of 8-10 GPa and the structure loses its stability.

3.2. High-pressure XRD

It is difficult to draw any conclusion about the structure of any system from Raman analysis alone. We performed detailed XRD measurements as a function of pressure. Some new Bragg peaks appear at around 20GPa. The new phase can be indexed to a monoclinic C2/m space group validating our prediction from high pressure Raman analysis. Also, the trigonality (calculated using c/a ratio) and bond angle variance, both related to structural stability, increases anomalously with pressure above 7.5 GPa indicating the structure becomes distorted and gradually leads to the structural transition.

3. CONCLUSION

- Structural instability is developed in the structure above 7.5GPa.
- The E_g mode (~28cm^{-1}) induces a structural transition from $R\bar{3}m$ phase to C2/m phase above 18 GPa.

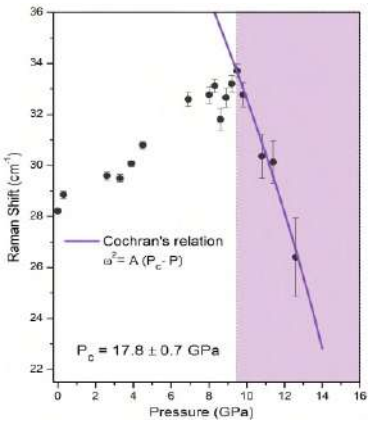

Fig.1. Pressure evolution of soft mode frequency.

ACKNOWLEDGEMENT

The authors acknowledge the financial support from DST, Govt. of India, to perform the experiment under the DST-DESY project in P02.2 extreme beam line condition at PETRA III, Germany. BM acknowledges the UGC, Govt of India, for the financial support to carry out the PhD work.

REFERENCES

[1] R. L Moreira et al, Phys. Rev. Materials, 2(5):054406, 2018.
[2] W Cochran. Advances in Physics,9(36):387–423, 1960.

X-Ray Absorption Spectroscopy of Neutron Irradiated SS 316L and SS316LN

Ran Vijay Kumar, K. Ashish, V. Karthik, R. Divakar
Indira Gandhi Centre for Atomic Research, Kalpakkam 603102, India
Email: (rvijay@igcar.gov.in)

Abstract: Austenitic stainless steel AISI 316 and its variants are widely used as the structural materials of Fast Breeder Reactors. The irradiation induced changes of SS 316L and SS 316LN were studied after test irradiations in Fast Breeder Test Reactor (FBTR) up to 5 dpa (displacement per atom) at 380-400ºC. The materials were characterized through mechanical test, XRD and X-ray Absorption spectroscopy.

1. INTRODUCTION

The synchrotron based X-ray Absorption spectroscopy (XAS) measurements were performed to study the influence of alloying elements on irradiation-induced changes in the local atomic environments around Cr, Ni, Mo and Fe atoms. XAS comprises of X-ray Absorption Near Edge Structure (XANES) and Extended X-ray Absorption Fine Structure (EXAFS).

2. EXPERIMENT

The irradiated specimens (Ø3mm and 0.5mm thick) were transported to RRCAT and XAS studies were carried out at BL 09 of INDUS II in fluorescent mode. The normalized XAS spectra plotted in K-space and Fourier transform was performed over a chosen K-range to get the plot in R-space to extract quantitative structural parameters for the atoms surrounding the central atoms such as Coordination number (CN), Bond length (BL) and Debye-Waller (DW) factors by fit the data with theoretical model for austenitic stainless steel.

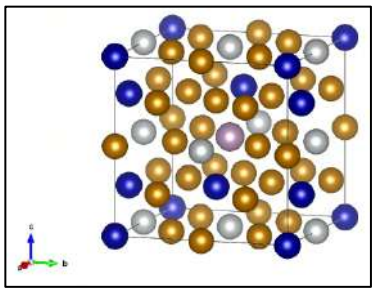

Fig. 1: Model for austenitic stainless steel

3. RESULTS

3.1 Fe K-Edge

Fe K-Edge data shows pronounced short-range ordering of Fe and N in un-irradiated SS316LN compare to SS316L. On irradiation, XANES spectrum of SS316L shifted towards un-irradiated SS316LN but negligible shift in spectrum of irradiated SS316LN. Quantitative interpretation also confirms that SS316LN has stable structure around Fe atoms.

3.2 Ni K-Edge

The spectrum of Ni K-Edge is similar to Fe K-Edge indicating Ni is strongly influenced by co-existence of ordered structure of Fe-N. However, quantitative interpretation indicates that, Ni does not form a direct bond with Nitrogen in un-irradiated SS316LN. On irradiation, the physical parameters do not change for SS316L but 316LN shows significant changes. This may be due to the local N saturation surrounding ϒ(Fe,Ni) phase during irradiation and induce decomposition, ϒ(Fe, Ni, N)→ ϒ'-Fe4N+Ni [1] a short range ordered structure.

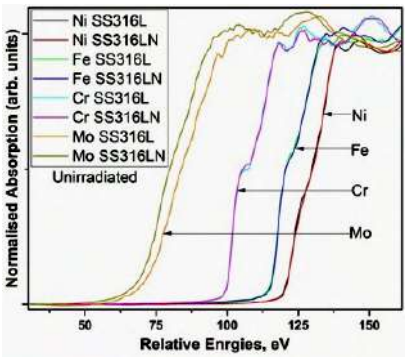

Fig. 2: Normalized XAS spectra for Fe, Ni, Cr and Mo K-Edge

3.3 Cr K-Edge

SS316LN spectrum for **Cr and Mo K-edge** shows low energy shift compare to SS316L. On irradiation, the decrease in CN is common for both the steels, indicating the accumulation of point defects around the Cr atom is more than the recombination. There were no significant change in BL for SS316L but for SS316LN, the BL decreases by 1% indicating short range ordered structure around Cr atoms.

3.4 Mo K-Edge

Mo K-edge spectra show a separation of the two broad peaks above the absorption K-Edge. The separation may be due to change in stability order, as parent metal (BCC) < carbide (HCP) < nitride (FCC) [2]. On irradiation, Mo shows short range ordering of Mo-N in SS316LN.

4. CONCLUSION

XAS has been employed to study the changes in chemical environments of neutron irradiated SS316.

REFERENCES

[1]. Martinavičius, Andrius. Doctoral thesis, SaechsischeLandesbibliothek- Staats- und Universitaetsbibliothek Dresden, 2011.http://nbn-resolving.de/urn:nbn:de:bsz:14-qucosa-68719.

[2]. Jingguang G. Chen, Chem. Rev. 1996, 96, 1477-1498

Structural, Optical and Temperature Dependent Ionic Conductivity Study of Green Chemical Synthesized Copper Sulphide Nanostructures in PVA Matrix

Sanatan Kr. Nath[1], P. K. Kalita[2]
[1]Department of Physics, B. H.College, Howly, Gauhati University
[2]Department of Physics, Rajiv Gandhi University, Arunachal Pradesh
Email: sanatankrnath@gmail.com

Abstract: Copper sulphide nanoparticles were synthesized by a green chemical route in PVA matrix using ammonia (aq.) as a complexing agent. Copper acetate monohydrate and thiourea were used as precursors. The particle sizes as obtained from X-Ray diffraction (XRD) results were found to be in good agreement with those of high-resolution transmission electron microscopy (HRTEM). The ultraviolet-visible (UV-Vis.) absorption and photoluminescence (PL) emission spectra exhibited a systematic blue shift of absorption and emission respectively confirming the quantum confinement effect in the synthesized nanoparticles. The band gap as estimated from Tauc-plot increased from 3.26eV to 3.92eV with a change in the concentration of the complexing agent. The fluorescence transmission infra-red (FTIR) spectra exhibited Cu-S stretching peaks characteristic of CuS. Ionic contributions of the electrolytic ionic CuS solution as measured by a standard conductivity cell clearly showed the semiconducting behavior of the product material. The synthesized material may be exploited in the fabrication of an optoelectronic device in the UV-blue region.

1. INTRODUCTION

CuS is a good prospective optoelectronic material that exhibits p-type electrical conductivity [1]. It is potentially used in solar cells, IR detectors, optical filters and other low-cost devices owing to its high absorption coefficient (10^4cm-^{1}) and narrow band gap (1.21 eV). In optoelectronics, it can be used as a light-emitting diode (LED) in the UV-Blue region.

2. METHODTOLOGY

2.1. MATERIALS AND METHODS

Copper acetate monohydrate and Thiourea were used as precursors for the copper and the sulphur source respectively. A green material, polyvinyl alcohol (PVA) acted as a capping agent and ammonia (aq.) as a complexing agent was used to adjust the pH value of the bath. An ionic conductivity cell was used to measure ionic conductivity at varying temperature.

2.2. Synthesis and Characterization

Copper Sulphide nanocrystalline thin films are deposited on glass substrates by a simple chemical route in PVA matrix.

The synthesized materials were characterized with XRD, HRTEM, UV- visible, PL, FTIR and Ionic conductivity.

3. Result and discussion

The XRD shows peaks of mixture of copper deficient phases such as $Cu_{1.96}S$, $Cu_{1.8}S$, and Cu_7S_4 as well as amorphous structure of the composite materials. Debye-Scherrer (D-S) and Williamson-Hall (W-H) [2] plot was used to estimate the different micro-structural parameters of the synthesized materials. The average particle size of the materials is in good agreement with those observed from HRTEM images. The UV- PL measurements show blue-green emission for both the copper sulphide samples characteristic of covellite phase of CuS. The materials exhibit temperature dependent ionic conductivity.

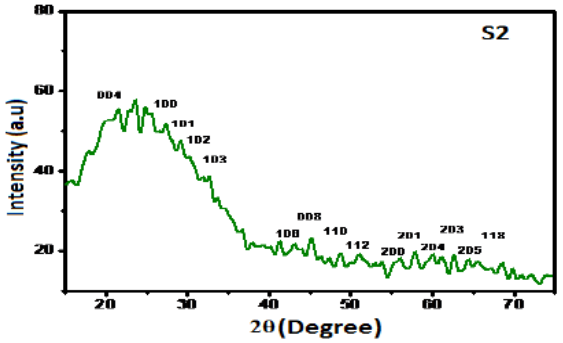

Fig.1.XRD Pattern of Sample S2

.

Table 1. The Table summarizes various parameters calculated in this work.

D (nm)	$\delta\times 10^{-3}$ lin. $(nm)^{-2}$	Williamson-Hall Method			
DS/ W-H		$\varepsilon\times 10^{-3}$	σ (MPa)	Y (GPa)	U $(Jm^{-3})\times 10^{-3}$
11/19	5.36	4.94	14.12	48.83	7.29

ACKNOWLEDGEMENT

The authors gratefully acknowledge all those associated with this work.

REFERENCES

[1].D. Nath et al, Mater. Chem. Phy.239 (2020) 1-9.
[2]. B. Barman et al, Solid State Sc.109 (2020) 1-7.

Topic Code:1

Increase in Hydrostatic Limit of Pressure Transmitting Medium Methanol -Ethanol with Temperature

Abhilash Dwivedi, Rahul Kaiwart, T. Balaganapathi and Himanshu Kumar Poswal
High pressure and Synchrotron Radiation Physics Division, Bhabha Atomic Research Centre, Mumbai-400085, India
Email: abhilash@barc.gov.in

Abstract: Methanol-Ethanol (4:1) mixture is the most widely used pressure-transmitting media (PTM) in high-pressure diamond anvil cell based experiments. The quasi hydrostatic limit of PTM is nearly 10.5 GPa. In the article, we have investigated the hydrostatic limit of Methanol-Ethanol (4:1) mixture at 100^0C, 150^0C and 200^0C with ruby fluorescence technique using internally heated diamond anvil cell. Our studies show that hydrostatic limit of the Methanol-Ethanol mixture can be extend up to 22 GPa by heating the mixture to 200^0C.

1. INTRODUCTION

Hydrostatic pressure conditions on the material plays a crucial role in its high pressure studies. Inhomogeneous strains due to non-hydrostatic pressures can change the phase transition pressure or even can change the phase diagram of the material [1]. Methanol-Ethanol (4:1) mixture is the most frequently used PTM medium which maintains the hydrostatic conditions inside the sample chamber of diamond anvil cell based high pressure experiments. It remains quasi hydrostatic up to ~ 10.5 GPa [2]. High pressure viscosity studies on Methanol- Ethanol mixture show that ~ 10 GPa, there is a sudden increase in viscosity to a value 10^{12} pascal-sec [3]. This indicates that the solidification of Methanol-Ethanol mixture at ~ 10 GPa. Therefore, It is considered that non hydrostatic stresses have been arises due to solidification of Methanol-Ethanol mixture above 10.5 GPa at ambient temperature. In the present studies, we have studied hydrostatic limits of Methanol-Ethanol mixture up to 200^0C.

2. EXPERIMENTAL DETAILS

High pressure ruby fluorescence experiments have been performed on Jobin Yvon triple-stage T64000 Raman spectrometer in a back-scattering geometry. Methanol-Ethanol mixture along with six ruby chips of size ~20 micron have been loaded on pre-indented tungsten gasket having hole of size ~200 micron. Pressures in the sample chamber have been measured by shifting in ruby fluorescence line [4]. For increasing the temperature of sample, a heater of tungsten coil is mounted inside the DAC. Three sets of high pressure experiments have been performed. In the first experiment, sample chamber containing methanol: ethanol (4:1) mixture is heated to 100 ^{0}C. Second and third experiments have been performed at temperature 150 ^{0}C and 200 ^{0}C respectively.

3. RESULTS AND DISCUSSION

There are three well established methods to measure the non hydrostatic stresses in the sample chambers. These are : (a) average width of ruby fluorescence R1 line; (b) average splitting in ruby fluorescence R1 and R2 lines; (c) the standard deviation of the pressures determined for the n ruby chips using R1 fluorescence line [7, 8]. It has been shown by klotz et al. [5] that the standard deviation of the pressures (σ) is the more reliable parameter for the detection of pressure variation in the sample chamber. Standard deviation of the pressures (σ) at different temperatures are showing in FIGURE1. For eliminating temperature induced shift in ruby fluorescence line R1, Datchi equation [6] has been used.

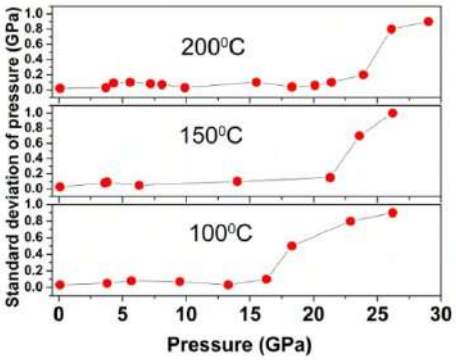

Figure 1. Standard deviation of the pressures measured from six ruby chips (present in the sample chamber) at different temperatures.

4. CONCLUSION

Our studies show that hydrostatic limit of Methanol-Ethanol (4:1) PTM can be extend up to 22 GPa by heating the mixture to 200^0C. The achieved hydrostatic conditions may be crucial for certain high pressure experiments, where spurious results are observed due to non hydrostatic conditions.

REFERENCES

[1]. A. Dwivedi, et al., High Pres. Re. 39 (2019), 81.
[2]. S. Klotz, et al., J. Phys. D Appl. Phys. 42 (1) (2009), 075413.
[3]. G. J. Piermarini et al., Rev. Sci. Instrum. 49 (1978), 1061.
[4]. H. K. Mao, et al., J. Geophys. Res. Solid Earth Planets. 91 (1986), 4673.
[5]. S. Klotz, et al., High Pres. Re. 29(2009), 649.
[6]. F. Datchi, et al., High Pres. Re. 27 (2007), 7.

A hybrid MC-MD Approach to study the irradiation behavior of Iron Phosphate Glasses

Manan Dholakia[1,*], Shakti Singh[2] and Sharat Chandra[1]
[1]Materials Science Group, Indira Gandhi Centre for Atomic Research, HBNI, Kalpakkam, 603102, Tamil Nadu, India
[2]Photonics Materials Technology Section, Materials Science and Advanced Technology Group, Raja Ramanna Centre for Advanced Technology, HBNI, Indore, 452013, MP, India
[*]manan@igcar.gov.in

Abstract: This study explores radiation damage in iron phosphate glass using a hybrid MC-MD approach. Random IPG structures are generated and melt-quenched via Molecular Dynamics simulations. It is seen that the energy dissipation in the cascade remains independent of PKA energy, with minimal defect recombination. The peak defect count scales linearly with PKA energy, matching NRT predictions.

1. INTRODUCTION

The rising global energy demand has intensified research on efficient energy production. The nuclear industry plays a key role but generates high-level nuclear waste (HLW), requiring robust encapsulation. Iron phosphate glasses (IPG) are one of the candidate materials as they are quite durable and understanding their irradiation characteristics is important. This work combines potential-free Monte Carlo and classical MD melt-quench methods to generate realistic amorphous IPG structures, overcoming limitations of ab-initio techniques. The next step is modeling radiation damage in glass via molecular dynamics (MD), which captures atomic-scale displacement cascades and defect recombination. Using realistic interatomic potentials, we analyze irradiation effects in the generated glass structures.

2. METHODOLOGY

Glass models are generated using a potential-free MC method [1,2], followed by MD melt-quenching in LAMMPS with a Buckingham + Coulomb + Stillinger-Weber potential [3]. The system is melted at 6000 K and quenched to 300 K over 120 ps, forming amorphous IPG. Radiation damage is simulated in an 80,000-atom cell, equilibrated at 300 K. A PKA (of 2, 4 and 6 keV energies) is introduced along the ⟨100⟩, ⟨110⟩, and ⟨111⟩ to study displacement cascades.

3. RESULTS AND DISCUSSION

Upon PKA initiation, atomic collisions transfer energy, causing velocity changes. The velocity autocorrelation function decays within 0.25 ps, coinciding with the peak defect number and thermal spike. PKA energy has minimal impact on the decay rate, suggesting energy dissipation is independent of PKA energy. The number of displaced atoms increases during the ballistic phase, with minimal defect recombination, highlighting the amorphous nature of IPG. Oxygen defects are most prevalent, while Fe^{2+} defects are rare, contrary to prior findings. The peak defect number increases linearly with PKA energy, matching NRT predictions.

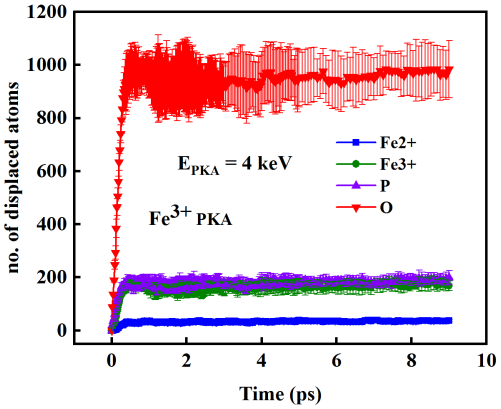

Fig.1. Variation of the number of displaced atoms with cascade simulation time

4. SUMMARY AND CONCLUSIONS

In summary, this work employs a hybrid approach to model the glass structure of IPG. Radiation damage studies indicate that point defects produced during the initial stages of the cascade do not anneal as effectively as they do in metallic systems, highlighting the amorphous characteristics of the glasses. Ongoing research is investigating the effects of different PKA species, temperature variations, and various IPG compositions on radiation damage characteristics.

REFERENCES

[1] Shakti Singh, Manan Dholakia, and Sharat Chandra, J. Phys. Chem. B, **128**, 3258-3272 (2024)
[2] Shakti Singh and Sharat Chandra, Comput. Mater. Sci., **202**, 110943 (2022)
[3] Kitheri Joseph, Kenny Jolley, Roger Smith, J. Non-Crystal. Solids, **411,** 137–144 (2015)

Topic Code: Advanced Characterization Techniques and equipment in Extreme Conditions

Nanoindentation studies on ordered and disordered iron aluminides

Pardhu Yella [1], Javed S. Ibrahim [2], Shivkumar Khaple [3], M.J.N.V. Prasad [2], M. Phani Raj [4, *]

[1] Department of Physics and Chemistry, Mahatma Gandhi Institute of Technology, Gandipet, Hyderabad 500075, India

[2] Department of Metallurgical Engineering and Materials Science, Indian Institute of Technology Bombay, Mumbai 400076, India

[3] Defense Metallurgical Research Laboratories, Hyderabad, 500058, India

[4] Department of Metallurgy and Materials Engineering, Mahatma Gandhi Institute of Technology, Gandipet, Hyderabad, 500075, India

***Email: mphaniraj_mme@mgit.ac.in**

Abstract: Light weight steels are known for their excellent high-temperature performance and outstanding oxidation resistance, particularly Fe3Al, have garnered attention in materials science as promising candidates for lightweight structural materials. Reports were dedicated for finding out the hardness and elastic modulus through nanoindentation for the alloys Fe7Al, Fe9Al and Fe16Al the strain rate sensitivity was not much explored. This paper aims to contribute valuable insights into the strain rate sensitivity of the specified alloys and thus the selection and application of iron aluminides, for future innovation with the light weight steels for automotive industries.

1. INTRODUCTION

Understanding the behavior of the light weight steels under stress and high temperature is essential for optimizing the performance in technological applications, such as aerospace and automotive industries[1]. Among the iron aluminides, the ordered and disordered variants present unique microstructural characteristics, which directly influence their mechanical properties such as yield strength and hardness, which are essential for applications in aerospace and automotive industries.

This study explores to evaluate the hardness and elasticity of iron aluminides, through the nanoindentation techniques to establish a correlation between microstructure and mechanical behavior with precise hardness and elastic modulus values, which are essential for evaluating the ductility and other mechanical properties.

2. EXPERIMENTAL DETAILS

The nanoindentation was performed on the iron aluminides Fe7Al, Fe9Al, Fe16Al samples to obtain the mechanical properties such as hardness, and strain rate sensitivity. The hardness values are measured from the load displacement data obtained from the load-unload cycle of nanoindentation [2]. A dwell time of 10 sec was maintained at the peak load for every indentation before unloading. This is done to minimize the effect of loading history on the unloading curve. The same peak load and loading rate conditions were maintained for 9 indents to obtain the consistency. The current investigation, the peak load utilized is 8000 µN with different loading rates 80, 160, 450, 800, 2500, 5000 and 7000 µN/s. The strain rate sensitivity is measured from the flow stress σ (where σ is calculated from Tabors relationship) with the strain rate έ in a uniaxial tension by using eqn. (1).

$$m = \frac{\partial ln\sigma}{\partial ln\dot{\varepsilon}} \qquad (1)$$

3. RESULTS AND DISCUSSION

Typical load displacement curves obtained for disordered and ordered FeAl samples are shown in Fig. 1 and it is clearly evident that the indentation response is uniform for a given test condition. The hardness was deduced from unloading part of the curve following the Oliver-Pharr method. This average hardness data obtained at various loading rates employed during nanoindentation is presented in table. (1)

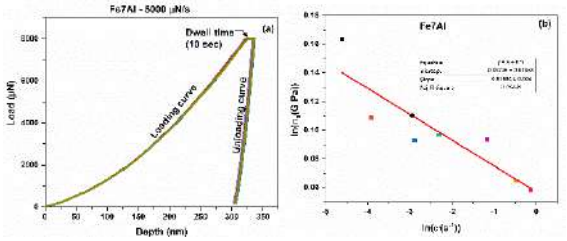

Fig. 1. (a) Load Vs depth curves of 9 indents for Fe7Al- 5000 µN/s, (b) SRS calculation.

Table 1. Hardness and elastic modulus of FeAl samples.

Sample	Hardness (GPa)	Strain rate sensitivity
Fe7Al	3.307012	-0.018
Fe9Al	3.688356	-0.0278
Fe16 Al	5.34829	-0.0168

4. CONCLUSIONS

The increment in hardness with increase in loading rate for a given test condition and a given sample suggests that the loading rate response is positive leading to positive strain rate sensitivity.

5. REFERENCES

[1]. S. Khaple et al., Defense Tech. **26** (2023) 1.

[2]. W. C. Oliver et al., J. Mat. Res. **7** (1992) 1564.

Topic Code:Advanced Characterization Techniques andequipment in Extreme Conditions

Positron maker: Intense positron facility at Dhruva Reactor

S. Mukherjee[1], D. Dutta[1], H. Chatterjee[2], M. Dev[2], S. Shrotriya[3], M. Pande[3], J. Kumar[4], T. Singh[4], P. K. Pujari[1], K. Sudarshan[1]
[1]Radiochemistry Division, [2]Reactor Technology Division, [3]Accelerator Controls Division, [4]Research Reactor Services Division, Bhabha Atomic Research Center, Trombay, Mumbai, MH-400085
Email: mukherjees@barc.gov.in

Abstract: The Design of Positron Maker facility- an intense positron beam to be installed in CS3003 beam cavity of Dhruva Research Reactor will be presented. Thermal neutrons from the reactor core will be intercepted by a thin cadmium sheet where they will undergo $^{113}Cd(n, \gamma)^{114}Cd$ reaction. This nuclear reaction will result in an intense capture gamma flux which will be incident on a suitably designed tungsten moderator assembly. The intensity of gamma ray incident on the moderator assembly will be ~0.01 photon per neutron with enough energy to induce electron-positron pair production. The high energy positrons produced in the moderator assembly will be self-moderated resulting in an intense flux of slow positron beam. The slow positron beam will be transported outside the biological shield through a ~3 m long solenoid tube which maintains a uniform axial magnetic field of ~ 7mT. After exiting the biological shield, the positron beam will be bend through a ~ 2m x 2m x 2m layered neutron and gamma shield which filters out the streaming radiation from the reactor core. The capture gamma production, transport and subsequent pair production process were simulated using FLUKA code [1]. Various parameters such as cadmium thickness, design of tungsten foil-based moderator assembly was optimized. Transport of the slow positrons was simulated using SIMION [2,3]. Design of outer radiation shielding assembly was carried out using FLUKA. Considerable effort was devoted to design the tip of the facility such that the maximum temperature rise could be limited to < 160 ^{o}C. Our simulations suggest an intensity of ~$7x10^{8}$ e+/s positrons in a ~20 mm diameter which is comparable to the various other similar facilities operating worldwide [3-6]. Once installation is complete, the intense positron beam will be used to study defect evolution in nanosecond time scale via single-shot spectroscopy techniques [7].

REFERENCES

[1]. C. Ahdida et al., Frontiers in Physics 705 (2022); Giuseppe Battistoni et al., Annals of Nuclear Energy 82 (2015)
[2]. D. A. Dahl, SIMION 3D 7.0, INEEL-95/4043, Revision 5, 2000
[3]. J. Moxom et al. Nucl. Instrum. Methods Phys. Res.A 579.1 (2007).
[4]. A. van Veen et al. Proc. of IAEA Symposium on Research Reactor Utilization, Safety and Management. IAEA, 2000.
[5]. C. Hugenschmidt et al., Applied Physics A 74 (2002).
[6]. K. Sato et al, Nucl. Instrum. Methods Phys. Res.B, 342 (2015)
[7]. D. B. Cassidy et al. Applied physics letters 88.19 (2006).

Poster Presentations

Topic Code:

Pressure and temperature-induced electron-phonon and spin-phonon coupling in $Cr_{3.04}Te_4$

Asish Kumar Mishra[1], Bidisha Mukherjee[1], S. Thirupathaiah[2], Goutam Dev Mukherjee[1*]
[1]National Centre for High-Pressure Studies, Department of Physical Sciences, Indian Institute of Science Education and Research Kolkata, Mohanpur Campus, Mohanpur 741246, Nadia,West Bengal India
[2]Department of Condensed Matter and Materials Physics, S.N.Bose National Centre for Basic Sciences, Kolkata,West Bengal 700106, India
Email: goutamdev@iiserkol.ac.in

Abstract: We have carried out a detailed high-pressure and low-temperature study using XRD and Raman spectroscopic measurements. The HP-XRD data shows no structural transition. The Raman data shows anomalies around 7.8 GPa pressure indicating the possibility of electronic transition. Further low-temperature investigation reveals that both the Raman peaks show signature of magnetic interaction below Neel temperature.

1. INTRODUCTION

Transition metal chalcogenides have sparked significant attention because of their application in spintronics and magnetic storage devices. $Cr_{3.04}Te_4$ crystalizes in the monoclinic structure. It is a room-temperature soft ferromagnet with alternating stacks of Cr-filled and Cr-vacant layers along the c direction [1].

2. EXPERIMENTAL DETAILS

High-quality Single crystals of $Cr_{3.04}Te_4$ were grown using the chemical vapor transport method [2]. High-pressure XRD measurements were carried out at the PETRA P02.2 beamline with a wavelength λ=0.2910 Å. A piston-cylinder type diamond anvil cell (DAC) was used to perform the high-pressure Raman measurements with an excitation wavelength of 488 nm. The low-temperature Raman measurements were carried out using a closed-cycle helium cryostat coupled with a microraman spectrometer with 532 nm laser wavelength.

3. RESULTS AND DISCUSSION

3.1. High-pressure Raman

The ambient Raman spectra of $Cr_{3.04}Te_4$ consist of two major peaks arising from the in-plane and out-of-plane vibration of the Te atom. Upon increasing the pressure the peak centered around 125 cm^{-1} shows red shift and the peak centered around 142 cm^{-1} shows blueshift. We have fitted the Raman data with the Fano function as the Lorentzian function does not fit well. The Fano coupling parameter indicates the presence of strong electron-phonon coupling in the system. The Raman shift of both peaks shows anomaly around 7.8 GPa pressure as shown in Fig.1. Interestingly, the coupling strength obtained from fano fitting drops to zero above 7.8 GPa, possibly due to a change in the material's electronic structure.

3.2. High-pressure XRD

To investigate the possibility of any structural transition we have carried out high-pressure synchrotron XRD up to 30 GPa. The ambient XRD pattern indexed to monoclinic structure with space group C 2/m. There is an isostructural transition happening around 17 GPa. Since no structural transition is observed around 7.8 GPa, the anomalies obtained in the Raman data around that pressure can be attributed to electronic transition.

3.3. Low-Temperature Raman measurement

To understand the effect of magnetic transition on the lattice vibration of the sample we have carried out low-temperature Raman measurement from 22 K to room temperature. The Raman shift of both the peaks show blue shift upon decreasing temperature up to the Neel temperature, below that softening of both the peaks observed. We have fitted three phonon decay scheme to eliminate the effect of anharmonicity, and it fits well up to 100 K . The deviation of experimental data below 100 K can be due to the spin-phonon coupling or electron-phonon coupling or both happening in the system [3]

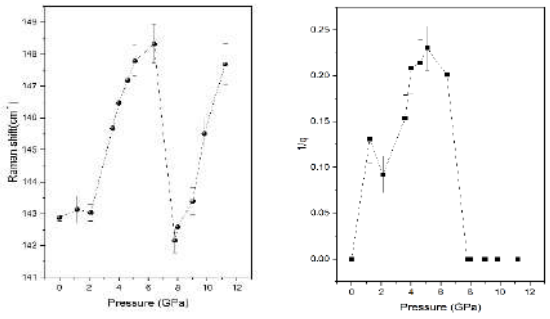

Fig.1. Variation of Raman shift and coupling strength with pressure for peak 2

ACKNOWLEDGEMENT

The authors acknowledge the financial support from DST, govt of India. A.K.M thankful to IISER Kolkata for the financial support to carry out the Ph.D. work.

REFERENCES

[1]. A wang et al, Phys. Rev. B 108, 094429 (2023) .
[2]. S. Purwar et al, Phys. Rev. Materials 7, 094204 (2023) .
[3].B. Mukherjee et al, J. Appl. Phys. 136, 095903 (2024).

Exploring the Pressure-Dependent Structural Transitions of $RE_3TM_4Sn_{13}$ (RE=Sr, Ca and La; TM=Rh) Compounds Through Synchrotron X-Ray Diffraction

Muthukumaran Sundaramoorthy[1,2], Arumugam Sonachalam[3], Boby Joseph[2]

[1]Centre for High Pressure Research, School of Physics, Bharathidasan University, Tiruchirappalli 620024, India

[2]Elettra-Sincrotrone Trieste S.C. p. A., S.S. 14, Km 163.5 in Area Science Park, Basovizza 34149, Italy

[3]Tamil Nadu Open University, Chennai 600015, India

Email: muthuk2501@gmail.com

The intermetallic $RE_3TM_4Sn_{13}$ (RE = rare-earth element, TM = transition metal) compounds, first discovered by Remeika et al., feature a fascinating cage-like structure that underpins their diverse physical properties, such as superconductivity, charge density wave behaviour, and heavy fermion effects. These materials crystallize in three distinct phases (I, II, and III), with the I phase ($Yb_3Rh_4Sn_{13}$ type) comprising $[Sn_1(Sn_2)_{12}]$ icosahedral cages and $[TM(Sn_2)_6]$ trigonal prisms. Phase II exhibits a Pesuedo tetragonal structure, while Phase III arises from structural instability or disorder of Phase I, evidenced by superstructural Bragg reflections and the doubling of the cubic unit cell. Synchrotron single crystal and powder X-ray diffraction studies on $Sr_3Rh_4Sn_{13}$, $Ca_3Rh_4Sn_{13}$, and $La_3Rh_4Sn_{13}$ reveal unique structural properties under ambient and high-pressure conditions. Both $Sr_3Rh_4Sn_{13}$ and $Ca_3Rh_4Sn_{13}$ crystallize in the $Pm\bar{3}n$ space group, with lattice parameters of 9.805 Å and 9.723 Å, respectively, while $La_3Rh_4Sn_{13}$ adopts a superlattice structure in the $I4_132$ space group. High-pressure XRD studies confirm smooth compression of $Sr_3Rh_4Sn_{13}$ up to 10 GPa, yielding a bulk modulus of 79.6 GPa. The structural properties of $Ca_3Rh_4Sn_{13}$, under ambient conditions, closely resemble those of $Sr_3Rh_4Sn_{13}$ at ~7 GPa, suggesting a "chemical pressure" analogy. In $La_3Rh_4Sn_{13}$, temperature-dependent synchrotron XRD reveals a structural transition from the $I4_132$ phase (III) to the $Pm\bar{3}n$ phase (I) between 340–350 K, while high-pressure XRD indicates a similar phase transformation above ~ 7.5 GPa, accompanied by the suppression of superlattice peaks. Raman spectroscopy further confirms the III to I transition, highlighting the interplay between pressure and structural distortions. This comprehensive study provides valuable insights into the pressure-induced structural behaviour of $RE_3TM_4Sn_{13}$ compounds, advancing the understanding of their intriguing physical phenomena.

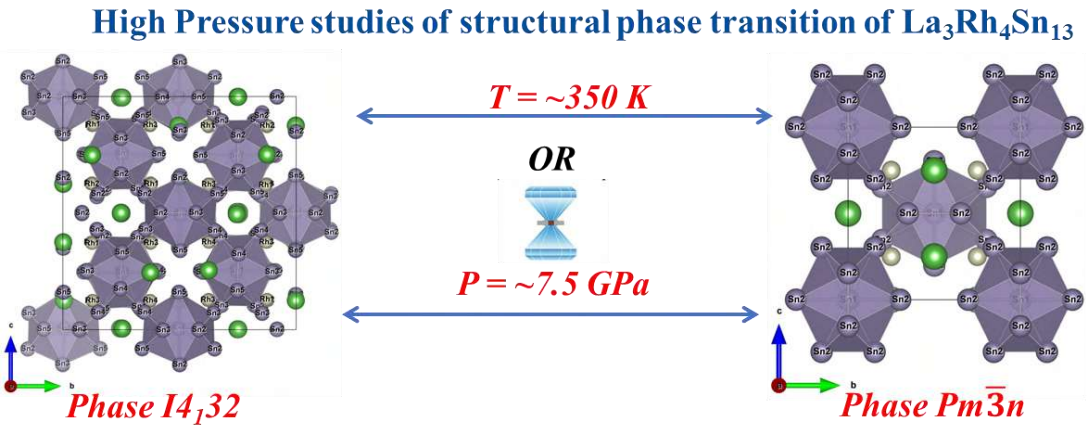

References:

[1] Muthukumaran Sundaramoorthy, Boby Joseph, et al. *Physica Status Solidi (RRL)–Rapid Research Letters* 17.12 (2023): 2300078.

[2] Muthukumaran Sundaramoorthy, Boby Joseph, et al *ChemPhysChem* 25.20 (2024): e202400286.

Topic Code: High-Pressure Materials Science

Unusual pressure-volume behaviour of Hf-Nb-Ta-Ti-V high entropy alloy

Nirmal Sharma[1], K. K. Pandey[1,2*], H. K. Poswal[1,2], Nilabja K. Sarkar[3] and Nandini Garg[1,2]
[1]*High Pressure & Synchrotron Radiation Physics Division, Bhabha Atomic Research Centre, Mumbai, India*
[2]*Homi Bhabha National Institute, Anushaktinagar, Mumbai, India*
[3]*Materials Science Division, Bhabha Atomic Research Centre, Mumbai, India*
*kkpandey@barc.gov.in

Abstract: High-pressure behavior of Hf-Nb-Ta-Ti-V high entropy alloy (HEA) has been investigated using X-ray diffraction (XRD) technique employing diamond anvil cell (DAC). Our study shows phase stability of the ambient *bcc* phase of Hf-Nb-Ta-Ti-V HEA up to the highest measured pressure of ~ 26.4 GPa, however with unusual pressure-volume (P-V) relationship between 7 to 11 GPa. This unusual behavior is concomitant with the reduction of macrostrain broadening, implying it to be an inherent character of the HEA system studied.

1. INTRODUCTION

High-entropy alloys (HEAs) are a class of materials that have attracted significant attention due to their unique properties, such as enhanced strength, corrosion resistance, and thermal stability. Due to these novel properties, HEAs are promising materials for various industrial applications. The HEA we studied was synthesized with the nominal composition of $Hf_{0.2}Nb_{0.2}Ta_{0.2}Ti_{0.2}V_{0.2}$. The alloy stabilizes in a single body-centered cubic phase with lattice parameter of 3.32Å at ambient condition [1]. We have investigated the high-pressure behaviour of this alloy up to ~ 26.4 GPa. Our study shows ambient phase stability up to the maximum studied pressure, however with unusual pressure-volume behaviour.

2. EXPERIMENTAL DETAILS

A few chips of the HEA sample of size ~ 20 μm were loaded in DAC along with Cu and silicone oil as pressure marker and pressure transmitting medium, respectively. The sample chamber was prepared by drilling ~ 200μm diameter hole in a pre-indented tungsten gasket. High-pressure X-ray diffraction (XRD) measurements were carried out at Extreme conditions XRD beamline, BL-11 at Indus-2 using monochromatic X-rays of wavelength λ=0.4861Å [2]. XRD images were recorded at MAR345 imaging plate detector in small pressure-steps of ~ 0.5 GPa up to ~ 26.4 GPa and subsequent release of pressure in a few steps, down to ambient conditions. 2D diffraction images were converted to 1D diffraction patterns using FIT2D software and subsequently analysed through Rietveld refinement using GSAS II software.

3. DISCUSSION AND RESULT

The ambient bcc phase has been found to be stable up to the maximum studied pressure, however, the pressure–volume (P-V) data exhibit unusual behaviour between 7 to 11 GPa (fig. 1). The P-V data could not be fitted with single equation of state (EoS). The experiments were repeated multiple times to verify if the unusual behaviour is an artifact or genuine behaviour of the studied HEA sample. We observed similar behaviour in all the measurements. The observed P-V behaviour can be described with two EoS. Fig. 1 shows two second order Birch-Murnaghan fittings to the observed P-V data in the pressure range of ambient to 7 GPa and 12 to 26.4 GPa.

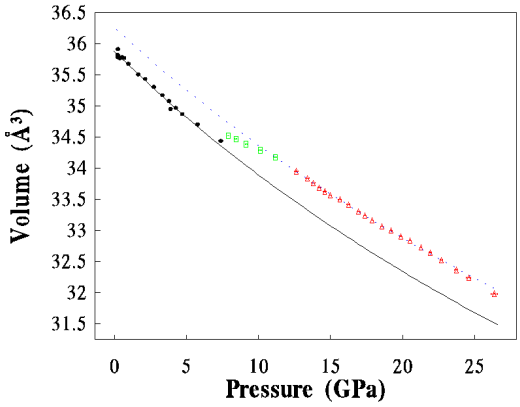

Fig.1: Pressure induced variation of unit cell volume.

Estimated bulk modulus are 156.3 GPa and 167.6 GPa for the first and second EoS fitting respectively. We observed significant reduction in macrostrain broadening of the sample XRD peaks in the unusual P-V region, implying the unusual behaviour to be inherent to the sample. Similar unusual P-V behaviour has been observed in nickelate [3], which is attributed to some internal structural changes. In our case different compression behaviour of different elements and concomitant changes in microstructure may have resulted in the unusual P-V behaviour. A detailed microstructural investigation on the studied HEA sample will be quite insightful for describing this observation.

REFRENCES

[1] N.K. Sarkar et al., Intermetallic 144,107503 (2022).
[2] K. K. Pandey et al. Pramana 80, 607 (2013).
[3] Sun, H., Huo, M., Hu, X. et al. Nature 621, 493–498 (2023).

Topic Code: High-Pressure Materials Science

Effect of plastic straining on *bcc-hcp* phase transition on pure iron: an in situ study

Suraj Kumar[1], K. K. Pandey[1,2]*, Valery I. Levitas[3,4]

[1]*High Pressure & Synchrotron Radiation Physics Division, Bhabha Atomic Research Centre, Trombay, Mumbai, India*
[2]*Homi Bhabha National Institute, Anushaktinagar, Mumbai, India*
[3]*Iowa State University, Departments of Aerospace Engineering and Mechanical Engineering, Ames, Iowa 50011, USA*
[4]*Ames Laboratory, Division of Materials Science and Engineering, Ames, IA, USA*

*kkpandey@barc.gov.in

Abstract: Synchrotron based in situ X-ray diffraction (XRD) study was carried out on pure iron under hydrostatic as well as under uniaxial compression to investigate the effect of plastic straining on the *bcc-hcp* phase transformation (PT) in pure iron. The *bcc-hcp* PT is found to be reversible in both the cases, however, plastic straining modifies the pressure-phase fraction hysteresis. Unlike hydrostatic condition, both forward and reverse PT initiate at nearly same pressure under plastic straining at high pressures. Under uniaxial compression, the *bcc-hcp* PT is found to be independent of compression-shear straining path and a function of accumulated plastic strain only.

1. INTRODUCTION

Phase transformations (PTs) induced by large plastic shear deformations under high pressures are critical in various material systems. Plastic shear can lower the pressure required for certain PTs, produce new phases unattainable without shear, and convert reversible transformations into irreversible ones [1]. These phenomena open new possibilities for synthesizing novel or known phases at reduced pressures [2]. High-pressure torsion in a rotational diamond anvil cell (RDAC) is an effective method for studying plastic strain-induced PTs [3]. We have carried out a similar X-ray diffraction (XRD) study on pure iron to investigate the effect of plastic straining on the well-known *bcc-hcp* PT in pure iron. Our study shows significant role of plastic straining on the *bcc-hcp* PT hysteresis at high pressures.

2. EXPERIMENTAL DETAILS

For hydrostatic compression experiments, small Fe chips of size ~20 µm were loaded in a symmetric type DAC with silicone oil as pressure transmitting medium and Cu as a pressure marker. For uniaxial compression experiments, a thin foil of iron of thickness ~ 150 µm was loaded in RDAC. In situ XRD experiments were performed at 16-BM-D beamline at HPCAT sector at Advanced Photon Source employing focused monochromatic X-rays of wavelength 0.3543 Å. For uniaxial compression case, XRD images were recorded across entire culet diameter of RDAC in steps of 10 µm. 2D diffraction images were converted to a 1D diffraction pattern using FIT2D and subsequently analysed through Rietveld refinement using GSAS II software for obtaining lattice parameters, phase fractions etc. of both *bcc* and *hcp* phases.

3. RESULTS AND DISCUSSION

The pressure-volume (PV) relationships of *bcc* and *hcp* Fe under compression in a DAC was obtained using a third-order Birch–Murnaghan equation of state (EoS) to determine the bulk modulus and its pressure derivative, which were found to be 141 GPa and 11 for *bcc* Fe, and 154 GPs and 5 for *hcp* Fe. The *bcc*-to-*hcp* PT resulted in an approximate 4.5% decrease in unit cell volume. Under hydrostatic compression, the PT begins at ~14 GPa and completes at ~17 GPa, while under uniaxial loading, it initiates at ~10 GPa and completes at ~17 GPa. On release, reverse PT initiates at ~ 8 GPa and 10 GPa under hydrostatic and uniaxial case, respectively. The PT hysteresis is found to be significantly modified under plastic straining (Fig. 1).

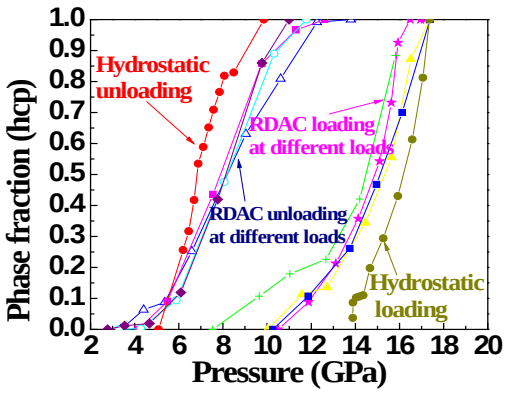

Fig. 1. Phase fraction hysteresis of hcp phase of iron under hydrostatic and uniaxial compression.

Under uniaxial compression, the PT initiation pressures for forward and reverse PT are found to be same at all radial positions of anvil where the stress conditions are quite different. This implies that the phase fraction of daughter phase is independent of the compression-shear pathway and a function of accumulated plastic strain only and hence the kinetic equation of plastic strain induced phase transition [1] is applicable to this case.

References

[1] V.I. Levitas, Phys. Rev. B 70, 184118 (2004).
[2] K. Edalati et al, Mat. Sci. Eng. A. 652, 325–352 (2016).
[3] K.K. Pandey et al, Acta Materialia 196, 338-346 (2020).

Spinel to perovskite transition in the Earth's lower mantle: Implication in Slab Dynamics

Rabindranath Mondal[1], Swastika Chatterjee[1]
[1]National Centre for High-Pressure Studies and Department of Earth Sciences,
Indian Institute of Science Education and Research Kolkata, Nadia, 741246, West Bengal, India
Email: ***rm19rs089@iiserkol.ac.in***

Abstract: Using first-principles density functional theory combined with quasi-harmonic approximation (QHA), we have investigated the thermodynamics of the ringwoodite to bridgmanite phase transition, which is known to be the cause behind the 660 km seismic discontinuity observed. Our calculations indicate that in the absence of water, the phase boundary has a high negative Clapeyron slope of -3.37 MPa/K and is located at a pressure of 21.15 GPa at 1873 K. However, previous experimental and theoretical calculations indicate that ringwoodite may contain a substantial amount of water (~1-2 wt.%) in its crystal structure, which can significantly impact on the phase transition. To investigate this effect, we analysed two distinct dissociation reactions at the same water concentration: (1) hydrous ringwoodite transforming into hydrous bridgmanite and periclase. This reaction yields a phase boundary that occurs at 21.98 GPa and 1800 K, with a high negative Clapeyron slope of -2.95 MPa/K at 1873 K. and (2) hydrous ringwoodite transforming into bridgmanite, periclase, and hydrous stishovite. Surprisingly, this reaction places the phase boundary at 23.85 GPa and 1800 K, close to the D660 discontinuity, with a slightly positive Clapeyron slope of +1.57 MPa/K at 1873 K. These findings indicate that the presence of water can strongly influence the 660 km discontinuity, particularly in the context of slab subduction dynamics.

1. INTRODUCTION

Olivine[$(Mg, Fe)_2SiO_4$] is the most dominant mineral in the upper mantle. It undergoes phase transition to wadsleyite, and further to ringwoodite with increasing pressure in the Earth's interior. These high-pressure phase transitions are known to be responsible for the observed seismic discontinuity at the depths of approximately 410 km and 520 km, respectively, within the mantle. Seismic tomography studies have further identified a global seismic discontinuity at a depth of ~660 km (~23.6 GPa and 1873 K) [1]. The dissociation of ringwoodite into an assemblage of bridgmanite [$(Mg, Fe) SiO_3$] and periclase [(Mg, Fe) O] is widely accepted to be the cause behind the ~660 km discontinuity [2]. It is a crucial structural boundary in the Earth's interior, as it separates the transition zone from the lower mantle. Water is an important volatile material on the Earth's surface and can be transported to the deep mantle through hydrous minerals in subducting slabs. Ringwoodite has been found to accommodate a significant amount of water (~1-2 wt.%) in its crystal structure [3], which can play an important role in Earth's evolution and dynamics.

2. COMPUTATIONAL DETAILS

All calculations have been carried out using first-principles density functional theory (DFT), which is implemented in VASP [4,5]. To estimate the phase boundary of the ringwoodite into bridgmanite and periclase at finite temperatures, we have used quasi-harmonic approximation to calculate the Gibbs free energy of each phase at constant pressure and temperature [6]. The first-principles phonon calculations were performed using the density functional perturbation approach (DFPT) [7].

3. PHASE TRANSITION BOUNDARY

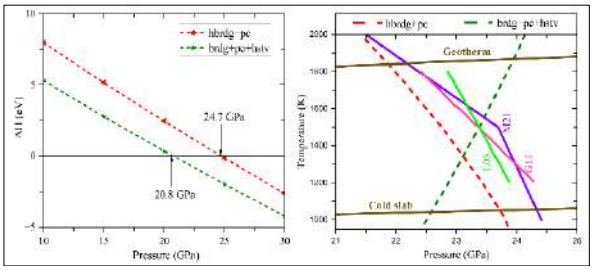

Fig.1. Phase boundaries for wet ringwoodite. The left panel shows the static conditions and the right panel shows different temperatures. Dotted lines: This study; solid lines: previous literature (L05= Litasov *et al*., 2005b; G13= Ghosh *et al.,* 2013; Muir *et al*., 2021).

ACKNOWLEDGEMENT

I acknowledge IISER Kolkata for providing financial support. I also express my gratitude to Prof. Jibamitra Ganguly for his valuable discussion and insights.

5. REFERENCES

[1]. Dziewonski & Anderson, PEPI, 25(4), 297-356, 1981.
[2]. Ito and Takahashi, JGR: solid Earth, 94(B8), 10637-10646, 1989.
[3]. Mondal *et al*., PEPI, 348, 107156, 2024.
[4]. Khon & Sham, Phys. Rev., 140(4A), A1133, 1965.
[5]. Kresse & Furthmüller, Phys. Rev. B, 54(16), 11169, 1996.
[6]. Wallace *et al*., AJP, 40(11), 1718-1719, 1972.
[7]. Baroni et al., Rev. Mod. Phys., 73(2), 515, 2001.

Structural stability and compressibility behaviour of $CeTe_2$ under pressure

K. Sanitha[1], P. Anand Kumar[1], S. Shyam Kumar[2], N. R. Sanjay Kumar[1, a)], Anuj Upadhyay[3], R. Sudha[2] and Rajesh Ganesan[2]

[1]Materials Science Group, [2]Materials Chemistry & Metal Fuel Cycle Group, Indira Gandhi Centre for Atomic Research, A CI of Homi Bhabha National Institute, Kalpakkam, 603 102, Tamil Nadu, India
[3]Accelerator Physics and Synchrotrons Utilization Division, Raja Ramanna Center for Advanced Technology, A CI of Homi Bhabha National Institute, Indore 452013
[a)]Corresponding author: sanju@igcar.gov.in

Abstract: The structural stability and compressibility behaviour of $CeTe_2$ was investigated using diamond anvil cell up to 25 GPa by high pressure x-ray diffraction experiments. $CeTe_2$ was synthesized in single phase by non-isothermal isopiestic method. At ambient, $CeTe_2$ crystallizes in a tetragonal (P4/*nmm*) phase. The sample does not undergo structural transition and is stable up to the maximum pressure studied. The bulk modulus of the tetragonal phase is estimated to be 62(1) GPa.

1. INTRODUCTION

$CeTe_2$, a member of the RTe_2 compounds, is well-known for its charge density wave (CDW) property with a high transition temperature of T_{CDW} ~ 1000 K [1]. At ambient, $CeTe_2$ generally crystallizes in the layered Cu_2Sb-type tetragonal structure (space group P4/*nmm*). There are two types of Te sites in the structure: Te(1) and Te(2). Te(1) atoms form planar square sheets, which are sandwiched along the *c* axis by the double layers of Ce-Te(2) slabs. The CDW phase in $CeTe_2$ coexists with magnetism and superconductivity (T_c = 2.7 K) under pressure [1]. In order to understand the underlying physics of pressure induced CDW phase, it is essential to investigate its crystal structure under pressure systematically. Hence, the aim of this study is to examine the structural stability of $CeTe_2$ under high pressure.

2. EXPERIMENTAL METHODS

$CeTe_2$ sample was synthesized by non-isothermal isopiestic method [2]. *In-situ* high-pressure experiments were carried out using a Mao-Bell type diamond anvil cell (DAC) with a culet size of ~ 500 μm. The sample was loaded into the central hole of a stainless steel (SS) gasket of diameter ~ 200 μm. The SS gasket was preindented to a thickness of ~60 μm. Silver was used as the pressure calibrant and silicone oil was used as the pressure transmitting medium. The HPXRD experiments were performed at BL 12 of Indus-II synchrotron source at RRCAT, Indore. A monochromatic X-ray beam of wavelength λ=0.7124 Å was used for the experiments. A MAR345 image plate detector was used to collect diffraction patterns.

3. RESULTS AND DISCUSSIONS

The analysis of ambient XRD data showed that $CeTe_2$ adopts tetragonal structure and belongs to the P4/*nmm* space group and the lattice parameters were estimated to be a = 4.507(4) Å and c = 9.065(1) Å. The obtained unit cell volume was V = 184.18(3) $Å^3$. Figure 1 shows the XRD patterns of $CeTe_2$ at various pressures up to 25 GPa. No new peaks emerged nor the existing peaks disappeared up to the highest pressure studied in this work. This suggests that $CeTe_2$ is structurally stable up to 25 GPa. The P-V data (Fig.2) is fitted with 3rd order Birch-Murnaghan equation of state and the bulk modulus was estimated to be 62(1) GPa. The pressure derivative of bulk modulus was estimated to be 5.2(1). The sample was found to be more compressible along *c*-axis than along the *a*-axis (inset in Fig.2). This kind of anisotropic reduction in lattice parameters is reported for transition metal dichalcogenides such as WSe_2 [3]. The total observed reduction in volume was around 20%.

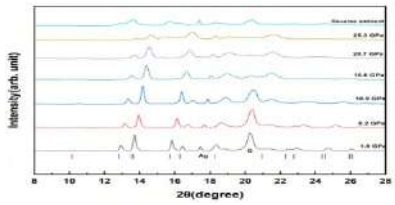

Fig.1. High pressure XRD patterns of $CeTe_2$ at various pressures up to 25 GPa

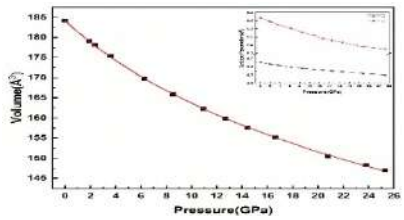

Fig.2. Pressure – volume data of $CeTe_2$ up to 25 GPa and variation of lattice parameters with pressure in inset.

4. CONCLUSION

In summary, high pressure x-ray diffraction studies were performed on the $CeTe_2$ powder to investigate the structural stability and compressibility behaviour. The lack of emergence or disappearance of peaks in the XRD patterns indicates no structural transition occurred in the sample. The bulk modulus of the tetragonal phase is estimated to be 62(1) GPa.

ACKNOWLEDGEMENT

The authors acknowledge IGCAR management for facility and administrative support. The authors are also grateful to all the members of HPSS, IGCAR for the help during experiment.

REFERENCES

[1]. M. H. Jung et al, Phys. Rev. B **67** (2003) 212504.
[2]. S. Shyam Kumar et al, Monatshefte für Chemie - Chemical Monthly **155**, (2024) 165–172.
[3]. X. Wang et al, Scientific Reports **7** (2017) 466.

Structural Stability of Gd^{3+} and Ce^{4+} co-doped Lanthanum Zirconates Under High Pressure: Insights into Actinide Host Matrices

Saideep Shirish Bhat[1], Irshad K. A[2], Boby Joseph[2], Gurumurthy S C[1], Raghavendra K G[3*]
[1]Nano and Functional Materials Lab (NFML), Department of Physics, Manipal Institute of Technology, MAHE, Manipal – 576104, Karnataka, India.
[2]Elettra-Sincrotrone Trieste S.C. p.A., S.S. 14, Km 163.5 in Area Science Park, Basovizza 34149, Italy.
[3]Department of Physics, Manipal Institute of Technology, MAHE, Manipal – 576104, Karnataka, India.
Email: raghavendra.kg@manipal.edu

Abstract: Rare Earth Zirconates with Pyrochlore and Flourite structures are considered potential host matrices for trapping long-lived actinides because of their irradiation resistance and high structural stability. The high-pressure behavior of actinide-loaded zirconates remains largely unexplored, yet understanding it is crucial. High pressure X-ray diffraction of Gd^{3+} and Ce^{4+} co-doped lanthanum zirconate (LZ) indicates an exceptional structural stability of the pyrochlore structure without any phase transition till ~17 GPa. The variations in the micro-strain along with the deviation in the compressibility above 5 GPa, suggest the possible changes in the micro-structure.

1. INTRODUCTION

Nuclear energy is vital for meeting growing energy demands and transitioning to carbon-free power sources, but managing radioactive waste remains a significant challenge. Used fuel pellets contain residual fissile materials and fission products, with some processed for uranium and plutonium, while the remainder becomes radioactive waste. Borosilicate glass is commonly used to immobilize high-level nuclear waste (HLW), but its stability, especially when exposed to water, is a concern [1]. Ceramic and glass-ceramic matrices, like pyrochlore and fluorite compounds, are being studied for their superior stability and lower leachability. Rare Earth Zirconates such as $La_2Zr_2O_7$, are known for their structural integrity with actinides in their A and B sites, however, their behavior under high pressure is not known. Gadolinium (Gd^{3+}) and cerium (Ce^{4+}) incorporation in A and B sites simulates a nuclear waste as they are used as surrogates for Americium (Am^{3+}) and thorium (Th^{4+}) ions. Considering this understanding the structural stability of Gd and Ce doped LZ is believed to shed light on this potential nuclear waste form [2]

2. EXPERIMENTAL DETAILS

The simulated waste form of $(La_{1.8}Gd_{0.2})(Zr_{1.8}Ce_{0.2})O_7$ was synthesised through co-precipitation method, using the inorganic salts as precursors. The pH was adjusted to 11 to aid the precipitate formation and the resultant precipitate were filtered, dried, ground, and calcined at 1300 °C for 5 hours. High-pressure X-ray powder diffraction (HPXRPD) studies were conducted at the Xpress beamline of Elettra synchrotron, Trieste, using a diamond anvil cell. Methanol-ethanol (4:1) is used as pressure transmitting medium and pressure was calibrated via ruby fluorescence. Diffraction data was recorded using a PILATUS3S-6M detector with an X-ray wavelength of 0.4956 Å. Rietveld method using GSAS software was employed for data analysis [3].

3. RESULTS AND DISCUSSIONS

HPXRPD data shown in the Fig. 1(a) indicate no structural phase transition till the highest pressure studied, thus indicating the large structural stability of the pyrochlore structure as actinide host matrix for the nuclear waste removal. With increasing pressure, all the diffraction peaks shifted to higher 2θ angles due to lattice contraction. The unit cell volume obtained from the Rietveld refinement indicate uniform compression with a bulk modulus of 133(4) GPa. However, the PV curve shown in Fig. 1(b) substantially deviates from the second order Birch-Murnaghan Equation of State fit (BM(II)-EoS). The monotonous and progressive increase in the micro-strain together with the deviations in the compression behavior above 5 GPa could be an indication of the microstructural changes occurring in the material. Further studies are being planned to explore this behavior.

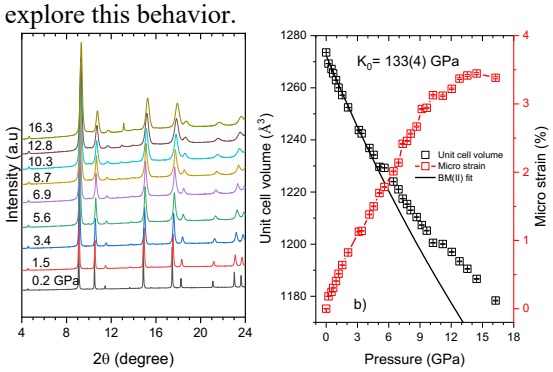

Fig.1(a) Synchrotron HPXRPD of $(La_{1.8}Gd_{0.2})(Zr_{1.8}Ce_{0.2})O_7$ recorded up to 16.3 GPa indicating the absence of structural phase transitions. (b) BM(II)-EoS fit to the pressure volume data and the variations in the micro-strain with increasing pressure.

ACKNOWLEDGEMENT

The authors acknowledge DST, India and Elettra, Italy for the financial assistance to carry out this research work.

REFERENCES

[1]. H. Kleykamp et al, Journal of Nuclear Materials **275** 1999.
[2]. M. Jafar et al, Journal of Alloys and Compounds **867** 2021.
[3]. B. Toby et al, *J. Appl. Crystallogr*. **46** 2013.

Pressure induced topological phase in intermetallic Zintl compound $RbZn_4As_3$

Ramesh Kumar[*], Mukhtiyar Singh[#]
Computational Quantum Materials Design (CQMD) Lab, Department of Applied Physics, Delhi Technological University, New Delhi, Delhi 110042, India
Email: [*]ramesh_2k19phdap506@dtu.ac.in, [#]mukhtiyarsingh@dtu.ac.in

Abstract: We reported the topological phase transition in an experimentally synthesized tetragonal Zintl compound $RbZn_4As$ via *first-principles* calculation. This compound has shown the topologically non-trivial phase under applied hydrostatic pressure and epitaxial strain of 38 GPa and 8%, respectively. The topological phase of this material has been verified with bulk band inversion at the *Γ-point* and the presence of surface states along the (001) plane. The Z_2 topological invariants have calculated with the help of parity analysis at time-reversal invariant momenta points and the evolution of Wannier charge centers.

1. INTRODUCTION

The topological phase of matter [1-2] is becoming increasingly popular after the discovery of topological insulators (TIs). Exploring a topologically trivial material that can be made topologically non-trivial by strengthening spin-orbit coupling (SOC) using external pressure and strain [3] is quite interesting. According to *first-principles* calculations, the structural phase transition has led to the topological phase transition in $NaCd_4As_3$ [4]. $RbZn_4As_3$ has an isoelectronic structure similar to $NaCd_4As_3$ but with a different space group. We examined, using *first-principles* calculations, the topological phase characteristics of the ternary Zintl compound $RbZn_4As_3$ under the influence of hydrostatic pressure and epitaxial strain.

2. RESULTS AND DISCUSSION

The ternary Zintl compound $RbZn_4As_3$ has a centrosymmetric tetragonal structure (*P4/mmm*), where Rb^+ cations are embedded between the $[Zn_4X_3]^-$ polyanions layers. These polyanionic layers contain tetrahedra $ZnAs_4$ and are stacked along the *c-axis* of the crystal structure as shown in Figure 1.

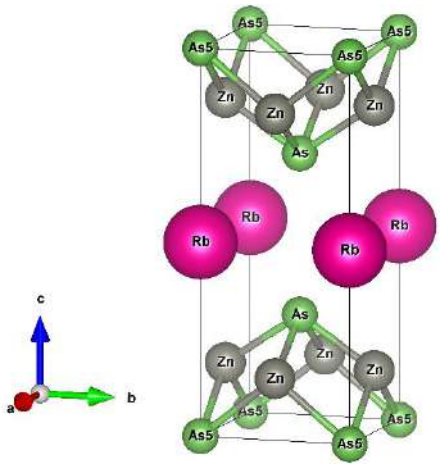

Fig.1. The crystal structure of the Zintl compound $RbZn_4As_3$.

The orbital projected electronic band structures of $RbZn_4As_3$ without and with the inclusion of SOC have shown that this material is topologically trivial with a direct band gap of 0.681 eV and 0.584 eV, respectively. It has observed that p_x, p_y, p_z*-orbitals* of As and *s-orbital* of Zn mainly contribute to the ground state eigenfunctions of this material near the Fermi energy. Under the applied hydrostatic pressure and epitaxial strain, the eigenstates of the system and order of eigenstates with projections p_x, p_y and p_z *-orbitals* of As near the Fermi energy changed. At the pressure of 38 GPa and epitaxial strain of 8% along the *c-axis*, this material has shown the transition from trivial to non-trivial phase and an inverted contribution of orbitals at the *Γ-point* has observed. This non-trivial phase has also verified from the presence of a topological surface state along the (001) plane. The Z_2 topological invariants have calculated using the product of parities of all the occupied bands at time-reversal invariant momenta (TRIM) points and the evolution of Wannier charge centers (WCCs) at ambient and elevated pressure/strain values.

ACKNOWLEDGEMENT

All the authors acknowledge the National Supercomputing Mission (NSM) for providing computing resources of 'PARAM Siddhi-AI', under the National PARAM Supercomputing Facility (NPSF), C-DAC, Pune and supported by the Ministry of Electronics and Information Technology (MeitY) and Department of Science and Technology (DST), Government of India. One of the authors (Ramesh Kumar) would like to thank the Council of Scientific and Industrial Research (CSIR), Delhi, for financial support.

REFERENCES

[1]. L. Kane, E.J. Mele, Phys. Rev. Lett. **95** (2005) 146802.
[2]. L. Fu, C.L. Kane, E.J. Mele, Phys. Rev. Lett. **98** (2007) 106803.
[3]. M. Singh, R. Kumar, R. K. Bibiyan, Eur. Phys. J. Plus **137** (2022) 633.
[4]. Y-Y. Wang, C. Zhong, M. Li, W-L. Zhu, W-J. Hou, W-H. Song, Q-X. Dong, Y-F. Huang, S. Zhang, Z-A. Ren, S. Wang, and G-F. Chen, Phys. Rev. B **102** (2020) 115122.

Prediction of High Pressure Phase Transition of ThO_2 using USPEX code

D. Sornadurai†
Condensed Matter Physics Division, Materials Sciemce Group, IGCAR, Kalpakkam – 603102, INDIA
†Homi Bhabha National Institute, IGCAR, Campus, Mumbai, INDIA
Email: sorna@igcar.gov.in

Abstract: To resolve the ambiguity in the structural phase transition of ThO_2, the crystal structure predicted using the USPEX code based evolutionary algorithm along with GULP code. It is identified that ThO_2 transformed from fcc (SG. No. 225) to orthorhombic structure (Pnma S.G. NO. 62) at 20 GPa with a volume collapse of 8.5 %.

1. INTRODUCTION

Thorium started to use as a nuclear fuel, because of high natural abundance of thorium in the earth's crust and a perception that uranium supplies may become limited. In liquid metal cooled fast breeder nuclear reactors (Th, Pu)O_2 containing 20–30% PuO_2 and 70–80% ThO_2 is used as fuel. UO_2, easily oxidizes to U_3O_8 and UO_3. Whereas ThO_2 is relatively inert and highly stable not oxidized beyond the stoichiometric composition and its thermal conductivity is higher than that of uranium dioxide. In reactor operation condition the rim of the fuel experiences more damage due to the temperature difference which induces pressure difference. Hence the high pressure study of ThO_2 carried out and the results are given.

2. COMPUTATIONAL DETAILS

Universal Structure Predictor:Evolutionary Xtallography (USPEX) code employs an evolutionary algorithm for structure prediction [2]. USPEX requires Chemical composition, number of elements their charge state and pressure. General Utility Lattice Program (GULP) requires the Buckingham potential parameters as given equation 1.

$$V(r_{ij}) = A_{ij}\, e^{-\frac{r_{ij}}{\rho_{ij}}} - \frac{C_{ij}}{r_{ij}^6} \qquad (1)$$

USPEX runs synergistically with the GULP code with the Buckingham potential parameters given in table 1.

Table 1. Buckingham Potential Parameters of ThO_2

Interacting atoms	A (eV)	ρ (Å)	C (eV. Å^6)
Th – Th	8.5215	0.16666	1530.173
Th – O	1379.866	0.398673	49.22
O – O	50259.34	0.15285	72.65339

For predicting the ambient structure the input pressure in the USPEX input file is 1x10^{-4} GPa. The predicted ambient structure matched well with the reported values. Then further the computation carried out up to 35 GPa in a step of 1 GPa. It was found that at 20 GPa ThO_2 transformed to orthorhombic structure. The PV data obtained from this computation is given in figure1. It can be seen that at 20 GPa there is a volume collapse of 8.5 % which reflected as a sudden jump in the density vs pressure curve. The P-V data of both the parent and daughter phases have been fitted separately using the third order Birch–Murnaghan equation of state to get the Bulk modulus values.

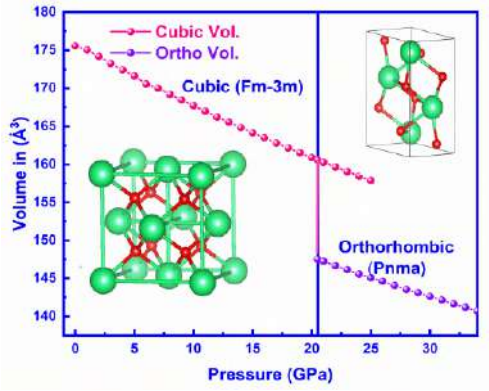

Fig.1The P-V data of ThO_2 curve showing the phase transition with the applied pressure.

3. RESULTS AND DISCUSSIONS

The BM EOS fitted graph is shown for both the phases are shown in figure 2.

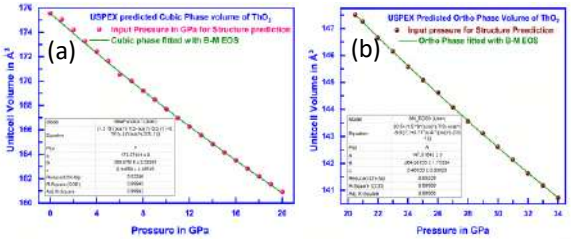

Fig.2 The B-M EOS fitted data for both the (a) Cubic and (b) Orthorhombic ThO_2.

The bulk modulus of ThO_2 in the ambient cubic structure closely matches with the experimental as well as the computational results. The high pressure orthorhombic phase shows a high bulk modulus of ~261 GPa with a considerable variation with the reported values.

REFERENCES

[1].Timothy Ault, Bradley Van Gosen, Steven Krahn, and Allen Croff, Nuclear Technology, **194,** 136–151 (2016).

[2]. A. R. Ogannov and C.W. Glass, The Journal of Chemical Physics, **124,** 2PP. 44704 (1-15) (2006).

[3]. Julian D. Gale and Andrew L. Rohl, Molecular Simulation, **29** (5), pp. 291–341 (2003).

Topic Code: High-Pressure Material Science

Structural Transition of Perovskite type $LaVO_3$ at High-pressures

A. K. Sivadasan[1], K. A. Irshad[2], I. Packia Selvam[1], Boby Joseph[2], S. N. Potty[1]
[1]Centre for Materials for Electronics Technology (C-MET), Thrissur, Kerala, India-680581
[2]Elettra-Sincrotrone Trieste S.C.p.A., S.S. 14 Km 163.5 in Area Science Park, Basovizza 34149, Italy
Email: *dr.a.k.sivadasan@gmail.com* & *snpotty@cmet.gov.in*

Abstract: Lanthanum vanadate ($LaVO_3$) is a Mott insulator with a tunable bandgap, suitable for the use of absorber layer in the solar cells. Our high-pressure studies indicate an unusual phase transition of orthorhombic centrosymmetric non-polar phase (*Pnma*) at 7.1GPa.

1. INTRODUCTION

Transition metal oxides (TMOs) with ABO_3-type perovskite structures exhibit tunable bandgaps ranging from near-infrared to ultraviolet, depending on their constituent elements. Generally, $LaVO_3$ adopts a typical distorted orthorhombic structure (*Pnma*, nonpolar and centrosymmetric) of rare-earth vanadates. Notably, $LaVO_3$ is a Mott insulator with a direct bandgap of 1.1 eV, the largest in the RVO_3 (R: rare-earth elements) series. This gap, formed between the *dxy* and *dyz/dzx* bands, falls within the optimal range (1-1.5 eV) for photovoltaic energy harvesting. External factors like pressure and temperature can significantly influence the Coulomb interactions and is expected to affect the Mott transitions [1,2]. Importantly, pressure is a versatile tool that can be used to fine tune the bandgap of these solar cell materials via structural modifications. Therefore, understanding the pressure-induced changes are crucial for exploring the photo voltaic applications of $LaVO_3$.

2. EXPERIMENTAL

$LaVO_3$ is synthesised via solid state reaction of lanthanum acetate hydrate [La $(CH_3CO_2)_3$. xH_2O] and vanadium acetyl acetonate [$V(C_5H_7O_2)_3$]. High-pressure X-ray powder diffraction (HP-XRPD) studies were performed at the Xpress beamline of Elettra Sinchrotrone Trieste, Italy using a membrane diamond anvil cell (DAC). A wavelength of 0.4957Å was used for the current study. High resolution diffraction data were collected using a PILATUS3 S 6M detector. Methanol ethanol mixture (4:1) was used as a pressure-transmitting medium. Pressure was calibrated from the ruby fluorescence.

3. RESULTS AND DISCUSSIONS

HP-XRPD data collected for $LaVO_3$ up to a maximum pressure of 19.5 GPa is shown in Fig. 1a. The diffraction data at ambient pressure could be indexed to the orthorhombic (*Pnma*) structure (ICDD ref: 01-081-2435). This structure remains stable up to ~7.1 GPa, beyond which we see the appearance of new reflections at several 2θ positions (a few are indicated with diamond symbol in Fig. 1a & 1b, indicating a structural phase transition). Though the onset of this transition is at 7.1 GPa, the high-pressure phase was co-existing with the parent phase till the highest pressure was reached in this study, indicating the sluggish nature of the transition. Our preliminary analysis indicates a phase transition to polar form, often involving a symmetry change from *Pnma* (orthorhombic, centrosymmetric, and non-polar) to $Pna2_1$ (orthorhombic, non-centrosymmetric, and polar) [3]. At higher pressures, $LaVO_3$ demonstrates the ability of the perovskite structure to densify through significant shortening of the La–V bond distances and distortion of the VO_6 octahedra, reflecting the structural flexibility of the perovskite framework and expected to change its space group symmetry [4]. These changes are fully reversible upon pressure release.

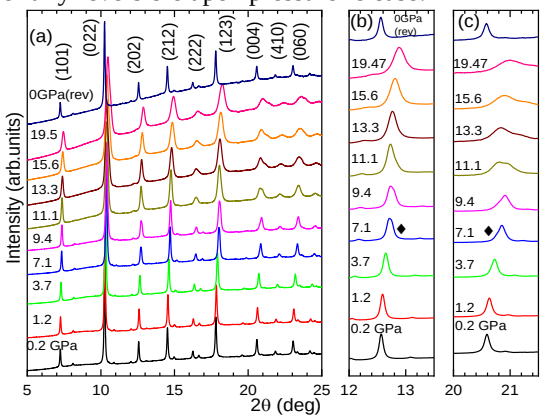

Fig.1. a) HPXRD data of $LaVO_3$ up to 19.5 GPa indicating the reversible transition, b) & c) shows new peaks at 7.1GPa.

4. CONCLUASIONS

HP behaviour of orthorhombic $LaVO_3$ is studied up to 19.5 GPa using the synchrotron HP-XRD. The study revealed a reversible structural phase transition from a centrosymmetric non-polar phase (*Pnma*) to a non-centrosymmetric polar phase $Pna2_1$ at 7.1 GPa

ACKNOWLEDGEMENTS

A.K.S thankful to KHEC, Govt of Kerala, for the financial assistance through CMNKPDF programme. A.K.S and I.P.S thank DST, Govt of India for the financial assistance to visit the Xpress beamline. K.A.I thank IISc Bengaluru and ICTP Trieste for the IISc/ICTP fellowship.

REFERENCES

[1] M. Brahlek *et al*, MRS Communications, **7** (2017) 27-52
[2] L. Wang *et al*, Phys. Rev. Applied, **3** (2015) 064015
[3] J. G. Cheng *et al*, PNAS, **10** (2013) 20003
[4] Jie Chen *et al*, Phys. Rev. B **108** (2023) 134106.

Topic Code: 05

Structural properties and phase transition of U_3Si under pressure: A DFT study

Prasanta Kumar Maharana[1,2], Gurpreet Kaur[1,2], Sharat Chandra[1,2], R Govindaraj[1,2]
[1]Materials Science Group, Indira Gandhi Centre for Atomic Research, Kalpakkam, TN-603102, India
[2]Homi Bhabha National Institute, Mumbai-400094, India
Email: pkmaharana459@gmail.com, gurpreet@igcar.gov.in

Abstract: We investigated the structural properties of U_3Si under hydrostatic pressure (0–100 GPa) using first-principles calculations based on density functional theory (DFT). A pressure-induced phase transition from the α-U_3Si to β-U_3Si structure is predicted at approximately 80 GPa. The optimized structural parameters at zero and high pressures were obtained and analyzed, providing valuable insights into the behavior of U_3Si under extreme conditions.

1. INTRODUCTION

The Fukushima nuclear accident highlighted the need for enhanced accident-tolerant fuels (ATFs). Uranium-silicides are proposed as the candidate for ATFs [1]. U_3Si has the highest uranium density among the U-Si compounds, making it an appealing contender for specialized reactor applications [2].

Utilization of U_3Si in reactor applications would require broad research to understand its performance under extreme reactor conditions such as high temperature and pressure. Out of different U-Si phases, USi, USi_2, U_3Si_2, U_3Si_5 have been examined at high-pressure conditions [3] but as of our knowledge, no experimental or theoretical study in literature for U_3Si under high-pressure.

In this work, we have performed density functional theory (DFT) calculations to study the structural properties and phase transition under high pressure (0-100 GPa).

2. COMPUTATIONAL DETAILS

Density Functional Theory (DFT) calculations were performed using the Vienna ab-initio Simulation Package (VASP) [4]. The projector augmented wave (PAW) method was employed to describe the ion-electron interaction, with the Perdew-Burke-Ernzerhof (PBE) functional within the generalized gradient approximation (GGA) for exchange-correlation potential. A plane wave basis with a 550 eV cutoff energy was used, and the Brillouin zone was sampled using a Monkhorst-Pack K-point mesh.

3. RESULTS AND DISCUSSION

U_3Si exhibits three crystal structures [5]: an orthorhombic (Fmmm) α-phase below 120 K, a tetragonal (I4/mcm) β-phase at 120 K, and a cubic (Pm-3m) γ-phase above 1050 K.. A third-order Birch-Murnaghan equation of state was fitted to the volume-energy curves, establishing α-U_3Si as the ground state. Equilibrium lattice parameters, volume, and energy for the ground state are presented in Table 1.

To investigate the effect of pressure on U_3Si phases, the structures were fully relaxed under varying pressures. The lattice parameters and volumes decrease monotonically with increasing pressure, attributed to the reduction in interatomic distances.

Table-1. Equilibrium structural parameters of U_3Si

	Lattice constants (Å)			Volume (Å^3)	Energy (eV)
	a	b	c		
α-U_3Si	8.4967	5.5115	8.4966	76.81	-39.867
β-U_3Si	6.0070	6.0070	8.5140	76.80	-39.862
γ-U_3Si	4.2553	4.2553	4.2553	77.05	-39.788

To study pressure-induced phase transitions in U_3Si, enthalpies of the three phases were calculated using $H = E + PV$ [6]. The stability of the phases decreases with increasing pressure. Relative enthalpies are calculated with respect to orthorhombic structure. Figure 1 shows an intersection between the α-U_3Si and β-U_3Si enthalpy curves at 80 GPa, indicating a phase transition from α to β phase. No prior studies are available to validate these findings.

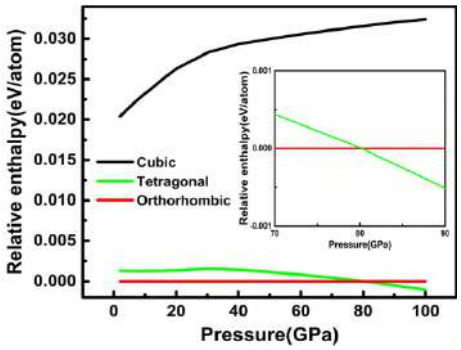

Fig. 1. The variation of relative enthalpy with pressure for the three structures of U_3Si.

4. CONCLUSION

This study examined the optimized lattice parameters and pressure-induced phase transitions of U_3Si using first-principles calculations, identifying an α-to-β phase transition at 80 GPa.

REFERENCES

[1]. Ulrich et al, Front. Nucl. Eng. 2 (2024) 1340426.
[2]. J.T. White et al, J. Nucl. Mater. 452 (2014) 304.
[3]. Baker et al, J. Nucl. Mater. 540 (2020) 152373.
[4]. J. Hafner et al, J. Comp. Chem. 29 (2008) 2044.
[5]. K. Remschnig et al, J. Solid State Chem. 97 (1992) 391-399.
[6]. Q.-J. Liu et al, J. Alloys Compd. 631 (2015) 192.

HIGH PRESSURE DENSITY FUNCTIONAL THEORY STUDIES ON $CaCu_2O_3$ COMPOUND

Aiswarya S M[1, 2], Somesh Chandra[1, 2], Gurpreet Kaur[3], G M Bhalerao[1*] and R Govindaraj[3]
[1]UGC-DAE CSR Kalpakkam Centre, Kokilamedu, Tamil Nadu - 603104
[2]University of Madras, Chennai, Tamil Nadu - 600005
[3]Material Science Group, IGCAR, HBNI, Kalpakkam, Tamil Nadu - 603102
***Email: gmbhalerao@csr.res.in**

Abstract: We present a Density Functional Theory (DFT) study on the structural properties of the pseudo spin ladder compound $CaCu_2O_3$ under ambient and high pressure conditions using VASP code. Structural optimization is performed using the PBEsol functional. Notably, significant structural changes occur, with the buckled angle approaching a planar configuration under higher pressure. The mechanical properties of the compound also studied.

1. INTRODUCTION

The two leg pseudo spin ladder compound $CaCu_2O_3$ has attracted significant interest within the scientific community due to its structural similarities with the high pressure phase of well-known two-leg spin ladder compound $SrCu_2O_3$ at 4.3 GPa. Although it resembles a two-leg ladder structurally, the ladder exhibits a "buckling" that results in a rung angle of 123° and stronger leg interactions compared to rungs.

In the present study, we perform DFT calculations using Vienna *ab-initio* Simulation Package (VASP) code [1] to understand the structural properties of the compound under external pressure. We investigated the change of bond angle with external pressure and also computed the Bulk modulus.

2. COMPUTATIONAL MEHOD

The (DFT) along with plane wave projector augmented wave (PAW) approach, as incorporated within the VASP code, are used for the first principle calculations. Revised PBE for solids (PBEsol) functional serves as an approximation for exchange correlation. The energy cut-off for plane waves was fixed at 500 eV. Brillouin zone integration is done utilizing a grid size of 3 × 6 × 7 using the Monkhorst–Pack method for optimizing the orthorhombic structure. Convergence in self-consistent field (SCF) calculations was determined by a threshold criterion of 10^{-8} eV for total energy change. Atom positions were relaxed until the force on each atom reached below 0.003 eV/Å.

3. RESULT AND DISCUSSION

To examine the effect of external pressure on the structural parameters of the $CaCu_2O_3$ compound, various pressure values (0-14 GPa) were applied in the VASP code, and the structural cell was optimized with respect to atomic positions, cell shape, and cell volume. The resulting structures were analyzed using VESTA software. Table 1 shows the lattice parameters that were calculated using the computational method at the appropriate pressure values.

Table 1. Lattice parameters at the respective pressure values

Pressure (GPa)	a (Å)	b (Å)	c (Å)	Rung angle (degree)	Leg angle (degree)
0	9.85	4.11	3.47	124.9	173.5
2	9.97	4.03	3.44	127.4	173.9
4	9.88	4.02	3.38	127.7	174.6
6	9.93	3.98	3.29	131.6	175.7
8	9.91	3.96	3.23	133.7	176.4
10	9.91	3.93	3.18	136.1	176.8
12	9.94	3.91	3.14	138.5	177.5
14	10.01	3.88	3.09	141.8	177.8

The compound exhibits expansion along ***a***, and contraction along ***b*** and ***c*** under pressure. Also the buckled structure approaches to a planar configuration under compression. The pressure vs. volume curve (Fig.1) fitted to the third-order Birch-Murnaghan equation of state (B-M EOS) [2] yields the bulk modulus of 57.6 GPa and its pressure derivative as 3.

$$P = \frac{3}{2}B_0\left[\left(\frac{V_0}{V}\right)^{\frac{7}{3}} - \left(\frac{V_0}{V}\right)^{\frac{5}{3}}\right]\left\{1 + \frac{3}{4}\left(B_0' - 4\right)\left[\left(\frac{V_0}{V}\right)^{\frac{2}{3}} - 1\right]\right\} \quad (1)$$

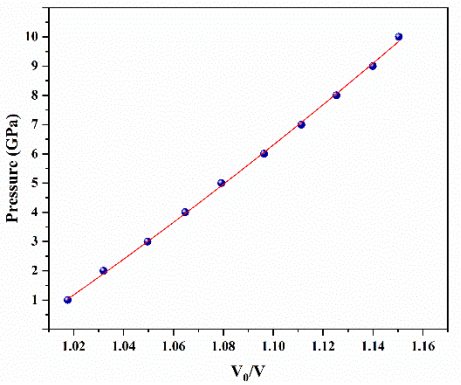

Fig.1. Pressure-volume curve fitted with B-M EOS

REFERENCES

[1] G. Kresse and J. Furthmüller, *Comput. Mater. Sci.* **6**, 1996.
[2] F. Birch, *Phys. Rev.* **71**, 1947.

Modification of Physicochemical and Optoelectronic Properties of CZTS Thin Films Using Post Deposition Treatments

Munjaji E. Dudhmal, Jayesh R. Pawar, Rajesh A. Joshi*

Thin films and Nanotechnology Laboratory,

Department of Physics,

Toshniwal Arts, Commerce and Science College, Sengaon Dist. Hingoli 431542 MS

*Corresponding Author: urajoshi@gmail.com

Abstract:

The CZTS thin films are widely studied for its potential optoelectronic application particularly as solar cell materials in combination with the other window materials like CdS etc. The optoelectronic properties of such heterojunction materials can be tailored/modified using post deposition techniques like annealing in air, ambient environment. In the present article CZTS thin films have been synthesized using the cost effective user friendly advanced chemical ion exchange method at room temperature on pre CdS deposited ITO glass substrate. These as deposited thin films are provided post deposition annealing treatments at 200, 300 and 400^0C and characterized for optoelectronic and physicochemical properties using X-ray diffraction technique, Raman spectrum analysis, Energy dispersive X-ray analysis along with surface morphology by scanning electron microscopy (SEM), the optical study conducted as absorbance mode. The results obtained in XRD have shown structural modification supported by the data obtained in Raman spectrum confirming annealing induced variation in composition and surface too as observed from SEM images. The optical absorbance has shown red shift in the absorbance peak may be inferred to compositional variations and updations.

EXPERIMENTAL INVESTIGATION OF ALUMINIUM OXIDE (Al_2O_3) DOPED YTTRIA STABILIZED ZIRCONIA (YSZ) THERMAL BARRIER COATINGS

Deva Priya P 1, Suresh Kumar J 2
Department of Mechanical Engineering, College of Engineering, Anna University Chennai
Email: sureshmitindia@gmail.com

Abstract: Thermal Barrier Coating (TBC) on IC Engine components were developed and manufactured from the last decade to maintain engine performance and decrease the emission rate. TBC is a ceramic layer coating provided on high temperature components which acts like a thermal insulation. pure Yttria Stabilized Zirconia (YSZ) coated on Aluminium alloy (AL 6061) is compared with three different compositions of Aluminium Oxide (Al_2O_3) doped with YSZ. The coating is done by Atmospheric Plasma Spray (APS) under the composition of (25%, 50% & 75%) Al_2O_3 and remaining YSZ. The Properties of the coating material under different tests for Wear, Bonding strength, SEM and Hardness test were evaluated

1. INTRODUCTION

The most commonly used TBC is Yttria stabilized Zirconate (YSZ) has its maximum operating temperatures limited to around 1200 °C. The efficiency of the IC-Engine increases with the increase in operating temperature and thus a TBC system needs to be developed that can operate at higher temperatures. Also according to studies made, Doped composites have better mechanical & thermal properties compared to un-doped one. So it seems that doping YSZ with Al_2O_3 can effectively increases the engine operating temperature and mechanical properties such as wear resistance. By employing doped materials the heat transfer rate inside the engine can be contained. Since only YSZ + Al_2O_3 coated material provide very good heat insulation compared to only YSZ coatings.

2. MATERIALS AND METHODS

Disk-shaped Aluminium 6061 with the dimension of 30mm in diameter and 20mm in thickness were used as the metallic substrate. Initially, the material was a cylindrical bar of 100mm length and 20mm thickness.

Figure 1 ceramic Coated Piston

3. EXPERIMENTAL METHODOLOGY

Before the Plasma Arc spraying process, to enhance the roughness of the sample surface, increase the mechanical bond between the deposited layer and substrate and consequently improve coating adhesion, the substrates have been sandblasted using alumina abrasive with the size of 125 μm at 80 psi air pressure and 100 mm standoff distance. METCO 3MB plasma spraying machine with Argon as primary plasma gas and hydrogen as the secondary gas was used to deposit the ceramic powders on the substrate.

4. RESULTS AND DISCUSSION

From the above graph the temperature distribution on the piston crown indicates, with 25% YSZ added with 75% Alumina has higher temperature withstand of 582.79 oC, whereas 75% YSZ added with 25% alumina has 565.95 oC and for 50% YSZ added with 50% Alumina is 569.06 oC which is all higher when compared to the uncoated sample values.

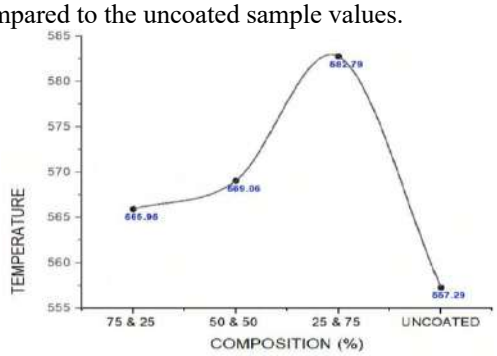

5. CONCLUSION

Results obtained show that 25% YSZ + 75% Al_2O_3 mixing proportion has less heat transfer rate from the piston crown to the bottom compared to the other coating composition by Adding Aluminium Oxide. The average Vickers hardness for the uncoated sample is 55.90 HV at 4.5 kg is the highest hardness value for the coated sample with YSZ and Al_2O_3. So hardness is improved by using Alumina as a major constituent to YSZ. This effect on hardness can be attributed to nanostructured stabilized zirconia powder which was plasma sprayed onto the aluminum substrate which increased the hardness.

REFERENCES

[1]. Keyvani, A., Saremi, M., Sohi, M.H., Valefi, Z., Yeganeh, M. and Kobayashi, A., 2014. Journal of alloys and compounds, 600, pp.151-158.

[2] Dai, H., Zhong, X., Li, J., Zhang, Y., Meng, J. and Cao, X., 2006. Materials Science and Engineering: A, 433(1-2), pp.1-7.

DEVELOPMENT OF TITANIUM HONEYCOMB SANDWICH STRUCTURE FOR THERMAL PROTECTION SYSTEMS IN HYPERSONIC VEHICLES

Suresh Kumar J 1, Kalaichelvan K 2
Department of Mechanical Engineering, College of Engineering, Anna University Chennai
Email: suresh@mitindia.edu

Abstract: The thermal protection system (TPS) is an essential structure in hypersonic aircraft skins as it prevents the hot air from entering vehicles. Sandwich structures are light weight structures with good mechanical properties can be integrated with TPS for application in hypersonic vehicles. Titanium alloy is used as the material to withstand the high temperature and also considering the formability in fabrication of honeycomb structure. The Ti-6Al-4V sheets were formed and brazed to fabricate the entire honeycomb structure. The fabricated structures were evaluated for their thermal resistance capability and these structures were good in high temperature applications.

1. INTRODUCTION

Recently there is a need for reusable launch vehicles which is facing lot of challenges in materials, design and propulsion. Titanium alloys are light weight and posses very good mechanical properties. Titanium sheets can be formed to fabricate the honeycomb sandwich structure. These structures are to be evaluated for extreme conditions such as high temperature environments. The usage of these materials under such environment has to be evaluated for their structural integrity. In this study the fabricated structure is tested for thermal resistance under high temperatures.

2. MATERIALS AND METHODS

Titanium alloy was used as the material for its good mechanical properties and very good formability.

Table 1. Chemical Composition of Ti-6Al-4V

Al	V	Fe	C	N	H	O	Ti
6.0	4.0	<0.30	<0.08	<0.05	<0.015	<0.20	Bal

The 0.5 mm thickness sheets were formed to half hexagonal structure using hot pressing process. Then these formed sheets were stacked one over another to form the hexagonal structure. The sheets were joined using vacuum brazing with the help of the soldering paste. The face sheets are also assembled to fabricate the entire honeycomb sandwich structure.

Figure 1 Die-set and Honeycomb structure

3. EXPERIMENTAL METHODOLOGY

The fabricated structures were tested for its thermal resistance. The testing was carried out in a furnace with One side of the skin is exposed to high temperature and other side skin temperatures were measured.

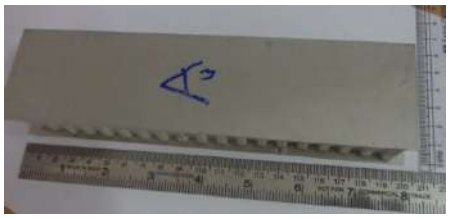

Fig.2. Ti-6Al-4V Honeycomb sandwich structure.

4. RESULTS AND DISCUSSION

The temperature time plot for the titanium honeycomb sandwich structure is shown in figure 3.

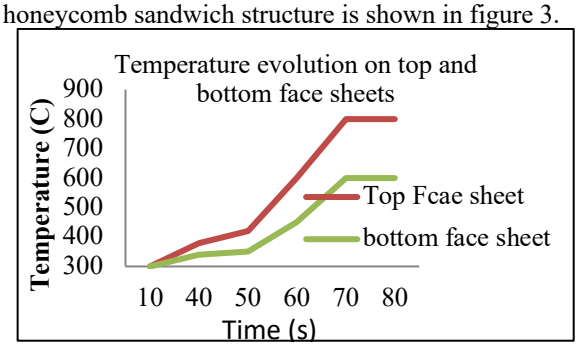

Figure 3 Temperature evolutions on top and bottom face sheets

From the figure it is clear the structure can be a good candidate for thermal resistance.

5. CONCLUSION

Ti-6Al-4V is the good candidate material for hypersonic aircraft skins due to its high thermal resistance capability. Further it can be formed to honeycomb structures to reduce its weight with very good mechanical properties.

ACKNOWLEDGEMENT

The financial support received under a grant-in-aid scheme from Structural division of Aeronautics Research Development Board (ARDB) is gratefully acknowledged [ARDB/01/2031830/M/I].

REFERENCES

[1]. Le, V.T., San Ha, N. and Goo, N.S., 2021. Composites Part B: Engineering, 226, p.109301.
[2] J, S. K., & K, K. (2024). International Journal of Crashworthiness, 29(6), 1011–1023.

Topic Code: Materials at High Temperatures and Thermal

Developing Empirical Relationship to Predict Hot-Wire TIG Welded Inconel 625 Alloy Using RSM and Machine Learning Approach

M.Reddeiah[1] S.Rajakumar[2] P.Hema[3] S.Kavitha[4] K. Devakumaran[5]

[1]Research scholar, [2,] Associate Professor, Department of Manufacturing Engineering, Faculty of Engineering and Technology, Annamalai University.

[3] Professor, Faculty of Engineering, S.V.University, Andhra, [4]Department of Electronics and Instrumentation Engineering [5]Deputy Manager,BHEL.Trichy

Corresponding Author Mail - **srkcemajor@gmail.com**

Abstract: HWGTAW is a modification of the traditional GTAW welding process. In this study, HWGTAW was used to weld Inconel 617 (Ni-Cr-Co-Mo alloy). Inconel 617 is a nickel-based super alloy that is widely used in high-temperature applications due to its excellent oxidation resistance, good creep strength, and excellent mechanical properties. This study focused on multi-pass welding of Inconel 617 pipes with a thickness of 12 mm and an outer diameter of 52.00 mm using HWGTAW. The core wire used in the experiment was ERNiCrMo-1. The main objective of this investigation is to optimize the HWGTAW parameters for enhancing the Mechanical properties and Microstructural Analysis bearing capability of Inconel 617 pipe joints for advanced Ultra supercritical (AUSC) power plants applications. The statistical response surface methodology (RSM) was utilized for generating strength prediction models (SPM) and validated using analysis of variance (ANOVA). The results from PSO were compared with RSM and the optimized input welding parameters for the electrode current, hot wire current and wire feed rate exhibited maximum ultimate tensile strength which was also confirmed from response and contour plots.

Keywords: Hot-Wire Gas Tungsten Arc Welding, Inconel, Hot Wire TIG Welding, Machine Learning.

1. INTRODUCTION

Inconel 617 (Ni–22Cr–12Co–9Mo) alloy (IN 617) is one of the candidate structural materials for next generation high temperature power plants. IN 617 is a solidsolution nickel-based superalloy with face-centered-cubic crystal. This superalloy has excellent creep strength at elevated temperature above 750 °C due to the effect of solution strengthening by the addition of Mo and Co, and also shows superior oxidation resistance at high temperature because of Al and Cr additions.

2. EXPERIMENTAL METHODOLOGY

The Inconel 617 was selected for experimental work, having an outer diameter of 52.27 mm and a thickness of 12 mm (as shown in Fig. 2). During welding, ErNiCrCoMo-1 filler metal with a diameter of 0.8 mm was provided. Samples was fabricated to measure through thickness weld-induced residual stresses at 180º in and around the weld start/end position of girth welded pipes. The welding procedure consists of the use of hot wire gas tungsten arc welding HW-GTAW processes. The welding was done in a horizontal rolled (1G) position, using pure argon shielding at a flow rate of 1 L/min in the case of welding. The HW-GTAW procedure only required 8 passes to finish the welding. In the case of welding process groove angle of 60º has been made with a root gap of 1 mm and root height of 1.5 mm. In the HW-GTAW process, the filler metal was preheated to 210 ◦C using the resistance heating method.

3. FIGURES AND IMAGES

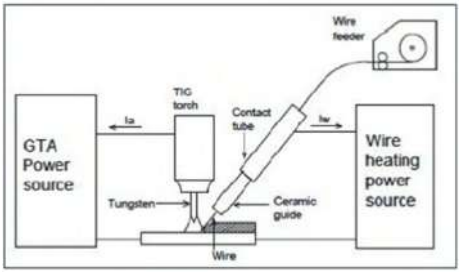

Experimental Set up

Schematic of the weld joint

4. TABLES

Table 1. Welding Process Parameters and their Levels (L4)

S.NO	Welding Current (amps)	Hot Wire Current (amps)	Wire Feed Rate (mm/sec)
1	150	70	1.5
2	150	100	2.0
3	180	70	2.0
4	180	100	1.5

Table 2. Mechanical Properties of the Weldments

Welding Current (amps)	Hot Wire Current (amps)	Wire Feed Rate (mm/sec)	Tensile Strength (Mpa)	Hardness (HV)
150	70	1.5	580.12	210
150	100	2.0	665.17	230
180	70	2.0	642.42	216
180	100	1.5	764.78	226

5. REFERENCE

[1] Silwal B, Walker J and West D. Hot-wire GTAW cladding: Inconel 625 on 347 stainless steel. Int J Adv Manuf Technol 2019; 102: 3839–3848.

[2] S. Sravan Sashank1 · S. Rajakumar2 · R. Karthikeyan3 "Influence of electrode current on mechanical and metallurgical characteristics of hot wire TIG welded SS304HCu austenitic stainless steel and P91 ferritic steel dissimilar joints"(2024)

[2]. S. Sravan Sashank1 · S. Rajakumar2 · R. Karthikeyan3 Kavitha Subramanian4 "Predicting hot wire tungsten inert gas welding parameters for joining P91 and 304HCu steel using multi-optimization techniques" 375-388 (2023).

[3] W. Mankins, J. Hosier, and T. Bassford: Microstructure and phase stability of Inconel alloy 617. Metall.Trans. 5(12), 2579 (1974)..

[4] Y. Guo, Z.B. Zhang, R.C. Zhou, S.F. Hou, B.H. Wang, Microstructure and mechanical properties of alloy 617B, Trans. Nonferrous Met. Soc. China (English Ed. 25 (2015) 1106–1113, https://doi.org/10.1016/S1003-6326(15)63704-9.

[5] R. Viswanathan, J. Henry, J. Tanzosh, G. Stanko, J. Shingledecker, B. Vitalis, and R. Purgert: US program on materials technology for ultra-supercritical coal power plants. J. Mater. Eng. Perform. 14(3), 281 (2005).

Experimental Characterization Diffusion Bonded Light Weight Blade-Rings for Aeroengine Application using Ti6Al4V Sheets with Ti6Al4V Wire Reinforcement

S Prakashkumar[1], S Rajakumar[2], S Sureshbabu[3]
[1-3,] Centre for Materials Joining and Research (CEMAJOR),
Department of Manufacturing Engineering, FEAT,
Annamalai University, Annamalai Nagar, Chidambaram, India-608002.
Email: srkcemajor@yahoo.com

Abstract: In this study, the lightweight Blade-Rings for Aeroengine Application using Ti6Al4V Sheets with Ti6Al4V Wire Reinforcement were bonded by using a solid state diffusion bonding process. The process parameters used to fabricate the lightweight Blade-Rings are bonding temperature of 700 C, bonding pressure of 50 MPa, and Holding Time of 60 Minutes. Mechanical and Metallurgical Characterization was carried. The experimental results showed that the bonded lightweight Blade-Rings have the TSFL of 38 kN, Bonding strength of 131 MPa, bonding ratio of 88.7 and reduction in thickness of 3.76 %. Bond interface Microstucture, Fracture surface and EDS analysis also revealed and the detailed results and discussion are presented in this paper.

1. INTRODUCTION

In this study, the lightweight Blade-Rings for Aeroengine Application using Ti6Al4V Sheets with Ti6Al4V Wire Reinforcement were bonded by using a solid state diffusion bonding process. The process parameters used to fabricate the lightweight Blade-Rings are bonding temperature of 7000 C, bonding pressure of 50 MPa, and Holding Time of 60 Minutes. Mechanical and Metallurgical Characterization was carried.The experimental results showed that the bonded lightweight Blade-Rings have the TSFL of 38 kN, Bonding strength of 131 MPa, bonding ratio of 98.7 and reduction in thickness of 3.76 %. Bond interface Microstucture, Fracture surface and EDS analysis also revealed and the detailed results and discussion are presented in this paper.

2. EXPERIMENTAL METHODOLOGY

Then the specimens to be bonded were placed in the high temperature (capacity 1600°C) diffusion bonding equipment comprised of a heating chamber under a vacuum environment with a sophisticated hydraulic pressurizing unit. After the completion of the diffusion bonding process, the specimen for microstructural examination and mechanical tests (lap shear test and ram tensile test) were extracted from the bonded specimen.

2.1. Equations

the thickness ratio was calculated based on the Equation.

Bonding ratio (%) = $((x_1+x_2+x_3\ldots.x_n)/l) \times 100$ .....(1)

3. FIGURES AND IMAGES

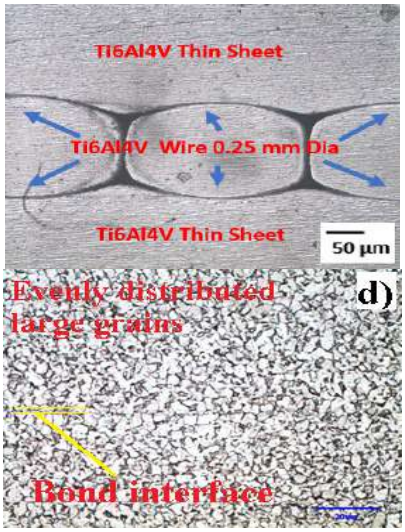

Microstructure of bonded lightweight Blade-Rings without carbon fibre reinforcement

4. TABLES

Table 1. Hot Tensile properties of MIM PAW welded Inconel 625 butt joints at different test temperatures.

Bonding temperature (°C)	Bonding pressure (MPa)	Holding time (minutes)	TSFL (kN)	Bonding strength (MPa)	Bonding ratio (%)
700	50	60	38	131	88.7

5. REFERENCING

[1] Pilling, J., Livesey, D.W., Hawkyard, J.B., and Ridley, N., "Solid State Bonding in Superplastic Ti-6Al-4V," Metal Science 18(3):117-122, 1984, https://doi.org/10.1179/msc.1984.18.3.117.

[2] Li, H., Li, M., Yu, W.-X., and Liu, H.-B., "Significance and Interaction of Bonding Parameters with Bonding Ratio in Press Bonding of TC4 Alloy," Rare Metals 35(3):235-241, 2014, https://doi.org/10.1007/s12598-014-0330-3.

Topic Code: Computational Materials Science in Extreme Conditions

Ab-initio study of SiC, Ti and V-doped SiC nanotubes for gas sensing application

***Nikhil M. Solanki* 1, *Suresh V. Chaudhari* 2, *Sanjeev K. Gupta* 3, *P. N. Gajjar* 4, ***

Affiliation, Address: [1,2,4] Department of Physics, University School of Sciences, Gujarat University, Ahmedabad 380 009, India
[3]Computational Materials and Nanoscience Group, Department of Physics, St. Xavier's College, Ahmedabad 380 009, India

Email: pngajjar@gujaratuniversity.ac.in
nikhilsolanki2708@gmail.com

Abstract: In response to the unprecedented advancement in the gas sensing technology, we have examined the effect of some noxious oxide gases such as CO and NO in the vicinity of bare SiC and transition metal such as Ti and V doped SiC nanotube (NT) using DFT calculations. First, for the structural stability point of view, we computed cohesive energy for bare SiCNT and formation energies for Ti/V SiCNT. The negative values of both energies ascertain the structural stability. The bare SiCNT is indirect semiconductor having 2.12 eV bandgap, while, the presence of Ti and V adatoms reduced this bandgap. Further, for the gas sensing ability and adsorption tendency of aforementioned NT is validated by parameters such as adsorption energy of gases, charge transfer and desorption time. Adsorption energies of CO/NO gases on aforementioned systems are -0.33 eV/-0.70 eV, -1.89 eV/-4.26 eV and -1.28 eV/-5.62 eV, respectively. From the analysis of adsorption energies, revealing that the effect of adatoms increase the sensitivity of the systems with chemisorption towards noxious gases, concurrently higher adsorption tendency for NO gas. Furthermore, the desorption times of CO and NO on these NTs are quite large (10^{9} to 10^{83} second), indicating the strong interaction, which allows the NT to detect even low concentrations of CO and NO gases. These interesting results of CO and NO gas sensing study on the bare and functionalized SiCNT, suggesting that these SiCNT based sensors can serve as good sensing devices for CO and NO gases.

Topic Code: Computational Materials Science in Extreme Conditions

Exploring thermal effects on dynamic uniaxial compression of single-crystal tungsten using molecular dynamics

A. Abhijith[1,2], K. Basavaraj[1,2], Anuradha S. Dwivedi[1,2], Apu Sarkar[1,2], Aditi Ray[1,2]
[1] Bhabha Atomic Research Centre, Mumbai-400085, India
[2] Homi Bhabha National Institute, Mumbai-400094, India
Email: (aabhijith@barc.gov.in)

Abstract: Molecular dynamics simulations are performed to investigate the mechanical response of single-crystal tungsten (W) under uniaxial compression along [001] crystallographic direction. Study examines the influence of elevated temperatures on stress-strain behavior, for strain rates relevant to shock compression. Observed reduction in yield and flow stress with temperature rise is explained from dislocation-based plasticity mechanism.

1. INTRODUCTION

The growing demand for materials with superior thermomechanical properties is driven by advancements in space exploration, fusion power, defense, and impact shielding. These applications often involve dynamic compression at ultrahigh strain rates, highlighting the need for a deeper understanding of thermomechanical responses and plastic deformation under such conditions. W, a refractory metal known for its exceptional mechanical strength, high melting point, and heat resistance, displays unique behavior under dynamic compression due to its complex microstructure and interatomic bonding. While uniaxial compression of W has been extensively studied for quasi-static and dynamic loading with strain rates up to 10^3/s [1, 2], its performance under ultrahigh strain rates, particularly in ballistic impact scenarios, remains largely unexplored. This study focusses on the thermal softening of single-crystal (sc) W under uniaxial compression at strain rate of 10^8/s.

2. METHODOLOGY

Simulations are conducted using molecular dynamics code LAMMPS [3], employing EAM potential of Olsson [4], which has successfully reproduced experimental shock Hugoniot data. The simulation box (24 nm × 24 nm × 48 nm along x, y, z axis) contains ~1.7 million atoms. Uniaxial compression is applied along [001] crystallographic direction aligning it with z-axis, while lateral directions (x and y) are held at zero pressure using NPT ensemble. Dislocation extraction algorithm as implemented in OVITO [5] is used for illustration and quantification of dislocations.

3. RESULTS AND DISCUSSIONS

The stress-strain curves for initial sample temperatures of 300 K, 700 K and 1500 K, presented in Fig. 1, exhibit a similar trend: stress increases almost linearly up to a peak value, then drops abruptly at the onset of plasticity, followed by plastic flow. Significant reduction in yield stress (~50%) is observed as the temperature rises from 300 K to 1500 K, with onset of plasticity shifting to lower strains for higher temperatures. Atomistic visualization of dislocations (Fig. 2), a signature of plastic deformation at high strain rate, reveals a dense dislocation network at 300 K, composed of both screw and edge line segments, which consistently diminishes with increasing temperature, demonstrating thermal softening. Corresponding dislocation density, shown in Fig. 1 (right axis), exhibits an order of magnitude decline from 300 K to 700 K, with minimal further reduction at higher temperatures, indicating that random thermal defects like vacancies and interstitials do not necessarily promote dislocation nucleation.

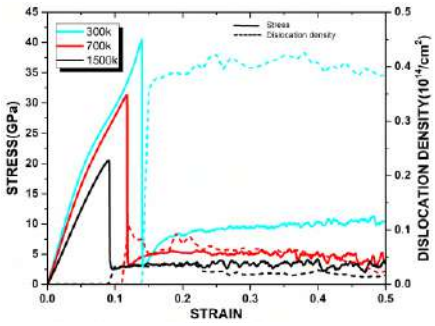

Fig. 1. Engineering stress-strain curve (solid) and strain-dependent dislocation density (dashed) of sc-W at a strain rate of 10^8/s for 300 K, 700 K and 1500 K.

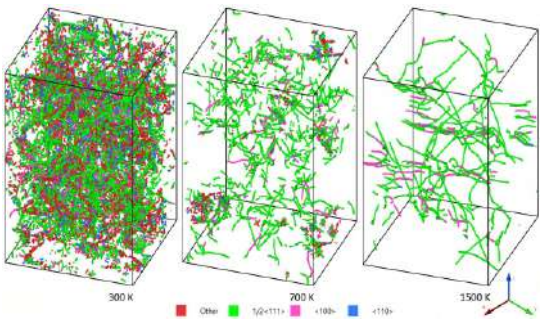

Fig. 2. Atomistic visualization of dislocation network for three different temperatures at strain of 0.2.

REFERENCES

[1] Q. Wei et al, Acta Materialia **54** (2006) 77.
[2] C.C. Zhu et al., J. Nucl. Mater. **469** (2016) 120.
[3] A. P. Thompson et al., Comput. Phys. Commun. **271** (2022) 108171.
[4] P. A. T. Olsson, Comput. Mater. Sci. **47** (2009) 135.
[5] A. Stukowski, Modell. Simul. Mater. Sci. Eng. **18** (2010) 015012.

Topic code: Computational Materials Science in Extreme Conditions

Optical properties of the NiB_6 monolayer*: In silico* study

Suresh V. Chaudhari 1[a], Nikhil M. Solanki 2[a], Sanjeev K. Gupta 3[b], P. N. Gajjar 4[*a]

[a]Department of Physics, University School of Sciences, Gujarat University, Ahmedabad 380009, India

[b]Computational Materials and Nanoscience Group, Department of Physics and Electronics, St. Xavier's College, Ahmedabad 380 009, India

Corresponding author: pngajjar@gujaratuniversity.ac.in

Abstract: NiB_6, is 2D atomically thin monolayer (ML) with Ni at centre coordinated with six boron atoms to make hexa-coordination. The calculated value of cohesive energy for the ML indicates its chemical stability while the ab-initio molecular dynamic (AIMD) simulation suggesting its thermal stability. From the electronic band structure computation, it can be concluded that ML exhibits metallic behaviour (Zero bandgap material) with formation of two *Dirac* cones near high symmetry k-points, showing graphene equivalent carrier mobility. In the present study, we have explored the optical response of the ML to check various optical properties like reflectance, transmission, absorption coefficient, real and imaginary dielectric constant etc. Owing to the zero band gap of the ML, it shows various peaks for reflectance in the wide range of spectrum, however peaks in the UV region are distinct. In the case of absorption coefficient, which is measure of absorption of electromagnetic radiation in the material, counter part of the reflectance with inverse behaviour. Hence, the broadband light absorption of ML allows for the development of high-speed and sensitive photodetectors operating across a wide spectral range.

Electrical and Thermoelectric properties of Bi_2Te_3 and Sb_2Te_3 single crystals

Nabarun Bera[1], Ayush Ramchandra Mokashi[1], Anoop M. D.[2], Sachin Sharma[1], Nisha Yadav[3], Deepika Kanwar[1], Balram Tripathi[4], D. K. Shukla[5] and Manoj Kumar[1*]

[1]Department of Physics, Malaviya Institute of Technology Jaipur (302017), India.

[2] Department of Advanced Science and Technology, Toyota Technological Institute, Nagoya, Aichi 468-8511, Japan.

[3]Malla Reddy Engineering College for Women Maisammaguda, Secunderabad (500100), India.

[4] S. S. Jain Subodh PG College Jaipur (302004), India.

[5]UGC-DAE Consortium for Scientific Research, Khandwa Road, Indore (452017), India

Email: mkumar.phy@mnit.ac.in

Abstract: Bismuth/Antimony Chalcogenides are well-known Thermoelectric materials as well as Topological insulators. The present article concerns itself with the synthesis, characterization, and analysis of the electronic and thermal transport properties of Sb_2Te_3., $BiSbTe_3$, and Bi_2Te_3. Rietveld refinement of x-ray diffraction data estimates the variation of lattice parameter for a=b from 4.261Å to 4.576 Å and unit cell volume from 478.67 $Å^3$ to 542.01 $Å^3$ while going from Sb_2Te_3 to Bi_2Te_3. Resistivity vs. temperature measurement between 4K-300K shows the metallic nature of all three crystals with a Fermi Liquid type behaviour below 50K. Magnetoresistance (MR) measurement yields nonsaturating linear type behaviour where MR% as high as 140% at 2K and 9Telsa was obtained for $BiSbTe_3$ with a signature of quantum oscillations above 5Tesla. Seebeck Coefficient measurement in the temperature range 10-240K shows all samples having positive Seebeck Coefficient throughout the temperature range and rises to a value as high as 250 μVK^{-1} for Bi_2Te_3 and $BiSbTe_3$, which is higher than the reported room temperature value for these materials.

1. INTRODUCTION

It's been known that inter-metallic compounds like Bi_2Te_3, $BiSbTe_3$, and Sb_2Te_3 [1]exhibit topological order. They possess gapless and robust surface states [2], which are protected by time-reversal symmetry [3] The existence of these surface states can prove vital in gauging the properties of these materials. The observed transport phenomena are analysed using the Boltzmann transport theory, Landauer formalism, and Fermi liquid theory. In doing so, we employ a combination of theoretical modelling and experimental characterization, enabling us to predict the behaviour at both low and high-temperature ranges. As we go to the low temperature, phonon scattering reduces considerably, helping to cite any contributions to the transport properties due to the existence of surface states.

2. EXPERIMENTAL WORK

2.1. Experimental Work & Material Characterization

Bi_2Te_3, $BiSbTe_3$, and Sb_2Te_3 were synthesized using the modified Bridgman method. [4] Scanning Electron Microscopy (SEM) and Energy Dispersive Spectroscopy (EDS) confirm the desired morphology and Homogenous Elemental Distribution. Rietveld analysis of x-ray diffraction (XRD) data affirms the formation of Rhombohedral crystal structure with Space Group R-3m.

3. RESULTS AND DISCUSSION

All samples show metallic behavior in their resistivity in the temperature range of 4K-300K shown in Fig1(a)..Their Resistivity behavior between 4-55K can be explained using Fermi Liquid theory. [5] Magnetoresistance was measured up to a field of 9Tesla at 2K, 5K,10K, and 50K temperatures that exhibits linear non-saturating MR at high field suggestive of the topological nature of the samples along with Quantum oscillations for $BiSbTe_3$. [6,7]Thermopower measurements in the temperature range of 10K-240K given in Fig1(b) show monotonic increase of Seebeck coefficient with temperature with a value of Seebeck coefficient of 256,250,80 μVK^{-1} at 240K for Bi_2Te_3, $BiSbTe_3$ & Sb_2Te_3 respectively.

3. FIGURES AND IMAGES

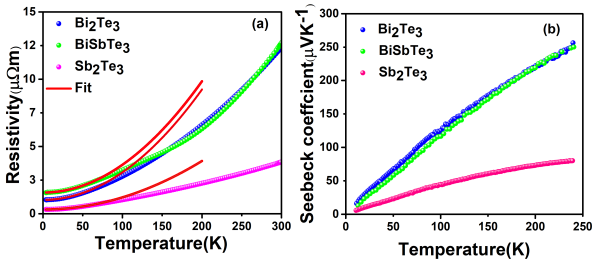

Figure1. (a)Resistivity vs Temperature (b)Seebeck coefficient vs Temperature

REFERENCES

[1]J. E. Moore, Nature **464**, 194 (2010).

[2]L. Fu and C. L. Kane, Phys. Rev. B - Condens. Matter Mater. Phys. **76**, 1 (2007).

[3]L. Fu, C. L. Kane, and E. J. Mele, Phys. Rev. Lett. **98**,1 (2007).

[4]M. D. Anoop *et al.*, Mater. Today Proc. **31**, 616 (2019).

[5]H. K. Pal, V. I. Yudson, and D. L. Maslov, Phys. Rev.B Condens. Matter Mater. Phys. **85**, 2 (2012).

[6]X. Wang *et al.*, Phys. Rev. Lett. **108**, 1 (2012).

[7]K. Shrestha *et al.*, Phys. Rev. B **95**, 1 (2017).

Analysis of AC Losses in High-Temperature Superconducting Tapes Using a Magnetic Formulation Based on the Thin Shell Model

Garkki B[1] and Revathi S[1]*
[1]Department of Electrical and Electronics Engineering
[1]National Institute of Technology Puducherry, Karaikal, India, 609609.
***Corresponding author: revathi.s@nitpy.ac.in**

Abstract:

The second-generation (2G) Yttrium Barium Copper Oxide (YBCO) superconducting tape is preferred for designing high-temperature superconductor (HTS) magnets due to its superior critical characteristics. However, the properties of HTS magnets are significantly affected by increasing AC losses. In this study, thin cuts are introduced to optimise the current injection into HTS tapes, aiming to reduce these losses. A thin-shell model is employed to analyse the magnetic behaviour and calculate the AC losses in the HTS tape. The proposed models are validated against the conventional H-formulation and T-A formulation, demonstrating their effectiveness in accurately estimating AC losses. In addition, analysed the magnetic field distribution and current density for HTS stacks. The results ensure that the proposed approach enhances the precision of AC loss calculations for HTS tapes, contributing to the development of a more efficient superconducting magnet system.

Keywords: High-temperature superconductors (HTS), AC losses, Yttrium Barium Copper Oxide (YBCO), Magnetic formulation

Atomic scale study of defects in Fe_2CrAl Heusler compounds

Ravi Kumar Yadav[1], R.Govindaraj[1], K Vinod[1] and V.Srihari[2]
[1]Materials Science Group, Indira Gandhi Centre for Atomic Research, HBNI,Kalpakkam-63102
[2]H P & SRPD, Bhabha Atomic Research Centre, Trombay, Mumbai 400085, India
Email:govind@igcar.gov.in

Abstract: Bulk structural studies using X-ray diffraction (XRD) indicate the presence of A2 type of disordering in the lattice of Fe_2CrAl. Significant deviation from Slater- Pauling rule has been observed. Curie temperature of the system has been found to be around 240K using bulk magnetic studies. Mössbauer studies with respect to Fe sites confirm the presence of significant structural as well magnetic disorders in Fe_2CrAl.

1. INTRODUCTION

Heusler compounds have potential to exhibit 100% spin polarization due to half metal ferromagnetism (HMF) and spin gapless semiconducting (SGS) nature which make them suitable candidate for spintronic applications [1]. General formula for full Heusler ternary compounds is X_2YZ where X and Y are transition metals and Z is the main group element. In the unit cell of $L2_1$ ordered (most desired structure) Heusler compounds, Z atoms occupy 4a (0,0,0) Y atoms occupy 4b (½,½,½) and X atoms occupy 8c (¼,¼,¼) Wyckoff sites with space group $Fm\bar{3}m$. In $L2_1$ ordered Heusler system, Slater Pauling (SP) rule predicts the total magnetic moment per formula unit as M_s/f.u. = $(Z_t\text{-}24)$ μ_B/f.u where Z_t is total no. of valence e^- in one f.u. [2]. SP rule is essential condition for HMF and SGS behaviour in Heusler systems for their spintronic applications. However, Heusler systems are susceptible to exhibit multiple types of lattice disorders such as B2, A2, $CuHg_2Ti$ type and $D0_3$ affecting their magnetic and spintronic properties. Hence, understanding of the lattice disordering in such type of systems is very crucial for tailoring magnetic as well as spintronic properties. Heusler compound Fe_2CrAl also has been predicted to HMF assuming $L2_1$ structure by Galanakis et al However, it does not follow SP rule with Curie temperature (T_c) ~240K but magnetisation does not become zero even up to 300K which indicate the possibility of ferromagnetic (FM) clusters in Fe_2CrAl [3]. These FM cluster can lead to local FM fluctuations in the matrix at atomic level Therefore, insight about these kinds of magnetic disorders can be obtained using local probes which are sensitive to both, structural as well magnetic properties at atomic level. Hence, Mössbauer spectroscopy (MS), being very sensitive tool to local structural and magnetic environment have been utilised to investigate structural and magnetic ordering/ disordering at atomic level in Fe_2CrAl Heusler system.

2. EXPERIMENTAL DETAILS

Fe_2CrAl Heusler compound has been prepared using arc melting. Angle dispersive XRD beamline -11 (BL-11) at Indus-2, synchrotron source, RRCAT) India in transmission mode has been utilised for bulk structural studies with wavelength (λ) 0.4952Å. Bulk magnetic studies have been carried out using vibrating sample magnetometer (VSM).

3. RESULTS AND DISCUSSIONS

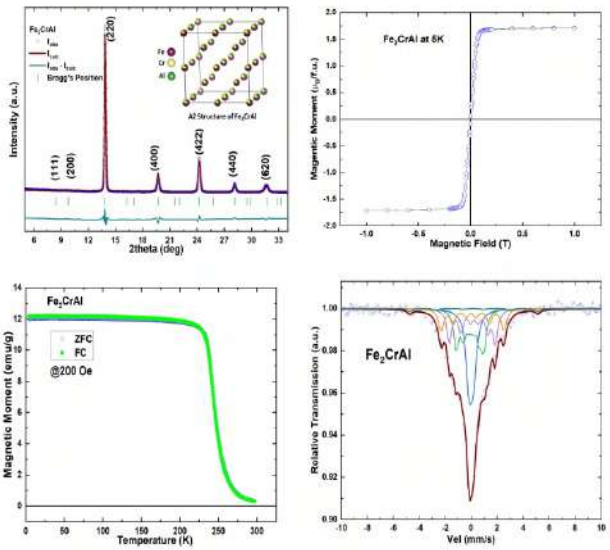

Fig.1 :.XRD pattern, variation of Magnetic moment with respect to magnetic field & temperature and Mössbauer spectrum of Fe_2CrAl at room temperature.

The Rietveld-refined XRD pattern of Fe_2CrAl, shown in Fig. 1, indicates the absence of (111) and (200) peaks, confirming dominant A2-type disorder in the system. The lattice parameter is determined to be 5.81 Å. The magnetic moment per formula unit (M_s/f.u.) for Fe_2CrAl is found to be 1.75 μ_B/f.u., deviating significantly from 1 μ_B/f.u. as predicted by the Slater-Pauling (SP) rule. The Curie temperature of the system is approximately 240 K, but magnetization remains nonzero even at 300 K. Mössbauer studies further confirm structural and magnetic disorder at room temperature, with evidence of ferromagnetic clusters in the sample.

Hence, it is concluded that Fe_2CrAl Heusler system exhibit the A2 type of lattice disordering which in turn results the significant deviation from SP rule as well as formation of ferromagnetic cluster beyond its T_c.

REFERENCES

[1]. X. L. Wang, Phys. Rev. Lett., (2008), **100**, 1–4.
[2]. I. Galanakis et al PRB (2002) **66**, 174429
[3]. M.Zhang et al Journal of Magnetism and Magnetic Materials (2004) **283,** 409–414.

Topic- Material Properties at Low-Temperature and Quantum Materials

Evolution of transport regimes from classical to quantum in $Bi_{1.95}Sb_{0.05}Se_3$ thin film by substrate Temperature

Shivani Soni[1,2], Edward Prabu Amaladass[1,2], Jegadeesan P[1], S. Amirthapandian[1,2], Kishore Kumar Madupu[1,2], Ramanathaswamy Pandian[1,2], Awadhesh Mani[1,2]

[1]*Material Science Group, Indira Gandhi Centre for Atomic Research, Kalpakkam, 603102*
[2]*Homi Bhabha National Institute, Training School Complex, Anushaktinagar, Mumbai, 400094*

E-mail: edward@igcar.gov.in

Abstract: We report the transition of transport phenomena from a classical behaviour characterized by a parabolic magnetoresistance ($\propto B^2$) to quantum behaviour characterized by weak antilocalization (WAL) in Sb-doped Bi_2Se_3 thin films grown using pulsed laser deposition (PLD) at different substrate temperature. The classical B^2 dependence of resistance arises from dominant bulk carrier contributions, while the WAL signature is attributed to strong spin-orbit coupling inherent to the topological surface states of Sb-doped Bi_2Se_3. The substrate temperature during deposition significantly influences the film's structural and electronic properties, impacting the interplay between bulk and surface transport mechanisms. At higher substrate temperatures, improved crystallinity and reduced defect density enhance surface state coherence, promoting quantum interference effects responsible for WAL. Conversely, lower substrate temperatures lead to increased disorder, resulting in stronger bulk carrier scattering and classical behaviour.

1. INTRODUCTION

Topological insulators (TIs) are characterized by insulating bulk states and topologically protected surface states, making them ideal candidates for spintronics and quantum computing[1,2]. Bi_2Se_3 is particularly notable for its well-defined bandgap and robust surface states. Here we have studied the role of substrate temperature on the electronic properties of Sb-doped Bi_2Se_3 thin films.

. 2. RESULT AND DISCUSSION

Films were deposited on a Si/SiO_2 substrate using PLD at substrate temperatures of 200°C, 250°C, 300°C, and 350°C. GI-XRD confirmed the rhombohedral phase of Bi_2Se_3, along with peaks corresponding to Sb_2Se_3. Scanning electron microscopy analysis in Fig.1 (a-d) reveals higher grain density for samples prepared at lower substrate temperatures of 200°C and 250°C, whereas the grain density drastically reduces for samples prepared at 300°C and 350°C. Temperature dependence of resistance is shown in Fig.1 (e-h) also depicts a transition from insulating to metallic behaviour as the substrate temperature increases. The calculated carrier density deduced from Hall data ranged from 1.41×10^{19} cm^{-3} to 1.62×10^{20} cm^{-3}. Magnetoresistance data displayed a transition from classical behaviour to WAL behaviour as the substrate temperature increases Fig.1 (i). The Hikami Larkin Nagaoka analysis yielded (α) of 6 and 5, with phase coherence lengths (L_ϕ) ranging from 50 nm to 160 nm. These features can be explained using the Ioffe-Regel criterion deduced using Eq. 1. For films prepared at lower temperatures, $k_F\ell<1$, indicating strong scattering and localization, resulting in insulating behaviour. Whereas films deposited at higher temperatures, $k_F\ell>1$, signifying reduced disorder and delocalized electronic states, leading to metallic behaviour.

$$K_f l_e = \frac{\hbar(3\pi^2)^{2/3}}{e^2 n^{0.33}} \quad \text{---------- Eq. 1}$$

3. FIGURES AND IMAGES

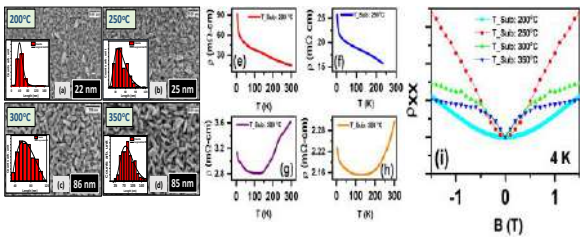

Figure 1. SEM images (a-d), temperature-dependent resistivity (e-h), comparison of MR data at 4 K (i,)

4. CONCLUSION

The study highlights the critical role of substrate temperature in Sb-doped Bi_2Se_3 films grown via PLD. Higher temperatures enhance crystallinity, reduce grain boundary scattering, and drive an insulating-to-metallic transition. Hall measurements confirm n-type carriers, while magnetoresistance analysis revealed a transition from classical quadratic behaviour to WAL.

6. REFERENCES

[1] Hasan M Z and Kane C L 2010 Colloquium: Topological insulators *Reviews of Modern Physics* **82** 3045-67

[2] Fu L, Kane C L and Mele E J 2007 Topological Insulators in Three Dimensions *Physical Review Letters* **98** 106803

Compositional Dependence of Magnetic Transition in Double Perovskite $Ho_2MnNi_{1-x}Cu_xO_6$ Systems

V R Pooja, A T Sathyanarayana, K Vinod and Awadhesh Mani
Materials Science Group, Indira Gandhi Centre for Atomic Research, A CI of Homi Bhabha National Institute, Kalpakkam, 603102, Tamil Nadu, India
Email: atsatya@igcar.gov.in

Abstract: The effect of Cu substitution at the Ni site on the magnetic behaviour of double perovskite Ho_2MnNiO_6 has been investigated. Room temperature XRD results show a systematic increase in the monoclinic lattice parameters implying that Cu substitutes into the lattice. The paramagnetic (PM) to ferromagnetic (FM) transition temperature (T_C), the Curie-Weiss temperature (Θ_C) and the effective magnetic moment (μ_{eff}) exhibit a systematic decrease with increase in Cu content.

1. INTRODUCTION

Double perovskites $A_2BB'O_6$ received renewed interest due to their interesting structural, electronic, magnetic and multi-ferroic behaviour [1]. The presence of multiple transition metal cations, different valencies and also their order/disorder can give rise to intriguing structural, electronic and magnetic properties. R_2NiMnO_6 (R = La, Pr, Nd, Sm, Gd, Tb, Dy, Y, and Ho) is one of the interesting series of compounds in which the ordering of cations exhibits ferromagnetic ground state due to super-exchange interaction between the Ni^{+2} and Mn^{+4} ions. By changing the radius of rare-earth R^{+3}ion, the transition temperature (T_C) can be systematically changed viz., from 270 K for La_2MnNiO_6 to 80 K for Ho_2MnNiO_6 [2]. We have investigated Cu substituted Ho_2MnNiO_6 in order to explore the effect of ionic radius, and change in spin state of B' cation on the magnetic transition.

2. EXPERIMENTAL METHODS

Poly-crystals of $Ho_2MnNi_{1-x}Cu_xO_6$ were prepared by solid state reaction method. Structural characterization was carried out by X-ray diffraction using STOE (Germany) diffractometer employing Cu Kα radiation. The magnetization measurements were performed using commercial Quantum Design make SQUID vibrating sample magnetometer.

3. RESULTS AND DISCUSSION

XRD analysis of the samples indicates that the crystallographic structure is consistent with monoclinic structure with space group $P2_1/n$ for all compositions (x). It is observed that the lattice parameters a, b and c systematically increase with increase x whereas the monoclinic angle β is found to be nearly constant. The increase in lattice parameters is expected as the ionic radius of Cu^{+2} ion (0.73 Å) is greater than the Ni^{+2} ion (0.69 Å) in the octahedral coordination. Magnetization measurements indicate a ferromagnetic (FM) to paramagnetic transition (T_C) that systematically shifts to lower temperatures with increase in x as shown in the inset of Figure 1a. The Curie-Weiss (CW) analysis in the PM region (see Figure 1b) indicates reduction of CW temperature Θ_C and effective magnetic moment μ_{eff} with increase of Cu content. The observed non-linear behavior of χ^{-1} for temperatures below 125 K, and larger values of observed μ_{eff} than the theoretically calculated values manifest the short-range magnetic interactions in the PM region. The increase in the lattice parameters with increase in Cu content and the smaller moment of Cu^{+2} ion as compared to Ni^{+2} ion reduce the strength of super exchange interaction which may be responsible for the reduction in T_C in these systems.

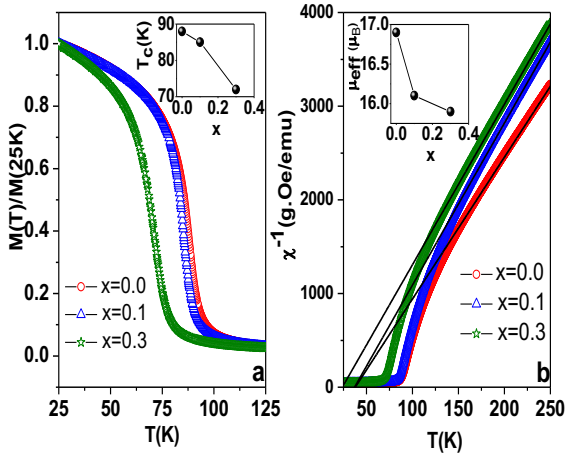

Fig.1. (a) Normalized magnetization (b) χ^{-1}vs T for different x of $Ho_2MnNi_{1-x}Cu_xO_6$ systems. The insets exhibit variation of T_C and μ_{eff} as a function of composition.

ACKNOWLEDGEMENT

The authors acknowledge Dr R Nithya for XRD measurements and UGC-DAE-CSR, Kalpakkam node for magnetization measurements.

REFERENCES

[1]. S Vasala et.al. Prog. Solid State Chem. **43** (2015) 1.
[2]. Tirthankar Chakraborty, et.al. J.Phys.: Condens. Matter **29** (2017) 025804.

Superconducting and Non-Superconducting States in $Nd_{1.85}Ce_{0.15}CuO_{4\pm\delta}$: Impact of Argon Annealing

Vinita Kumawat[1*], Riya Sindhwani[1], K. Vinod[1], Kishore Kumar Madupu[1], T. Geetha Kumary[1], Awadhesh Mani[1,2,]

[1]Materials Science Group, Indira Gandhi Centre for Atomic Research, Kalpakkam – 603 102, India

[2]HomiBhabha National Institute, Anushakthi Nagar, Mumbai, Maharashtra, India – 400 094

***vinitak@igcar.gov.in**

Abstract: In the present work, the role of Argon annealing in inducing superconductivity in the bulk $Nd_{1.85}Ce_{0.15}CuO_{4\pm\delta}$ (NCCO) system is studied. Additionally, thin films of superconducting NCCO were prepared by pulsed laser deposition method, followed by ex-situ annealing in argon atmosphere. Structural and electrical characterizations were performed on the films. Resistivity measurements demonstrated superconducting behaviour in the argon annealed thin film.

1. INTRODUCTION

In the electron doped superconductor $Nd_{2-x}Ce_xCuO_{4\pm\delta}$, superconductivity is observed within a specific range of cerium doping of $0.14 \leq x \leq 0.18$. The compound is reported to exhibit the largest superconducting critical temperature (T_C = 24 K) for x ~ 0.15[1]. The study of thin films of NCCO is often constrained by challenges in sample preparation, particularly with respect to the critical levels of Ce content and oxygen vacancies needed to induce superconductivity in this system. The present work aims to explore the role of Argon annealing in inducing superconductivity in the NCCO system; both in bulk and thin films.

2. EXPERIMENTAL

Bulk NCCO samples were synthesized via the solid-state reaction method, followed by Argon annealing. Thin films were prepared by pulsed laser deposition on (100)-oriented $SrTiO_3$ substrates and are subjected to different annealing procedures [2]. The samples were characterized using X-ray diffraction (XRD) and Raman spectroscopy. Temperature (T) dependence of resistance (R) measurements were performed using a dipstick, in the temperature range 4.2 K to 300 K.

3. RESULT AND DISCUSSION

The *R vs. T* data for the bulk NCCO before and after Argon annealing is shown in figure 1(a). The figure clearly indicates the necessity of Ar annealing in inducing superconductivity in the system. The bulk NCCO system before Ar annealing exhibits semiconducting nature in the entire temperature range studied. After Ar annealing the NCCO exhibits superconductivity, with the superconducting transition temperature around 25 K (T_{Conset}).

For bulk NCCO, the XRD measurements indicates tetragonal T' structure (space group 14/mmm), with lattice parameters $a = b = 3.945$ Å and $c = 12.082$ Å. No significant change in the lattice parameters was observed before and after Ar annealing of the NCCO bulk. However, a noticeable difference is observed in the Raman spectra (excited by a 532 nm laser) before and after annealing, as shown in fig. 1(b). The peak at 582 cm^{-1}, likely associated with the vibration of O and Cu in the CuO_2 planes, sharpens after Ar annealing. This may be indicating that the reduction process causes the localized electrons near the Nd/Ce sites to transfer to the CuO_2 planes, thereby converting them into free electrons [3], which has to be corroborated by other experiments.

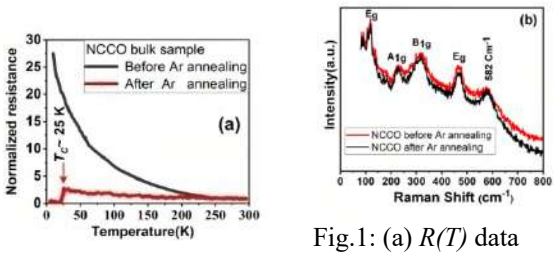

Fig.1: (a) *R(T)* data and (b)Raman data of bulk NCCO

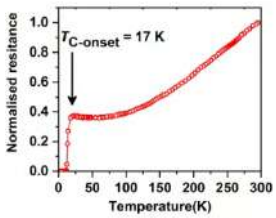

Fig. 2: *R vs. T* data for NCCO thin film.

The thin films (*R vs. T* data shown in Fig 2) exhibited a superconducting transition temperature of 17 K after vacuum annealing at 750°C and protect Ar annealing [2].

4. CONCLUSION

As prepared bulk NCCO exhibits semiconducting and becomes superconducting only after a specific reducing annealing process. By following an annealing method, superconducting thin films of NCCO system also prepared.

REFERENCES

[1]. Y. Tokura, H. Takagi, and S. Uchida, Nature 337, 345 (1989).

[2]. Horio M, *et.al.* Nature Communications, **7,** 10567 (2016)

[3]. Meng-Yan Shen and Shu-Lin Zhang,Physica C 196(1992)

Cryogenic Testing of Niobium Material for Superconducting RF Cavity Applications using the RRR measurement Technique

Anand Yadav*, Vinesh K. Verma, Ajay Yedle, Suresh Maloth, Vikas K. Jain, Sanjay Chouksey & Mahendra Lad.

Superconducting Cavity Development Division, Proton Accelerator Group
Raja Ramanna Centre for Advanced Technology, Indore - 452013, India

**E-mail ID: anandyadav@rrcat.gov.in*

Superconducting radiofrequency (SCRF) technology is critical for developing high-energy particle linear accelerators. Department of Atomic Energy (DAE) is working on development of superconducting radiofrequency (SCRF) technology for high energy particle linear accelerators which includes development of SCRF cavities. Majority of SCRF cavities used in accelerator applications are made out of high purity bulk Niobium (Nb) sheets. These SCRF cavities operating at extremely low temperature (~2K) have significantly high-quality factor (>10^{10}) and operates at high accelerating gradients (>20 MV/m). The low availability of high RRR rare-earth Nb material, precise cavity fabrication techniques, advanced cavity processing procedures and cryogenic testing eventually end up in making delicate and costly component of accelerator. Any degradation in material due to gaseous infusion (in ppm level) or impregnation of impurity (in µm size) degrades the specified performance of the SCRF cavity at cryogenic temperature. In order to qualify the stringent functional and technical requirement specifications of these cavities, it requires to maintain the purity of the Niobium and its surface throughout the cavity fabrication and processing procedures.

Residual Resistivity Ratio (RRR) evaluation is a widely used ~~and~~ practical technique for comprehensively assessing Nb quality at various fabrication stages. RRR is an indicator of the purity of material and its thermal conductivity at cryogenic temperature. The significance of RRR evaluation in assuring exceptional SCRF cavity performance is presented and discussed in this paper. By optimizing the RRR evaluation process along with processing, we can ensure consistent production of high-purity Nb SCRF cavities, ultimately contributing to the advancement of SCRF technology for next-generation accelerators. This paper details the RRR evaluation setup, noteworthy test results, and plans for further development.

REFERENCES:

1. W. Singer, A. Ermakov, X. Singer “RRR-Measurement Techniques on High Purity Niobium”inTTC-Report 2010-02
2. H. Padamsee, J. Knobloch, and T. Hays, RF superconductivity for accelerators, J. Wiley & Sons, New York, 1998
3. K. K. Schulze, “Preparation and characterization of ultra-high-purity niobium,” J. Met., vol. 33, pp. 33–41, 1981
4. L. F. Goodrich, T. C. Stauffer, J. D. Splett, D. F. Vecchia, “Measuring residual resistivity ratio of high-purity Nb”, Advances in Cryogenic Engineering Materials, Vol. 50A, pp. 41-48, 2004
5. P. Bauer, T. Berenc, C. Boffo, M. Foley, M. Kuchnir, Y. Tereshkin, T. Wokas, RRR measurements on niobium for superconducting RF cavities at FERMILAB, Proceedings of 11th workshop on RF superconductivity (SRF2003), 8-12 Sept. 2003, Lubeck/Travemunde, Germany

Effect of Substrate Temperature on the Structural and Magnetic Properties of Cobalt Ferrite ($CoFe_2O_4$) Thin Films Grown by Pulsed Laser Deposition

Vinay Shrivastava[1],Ambrish Dwivedi[1],Yksh Gupta[2],Keval Gadani[3],Sanjay Kumar Upadhyay[4],Sourav Chowdhury[5],Anil Gome[6,7],Ratnesh Gupta[2],Sagar Sen[1]*

[1]Department of Physics, Maharaja Bhoj Govt. P.G. College, Dhar 454001, India.
[2]School of Instrumentation, Devi Ahilya Vishwavidyalaya, Indore, India.
[3]Centre of Education, Faculty of Physics, Indian Institute of Teacher Education (IITE), Gandhinagar, India.
[4]HNB Garhwal University Srinagar Garhwal, Uttarakhand-246174, India.
[5]Deutsches Elektronen-Synchrotron DESY Notkestrasse 85, 22607, Humburg, Germany.
[6]UGC-DAE Consortium for Scientific Research, Indore 452010, India.
[7]Depaetment of Physics, Medi-Caps University, Indore, India.
Email: sssagarsen@gmail.com

Abstract: Thin films of cobalt ferrite ($CoFe_2O_4$) were deposited on Si substrates using pulsed laser deposition at various substrate temperatures. Structural analyses via XRD and AFM revealed that higher deposition temperatures improve crystallinity and increase average grain size. XPS and XAS studies indicate significant temperature-driven variations in cation distribution between octahedral and tetrahedral sites. Magnetic measurements using SQUID-VSM and XMCD confirm that films deposited at higher temperatures exhibit enhanced magnetic moments, aligning well with predictions from the Néel superlattice model. These results highlight the pivotal role of substrate temperature in tailoring the magnetic properties of $CoFe_2O_4$ thin films.

1. INTRODUCTION

Bulk $CoFe_2O_4$, an inverse spinel ferrite, is widely recognized for its exceptional properties, such as high coercivity, chemical stability, magneto-crystalline anisotropy, and magnetostriction. These attributes make it highly suitable for applications including catalysis, data storage, drug delivery, ferrofluids, and magnetic refrigeration [1,2].

The magnetic properties of $CoFe_2O_4$ thin films, including saturation magnetization (M_s), coercivity (H_c), magnetic easy axis, and anisotropy constant, are significantly influenced by growth conditions such as growth temperature, oxygen pressure, substrate type, laser fluence, and laser wavelength [3]. In this context, understanding the relationship between crystalline growth and magnetic properties in $CoFe_2O_4$ thin films, particularly with variations in substrate temperature, is essential for optimizing the overall magnetic moment. This study compares the structural and magnetic properties of $CoFe_2O_4$ films deposited at three different substrate temperatures—room temperature, 400°C, and 600°C—on Si (1 0 0) substrates [4].

A robust method is required to investigate the magnetic and cationic structure of cobalt ferrite thin films. X-ray Magnetic Circular Dichroism (XMCD) at the cation $L_{2,3}$ edges provides such a tool. In this work, along with XPS, XMCD analysis was also performed on cobalt ferrite thin films at the Fe and Co $L_{2,3}$ edges to investigate their magnetic structure and cationic distribution

2. EXPERIMENTAL

Cobalt ferrite powder (99.9%) was sintered at 500°C for 2 hours and 1100°C for 12 hours to prepare the target. Thin films were deposited using Nd:YAG PLD (λ = 355 nm) at substrate temperatures: S0 (room temperature), S1 (400°C), and S2 (600°C). GIXRD and XRR were conducted with a D8 Bruker diffractometer, AFM with Bruker's Bioscope Resolve, and magnetization measurements using a 7-tesla SQUID-VSM. XPS was performed at RRCAT Indore, while XAS and XMCD were carried out at PETRA III DESY.

3. RESULTS AND DISCUSSION

The XRD patterns confirm the presence of cobalt ferrite with a cubic spinel structure. The peaks at 35.5° and 43.2° correspond to the (311) and (400) reflections of cobalt ferrite. The intensity of the (311) diffraction peak increases with substrate temperature, suggesting an increase in atomic grain size. XRR measurements indicate that the substrate roughness and film thickness increase with substrate temperature while the surface roughness decreases with increasing substrate temperature. SQUID-VSM measurements show that the magnetic moment increases with substrate temperature, with values of 1.40 μ_B, 2.05 μ_B, and 2.80 μ_B for S0, S1, and S2 thin films, respectively. XPS measurements reveal the cation distribution in cobalt ferrite thin films. In the S0 sample, Co^{2+} ions are mainly located in tetrahedral sites, while Fe^{3+} ions are more evenly distributed between octahedral and tetrahedral sites. In the S2 sample, Co^{2+} ions are more evenly distributed between octahedral and tetrahedral sites, while Fe^{3+} ions are predominantly found in octahedral

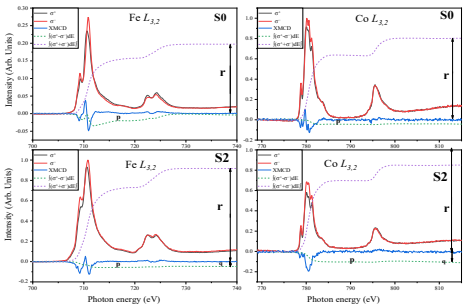

Fig.1. XAS and XMCD of S0 and S2 cobalt ferrite thin films.

sites. The magnetic moment was theoretically calculated using Neel's theory:

$$M_{cal} = M_{Octa}(x) - M_{Tetra}(x) \quad (1)$$

Where M_{Octa} and M_{Tetra} represent the saturation magnetization of the octahedral and tetrahedral sites. Using this relation, the total magnetic moments for S0 and S2 were calculated as 1.3 μB and 2.33 μB, respectively. The VSM measurements for both samples closely match the theoretical values predicted by the Neel superlattice model. The increase in Co^{2+} ions in octahedral sites and the redistribution of Fe^{3+} from tetrahedral to octahedral sites enhance the magnetic properties. Fig 1 shows XAS and XMCD measurements show a similar distribution of cobalt ferrite in octahedral and tetrahedral sites, and the magnetic moment was calculated using the sum rule, which comes out 2.71 μ_B and 1.50 μ_B for S2 and S0 thin films, respectively.

4. CONCLUSION

In conclusion, $CoFe_2O_4$ thin films grown via PLD at varied substrate temperatures display distinct structural and magnetic characteristics. XRD and AFM analyses confirm that higher substrate temperatures enhance crystallinity and increase average grain size. XPS and XAS investigations reveal temperature-dependent shifts in the distribution of Co^{2+} and Fe^{3+} ions. Magnetic measurements show that the S2 sample exhibits a higher magnetic moment compared to the S0 sample. Overall, substrate temperature is a critical parameter for tailoring the films' structural and magnetic properties.

ACKNOWLEDGEMENT

Mr Vinay Shrivastava is a project fellow in the project supported by Inter-University Accelerator Centre (IUAC) Delhi (project no. IUAC/13.3A/74320 and dated 17.07.2023). Financial assistance from the same is thankfully acknowledged. The authors are thankful to UGC DAE CSR Indore for providing the experimental facilities.

REFERENCES

1. Synthesized cobalt substituted magnetite (CoxFe3-xO4) nanoparticles – evaluation of structural, opti | Enhanced Reader.

2. Hochepied, J. F., Sainctavit, P. & Pileni, M. P. X-ray absorption spectra and X-ray magnetic circular dichroism studies at Fe and Co L2,3 edges of mixed cobalt–zinc ferrite nanoparticles: cationic repartition, magnetic structure and hysteresis cycles. *J Magn Magn Mater* **231**, 315–322 (2001).

3. Sagu, J. S., Wijayantha, K. G. U. & Tahir, A. A. The Pseudocapacitive Nature of CoFe2O4 Thin Films. *Electrochim Acta* **246**, 870–878 (2017).

4. Raghunathan, A., Nlebedim, I. C., Jiles, D. C. & Snyder, J. E. Growth of crystalline cobalt ferrite thin films at lower temperatures using pulsed-laser deposition technique. *J Appl Phys* **107**, 44502 (2010).

Exploring the magnetic properties of La_2MMnO_6 (M = Cr, Zn) double perovskites

K. Jeevanandham, K. Vinod, A. T. Sathyanarayana and Sujoy Sen
Condensed Matter Physics Division, Materials Science Group, Indira Gandhi Centre for Atomic Research, A CI of Homi Bhabha National Institute, Kalpakkam, Tamil Nadu, 603102, India
Email: (vinod@igcar.gov.in)

Abstract: The low temperature magnetic properties of La_2CrMnO_6 and La_2ZnMnO_6 double perovskites were studied. The results revealed that the nature of B site ion influences the magnetic property of these systems. Cr atoms at the B site promote strong ferromagnetic ordering, while Zn at the B site breaks the long-range magnetic ordering, resulting in paramagnetic La_2ZnMnO_6.

1. INTRODUCTION

Double perovskites exhibit multiferroic properties and have applications in spintronics. Numerous studies have reported on their magnetic, structural, and dielectric properties. Jasnamol *et al*. [1] reported that La_2CrMnO_6 exhibits ferromagnetic properties and spin-glass behavior above the Curie temperature (T_C) along with Griffith's phase-like characteristics. Yoshimatsu [2] demonstrated ferrimagnetic behaviour in La_2CrMnO_6. Similarly, Dexin Yang [3] investigated the magnetic exchange interactions in La_2CrMnO_6, providing evidence of ferrimagnetic behaviour. In this study, we investigate the magnetic properties of La_2CrMnO_6 as well as the La_2ZnMnO_6 double perovskites.

2. EXPERIMENTAL

The La_2CrMnO_6 and La_2ZnMnO_6 samples were prepared in bulk polycrystalline form, using the solid-state reaction method. The magnetic ground state in these samples was studied in detail.

3. RESULTS AND DISCUSSIONS

The iso-field magnetization measurement performed at a magnetic field (H) of 1000 Oe for the La_2CrMnO_6 sample is shown in figure 1. The magnetization (M) as a function of temperature (T) for both zero field cooled (ZFC) and field cooled (FC) conditions show a clear ferromagnetic transition. The first derivative of M with respect to T (dM/dT) indicates the ferromagnetic transition temperature (Curie temperature, T_C) around 122 K. Another weak magnetic transition is also observed around 59 K.

The upper inset in figure 1 shows the $1/\chi$ *vs.* T plot (χ is the magnetic susceptibility) along with Curie-Weiss fit, performed over the temperature range 200-300 K. From this fit, the Curie-Weiss temperature (Θ_C) and the effective paramagnetic moment (μ_{eff}) were determined. The lower inset in figure 1 displays the isothermal M *vs.* H data measured at 4 K. The saturation magnetization (μ_{sat}) is calculated from the M *vs.* H data. These results are summarized in table 1.

The La_2ZnMnO_6 system shows (data not shown) simple paramagnetic behavior, without any magnetic phase transitions, in the temperature range studied (4-300 K). This results support the idea of complete breaking of B-B' site magnetic exchange interactions by the introduction of a non-magnetic ion (Zn) at the B site.

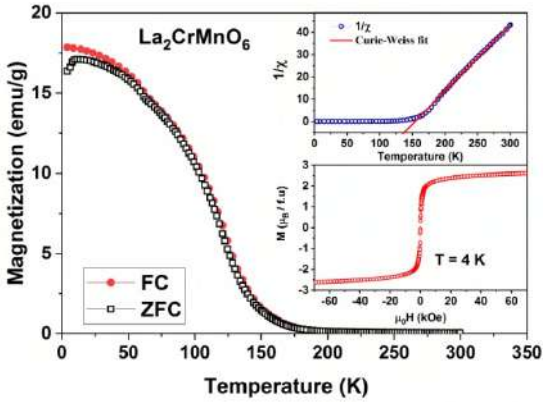

Fig.1. ZFC and FC M *vs.* T data for H = 1000 Oe. The upper inset shows $1/\chi$ *vs.* T data along with the Curie-Weiss fit. Lower inset displays isothermal M *vs.* H data for T = 4 K.

Table 1. Magnetic properties of the samples.

Sample	μ_{sat} $(\mu_B/f.u)$	μ_{eff}^{exp} (μ_B)	μ_{eff}^{theor} (μ_B)	Θ_{CW} (K)
La_2CrMnO_6	2.6	5.24	6.24	151.2
La_2ZnMnO_6	-	4.47	3.87	43.8

4. SUMMARY

The magnetic ground states of the double perovskite oxide systems La_2CrMnO_6 and La_2ZnMnO_6 have been evaluated. The La_2CrMnO_6 system exhibits ferromagnetic behaviour with T_C around 122 K, while the La_2ZnMnO_6 remains paramagnetic in the temperature range of 4 K to 300 K.

ACKNOWLEDGEMENT

K. Jeevanandham acknowledges IGCAR and HBNI for the research fellowship.

REFERENCES

[1]. Jasnamol *et. al.* J. Appl. Phys. **122**(2017) 073907.
[2]. K. Yoshimatsu, *et. al.* Phys. Rev. B **99** (2019) 235129.
[3]. D. Yang *et. al.* Results in Physics. **12** (2019) 344.

Structural Investigations in Gd^{3+} and Ce^{4+} co-doped Lanthanum Zirconate Pyrochlores

Vidya M[1*], Raghavendra K G[1]

[1]Department of Physics, Manipal Institute of Technology Manipal Academy of Higher Education (MAHE), Manipal–576104, India.

**Email:vidyam20112001@gmail.com*

Abstract: This study investigates the phase stability and microstructural evolution of Gd^{3+} and Ce^{4+} co-doped $La_{2-x}Zr_{2-y}O_7$ at high temperatures. It aims to provide a comprehensive understanding of the impact of high-temperature exposure on the structural integrity of the material, offering key insights into the thermal stability and behavior of these doped zirconates under extreme conditions.

1. INTRODUCTION

The growing demand for advanced ceramic materials from aerospace and nuclear industries, that can withstand extreme environmental conditions has driven the exploration of zirconate pyrochlores ($A_2Zr_2O_7$) due to their exceptional thermal stability, low thermal conductivity, resistance to chemical corrosion and irradiation stability [1]. For aerospace applications, these materials are candidate for critical high temperature applications such as thermal barrier coatings (TBCs) in jet engines. In nuclear applications, rare earth zirconates are a potential host matrix for providing a stable and durable solution for the long-term containment and safe disposal of high level radioactive wastes. Among the family of rare earth zirconates, lanthanum zirconate ($La_2Zr_2O_7$) (LZ) is one of the most potential candidates for these critical applications and widely studied. Towards further improving their mechanical properties, the A and B site co-doped variants of LZ has shown potential and the co doped LZ also act as a simulated nuclear waste. Under this context, understanding the structural stability of this material is of paramount importance [2-3]. Considering this, the current study examines the effects of Gd^{3+} and Ce^{4+} co-doping on the material's microstructure and phase evolution at elevated temperatures using X-ray diffraction studies and local structure analysis through Raman spectroscopy.

2. SYNTHESIS AND MICROSTRUCTURAL ANALYSIS

Gd^{3+} and Ce^{4+} co-doped samples with chemistry $La_{1.8}Gd_{0.2}Zr_{1.8}Ce_{0.2}O_7$ (LZC) and $La_{0.2}Gd_{1.8}Zr_{1.8}Ce_{0.2}O_7$ (GZC) were synthesized via chemical co-precipitation method and calcined from 700°C – 1300°C. X-Ray diffraction and Raman spectroscopic techniques are employed to study their phase and structural evolution. An ordered pyrochlore structure is observed in LZC at high temperatures as shown in Fig. 1(a) and (b) whereas defect fluorite is observed in GZC sample. Further microstructural studies through electron microscopy, thermal property assessments and ion irradiation studies are in progress which is necessary to qualify this material for its intended nuclear and thermal applications. The critical insights from our extensive investigation will be discussed in detail during the conference.

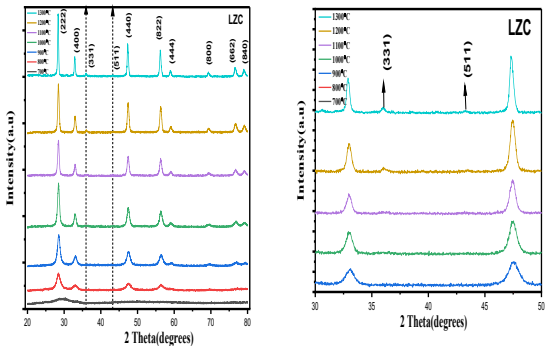

Fig.1a Fig.1b

Fig1a. XRD patterns for LZC sample calcined from 700°C to 1300°C.
Fig1b. Enlarged view of superlattice reflections of LZC

ACKNOWLEDGMENT

The authors gratefully acknowledge the financial support from MAHE through seed money grant and PG students research fund.

REFERENCES

1 . A. Panghal, Y. Kumar, P.K. Kulriya, P.M. Shirage, N.L. Singh, Structural assessment and irradiation response of La2Zr2O7 pyrochlore: Impact of irradiation temperature and ion fluence, J Alloys Compd. 862 (2021) 158556.

2. . Mathanbabu, M., Thirumalaikumarasamy, D., Thirumal, P., & Ashokkumar, M. (2021). Study on thermal, mechanical, microstructural properties and failure analyses of lanthanum zirconate based thermal barrier coatings: A review. *Materials Today Proceedings*, *46*, 7948–7954.

3. Xiang, J., Chen, S., Huang, J., Zhang, H., & Zhao, X. (2012). Phase structure and thermophysical properties of co-doped La2Zr2O7 ceramics for thermal barrier coatings. *Ceramics International*, *38*(5),3607–3612.

Study on structural and dye degradation property of Mn doped MoO_3/SiO_2 nanocomposites

Boobesh S[1], Abuthahir J[2], Janardhanan P[1], Elango M[1*].
Department of Physics, PSG College of Arts and Science, Coimbatore, Tamilnadu, India
Department of Physics, Government College of Technology, Coimbatore, Tamilnadu, India
Email: elango@psgcas.ac.in

Abstract

Mn-doped MoO_3/SiO_2 composites were synthesized using a modified wet-chemical approach, altering the pH with NH_3. XRD confirmed an orthorhombic phase (ICDD 029-0569), with Mn doping reducing crystallite size (38–47 nm to 31–36 nm). Raman analysis revealed lattice strain and structural defects due to Mn incorporation. The catalyst exhibited enhanced photocatalytic degradation of Crystal Violet dye via improved charge separation and reactive oxygen species (ROS) generation, demonstrating its potential for wastewater remediation.

1. INTRODUCTION

MoO_3-based composites are promising for wastewater treatment due to their stability, broad bandgap (2.69–3.6 eV), and ability to absorb visible and UV light (Liu et al., 2014). MoO_3-coated micro/nano SiO_2 functions as an efficient n-type semiconductor and is widely used in sensors, batteries, supercapacitors, solar cells, and photocatalysis (Chidambararaj et al 2013). Crystal Violet, a synthetic triphenylmethane dye with amino-substituted phenyl rings, exhibits high chemical resistance and strong coloration (Radia et al., 2024). Its complex molecular structure makes removal from water systems difficult, contributing to environmental pollution and inhibiting biological degradation, thereby harming ecosystems.

2. EXPERIMENTAL METHODS

Core SiO_2 was synthesized following Tamta et al. (2023). Mn-doped MoO_3/SiO_2 was prepared using Mo precursor, NaOH, and HNO_3, with pH adjustment via NH_3, modifying Huang et al. (2013) protocol.

3. RESULTS AND DISCUSSION

3.1. Microstructural analyses

XRD analysis (Fig 1) confirmed the orthorhombic MoO_3 phase (ICDD 029-0569, space group *Pbnm*) for both undoped and Mn-doped MoO_3/SiO_2. The absence of an amorphous SiO_2 peak suggests complete shell formation or a non-interactive layered structure. Mn^{2+} incorporation caused peak shifts and reduced crystallite size (38–47 nm to 31–36 nm). Increased texture coefficient favored photocatalytic activity. Raman spectroscopy revealed characteristic MoO_3 bands at 670, 822, and 1000 cm^{-1}, with the 670 cm^{-1} band confirming the symmetric stretching of triply coordinated oxygen bridges. Mn doping induced peak broadening, indicating lattice strain, bond length fluctuations, and structural defects.

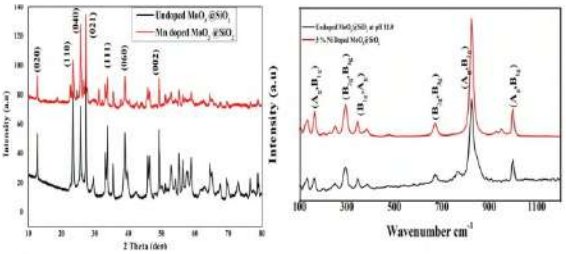

Fig.1 XRD and Raman spectra of bare and Mn doped MoO_3/SiO_2

Higher lattice strain and bond length fluctuations are indicated by the intensity changes and peak shifts (820 to 823 cm^{-1}). The Raman peaks in this region are greatly broadened by Mn doping confirming the severe lattice disorder.

3.2. Dye degradation analysis on Crystal violet

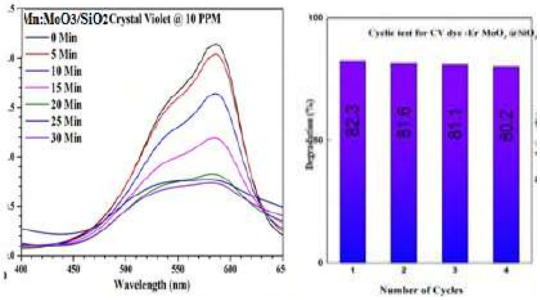

Fig 2 Dye degradation analysis against CV dye

Dye molecules adsorb onto the catalyst via electrostatic and van der Waals forces, aided by the high surface area of SiO_2. Light excites electrons from the valence to conduction band, generating superoxide and hydroxyl radicals that degrade dyes into non-toxic byproducts. Mn doping enhances charge separation and reactive oxygen species (ROS)

Conclusion

Mn-doped MoO_3/SiO_2 composites were successfully synthesized, with XRD confirming an orthorhombic phase and Raman analysis revealing structural distortions due to Mn incorporation. The reduced crystallite size and increased texture coefficient enhanced photocatalytic performance. Mn doping improved charge separation and ROS generation, leading to efficient Crystal Violet dye degradation. These findings highlight the potential of Mn-doped MoO_3/SiO_2 as a promising photocatalyst for wastewater treatment applications.

REFERENCES

[1].Liu, T et al., *Chemical Engineering Journal*, *244*, pp.382-390. 2014.

[2]. Chithambararaj et al *Physical Chemistry Chemical Physics*, *15*(35), pp.14761-14769.2013

[3].Joya, et al, *Current Science*, *116*(10), pp.1690-1695. 2019.

[4].Tamta et al *Physica B: Condensed Matter*, *638*, p.413971. 2022

.[5]. Huang et al *Applied surface science*, *283*, pp.25-32. 2013.

Topic Code: Advanced Characterization Techniques and equipment in Extreme Conditions

Assessing the Corrosion Resistance, Structural, and Energy Consumption Properties of TiO2-based PEO coatings for photo catalysis on pre-anodized AA2024-Al

Sanjeev Kumar Singh[1], Dr. P Naresh[2],

[1]Department of Physics, Avanthi Degree & PG College, Hyderabad, Telangana, India - 500027
[2]Department of Physics, Osmania University, Hyderabad, Telangana – 500007

Email address for correspondence: sks211979@gmail.com

Abstract

In this work, a thorough investigation was conducted to develop plasma electrolytic oxidation (PEO) coatings on pre-anodized AA2024-Al alloy. The coatings were developed at various concentrations of TiO2 dispersed in a water-based electrolyte containing sodium silicate, sodium phosphate dodecahydrate, and potassium hydroxide. The aim was to determine the effect of TiO2 incorporation on energy consumption, coating growth, surface morphology, photocatalytic behavior, and long-term corrosion resistance properties. The pre-anodization time was controlled to develop a (20.0±1.6) µm-thick anodic film. Compared to PEO developed without pre-anodic precursors, a reduction of ~66% in energy consumption (kW.h.m2.µm-1) was observed. The addition of TiO2 nanoparticles (Degusa-P25) into the base electrolyte resulted in reductions of ~68%, 64%, and 51% for the PEO coatings developed at 2, 5, and 10 g/L TiO2 concentrations, respectively. The photocatalytic activity of TiO2 was investigated by photodegrading phenol under simulated sunlight conditions, where higher TiO2 concentrations led to improved phenol photodegradation efficiency. The effectiveness of TiO2 concentration on the corrosion resistance properties of PEO coatings was observed, with nearly one order of magnitude higher impedance magnitude (after 336 h) than the PEO layer without TiO2.

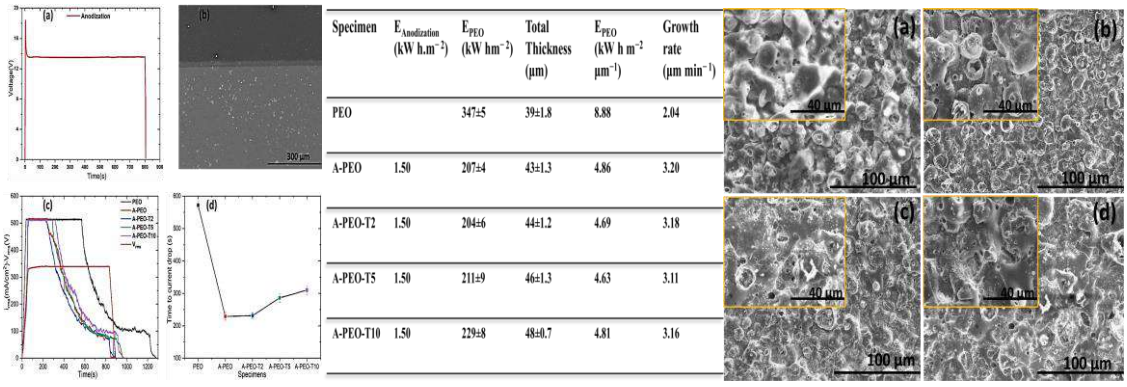

Specimen	$E_{Anodization}$ (kW h.m^{-2})	E_{PEO} (kW hm^{-2})	Total Thickness (µm)	E_{PEO} (kW h m^{-2} µm^{-1})	Growth rate (µm min^{-1})
PEO		347±5	39±1.8	8.88	2.04
A-PEO	1.50	207±4	43±1.3	4.86	3.20
A-PEO-T2	1.50	204±6	44±1.2	4.69	3.18
A-PEO-T5	1.50	211±9	46±1.3	4.63	3.11
A-PEO-T10	1.50	229±8	48±0.7	4.81	3.16

ACKNOWLEDGMENT

This work is financed by the European project UNA4CAREER (Marie Skłodowska Curie grant No 847635). The authors also gratefully acknowledge the support of PID2021-124341OB-C22 (MCIU/AEI/FEDER, UE). M. Mohedano is grateful for the support of RYC-2017-21843.

References

1. Blawert, C., Heitmann, V., Dietzel, W., Nykyforchyn, H.M. and Klapkiv, M.D., 2007. Influence of electrolyte on corrosion properties of plasma electrolytic conversion

coated magnesium alloys. *Surface and Coatings Technology*, *201*(21), pp.8709-8714.

2. Mengesha, G.A., Chu, J.P., Lou, B.S. and Lee, J.W., 2020. Corrosion performance of plasma electrolytic oxidation grown oxide coating on pure aluminum: effect of borax concentration. *Journal of Materials Research and Technology*, *9*(4), pp.8766-8779.

3. Snizhko, L.O., Yerokhin, A.L., Pilkington, A., Gurevina, N.L.,Misnyankin, D.O., Leyland, A. and Matthews, A.J.E.A., 2004. Anodic processes in plasma electrolytic oxidation of aluminium in alkaline solutions. *Electrochimica Acta*, *49*(13), pp.2085-2095.

Ballooning Behavior in End Plug Repaired Welds of Fuel Clad Tubes at Extreme Conditions

Rosy Sarkar, R. Suresh Kumar, R. Manu, K. Mohan, K.Natesan
Reactor Design Group, IGCAR, Kalpakkam - 603102
Email: rosy@igcar.gov.in

Abstract: In fast breeder reactors, the integrity of fuel clad tubes is essential for reactor safety and performance. This investigation focuses on the potential for ballooning in the end plug welds of these tubes, considered weak points due to the welding process. Ballooning typically initiates in the weakest regions under high temperature and pressure. Through detailed experiments, the clad tube was observed to balloon and burst at 1070°C, away from the weld, indicating initiation in a more ductile region. Additional tests on tubes with multiple weld repairs showed similar results, highlighting that ballooning occurs away from the brittle weld region. These findings provide valuable insights into material behavior under extreme conditions, crucial for enhancing the safety and reliability of fast breeder reactors.

1. INTRODUCTION

The integrity of fuel clad tubes in fast breeder reactors is crucial for reactor safety. Ballooning, which can severely compromise these tubes under high temperature and pressure, is a significant issue. Welds, especially at end plugs, are potential weak points due to brittleness from welding and the solid end plug's restriction on bulging. This study investigates whether ballooning occurs at these welds, where brittleness, weak links, and constraints to bulge coexist. Insights from this study on material behavior under extreme conditions aim to enhance the safety and reliability of fast breeder reactors.

2. EXPERIMENTAL FRAMEWORK

2.1. Test Facility

The Rupture And Ballooning In Tubes (RABITS) facility in SML is used to test fuel clad tubes at various temperatures and heating rates [1].

2.2. Calibration of the Furnace

A calibration test was conducted using a dummy sample with temperature sensors placed along its height, and the distribution with time was recorded as shown in Fig.1.

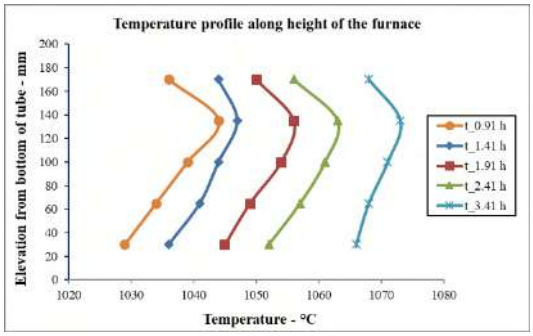

Fig.1. Temperature profile along height of furnace

The highest temperature was observed just below the top of the furnace due to natural convection currents and design. This profile closely matches that of PFBR fuel pins, ensuring representative conditions.

2.3. Specimen Positioning and Testing

The specimen (with 0 repaired weld) was positioned in the highest temperature zone (Fig. 2a), pressurized to 100 bars, and heated to 1100°C. It ballooned and burst at 1070°C, after 35 minutes, away from the weld (Fig. 2b), indicating initiation in a ductile region. A similar test with three repairs in the end plug weld showed the tube ballooning and rupturing away from the weld, (Fig. 2c), at a similar burst temperature and time. Previous creep tests revealed crack initiation near the weld in multiple repaired pins [2]. This suggests that ballooning involves higher ductility, making the brittle weld region unfavorable for ballooning.

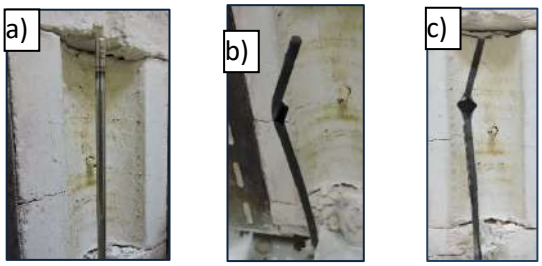

Fig.2. a) Specimen position b) Zero repaired ballooned pin c) Three repaired ballooned pin

3. CONCLUSION

This study provides key insights into ballooning in fuel clad tubes at the end plug welds, which are potential weak points due to welding brittleness. Experimental results showed that the clad tube ballooned and burst at 1070°C, away from the weld, indicating initiation of ballooning in a ductile region. Additional tests on tubes with multiple weld repairs also showed that ballooning occurred away from the weld, reaffirming the findings. Understanding ballooning conditions is crucial for reactor safety and reliability.

ACKNOWLEDGEMENT

The authors thank the lab personnel for their assistance with the tests and IGCAR for providing the necessary facilities.

REFERENCES

[1] Rosy Sarkar et al, International Journal of Pressure Vessels and Piping, 160 (2018)24–33.
[2] Rosy Sarkar et al., Nuclear Engineering and Design, 252 (2012) 192-200.

Mechanical characterization of multi-directional C_f-SiC_m composites

Saurav Kumar Sahoo[1], Arjun Mahato[1], Samar Mandal [1,2], M. Thangarasua[1], Shibayan Roy [1]
[1]Materials Science Centre, Indian Institute of Technology Kharagpur, Kharagpur, India, 721302
[2]Advanced Systems Laboratory (ASL), Hyderabad, India, 500058
Email: sauravkumarsahoo@kgpian.iitkgp.ac.in

Abstract: Carbon fiber reinforced silicon carbide (C_f-SiC_m) composites offer promising solutions as a structural material for aerospace applications due to their ability to withstand extremely high temperature. In the present study, non-crimped fabrics (NCFs) were employed for the fabrication of C_f-SiC_m composites having multi-directional (1D, 2D, 3D, 4D) fiber architecture through LSI method. The composites were initially characterized for density and microstructure evolution. Additionally, x-ray micro computed tomography (Xμ-CT) was performed to assess the volume fraction of porosity, residual silicon, carbon and formed silicon carbide. Fiber orientation's effect on mechanical properties was evaluated through tensile, compression, and flexural tests.

1. INTRODUCTION

Multidirectional carbon-fiber reinforced silicon carbide matrix composites (C_f-SiC_m) are ideal for aerospace components like jet vanes and thrusters. Liquid-silicon-infiltration (LSI) is preferred over chemical vapor deposition and polymer impregnation for producing thicker, high-performance parts. This study explores the tailoring of various mechanical properties (tensile, compressive, and flexural) by selecting appropriate fiber architectures, specifically uni-directional (1D), multi-directional (2D,3D, 4D) non-crimped continuous carbon fiber preforms, for the production of C_f-SiCm composites via the liquid silicon infiltration (LSI) technique. It focuses on the microstructure and phase evolution of the composites and investigates the impact of fiber architecture on their mechanical properties. A high carbon content (V_f = 36%) is chosen for the fiber preforms to ensure the structural integrity of the composite after the LSI process.

2. EXPERIMENTAL PROCEDURE

2.1. Materials and Fabrication

T-300 3k carbon fiber tows were used to create non-crimped preforms with various fiber orientations (1D, 2D, 3D, 4D). The preforms were densified with coal-tar pitch, siliconized with silicon metal, and rigidized at 200–300°C. Carbonization and graphitization were performed at 900–1000°C and 2500–2600°C, respectively. Further densification included vacuum impregnation with coal-tar pitch and SiC slurry, followed by HIPIC at 700–800°C. C-C components were impregnated with molten silicon at 1650°C to form C-SiC, then machined for characterization.[1].

2.2. Composition Determination

The composition of the siliconized blocks was determined by acid digestion method [2].

2.2. Microstructure characterization and phase evolution

Microstructural morphologies were analysed using high-resolution X-ray micro-CT, optical microscopy, and SEM. Phase identification of C_f-SiC_m composites was done by XRD with Ni-filtered CuKα radiation (λ=1.5406 Å) in the 2θ range of 10-80° and a step size of 0.0065°.

3. FIGURES AND IMAGES

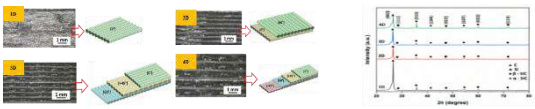

(a) (b)

Fig.1. (a) Optical and Schematic images (b) X-ray diffraction profile captured from the longitudinal surfaces of 1D, 2D, 3D and 4D C_f-SiC_m composites.

4. TABLES

Table 1. The Table summarizes the volume fraction of each phase in the C-SiC composites was analysed using XμCT.

C-SiC composites	Matrix (Vol%)	Fiber (Vol%)	Free Silicon (Vol%)	Pore (Vol.%)
1D	56.51	37.15	1.15	5.19
2D	55.73	37.04	2.76	4.45
3D	56.82	37.26	1.68	4.23
4D	58.02	37.81	0.32	3.84

ACKNOWLEDGEMENT

We acknowledge Advanced Systems Laboratory (ASL), Hyderabad, India, for composite specimen preparation and some characterization facilities, and the DIST-FIST program for the FESEM facility at IIT Kharagpur's Materials Science Centre.

REFERENCES

[1] Kumar, Suresh, et al. "Preparation of 3D orthogonal woven C–SiC composite and its characterization for thermo-mechanical properties." Materials Science and Engineering: A 528.19-20 (2011)

[2] Mandal, S., et al., Fabrication, Characterization and Suitability of 3D Non-woven Needle-Punched Preform C_f-SiC_m Composites for Ultra-High Temperature Applications. Metallurgical and Materials Transactions A, 2024. 55(10): p. 4122-4145.

Altercations in Physicochemical Properties of Soft Chemical Route Synthesized ZnO Thin Film

Jayesh R. Pawar, Munjaji E. Dudhmal, Rajesh A. Joshi*

Department of Physics,

Toshniwal Arts, Commerce and Science College, Sengaon-425343 Dist. Hingoli MS India

Abstract

The Zinc Oxide (ZnO) thin films were deposited onto the glass substrates by a successive ionic layer adsorption and reaction method, which is based on the alternate dipping of substrate in a zinc nitrate solution complexes with NH4OH and distilled water heated at 75 ◦C. The time duration for which a substrate is dipped in the distilled water, plays an important role and it has been shown in this work that the time period for which a substrate is dipped in distilled water, which we referred as rinsing period, affects significantly on the structural and optical properties. One of the samples is not annealed and others are annealed at 100, 200, 300 and 400 °C. These samples are used to investigate the effect of annealing and aging on the properties of ZnO. Nano crystalline diamond like ZnO thin film is characterized by different characterization techniques such as X-ray diffraction (XRD), Atomic Force Microscopy (AFM), Raman spectrometer, Scanning Electron Microscopy (SEM) with Energy Dispersive X-Ray Analysis (EDAX) and optical absorption.

Keywords

ZnO thin film, SILAR, Annealing, XRD, AFM, SEM, EDAX, Raman Spectroscopy.

Topic Code:

Reducing low thermal conductivity of GeTe compounds via nanostructure modulation by spark plasma sintering method

A. Sampathu[1], Chellakumar. R[2], Narendran. D[3] and M. Balakrishnan[1]*

[1]PG and Research Department of Physics, Kalaignar Karunanidhi Government Arts College, Tiruvannamalai 606 603, Tamil Nadu, India
[2]Department of Nuclear Physics, University of Madras, Chennai 606 603, Tamil Nadu, India
[3]Sr. Engineer-Lubrication- Vestas Wind Technology, India
Email: aspsampathu@gmail.com

Abstract: GeTe intensively studied in recent years as promising p-type semiconducting lead-free mid temperature range thermoelectric (TE) material. It also displays a second-order phase transition nature (700 K) from high-temperature cubic (Fm-3m) to a low temperature rhombohedral (or hexagonal) structure R3m. The reduction of total thermal conductivity ($3Wm^{-1}K^{-1}$) was achieved for **$Ge_{0.88}Mg_{0.06}Bi_{0.06}Te$** materials.

1. INTRODUCTION

Thermoelectric materials are efficient for the bidirectional conversion of waste heat into electric energy and propitious remedies for the global energy problem [1]. GeTe, as p-type semiconductor, has been diligently studied in recent years as a promising lead-free mid temperature range thermoelectric material. In this field, materials need to possess high value of dimensionless thermoelectric figure of merit,

$$ZT = \frac{S^2 \sigma T}{k_t}$$

Where, $k_t = K_L + K_e$, σ electrical conductivity, S Seebeck coefficient, K_t total thermal conductivity, K_L lattice thermal conductivity, K_e electronic thermal conductivity and T absolute temperature. Significant improvement in the ZT value has been achieved with the reduction of K_L via phonon scattering because of complex nano structuring, [2] point defects (substitutional, interstitial and vacancy), mesoscale grain boundaries, second phase nanoprecipitation and intrinsic bond anharmonicity [3].

2. EXPERIMENTAL MATERIALS AND METHODS

In this present research work, purity of Ge shots (99.999%), Te powder (99.999%), Mg Granulas (99.99%) and Bi powder (99.999%) are taken in stochiometric amount and loaded to vacuum sealing in quartz tube with 10-5 Torr than annealed at 1173K for 18h, than obtained ingots are grinded. The fine powder allows the process of spark plasma sintering on 723 K for 5 min.

3. RESULTS AND DISCUSSION

The structural property analyzed by X-ray diffraction it shows the rhombohedral structure and calculated the variation of rhombohedral angle. The strain and mass fluctuation calculated by modified Debye-Callaway model equations. The Hall Effect measurements confirmed the p-type nature of carrier concentration and determined the conductivity as well as resistivity also mobility, the carrier concentrations are optimized in the range of high Seebeck coefficients. The thermal conductivity was measured using the relation $k = dC_PD$, where D is the thermal diffusivity measured by laser flash technique, d density of the pellet and C_P is the heat capacity.

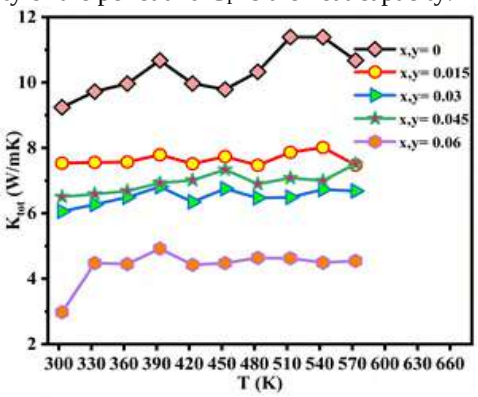

Fig.1. Thermalconductivity of Mg and Bi co-doped GeTe materials.

4. CONCLUSION

We report low thermal conductivity (k) achieved by tuning the carrier concentration and complex nanostructure successfully modulated through co-doping of Bi and Mg in GeTe compounds via large differences in strain and mass fluctuations and structural angle. The bi-functional nature of TE materials makes it possible to also achieve thermoelectric cooling for devices or personal thermal management. These kinds of materials could play a crucial role in development of future thermoelectric devices.

5. REFERENCES

[1]. Tan, G.; Zhao, L. D.; Kanatzidis, M. G. Rationally Designing High-Performance Bulk Thermoelectric Materials. Chem. Rev. 2016, 116, 12123−12149.

[2]. Chen, Z.; Zhang, X.; Pei, Y. Manipulation of Phonon Transport in Thermoelectrics. Adv. Mater. 2018, 30, 1705617.

[3] X.L. Shi, J. Zou, Z.G. Chen, Advanced thermoelectric design: from materials and structures to devices, Chem. Rev. 120 (2020) 7399–7515.

Effect of Vacuum Annealing on the Cationic Distribution and Magnetic Properties of $NiFe_2O_4$ Thin Films

Ambrish Dwivedi[1] ,Vinay Shrivastava[1],Yksh Gupta[2],Keval Gadani[3],Sanjay Kumar Upadhyay[4],Sourav Chowdhury[5], Jayjit Kumar Dey[5] Moritz Hoesch[5] Anil Gome[6,7],Ratnesh Gupta[2],Sagar Sen[1]*

[1]Department of Physics, Maharaja Bhoj Govt. P.G. College, Dhar 454001, India.

[2]School of Instrumentation, Devi Ahilya Vishwavidyalaya, Indore, India.

[3]Centre of Education, Faculty of Physics, Indian Institute of Teacher Education (IITE), Gandhinagar, India.

[4]HNB Garhwal University Srinagar Garhwal, Uttarakhand-246174, India.

[5]Deutsches Elektronen-Synchrotron DESY Notkestrasse 85, 22607, Humburg, Germany.

[6]UGC-DAE Consortium for Scientific Research, Indore 452010, India.

[7]Depaetment of Physics, Medi-Caps University, Indore, India.

Email: sssagarsen@gmail.com

Abstract: Thin films of $NiFe_2O_4$ were deposited on Si substrates using pulsed laser deposition and subsequently annealed under vacuum at different temperatures. XPS analysis revealed a temperature-driven reduction of Ni^{3+} to Ni^{2+} and the emergence of Fe^{2+}, indicating cation redistribution influenced by oxygen vacancies. XMCD measurements confirmed these changes, showing increased Ni^{+2} intensity and decreased Fe^{3+} contribution. Structural and electronic modifications induced by annealing significantly impact the material's magnetic properties. These findings demonstrate the crucial role of vacuum annealing in tuning the electronic and magnetic characteristics of $NiFe_2O_4$ thin films for spintronic applications.

1. INTRODUCTION

Nickel ferrite ($NiFe_2O_4$) is a soft magnetic material with a normal spinel structure, known for its excellent chemical stability, moderate saturation magnetization, and low coercivity [1.2]. These properties make $NiFe_2O_4$ thin films highly desirable for various technological applications, including spintronics, microwave devices, and magnetic sensors. The magnetic and structural properties of $NiFe_2O_4$ thin films are strongly influenced by fabrication parameters such as deposition technique, annealing conditions, and environmental factors like oxygen partial pressure [3].

Vacuum annealing is a crucial post-deposition treatment that can significantly modify the cation distribution, strain relaxation, and defect concentration in ferrite thin films, ultimately affecting their magnetic properties. By altering the oxygen content and promoting cation redistribution between tetrahedral and octahedral sites, vacuum annealing can tune key parameters such as saturation magnetization (M_s), coercivity (Hc), and magnetocrystalline anisotropy [4]. Despite extensive studies on bulk and thin-film ferrites, the impact of vacuum annealing on the structural and magnetic characteristics of $NiFe_2O_4$ thin films remains an area of active research.

This study investigates the effect of vacuum annealing on the structural and magnetic properties of $NiFe_2O_4$ thin films. By employing X-ray diffraction (XRD), X-ray photoelectron spectroscopy (XPS), and vibrating sample magnetometry (VSM), we analyze the changes in crystallinity, oxidation state, and magnetic behavior induced by vacuum annealing. Understanding these effects is essential for optimizing $NiFe_2O_4$ thin films for advanced technological applications.

2. EXPERIMENTAL

$NiFe_2O_4$ thin films were deposited using pulsed laser deposition (PLD) at the PLD lab, School of Instrumentation, DAVV, Indore. A $NiFe_2O_4$ target was ablated using a Nd:YAG laser with a wavelength (λ) of 355 nm under a deposition pressure of ~2×10^{-6} mbar. The films were deposited on Si (100) substrates at room temperature under high vacuum (10^{-6} mbar).

To study the effect of vacuum annealing, the deposited films were annealed at different temperatures: S1 (room temperature), S2 (300°C), and S3 (400°C).

3. RESULTS AND DISCUSSION

The XRD patterns confirm the presence of cobalt ferrite with a cubic spinel structure. The peaks at 35.5° correspond to the (311) reflections of Nickel Ferrite. The intensity of the (311) diffraction peak increases with annealing temperature suggesting an increase in atomic grain size. As a function of annealing temperature, the film thickness and surface roughness decrease, while substrate roughness slightly increases. SQUID-VSM measurements indicate that increasing temperature induces perpendicular magnetic anisotropy (PMA) in the NFO film and increases its saturation magnetic moment. XPS measurements reveal the cation distribution in $NiFe_2O_4$ thin films. With increasing annealing temperature, Ni^{2+} concentration increases while Ni^{3+} decreases, indicating a reduction of Ni^{3+} to Ni^{2+}, likely due to changes in oxygen vacancy concentration or cation redistribution. After annealing, Fe^{2+} emerges and increases, suggesting a partial reduction of Fe^{3+} to Fe^{2+}. Additionally, Fe^{3+} ions from octahedral sites migrate toward tetrahedral sites, further confirming cation redistribution within the spinel structure. These changes in oxidation states and site occupancy significantly influence the electronic and magnetic properties of the annealed films.

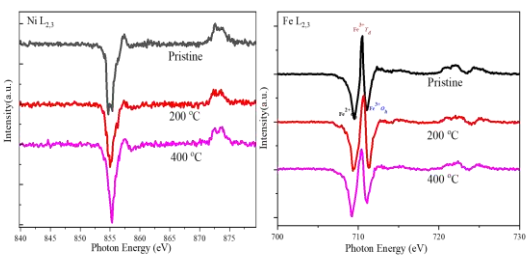

Fig.1. XMCD of pristine and annealed nickel ferrite thin films.

4. CONCLUSION

Vacuum annealing of $NiFe_2O_4$ thin films induces significant cationic and electronic modifications. The reduction of Ni^{3+} to Ni^{2+} and the emergence of Fe^{2+} indicate cation redistribution influenced by oxygen vacancies. XMCD analysis confirms these changes, showing increased Ni and decreased Fe^{3+} intensity. These alterations play a crucial role in tuning the magnetic and electronic properties of $NiFe_2O_4$ films, making them promising for spintronic applications.

ACKNOWLEDGEMENT

The authors sincerely acknowledge the financial support from the Inter-University Accelerator Centre (IUAC), Delhi (Project No. IUAC/13.3A/74320, dated 17.07.2023), and the Madhya Pradesh Council of Science and Technology (MPCST). The financial assistance from these agencies is gratefully acknowledged. The authors also extend their gratitude to UGC-DAE CSR Indore for providing the necessary experimental facilities.

REFERENCES

[1] J. Dash, S. Prasad, N. Venkataramani, R. Krishnan, P. Kishan, N. Kumar, S.D. Kulkarni, S.K. J. Appl. Phys 86 (1999) 3303. https://doi.org/10.1063/1.371206.

[2] J. F. Hochepied, P. Sainctavit, and M. P. Pileni, ‘X-ray absorption spectra and X-ray magnetic circular dichroism studies at Fe and Co L2,3 edges of mixed cobalt–zinc ferrite nanoparticles: cationic repartition, magnetic structure and hysteresis cycles’, *J Magn Magn Mater*, vol. 231, no. 2–3, pp. 315–322, Jun. 2001, doi: 10.1016/S0304-8853(01)00182-2.

[3] J. S. Sagu, K. G. U. Wijayantha, and A. A. Tahir, ‘The Pseudocapacitive Nature of CoFe2O4 Thin Films’, *Electrochim Acta*, vol. 246, pp. 870–878, Aug. 2017, doi: 10.1016/j.electacta.2017.06.110.

[4] A. Raghunathan, I. C. Nlebedim, D. C. Jiles, and J. E. Snyder, ‘Growth of crystalline cobalt ferrite thin films at lower temperatures using pulsed-laser deposition technique’, *J Appl Phys*, vol. 107, no. 9, p. 44502, May 2010, doi: 10.1063/1.3357315.

Topic Code: Radiation-Resistant Materials and Radiation-Induced Defects

Gamma-ray effects on Gd^{3+} doped Borophosphate Glass for radiation shielding and TL-Dosimetry Applications

Paul Dhinakaran A[a*], P. Vinothkumar[a*]

[a] Department of Physics, Saveetha Engineering College, Thandalam, Chennai 602105, Affiliated to Anna University, Guindy, Chennai, Tamil Nadu 600025

Email: sagaidhina24@gmail.com

Abstract: Radiation-resistant glass development is crucial for possible uses in optics, displays, and nuclear or space conditions. With a Gamma Chamber 5000, Co-60 Gamma Irradiator (Atomic Energy Regulatory (AERB), India), the γ-ray resistance of Gd^{3+}-doped Borophosphate glass is examined in this work under 10kGy gamma irradiation. The melt-quench method was used to create the Gd^{3+}-doped Borophosphate glass [$40B_2O_3$ - $39P_2O_5$ - $5Al_2O_3$ - 10ZnO - $5KF_2$ and $1Gd_2O_3$ (wt%)], and its properties were investigated both before to and following gamma irradiation. The effects of 10kGy of γ-radiation on the glass were examined using XRD, SEM, optical absorption, FTIR, photoluminescence, CIE-1931 color chromaticity, ESR, Phy-x analysis for gamma ray shielding and Thermoluminescence (TL).

1. INTRODUCTION

The creation of irradiation materials has significantly aided the advancement of nuclear technology over the past several decades. Consequently, applying radiation-resistant materials and comprehending their basic idea is crucial. The purpose of radiation-resistant glass is to attenuate, reflect, and absorb ionizing and non-ionizing radiation [1]. Transparency is preserved while optimum protection is achieved by the optimization of composition and thickness. Common materials include glass, which provides resistance to thermal shock, and lead glass, which is renowned for its great density and efficiency in preventing ionizing radiation [2]. In the glass network, ionizing radiation can produce a variety of flaws, including extrinsic faults brought on by radiation exposure and intrinsic defects created during preparation [3]. These flaws may change the glass's optical characteristics and have practical uses in lighting or sensing applications. Glass that is resistant to radiation is essential for protecting against radiation exposure, but it also has drawbacks in terms of defect generation when exposed to radiation. Research is still being done to improve these materials' performance in demanding environments [4].

2. MATERIAL AND METHODS

The melt-quenching process, a popular glass-making method, was used to create the Gd^{3+}-doped Borophosphate glass. The initial elements that need to be collected are $40B_2O_3$ - $39P_2O_5$ - $5Al_2O_3$ - 10ZnO - $5KF_2$ and $1Gd_2O_3$. In a mortar and pestle, thoroughly mix these ingredients to create a uniform consistency. Heat-treat the furnace after placing the mixed powders in an alumina crucible. Heat the furnace gradually to the mixture's melting point, which is 1100°C, to ensure that the glass is fully melted and uniform. After that, leave it there for an hour or two. To guarantee homogeneity and get rid of bubbles, swirl the molten glass liquid using a glass stirring rod. To create the appropriate forms, carefully pour the molten glass into hot molds. Then, let the glass cool slightly inside the molds. To remove internal tensions, move the molded glass to an annealing furnace and anneal it by lowering the temperature progressively from the molding temperature to room temperature. Glass samples were exposed to 10 kGy of gamma radiation for 13 hours to examine them and both the before and after gamma-ray glass images shown in figure 1.

2.2. CHARACTERIZATION STUDIES

The measurements for the samples obtained during the Gd^{3+}-doped Borophosphate glass research are as follows. The Bruker D2 XRD diffractometer, FTIR by ATR-IR. The optical absorption by V-670 double UV-VIS-NIR Spectrophotometer. Emission by JY Fluorolog-3-11 PL Spectrofluorometer. The CIE 1931 Color Calculator tool was used to get the CIE x, and y coordinates, CCT, and Purity values. TL reader (Nucleonix TL research reader (Type: TL 1009I)) was used. The JES200 ESR spectrometer was used to examine electron spin resonance (ESR) spectroscopy.

Fig.1. The Gd^{3+}-doped Borophosphate glass before and after 10kGy Gamma irradiation.

REFERENCES

[1]. Li G, Li C, Hou Z, Peng C, Cheng Z, Lin J (2009) Opt Lett 34:3833

[2]. Nogami M, Abe Y (1997) J Appl Phys 81:6351

[3]. Arai K, Namikawa H, Kumata K, Honda T, Ishii Y, Handa T (1986) J Appl Phys 59:3430

[4]. Zhang H, Liu XY, Zhao FY, Zhang LH, Zhang YF, Guo H (2012) Opt Mater 34:1034

Morphological evolution of MBE grown Antimony nanocrystals under ion irradiation

Jinu Job[1,2], Vikas Singh Gahlot[1,2], P. Jegadeesan[1], Sujoy Sen[1,2], S. Amirthapandian[1,2], B. Sundaravel[1,2]
[1]Materials Science Group, Indira Gandhi Centre for Atomic Research, Kalpakkam- 603 102
[2]Homi Bhabha National Institute, Indira Gandhi Centre for Atomic Research, Kalpakkam - 603 102
Email: jinu@igcar.gov.in, bsundar@igcar.gov.in

Abstract: Antimony thin films are grown using molecular beam epitaxy (MBE) method at 245 °C. The evolution of morphology of these films under 2 MeV Al^+ ion irradiation is studied using In-situ ion irradiation and imaging with field emission scanning electron microscope (i^4- FESEM) facility. Our results shows that the facets of square pyramidal antimony nanocrystals changes significantly compared to triangular-structured antimony nanocrystals under ion irradiation. This observation is discussed in the light of basic ion-solid interactions.

1. INTRODUCTION

The bandgap of bulk antimony is 0.15 eV whereas the band gap of antimonene (monolayer of antimony) 1.55 eV and it is tunable [1]. Ion irradiation causes damage which results in change in the properties like energy band gap, transmittance, reflectance and refractive index of the antimony thin film. The morphological evolution of antimony nanocrystals under ion irradiation is studied with i^4-FESEM.

2. EXPERIMENTAL

The cleaned *c*-plane sapphire substrates are annealed at 1200 ℃ for 5hrs under an oxygen atmosphere. Prior to deposition of film, the substrate was heated up to 250 ℃ for 20 minutes in UHV (2×10^{-10} mbar) conditions. The Sb(500Å)/*c*-Al_2O_3 was deposited with the substrate temperature of 245 °C and the deposition rate is 0.25 Å/s. The morphological evolution of antimony thin films for various ion fluences (ranging from 2.24 $\times10^{14}$ ions/cm^2 to 4.08 $\times10^{16}$ ions/cm^2) of 2 MeV Al^+ ion irradiation is studied using i^4 – FESEM facility [2].

3. RESULTS AND DISCUSSION

Figure 1(a) shows the SEM image of the as-prepared Sb(500Å)/*c*-Al_2O_3 thin film. It shows square pyramids and triangular nanocrystals of antimony. Figure 1(b) shows the SEM image of the 2 MeV Al^+ ion irradiated sample with a ion fluence of 4.08 $\times10^{16}$ ions/cm^2. The diagonal length of square pyramids (marked in Fig 1(a) and 1(b)) are measured using imageJ software and the diagonal length as a function of ion fluence is shown in Figure 1(c). It is observed that, with the increase in ion fluence, the diagonal length of square pyramids are decreasing whereas triangular structures remain unaffected. The electronic energy loss of 2 MeV Al^+ ions in Sb is 1.69 keV/nm and sputtering yield is 0.35 atoms/ion, which are estimated from stopping ranges of ions in matter (SRIM-2013 software) [3]. The deposited energy density (ion fluence × electronic stopping power) is 689 keV/nm^3 in the film which can raise the temperature and cause desorption of antimony. Sputtering also will give raise to material loss. These processes can give raise to the shrinking of the antimony square pyramids, thereby the reduction in diagonal length was observed. Preferential sputtering of square pyramids compared to triangular islands is attributed the facet orientation dependent sputtering yield.

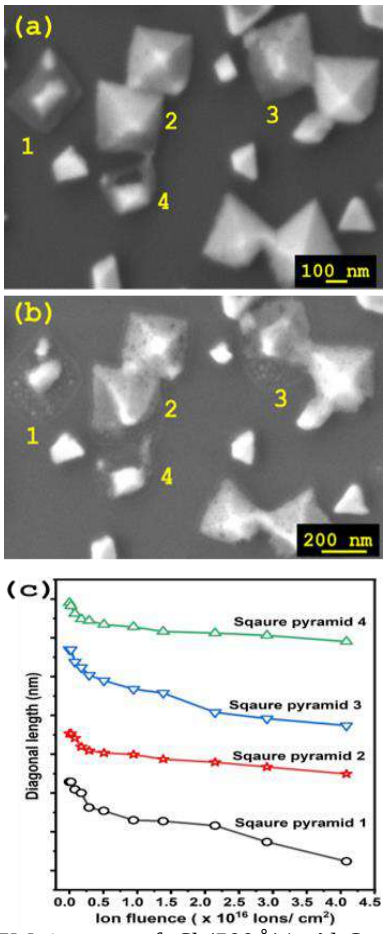

Fig.1. SEM images of Sb(500Å)/*c*-Al_2O_3 thin film (a) before irradiation and (b) after ion irradiation with fluence of 4.08 $\times10^{16}$ ions/cm^2 and (c) the graph diagonal length versus various ion fluencies on square pyramids marked 1,2,3 and 4 in SEM images.

REFERENCES

[1]. Aktürk, O. Ü, et.al. Physical review B. **91** (2015) 235446.
[2]. Jegadeesan P, et al. In-situ ion irradiation and imaging with field emission scanning electron microscope (i^4-FESEM) facility at IGCAR (Communicated to NIMB)
[3]. J. Ziegler, James Ziegler - SRIM & TRIM, (2017). http://www.srim.org/

Comparative analysis of the radiation hardness of PM6 and PTB7-th for space application in organic solar cell

Anuradha
Malaviya National Institute of Technology ,JLN Marg ,
Malviya Nagar ,Jaipur - 302017, India.
2022rpy9512@mnit.ac.in

Abstract:

This study investigates the impact of gold ion irradiation on the stability of two organic materials, PM6 and PTB7-Th. The materials were spin-coated at various speeds and subsequently irradiated with 70 keV gold (Au) ions at a fluence of 1×10^{13} ions per cm^2. To assess the changes in material properties, a range of characterization techniques were employed, including photoluminescence, Raman spectroscopy, UV-visible spectroscopy, X-ray photoelectron spectroscopy (XPS), atomic force microscopy (AFM), and scanning probe microscopy (SPM). The Gibbs free energy was used to evaluate the materials' stability under irradiation, with the goal of identifying which material demonstrates greater durability for use in organic solar cells, particularly in space missions where exposure to cosmic radiation is a concern.

1. INTRODUCTION

Gold ions have the ability to enhance the strength and stability of materials by directing the flow of electrons or ions, especially under radiation exposure. This interaction increases the material's resistance to cosmic radiation, making it ideal for space applications. Perovskite solar cells, modified with cations like europium (Eu^{3+}) and dysprosium (Dy^{3+}), offer improved radiation resistance but contain toxic lead (Pb), posing significant environmental risks. The lead could corrode spacecraft and accumulate in space, creating long-term pollution.[1-2].

2. MAJOR SECTIONS

2.1 EXPERIMENTAL WORK

PM6 and PTB7-Th (5 mg each) were dissolved in 2.5 mL chlorobenzene and sonicated. Thin films were spin-coated onto glass substrates at varying speeds (600-3000 rpm) using an NXG-m1 spin coater. The films were irradiated with Au ions at a fluence of 1×10^{13} ions/cm^2 and 70 KeV using an ion implanter. Material properties were characterized using photoluminescence, Raman spectroscopy, UV-visible spectroscopy, XPS, AFM, and SPM.

2.2. Equations

$$\Delta G = \Delta H - T\Delta S \qquad (1)$$

The above equation is used to find out stability of organic thin films

3. FIGURES AND IMAGES

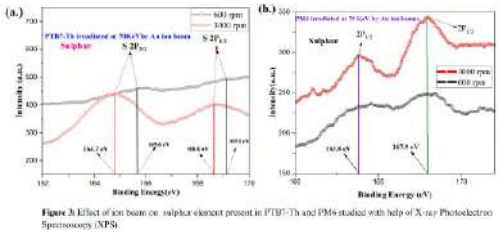

Figure 3: Effect of ion beam on sulphur element present in PTB7-Th and PM6 studied with help of X-ray Photoelectron Spectroscopy (XPS).

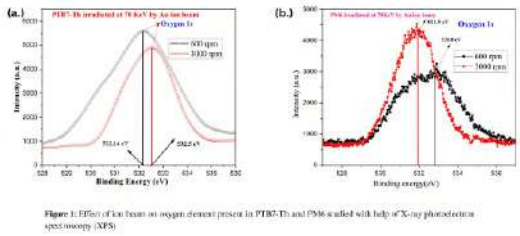

Figure 1: Effect of ion beam on oxygen element present in PTB7-Th and PM6 studied with help of X-ray photoelectron spectroscopy (XPS)

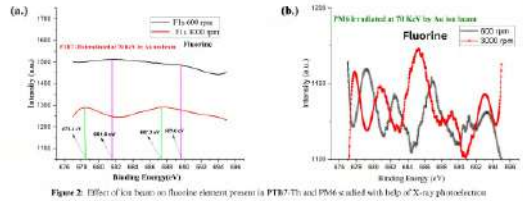

Figure 2: Effect of ion beam on fluorine element present in PTB7-Th and PM6 studied with help of X-ray photoelectron spectroscopy (XPS)

4. TABLES

Table 1. The Table summarizes the roughness of PM6 and PTB7-Th thin films.

spinning speed	PM6(roughness)	PTB7-Th(roughness)
600 rpm	8.88 nm	2.182 nm
800 rpm	11.71 nm	4.711 nm
1500 rpm	16.17 nm	3.712nm
3000 rpm	28.42 nm	2.158 nm

ACKNOWLEDGEMENT

The authors express their gratitude to their supervisor Dr. Rahul Singhal for his invaluable supervision and continuous guidance throughout the experiment.

REFERENCES

[1]. Ustinova, M. I., et al. (2024). *Eu Shuttle for Perovskites: Eu^{2+}/Eu^{3+} Redox to Boost Stability*. J. Mater. Chem. A, 12.

[2.] Ustinova, M. I., et al. (2024). *Radiation Hardness of Perovskites via Dy^{2+}*. Chem. Eng. J., 493, 152522.

Energy Storage study on gamma irradiated PANI – CuO nano Composites.

S. Ramakrishnan[1] and S. Rajakarthihan[2]
[1]Department of Physics (SF), Madura College, Madurai.
[2]Department of Physics, Thiagarajar College, Madurai.
Email: rajakarthihan@gmail.com

Abstract

The polyaniline - copper oxide (PANI– CuO) nano composite was synthesized by grinding technique and the samples were irradiated using gamma ray source of Co^{60}. The polymer composites have been subjected to gamma radiation from 4 to 20 kGy dosages. The structural, vibrational, optical and morphological characteristics of every materials have been determined by X-ray diffraction (XRD), Fourier Transform Infrared (FTIR) spectroscopy, Ultra Violet spectroscopy (UV), Photoluminescence spectroscopy (PL), Scanning electron microscopy (SEM) and EDAX analysis. Cyclic voltammetry (CV) has been used to access application of the prepared and irradiated samples. The 20 kGy irradiated PANI– CuO sample had a maximum specific capacitance and energy storage capacity than pure one, measuring 184.19 F/g and 23.02Wh/Kg respectively. According to the results, irradiation composites may be appropriate for the use as super capacitive electrode materials.

Keywords: CuO, PANI, Composites, Irradiation, Capacitance, Energy storage

Nanostructuring of Germanium surface using low energy Ga ion implantation

Hrudya Radhakrishnan, Kamalesh N, Ramanathaswamy Pandian*
[1]Surface and Sensors Studies Division, Materials Science Group, Indira Gandhi Centre for Atomic Research, A CI of Homi Bhabha National Institute, Kalpakkam 603102, Tamil Nadu, India
***Email: rpandian@igcar.gov.in**

Abstract: We report the formation of porous nanostructures on crystalline Ge by low energy Ga^+ ion implantation using focused ion beam microscopy. The morphology of the nanostructures formed was characterized by scanning electron microscopy. The Raman spectra of the nanostructured Ge showed a broad peak associated with the amorphous Ge. The origin of decomposition of the structure upon ion irradiation can be correlated to the vacancy clustering and/or micro-explosions occurring beneath the surface.

1. INTRODUCTION

Nanostructured semiconductors like Si, Ge are preferred largely because of its compatibility with complementary metal oxides (CMOS). Unlike Si, Ge has not been widely used due to factors, including low bandgap, low absorption in visible region and high optical loss in infrared region. However, the nanostructured Ge owing to its several advantages such as high surface area, high theoretical specific capacitance, has potential applications including photodetectors, chemical sensors and energy storage [1-2]. The nanostructured morphology can be prepared by various methods such as physical/chemical vapor deposition, electrochemical cycling and ion implantation.

Generally, the nanostructuring of Ge by ion implantation occurs via two major steps. When an ion beam of relatively high mass, is incident on the surface of the crystalline Ge (c-Ge), an amorphous layer of Ge, (a-Ge) is formed when a critical dose is used. When the dose is further increased, after the critical dose (~ 10^{15} ions/cm^2), the amorphous layer collapses (or decomposes), exhibiting voids and porosity. An interconnected network of nanograsses or nanowalls will be formed for higher doses [3]. The nanostructuring, or often termed as nanotexturing, depends on the energy of the incident ion, mass of the ions, fluence and angle of incidence. In this work, we study the effect of fluence of the Ga^+ ion on the surface modification of Ge for the normal incidence of Ga ion beam on Ge.

2. EXPERIMENTAL METHODS

A polished and cleaned single crystal Ge wafer with (111) orientation and thickness of 0.5 mm was irradiated with Ga ions using a focused ion beam microscopy. Beam energy of 30 keV was used and fluence was varied from 10^{15} to 10^{16} ions/cm^2. The distribution of Ga ions in the Ge subsurface was estimated using SRIM 2013 software. The morphology of the nanostructured Ge, was analyzed using scanning electron microscopy (SEM, Model - Supra 55 by Carl Zeiss, Germany). The structural property was analyzed using a 532 nm excitation source, Raman spectrometer (Renishaw) in a backscattered geometry.

3. RESULTS AND DISCUSSION

SEM images of the nanostructured Ge are shown in Fig. 1. Fig. 1a shows the pristine or unmodified c-Ge consisting of smooth surface and Fig. 1b and 1c shows the modified or nanostructured Ge after ion irradiation at fluence of 10^{15} ions/cm^2 and 10^{16} ions/cm^2, respectively. A less dense porous nanostructure is obtained for the fluence of 10^{15} ions/cm^2 and while increasing the fluence to 10^{16} ions/cm^2, the porous surface collapses to form an interconnected network of nanowalls. Figure 2 shows the Raman spectra for samples irradiated with different fluences. The absence of sharp intense peak at 301 cm^{-1}, indicates the amorphous structure formed. The structural decomposition upon the ion irradiation is correlated to the vacancy clustering and/or micro-explosions occurring beneath the surface [3].

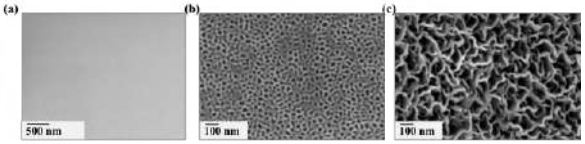

Fig.1. SEM images of a) pristine c-Ge, b) irradiated with 10^{15} ions/cm^2, c) irradiated with 10^{16} ions/cm^2.

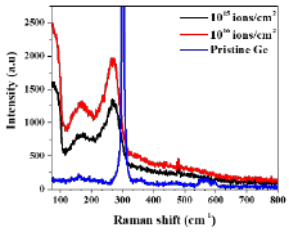

Fig.2. Raman spectra of pristine and irradiated Ge.

4. CONCLUSION

The influence of implantation parameters of low energy Ga ion on the surface modification of Ge was investigated. The change in the structural and morphology was confirmed with Raman spectra and scanning electron micrographs.

ACKNOWLEDGEMENT

HR acknowledges Department of Atomic Energy for the financial support.

REFERENCES

[1]. L. Romano et al, J. Appl. Phys., **107**(8) 2010.
[2]. T. P. Pasanen et al, Adv. Opt. Mater., **8**(11), 2020.
[3]. N. G. Rudawski et al, J. Mater. Res. **28**(13), 2013.

Insights into the Behaviour of Shape Memory Alloys under Extreme Conditions: A Candidate Material for the Passive Systems in Future FBR

Salil Verma, Rosy Sarkar, Bhuwan Chandra Sati, R. Suresh Kumar, K. Natesan
Reactor Design Group, IGCAR, Kalpakkam - 603102
Email: salil@igcar.gov.in

Abstract: Shape Memory Alloys (SMAs) are metallic materials capable of reverting to a predefined shape upon temperature variation due to reversible phase transformations. This paper examines their properties, behaviour under extreme conditions, and potential applications in the future FBR, particularly focusing on passive damper opening for the Safety Grade Decay Heater Removal (SGDHR) system.

1. INTRODUCTION

Shape Memory Alloys (SMAs) are metallic materials capable of returning to a predefined shape after heating. This behaviour results from a transition from a low-temperature martensite phase to a high-temperature austenite phase, a process known as the Thermal Shape Memory Effect (SME). This characteristics introduces shape memory effect on material against temperature. Another key property of these alloys is superelasticity, or pseudoelasticity, allowing them to endure significant deformation without permanent change and snap back to their original shape. The stress-strain behaviour of typical SMA is shown in Fig.1.

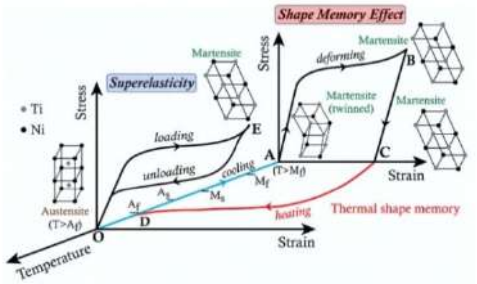

Fig.1. Stress-Strain-Temperature diagram of SMA [1]

2. LITERATURE REVIEW

Since their discovery in the 1960s, extensive research has been conducted on SMAs, focusing on understanding phase transformation mechanisms, optimizing alloy compositions, and improving mechanical properties. Recent advancements include high-temperature SMAs for extreme environments and new alloy systems to enhance performance [2, 3].

3. EXTREME CONDITION PROPERTIES

3.1 Types of SMAs and Temperature Limits

- *Nickel-Titanium (Ni-Ti) Alloys (Nitinol):* Operate within -200°C to 110°C; preferred for biocompatibility and mechanical properties.
- *Copper-Based Alloys (Cu-Al-Ni, Cu-Zn-Al):* Function up to around 200°C; suitable for moderate temperature stability.
- *β-Titanium Alloys:* Suitable up to 600°C; ideal for extreme environments like aerospace and industrial applications.

3.2 Thermo-Mechanical Behavior

SMAs exhibit thermal shape recovery and superelasticity under extreme conditions.

3.3 Cryogenic Behavior

Enhanced damping properties at low temperatures make SMAs ideal for cryogenic applications.

3.4 Corrosion Resistance

Ni-Ti alloys offer good corrosion resistance; additional coatings or alloying elements (e.g., Cr, Pd) may be required in aggressive environments.

4. POTENTIAL APPLICATIONS FOR FUTURE FBR

SMAs, especially β-Titanium alloys, can be utilized in the future FBR as a temperature-sensitive actuator mechanism for the damper opening for the Safety Grade Decay Heat Removal (SGDHR) piping system (Fig.2). Their high-temperature stability and reliable actuation properties make them ideal for this function under extreme conditions. Current studies are focusing on the design of passive damper openings shown in Fig.2. Additionally, SMAs have potential applications in electrical safety switches and smart valves.

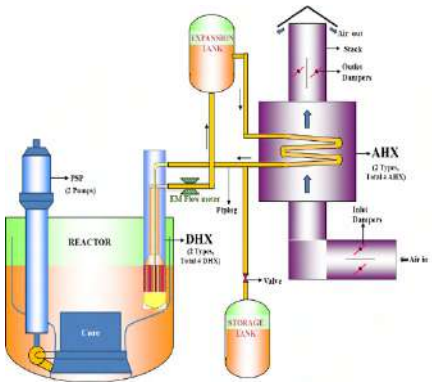

Fig.2. SGDHR showing AHX dampers in PFBR.

5. CONCLUSION

SMAs possess unique properties that make them ideal for extreme conditions and various applications. Ongoing research aims to optimize these materials for passive damper opening for the SGDHR piping system.

REFERENCES

[1]. Srivastava, R, et al, (2022), Sensors.
[2]. Otsuka, et al, (1998), Cambridge University Press.
[3]. Lagoudas, D.C (2008), Springer.

Topic category: Radiation Resistant Materials and Radiation Induced Defects

Real-time reliability analysis of 8051 microcontroller in gamma and proton environments

Charu Sharma[1,2], R. P. Behera[2], Saif A. Khan[3], Puspalata Rajesh[4], S. Amirthapandian[1,5]
[1]Homi Bhabha National Institute, Indira Gandhi Centre for Atomic Research, Kalpakkam – 603102
[2]Real Time System Division, Indira Gandhi Centre for Atomic Research, Kalpakkam -603 102
[3]Materials Science, Inter University Accelerator Centre, New Delhi -110 067
[4]Water and Steam Chemistry Division, BARC Facilities, Kalpakkam -603 102
[5]Materials Science Group, Indira Gandhi Centre for Atomic Research, Kalpakkam - 603 102
Email: 93charusharma@gmail.com, pandian@igcar.gov.in

Abstract: The instrument and control (I&C) system is critical in maintaining the safety, efficiency, and reliability of a nuclear power plant. The harsh radiation environment impacts the performance of the I&C system. The present study investigates the reliability of an AT89C51RD2 microcontroller under radiation (gamma and proton) exposure in real-time. Custom circuits were designed to expose the microcontroller to varying doses of gamma radiation from a ^{60}Co source and proton irradiation. The results indicated that the device could operate without failure and performance degradation up to a total absorbed dose of approximately 0.6 kGy for gamma radiation and 1.5 kGy for proton irradiation, indicating its potential robustness in radiation environments.

1. INTRODUCTION

The I&C system of prototype fast breeder reactor (PFBR) utilizes remote terminal units (RTUs) for real-time monitoring and control of safety functions. In present work, the 8051 microcontroller, which is used in RTU boards, is subjected to radiation testing to validate its performance and functional integrity. The microcontroller is exposed to gamma and proton irradiation, and its performance is analyzed.

2. METHODS

Custom PCBs were designed for the microcontroller testing, including circuitry for biasing during irradiation and *in-situ* measurements. The PCB consists of a MAX232 to establish a link for serial communication with a personnel computer (PC). LEDs are connected to the microcontroller, to test its functionality by switching them on and off.

The gamma irradiation experiments were conducted using a GC-5000 self-shielded gamma irradiation chamber, with a ^{60}Co radiation source and a measured dose rate of 1.94 kGy/h.

For proton irradiation, 25 MeV proton beam from 15 UD pelletron accelerator at the Inter-University Accelerator Centre (IUAC), New Delhi, was used. The PCB with device under test (DUT) was mounted on the adjustable sample holder in the irradiation chamber, with connections *via* BNC cables and vacuum feed-throughs. The proton flux was 6×10^9 p/cm^2/s. The cumulative total dose equivalent of proton fluence in rad (100 rad =1 Gy) is given by dose (rad)=$1.6\times10^{-5}\times\phi\times$LET [1], where ϕ and LET are ion fluence and linear energy transfer.

3. RESULTS

The performance of the DUT was observed by analyzing the memory array of the DUT written with a specific program to flash the LEDs and transmit the output data to the PC. The experiment is ended when the output data stopped displaying on the PC. It was observed that gamma radiation degrades device functionality beyond 0.6 kGy, causing permanent failure where the DUT cannot be reprogrammed due to total ionizing dose effects.

For each DUT, the maximum dose at which the device failure was observed, is given in Fig.1. In both experiments, bit flips were observed in the memory array and LED blinking and serial data transmission was affected. The pin output voltage decreased and device input current increased with higher absorbed doses. It was found that the proton dose beyond which the device will fail is twice as high as compared to gamma irradiation. During gamma irradiation, ionization is the dominant damage process, while proton irradiation causes both ionization and displacement damage.

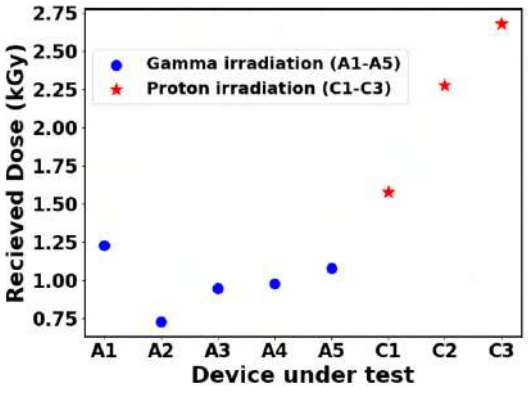

Fig. 1 Total dose received by DUTs during gamma irradiation (A1-A5) and proton irradiation (C1-C3)

REFERENCES

1. B. Kocaman, et. al., AIP Conf Proc **2700** (2023) 20042.

Defect Evolution in Sequential He and Ni Ion Implanted FeCrMnNi High Entropy Alloy

S. Vinitha[1], S. Abhaya[1, 2], C. David[1, 2]
[1]Homi Bhabha National Institute, Kalpakkam, TamilNadu-603102, India
[2]Material Science Group, Indira Gandhi Centre for Atomic Research, Kalpakkam- 603102, TamilNadu, India
Email: vinitha@igcar.gov.in

Abstract: Multicomponent alloys with near- equiatomic composition exhibit remarkable properties, which makes them potential candidates for nuclear structural materials. In this present work, the radiation response of a quaternary FeCrMnNi alloy is explored. Defect evolution of implantation- induced defects in He plus Ni ion-implanted FeCrMnNi has been studied using depth-resolved positron beam as a function of annealing temperature. The growth of He bubbles is observed from the Doppler S-parameter beyond 823 K.

1. INTRODUCTION

Medium and High Entropy Alloys are the area of great interest due to their unique material properties. Equiatomic or near-equiatomic composition of the alloys results in enhanced properties that make them tunable for different functional applications [1, 2]. Improved radiation resistance of HEAs with adequate mechanical properties makes them potential candidates for nuclear structural applications [2]. Variable Low Energy Positron Beam technique is a sensitive tool that can be used to study implantation-induced vacancy-like defects in materials [3]. Doppler S-parameter based Positron beam measurements were carried out on the alloy to study the microstructural evolution of implantation-induced defects in the alloy.

2. EXPERIMENTAL DETAILS

A near-equiatomic $Fe_{27}Cr_{18}Mn_{27}Ni_{28}$ alloy was prepared by the arc melting technique, followed by homogenization at 1373 K for 6 hrs. XRD measurements were carried out to find the phases formed in the prepared sample. The homogenized sample was then 18% cold worked. He^+ ion implantation (130 keV, 1×10^{16} ions/cm^2, 5630 appm) followed by Ni^+ ion implantation (1.5 MeV, 5×10^{16} ions/cm^2, 100 dpa) was performed on the cold-worked samples at room temperature. Depth-resolved Doppler broadening measurements with varying positron beam energies (E_p) were carried out on cold-worked implanted samples post-annealed at different temperatures.

3. RESULTS AND DISCUSSION

3.1. Material Characterization

The XRD pattern of the homogenized sample reveals an FCC structure with a lattice parameter of 3.59 Å. The calculated criteria for the formation of solid solution show FCC phase, which matches with the XRD results.

3.2. PAS Results

S vs. Ep curves of the implanted samples post-annealed at different temperatures were obtained. Fig. 1 shows the S parameter (averaged between 8 and 18 keV, corresponding to a range of depth between 138 and 506 nm) as a function of annealing temperature. The S parameter value of 0.555 for the room temperature implanted sample corresponds to the presence of implantation-induced vacancy-like defects. At 723 K, there is a decrease in S-parameter attributed to the formation of He-vacancy complex. Further increase in annealing temperature leads to an increase in the S-parameter corresponding to the formation and growth of He bubbles due to He plus Ni ion implantation. A detailed analysis of defect microstructure will be presented.

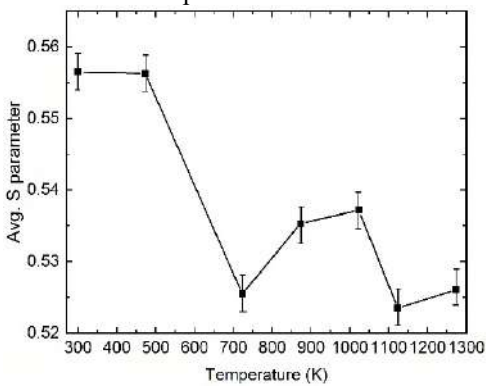

Fig.1. S parameter (averaged) as a function of annealing temperature for sequential He and Ni ion implanted samples.

ACKNOWLEDGEMENT

The authors like to acknowledge Dr. Chanchal Ghosh for the preparation of arc melted FeCrMnNi and Dr. Nithya Ravindran for XRD measurement.

REFERENCES

[1]. Ed J. Pickering et al, Entropy 23 (2021) 98.
[2]. Michael Moschetti et al, Journal of Nuclear Materials 567 (2022) 153814.
[3]. Amarendra G et al, Current Science 73, no.5, (1997) 409-17.

Study of ion beam-induced luminescence in β-Ga_2O_3 by 100 keV He^+ ions

Monu Kataria[1], Fouran Singh[1], Sujoy Sen[2], Christopher David[2] and Debdulal Kabiraj[1]
[1]Inter-University Accelerator Centre, Aruna Asaf Ali Marg, New Delhi 110067, India
[2]Indira Gandhi Centre for Atomic Research, HBNI, Kalpakkam 603102, India
Email: mkmonukataria@gmail.com

Abstract: Ion beam-induced luminescence (IBIL) spectra of β-Ga_2O_3 wafer under irradiation by a 100 keV Helium ions beam were analyzed as a function of the dose in order to understand the kinematics of quenching of photoemission and possible formation of photoluminescence of luminescence defects. The results indicate that the intensity decreases with increasing fluence due to the formation of defects, which serve as non-radiative recombination centres competing with radiative processes.

1. Introduction

Gallium oxide (β-Ga_2O_3), well known for its unique optical and electrical properties as a semiconductor with a wide band gap (4.5–5.3 eV), has shown a constantly growing interest as a promising material in different fields of power electronics, optoelectronics, and photonics in recent years. Moreover, β-Ga_2O_3 demonstrates significant promise in photocatalysis, gas sensors, ultraviolet (UV) photodetectors. [1]

The performance of these devices depends heavily on the quality of the material, and defects in the crystal structure. These defects include vacancies, interstitials, and substitutions, which can introduce localized energy states within the band gap and directly influence the material's optical and electronic properties.

Furthermore, understanding the interaction of radiation with this material is important to assess its potential for electronics used in radiation environments or even as a radiation detector. In this context, ion beam analysis techniques with depth and lateral resolution and the potential to modify the intrinsic properties by creating different types of defects are especially suitable for studying/optimizing these electronic devices. IBIL is an effective and direct technique during in situ ion irradiation, specifically used to investigate the optical properties and the dynamic changes of defects.

2. Experimental Setup

Single-crystal (-201) oriented β-Ga_2O_3 wafers were irradiated with 100 keV He^+ ions, and IBIL spectra were recorded during irradiation at various ion fluences reaching up to 5E16 ions/cm² as shown in Fig.1 performed at IGCAR, Kalpakkam [2]. We studied the intensity evolution across different emission wavelengths within a broad spectral range from UV to visible light. The projected range of 100 keV He ions in β-Ga_2O_3 is ~ 420 nm with electronics energy loss 26.54 eV/Å and nuclear energy loss 0.49 eV/Å as calculated using SRIM (Stopping and Range of Ions in Matter) software).

3. Results and Discussion

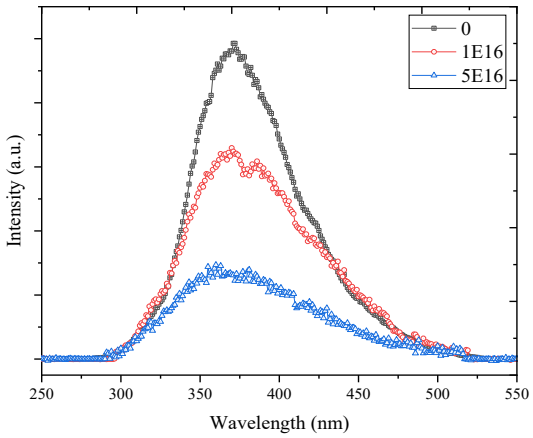

Fig.1. Evolution of the IBIL spectra with increasing fluences, upon irradiation with 100 keV He^+ ions

As fluence increases, the accumulation of beam-induced defects leads to a reduction in luminescence intensity. These defects do not change the capture probability of recombination centres but inhibit radiative emission by either enhancing non-radiative pathways or obstructing the formation of radiative states. Consequently, the proportion of luminescence events decreases with higher doses due to these competing non-radiative recombination centres. [3,4]

Acknowledgement

The author, MK, acknowledges K. Suresh, IGCAR, Kalpakkam for facilitating the irradiation and CSIR, New Delhi, for providing the Senior Research Fellowship.

References

[1]. Galazka et al. Semicond. Sci. Tech, 33, no. 11 (2018): 113001.
[2]. Srivastava et al. AIP Advances 10, no. 9 (2020).
[3]. Huddle et al. NIM B 261, no. 1-2 (2007): 475-476.
[4]. Esteves et al. Scientific Reports 13, no. 1 (2023): 4882.

Proton irradiation studies on pristine & 20 % cold work D9 samples using Medical Cyclotron Facility

Binoy Kumar Maji[1,*], Dipak Kumar Baisnab[1], B. Sundervel[1], Gayathri N. Banerjee[2], C. David[1] and Paramita Mukherjee[2]

[1]Defects & Damage Studies Division, MSG, IGCAR, Kalpakkam-603102, India, [2]Matrials Science Studies Division, MS&MG, VECC, Kolkata-700064, India

Email[*]: bk.maji@vecc.gov.in

Abstract: Proton irradiation experiments were carried out on D9 and 20% cold work D9 samples to see the effect of microstructural changes on proton irradiation. The line profile analysis using W-H method were done before and after the irradiation.

1. INTRODUCTION

Austenitic stainless steel like D9 alloy has been chosen for clad and wrapper tubes for the initial core of PFBR as a structural material in view of their good high temperature mechanical properties, oxidation resistance, excellent compatibility with liquid sodium and also its satisfactory behaviour established in reactors based on the accumulated international experience. The irradiation damage studies on D9 by the high intensity proton beams from material science beamline at Medical Cyclotron Facility provide a useful tool for simulating the bulk damage induced by fast neutrons in a reactor. In this aspect, an irradiation experiments were planned on D9 and 20% cold work D9 samples to see the effect of microstructural changes on proton irradiation.

2. EXPERIMENTAL

3 nos. of each set of D9 and D9-20% CW samples has been prepared. The XRD and hardness measurements of D9 and D9-20CW D9 were done by using Bruker made D8 Advance X-ray Diffractometer, Germany. Finally, the proton irradiation experiments were carried out at 3 different doses of 1E17, 5E17 and 1E18 p/cm^2 at 16 MeV proton beam energy which was reduced to 5 MeV by using Al-degrader and 10 µA current at MCF, Kolkata.

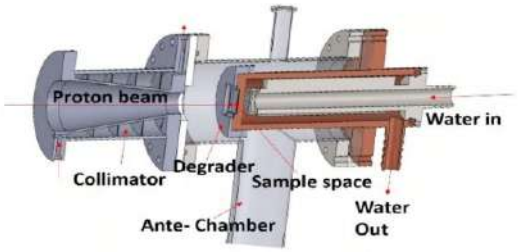

Fig. 1: Schematic of irradiation sample assembly

3. RESULTS AND DISCUSSIONS

Fig. 2 shows the XRD patterns of unirradiated sample of pristine D9 and 20 CW-D9. XRD LPA on D9 and 20 CW-D9 were carried out by W-H method to determine the domain size and lattice strain in the material. Using the Scherer and Wilson equations, we can express integral breadth in terms of volume weighted domain size (D_v) and the microstrain (ε) following equation

$$(\beta \cos \theta/\lambda) = 0.9/Dv + 2\,\varepsilon((2 \sin \theta)/\lambda) \quad \text{.....(1)}$$

Where, λ is the wavelength of X-ray and is the exact Bragg angle of diffraction. From the ordinate intercept and slope of the plot of ($\beta \cos \theta/\lambda$) vs. ($2 \sin \theta$)/$\lambda$), the volume-weighted domain size and microstrain can be determined respectively.

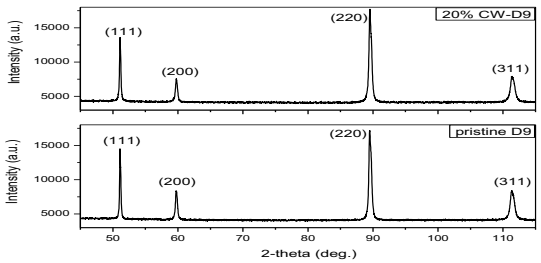

Fig. 2. XRD Patterns of D9 and 20CW-D9 samples

D9			20CW-D9		
2θ	β cos θ/ λ	2 sin θ/ λ	2θ	β cos θ/ λ	2 sin θ/ λ
51.0888	1.4193	0.4821	51.0832	1.6304	0.4820
59.7252	2.9452	0.5567	59.7285	3.3603	0.5567
89.4946	2.5464	0.7870	89.5136	2.7000	0.7872
111.3207	3.4980	0.9231	111.3575	4.4505	0.9233

Table 3: Domain Size and microstrain of pristine D9 and 20CW D9 samples.

The irradiation of D9 and 20 CW-D9 samples were irradiated at 3 different doses and sample are in hot store and the irradiated sample LPA will be carried out shortly.

5. CONCLUSIONS

The XRDLPA studies shows cold work D9 samples have more strain and lower domain size compare to pure D9 sample.

ACKNOWLEDGEMENT

The authors are thankful to Head, DDSD/MSG and Director, MSG for their constant supports.

REFERENCES

[1]. V. Kartik et al, JNM. **565** (2022) 153711.
[2]. T. Chenet al., Acta Materalia, **195** (2020) 433-454.
[3]. S. Dey et al. REDS, **173:3-4**, (2018) 300-317.

Ion Beam-Induced Modification in the Microstructural and Mechanical Properties of 15-5PH Steel Fabricated by Selective Laser Melting

Pritam Patra[1], Ambuj Tripathi[2], Sagar Sarkar[1]
[1]Indian Institute of Technology Delhi, New Delhi, India
[2]Inter University Accelerator Center, New Delhi, India
Email: pritampatra63@gmail.com

Abstract: Additive manufacturing (AM) is progressively investigated for nuclear reactor components due to its ability to produce intricate geometries, minimize material waste, and enable quick prototyping and repair operations. Amongst other AM processes, Selective Laser Melting is remarkably versatile, capable of fabricating intricate components without needing exorbitant fixtures, tooling, or other auxiliary equipment. This study experimentally investigates the effect of 3 MeV xenon ion irradiation on the micromechanical and microstructure of 15-5PH stainless steel fabricated by SLM. The findings are pertinent given the alloys' applications in producing components subjected to irradiation and extreme operational conditions, which are essential in evaluating the efficacy of additive manufacturing for fabricating complex nuclear components.

1. INTRODUCTION

Selective Laser Melting (SLM), also known as Laser Powder Bed Fusion (LPBF), is an AM technique in which a thin layer of metal powder is applied on a build plate, and a focused laser beam is scanned along the powder bed using a specific scan route in an inert gas environment. Due to the laser's intense heat flux, the material melts in a regulated amount where the laser beam is directed, then undergoes rapid solidification once the laser beam moves away. The laser scan approach determines the patterns of these solidified tracks, and merging these individual tracks within a plane results in a thin metal layer. These steps are repeated layer by layer until the entire part is built.

Precipitation hardening (PH) stainless steels have grown increasingly popular because of their superior mechanical and corrosion properties at extreme conditions. These properties can be further improved by undergoing aging heat treatment. 15-5 PH stainless steel is martensitic/austenitic and extensively utilized in aerospace, nuclear, chemical, and other engineering applications. 15-5 PH steel's high strength and hardness make it difficult to machine traditionally, but its good weldability makes it ideal for being fabricated by SLM.

Sagar et al. [1-3] investigated the effect of various heat treatments on SLM 15-5PH steel and its corresponding effect on fatigue, wear and corrosion. The findings indicate that aging heat treatment (H900) produces fine spherical ε-Cu-rich precipitates that increase yield strength, hardness, and corrosion resistance. However, it also makes the specimens brittle, which increases wear rate and decreases impact energy.Materials used in the harsh conditions of nuclear reactor require a standard level of physical stability, especially at extreme temperature, corrosion and radiation environments. Zheng et al. [4] investigated the effect of ion irradiation on 13-8 PH steel. Uddin et al. [5] reported the effect of 1 MeV proton irradiation on 17-4 PH steel fabricated by LPBF. Average grain size were noted to become slightly finer due to irradiation. Additionally, it impacts the yield strength, increases the maximum shear strength, and hardens the alloy in terms of nano hardness. Lutfun et al. [6] investigated the effect of build orientation and Hot isostatic pressing on LPBF 17-4 PH steel under ion irradiation.

Therefore, the current study aims to ascertain how highly energetic heavy ion irradiation affects 15-5 PH stainless fabricated by SLM. Some as-build specimens underwent H900 aging heat treatment as post-processing. 3 MeV Xe ion irradiation was carried on specimens of both vertical (along build direction) and horizontal orientation of both as-build and H900 condition.

REFERENCES

[1]. Sagar Sarkar et al, Effects of heat treatment and build orientations on the fatigue life of selective laser melted 15-5 PH stainless steel, Materials Science and Engineering: A. **755** (2019).

[2]. Sagar Sarkar et al, Effects of heat treatment on microstructure, mechanical and corrosion properties of 15-5 PH stainless steel parts built by selective laser melting process, Journal of Manufacturing Processes. **50** (2020).

[3]. Sagar Sarkar et al, Three-body dry abrasive wear properties of 15–5 precipitation hardening stainless steel produced by laser powder bed fusion process, Wear **470–471** (2021).

[4] Ce Zheng et al, Ion irradiation effects on commercial PH 13-8 Mo maraging steel Corrax, Journal of Nuclear Materials. **514** (2019).

[5] Mohammad Jashim Uddin et al, Effects of proton irradiation on nanoindentation strain-rate sensitivity and microstructural properties in L-PBF 17–4 PH stainless steels, Materials Science and Engineering: A. **837** (2022).

[6] Nipa, L, et al, "Irradiation and Hip Impact on Microstructure and Small-Scale Mechanical Properties of AM Nuclear Reactor Materials." Proceedings of the ASME 2024 19th International Manufacturing Science and Engineering Conference. Knoxville, Tennessee, USA. June 17–21, 2024.

Irradiation studies on mechanical properties of silicon rubber compound

Suba. M, Prakash. S, Falix Lawrence D, Kodandaraman. J, Venkatesan. K. A and Rajan. K
Reprocessing Group, IGCAR, Kalpakkam-603102
Email: kavenkat@igcar.gov.in

Abstract: Irradiation studies were carried out for silicon rubber in order to evaluate its suitability for reprocessing plant applications. The test specimens (for hardness, tensile properties and compression set) were prepared from the silicon rubber compound and were irradiated. Degradation of mechanical properties were observed on irradiation. Radiation resistance of silicon compound was evaluated to be 4 x 10^4 Gy.

1. INTRODUCTION

In fast reactor reprocessing, the components used in the reprocessing plants are exposed to the radiation environment, hence it is necessary that these components must be fabricated from radiation resistant materials. Hence to evaluate suitability of silicon rubber for gasket and O-ring application in radiation atmosphere a study was carried out.

2. EXPERIMENT

Compound of silicon rubber for O-ring and gasket application was prepared. Test specimens (tensile as per ASTM D412, hardness as per ASTM D2240 and compression set as per ASTM D395) were fabricated from the silicon compound and were irradiated to doses of 10, 100 and 1000 kGy in ambient condition (with Co^{60} as the source, supplied by Board of Radiation and Isotope Technology, Mumbai, India). The irradiated and unirradiated samples were tested for tensile, hardness and compression set properties.

3. RESULTS AND DISCUSSION

Plot of tensile strength and elongation at break with radiation dose is shown in fig.1 and fig. 2 respectively. On irradiation tensile strength and elongation at break of silicon compound was found to decrease. This is due to degradation occirung by irradiation. From elongation at break values at various doses, radiation resistance of silicon compound was evaluated to be 4 x 10^4 Gy (criteria as per IEC 544). Hardness was found to increase with radiation which is due to chain scission. Fig. 3 shows plot of hardness with radiation dose.

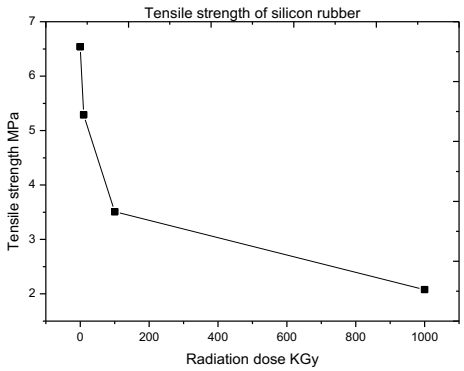

Fig.1 Plot of tensile strength of silicon compound with radiation dose

Variation of compression set of the silicon compound with radiation is shown in table. 1. It can be seen that there is not much variation in the compression set.

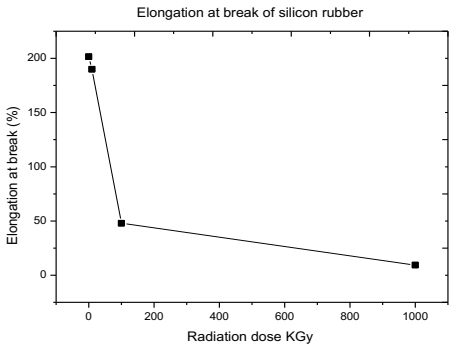

Fig. 2 Plot of elongation at break of silicon compound with radiation dose

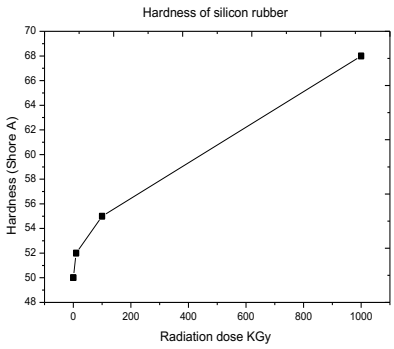

Fig.3 Plot of hardness of silicon compound with radiation dose

Table. 1 Compression set of silicon compound at various radiation dose

S. No	Dose (kGy)	Compression set (%)
1.	0	4.34
2.	10	4.49
3.	100	4.33
4.	1000	4.60

4. CONCLUSION

Mechanical properties of silicon rubber was found to degrade on irradiation. Radiation tolerance of the silicon compound was evaluated to be 4 x 10^4 Gy. Hence, the silicon compound can be used for gasket and O-ring application in plant up to radiation dose of 4 x 10^4 Gy.

Unveiling the structural, radiation sheilding properties of $BiVO_4$ - epoxy resin nanocomposites

Vikram T[1], Abuthahir J[2], Sanjeevi P[1], Saravanakumar A[3], Elango M[1*].
Department of Physics, PSG College of Arts and Science, Coimbatore, Tamilnadu, India
Department of Physics, Government College of Technology, Coimbatore, Tamilnadu, India
Department of Medical Radiology, PSG IMSR, Coimbatore, Tamilnadu, India.
Email: elango@psgcas.ac.in

Abstract: Bismuth vanadate ($BiVO_4$)/epoxy resin nanocomposites were identified as suitable substitute for lead based radiation blocking agents. Filler particles were prepared via precipitation method followed by apron preparation by drop-casting method using epoxy resin. Material and size confirmation were done by XRD, Raman and HRTEM . X-ray attenuation properties of the composite was analysed and the results are accounted. It was unveiled that the filler particles significantly enhanced the shielding properties of the composite and it is on par with the Pb based composites.

1. INTRODUCTION

The higher reliance on X-rays raises the risk of overexposure, which can cause severe and irreversible health damage to practitioners [1,3]. Therefore, developing advanced X-ray shielding materials with ensured safety while remaining practical and comfortable is the crucial for protecting those who are frequently exposed to X-ray radiation. Traditional shielding materials like lead and concrete favour their high attenuation coefficients and cost-effectiveness but are hindered by their weight, lack of flexibility, and limited structural adaptability, making them unsuitable for protective garments. Bimetallic oxides are identified as an alternate system for replacing the toxic Pb based materials for radiation protections measures . Herein we report the Bi and V based novel bimetallic oxide system with appreciable stability over wide range of tube voltage against X-ray exposures.

2. EXPERIMENTAL METHODS

Bismuth nitrate ($BiNO_3.5H_2O$) and ammonium meta vanadate (NH_4VO_3) are used as the precursor to prepare the $BiVO_4$ by co precipitation method followed with modification in the protocol reported by [1].

3. RESULTS AND DISCUSSION

3.1. Microstructural analyses

XRD analysis (Fig. 1) confirms that the synthesized $BiVO_4$ system follows monoclinic ordering, with diffraction intensities indicating multifaceted growth. The predominant peak at 28.9° was used to determine crystallite size and microstructural properties, aligning well. Peak broadening suggests defect-induced lattice strain and dislocation densities. Crystallite size, calculated using the Scherrer formula, was found to be 12 nm, consistent with HRTEM analysis. Micrographs reveal particle aggregation due to Ostwald ripening, with distinct particle boundaries confirming complete formation [3]. Selected area electron diffraction (SAED) patterns further validate the crystalline nature. Raman spectroscopy identified vibrational and rotational bands at 213, 324, 366, 610, and 811 cm^{-1}, confirming $BiVO_4$ formation. The 213 cm^{-1} band represents rotational and translational modes of VO_4^{3-}, while the 324 and 366 cm^{-1} bands correspond to VO_4^{3-} tetrahedral deformations. Bi-O symmetric bending modes were observed at 610 cm^{-1}, supporting the successful synthesis of $BiVO_4$ [2].

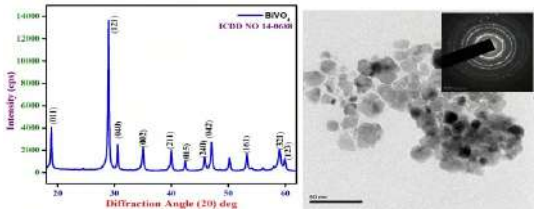

Fig 1 XRD spectrum & TEM image of $BiVO_4$ system

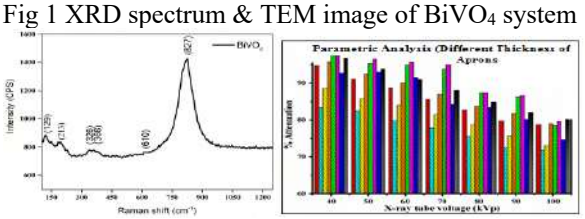

Fig 2 Raman spectrum & X-ray attenuation study of $BiVO_4$ system with different thickness

Nanomaterials enhance particle-radiation interactions, improving attenuation. The superior shielding performance of $BiVO_4$ nanoparticles is attributed to reduced crystallite size and increased texture coefficient, as confirmed by XRD. Figure 2 shows the correlation between tube voltage and X-ray exposure for different apron thicknesses. Among tested samples, the 3.2 mm thick apron containing $BiVO_4$ nanoparticles exhibited the lowest X-ray exposure, demonstrating its effectiveness in radiation shielding applications.

4. CONCLUSION

$BiVO_4$ nanoparticles were successfully synthesized using a modified co-precipitation method, with XRD confirming monoclinic ordering and a crystallite size of 12 nm. Raman spectroscopy validated the structural integrity, while X-ray attenuation studies demonstrated enhanced radiation shielding. The 3.2 mm thick $BiVO_4$-based apron exhibited the highest shielding efficiency, proving its effectiveness.

REFERENCES

[1]. Jianqiang Yu et al., *J Solid State Chem*. 182. 223-228. 2009.
[2]. Jang *et al., Jpn. J. Appl. Phys.* **24** 506. 1985.
[3]. Sambhudevan et al *J. Elastomers Plast*. 49 527–544. 2017.

Topic Code: 05

Molecular dynamics study of self diffusion in Iron Phosphate glass

Aishwarya K[1, 2], Manan Dholakia[1, 2], Sharat Chandra[1, 2]
[1]Materials Science Group, Indira Gandhi Center for Atomic Research, Kalpakkam, TN-603 102, India
[2]Homi Bhabha National Institute, Mumbai – 400 094, India
Email: aishwarya@igcar.gov.in

Abstract: Iron phosphate glasses are promising candidate materials for immobilization of high level nuclear waste. Self diffusion is a characteristic property that constrains the practical applicability of the glass. Thus it is important to study the self diffusion of glass elements. In the current study iron phosphate glasses are modeled using classical molecular dynamics by performing melt quench simulations on $Fe_3(P_2O_7)_2$ crystal structure. Modeled glasses are validated by computing properties such as density, radial distribution function and void fraction. Effect of a broad range of temperature on self diffusion coefficient of all the elements of the modeled glass is studied.

1. INTRODUCTION

One of the efficient ways of storing the radioactive nuclear waste is through the process of vitrification where the highly radioactive substances are immobilized within the glass matrix. Conventionally borosilicate glasses are being used for this purpose. However, iron phosphate glasses (IPG) are emerging as better suitable candidate for the storage of heavy metal waste than borosilicate glasses. As the migration of glass elements is one of the factors that may limit its potential usefulness towards waste immobilization, it is important to study the diffusive nature of elements of the glass matrix. Thus in this study we focus on modeling IPG of composition $60P_2O_5$–$40Fe_2O_3$ mol% and computing the self diffusion coefficient of each species of elements through the mean square displacements (MSD) which are recorded during the simulation.

2. COMPUTATIONAL DETAILS

The classical molecular dynamics simulations were carried out using LAMMPS. Initial structure was 2×2×1 super cell of orthorhombic crystal structure of $Fe_3(P_2O_7)_2$ from materials project database [1]. This crystal contains 336 atoms (16 Fe^{II+}, 32 Fe^{III+}, 64 P, and 224 O) and has the same composition as that of IPG. Interatomic potential used consists of the Buckingham potential along with Coulomb potential, and for the three body terms, Stillinger Weber potential is used with parameterizations as given in [2]. The melt quench scheme followed was same as that of Deng et al [3] with a quench rate of 5×10^{12} K/s.

3. RESULTS AND DISCUSSION

The snapshot of final glass structure is shown in Fig. 1. The optimized structure has a density of 3.2 g/cc. It has a cohesive energy of -19.7 eV. From the RDF plot given in the Fig. 2, the bond length for P-O, Fe-O, and O-O are found to be as 1.6 Å, 1.8 Å and 2.6 Å respectively which match well with other theoretical models [4]. The void fraction of the glass structure was calculated using MOF explorer which was found to be 0.202 which also agrees well with experimental value which is 0.207. The self diffusion calculations are ongoing and the data analysis will be presented during the conference.

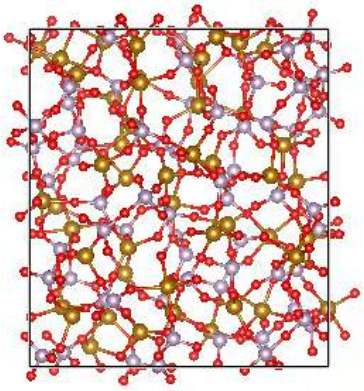

Fig.1. Snapshot of final glass structure

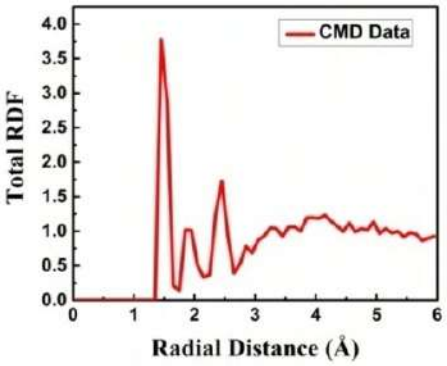

Fig. 2. Plot of radial distribution function.

REFERENCES

[1]. A. Jain et al, APL Mater. 1 (2013) 011002.
[2]. F. H. Stillinger et al, Phys. Rev. B. 31 (1985) 5262.
[3]. L. Deng et al, J. Non. Cryst. Solids 453, (2016) 177-194.
[4]. S.S. Jena et al, J. Non. Cryst. Solids 637 (2024) 123035.

Topic Code:(4) Radiation Resistant Materials and Radiation Induced Defects

Investigation of Vacancy Formation Energy and Mechanical Properties in FeCrMnNi Alloy

Vallinathan K[1,2], Gurpreet Kaur[1], Sharat Chandra[1]
[1]Material Science Group, Indira Gandhi Centre for Atomic Research, Kalpakkam 603102, Tamil Nadu
[2]HBNI, Anushakti Nagar, Mumbai 400094, India
Email: vallinathan8@igcar.gov.in, gurpreet@igcar.gov.in

Abstract: In this work, we have investigated the mechanical properties of FeCrMnNi High Entropy Alloy (HEA) using first-principles density functional theory (DFT) based calculations and Molecular Dynamics (MD) simulations. For DFT calculation HEA is modelled using a special quasi-random structure (SQS). The vacancy formation energies for different sites are studied. The calculated formation enthalpy is -1.56 eV which shows that the modelled FeCrMnNi is stable.

1. INTRODUCTION

High Entropy Alloy (HEA) is defined as consisting of five or more principle elements, without any minor elements [1]. The elements included must obey the Hume-Rothery rule. HEAs enhance the material property compared to the conventional alloys. HEAs exhibit good wear resistance, high-temperature stability and high corrosion resistance. Most HEAs form single phase structures such as face-centred cubic (FCC), body-centred cubic (BCC) and hexagonal closed packed (HCP) structure (HCP). CoNiFeCrMn and CoNiFeCr HEAs are well-studied, but for nuclear reactor applications, Co is less preferable due to its high induced radioactivity [2]. Therefore we have removed Co from the CoNiFeCrMn alloy and worked with FeCrMnNi instead. We have used equiatomic FeCrMnNi alloy, which forms a single-phase FCC structure [3].

2. METHODOLOGY

To construct the FeCrMnNi HEA, we used Alloy Theoretic Automated Toolkit (ATAT) to generate the SQS for a 2×2×2 fcc supercell with an equal composition of atoms in the alloy. Calculations were carried out using the Vienna ab initio Simulation Package (VASP) with the Perdew-Burke-Ernzerhof (PBE) generalized gradient approximation. Projector augmented wave (PAW) potentials were employed, with an energy cutoff of 500 eV and a 5×5×5 k-points grid in the Monkhorst-Pack scheme. The relaxation was performed until the forces acting on the atoms converged to 10^{-3} eV/Å. For classical molecular dynamics (CMD), we have constructed a 15×15×15 fcc supercell containing 13,500 atoms arranged randomly and simulations are done in LAMMPS using FeCrMnNi interatomic potential [4].

3. RESULT AND DISCUSSION

The calculated lattice parameters using DFT are 3.525 Å, 3.513 Å, 3.496 Å. The calculated mechanical properties such as bulk modulus (B), shear modulus (G), Young's modulus (Y) and Poisson's ratio (ν) are calculated through CMD and DFT for HEA and the results are compared with fcc-Fe as given in the table.

	B (GPa)	G (GPa)	ν
CMD	**195.84**	**95.56**	**0.29**
DFT	**248.87**	**94.64**	**0.33**
FCC-Fe [6]	**253.90**	**168.13**	**0.23**

The vacancy formation energy (E_f) of all sites in the supercell are calculated using formula:

$$E_f = E_{def} - E_{perf} + \mu_{xi} \quad (1)$$

E_{def} , E_{perf} are the total energy of defected supercell and perfect supercell resp., μ_{xi} is the chemical potential of element x_i (Fe, Cr, Ni, Mn). E_f for different sites is plotted in Figure 1. Average vacancy formation for all types of atoms is lower than the vacancy formation energy in fcc Fe for almost all the sites.

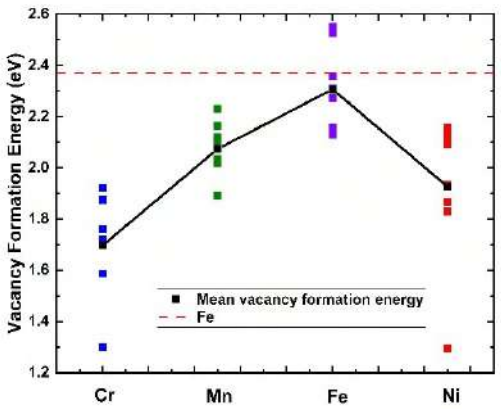

Fig.1. The vacancy formation energy of Fe, Cr, Mn and Ni atoms in FeCrMnNi HEA compared with e [5].

REFERENCES

[1] Mizuno et al, Comput. Mater. Sci. **170** (2019) 109163.
[2] Fan et al, Mater. Sci. Eng. **598** (2014) 244-250.
[3] Wu et al, Mater. Sci. Eng. **640** (2015) 217-224.
[4] A. Daramola et al, Comput. Mater. Sci. **203** (2022) 111165.
[5] Kangming Li et al, Phys. Rev B **104** (2021) 104406.
[6] Yang Lin et al, Metals **11** (2021) 1988.

Topic category: Radiation Resistant Materials and Radiation Induced Defects

Irradiation induced dissolution of precipitates in P91 steel – in-situ SEM investigation

Vikas Singh Gahlot[1,2], P. Jegadeesan[1], V. D. Vijayanand[3], S. Amirthapandian[1,2]
[1]Materials Science Group, Indira Gandhi Centre for Atomic Research, Kalpakkam - 603 102
[2]Homi Bhabha National Institute, Indira Gandhi Centre for Atomic Research, Kalpakkam - 603 102
[3]Materials and metallurgy Group, Indira Gandhi Centre for Atomic Research, Kalpakkam - 603 102
Email: v.s.gahlot@igcar.gov.in, pandian@igcar.gov.in

Abstract: Atomic displacements created within collision cascades can drive the atoms in a precipitate into the surrounding matrix through recoil processes, thus contributing to the dissolution of the precipitates. The dissolution of precipitates in P91 steel under 3 MeV Fe^+ ion irradiation is investigated using the in-situ ion irradiation and imaging with field emission scanning electron microscope (i^4-FESEM) facility. As ion fluence increases, the precipitates are either dissolve into the matrix or form core-shell precipitates. This observation is discussed in the light of basic ion-solid interaction in materials.

1. INTRODUCTION

P91 ferritic steel is one of the candidate material proposed for structural materials in nuclear reactors due to less void swelling, however it the embrittlement due to irradiation induced hardening is the problem[1]. Here we have studied the dissolution of precipitates in the P91 steel upto 50 dpa using our newly established i^4-FESEM facility[2].

2. EXPERIMENTAL

The P91 steel was prepared for irradiation by subjected to normalizing at 1040 °C for 1 hr followed by tempering at 760 °C for 2.5 hrs. The sample was prepared using standard metallographic preparation up to a surface finish of 1 µm. Etching was carried out using Villela's reagent. The $M_{23}C_6$ precipitates were observed along the grain boundaries in the steel. The sample was examined with in-situ SEM where 3MeV Fe^+ ion irradiation at 45° and SEM imaging were carried out sequentially using the i^4-FESEM facility [2]. The ion irradiation was carried out at 45° with respect to the ion beam. The evolution of the precipitates in P91 steel was studied for various ion fluences, ranging from 2.78×10^{14} ions/cm^2 to 1.39×10^{17} ions/cm^2.

3. RESULTS AND DISCUSSION

Figure 1(a) shows the SEM image of P91 steel, where the $M_{23}C_6$ precipitates decorate in both grain boundaries and grains. The same $M_{23}C_6$ precipitates were observed after ion irradiation(ion fluence 1.39×10^{17} ions/cm^2) and shown in Fig.1(b). SEM images were also recorded at various intermediate ion fluences (images not shown). At low ion fluences, *i.e.,* upto 1.08×10^{15} ions/cm^2, there was no significant change in the morphology of the precipitates, but as the ion fluence reached 8.49×10^{15} ions/cm^2, the facets of the precipitates began to level out and become spherical in shape. When the ion fluence was increased further, small precipitates dissolved completely in the matrix as marked by circle 2 (in Fig 1). Almost all particle have developed a core-shell structure and the shell is visible in the top of the precipitates (marked as 1 and 3 in Fig.1). The shell is found to protrude along the ion beam direction, as evident in top-side of the precipitates.

Nelson, Hudson and Mazey(NHM) [3] model explains the competition between recoil dissolution and temperature dependent diffusion. The diffusion process enhances the growth of precipitate while recoil mixing increases the dissolution of precipitates. In the present experiments, the irradiation was carried out at room temperature, the thermal diffusion is significantly low. Hence the dissolution of precipitates and recoil mixed shell structures in the precipitates are observed.

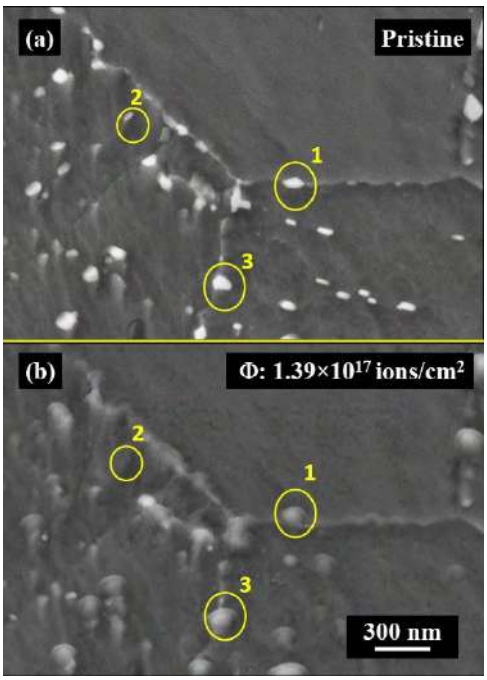

Fig.1. SEM images of P91 steel sample before (a) and after ion irradiation (ion fluence: 1.39×10^{17} ions/cm^2)

REFERENCES

[1]. Murty K.L *et. al.* J. Nucl. Mater. **383** (2008) 189.
[2]. Jegadeesan P, *et. al.* In-situ ion irradiation and imaging with field emission scanning electron microscope (i^4-FESEM) facility at IGCAR (Communicated to NIMB)
[3]. Nelson R.S., *et. al.* J. Nucl. Mater. **44** (1972) 318.

Microstructural Characterization of carbide fuel elements of FBTR at linear heat rating of 400W/cm

[1,2]Bhabani Shankar dash, K. G. Chaithanyaa, M. Padalakshmi, [1,2]V. V. Jayaraj, C. Padmaprabu, [1,2]V. Karthik &[1,2]R. Divakar

Affiliation, 1. Metallurgy and Materials Group (MMG), Indira Gandhi Centre for Atomic Research (IGCAR), Kalpakkam; 2. Homi Bhabha National Institute (HBNI)

bhabani@igcar.gov.in

Abstract:

Microstructural characterization using Electron microscopy (EM) plays a vital role in the Post Irradiation Examination (PIE) of fast reactor fuels and structural materials. The challenges include high levels of radioactivity (α,β,γ), limited volumes of homogenous materials, remote specimen preparation and handling, customisation of analytical equipment etc. The EM characterization of irradiated Mark I Mixed Carbide (Mk I MC) fuel and SS316 clad of Fast Breeder Test Reactor (FBTR) is presented here.

1. INTRODUCTION

The in-reactor performance of fuel & clad materials is closely related to the microstructure & microchemical changes caused due to neutron irradiation and depends on reactor operating parameters such as neutron flux, linear heat rating (LHR), burnup/dpa and their gradients etc.

PIE has been carried out on Mk-I MC fuel sub-assembly of FBTR irradiated to 105 GWd/t burn-up (BU) at a LHR of 400 W/cm & sodium inlet temperature of 380°C. To study the structure property correlation of fuel & clad, microstructural & microchemical characterisation was carried out.

2. MICROSTRUCTURAL EXAMINATION

Transverse sections with different combination of temperature and burnup/dpa extracted from the irradiated fuel pin were metallographically prepared inside the hot cell. A dedicated customised facility housing a Scanning Electron Microscope (SEM) with a glove box interface and accessories was used for examination of carbide fuel. Sample transfer from hot cell to SEM was carried out using shielded cask and alpha tight double door transfer systems. Samples from defueled clad tubes were thinned to electron transparency by a specialised procedure involving hot cell and fume hoods for examination in Transmission Electron Microscope (TEM).

2.1. Fuel (70%PuC-30%UC)

The microstructure of fuel pin cross section indicated complete closure of fuel clad gap (Fig.1) with dense region at fuel periphery and a relatively porous region at the center. WDS spot scan along radial direction revealed Cs peaks towards fuel periphery.

2.2. Clad (20% CW SS316)

TEM analysis (Fig.2) of clad material indicated formation of irradiation induced defects, network of dislocations, precipitation, dislocation loops and stacking faults. The volume fraction of voids in clad quantified using image analysis is found to be ~10%. The void size and number density found to increase with temperatures and dpa respectively.

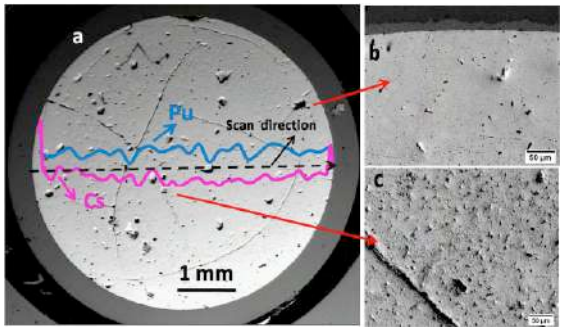

Fig. 1(a) Micrograph of fuel-clad transverse section with overlay of Pu & Cs radial distribution. Porosities at (b) periphery & (c) central regions of fuel.

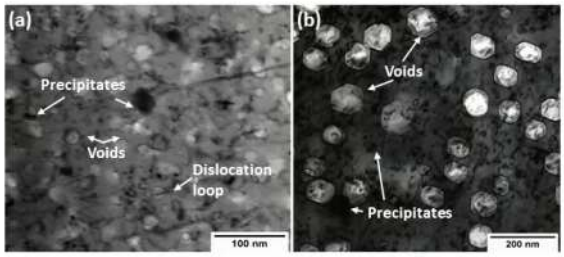

Fig 2. Bright Field image of the clad material indicating irradiation induced defects (a) 62 dpa, 462˚C and (b) 64 dpa, 528˚C

3. CONCLUSION

Microstructural examination of fuel using SEM indicated that fuel can accommodate further swelling due to availability of pores. However, higher void volumes & defects in SS316 cladding and the associated loss in ductility of cladding are the major life limiting factors influencing the extension of fuel burn-up beyond 105 GWd/t.

4. ACKNOWLEDGEMENT

The contribution of whole PIED team during the study is gratefully acknowledged.

REFERENCES

[1] C.N. Venkiteswaran, et al, Energy Procedia, Volume 7, 2011, Pages 227-233

[2] A. Renault, et al, Journal of Nuclear Materials, Volume 460, 2015,Pages 72-81,

Studies on Fatigue Behavior of neutron irradiated SS316 using small specimens

Aishwary Vardhan Pandey[a], V. Karthik[a,b], Ashish Kolhatkar[b], Divakar R.[a,b]
[a] Homi Bhabha National Institute (HBNI), Kalpakkam, 603102, Tamil Nadu, India
[b] Indira Gandhi Centre for Atomic Research (IGCAR), Kalpakkam, 603102, Tamil Nadu, India
Email: avpandey@igcar.gov.in

Abstract: Effect of neutron irradiation on cyclic deformation behavior of SS 316 disc samples are evaluated, under asymmetrical load cycling, using small punch fatigue (SPF) test. The test response shows a continuous shift in load – displacement loops as a result of inelastic displacement accumulation, similar to uniaxial ratcheting. Increase in displacement damage result in decrease in fatigue life. The study also discusses the effect of various test parameters such as mean load, load amplitude, specimen thickness on fatigue response of neutron irradiated SS 316.

1. INTRODUCTION

Structural components of fast breeder reactor are subjected to complex thermo – mechanical cycling and asymmetrical load cycling due to frequent startup, shut downs and load variations. In addition, microstructural changes due to neutron irradiation further degrades the material's performance under such complex loading. Hence periodic assessment of irradiation induced changes in material's cyclic behavior is of paramount importance to ensure integrity of reactor components. However, fatigue property evaluation requires large specimens, difficult to accommodate in sufficient numbers in available reactor space for neutron irradiation. This motivates the miniaturization of test specimens such as small disc specimen. Due to small volume, large numbers of disc specimen (ϕ 8 mm and 0.5 mm thick) can be fit in reactor space or even can be extracted from tested conventional samples. Disc samples are recognized for determining tensile, creep and ductile-to-brittle transition temperatures of irradiated materials through small punch (SP) test [1]. Nevertheless, in authors' knowledge, SP test for cyclic behavior analysis of irradiated material is so for not reported. Hence, this work is motivated from the authors' recent study, in which a novel correlation between SPF and uniaxial ratcheting was presented for SS 316LN and P91 steels [2]. The present study explores the effect of different factors such as mean load, load amplitude, specimen thickness, and the impact of irradiation damage (0, 2.45, 4.93 and 6.75 dpa), on the cyclic response of SS 316.

2. RESULTS

Pre-fabricated disc specimens of archive AISI 316 SS grid plate material were irradiated in FBTR to a neutron does range of 2.45 dpa to 6.75 dpa. These specimens were tested, under different cyclic load conditions with positive load ratio (R>0). The test outcomes and analysis results are discussed in the following sections.

2.1. Effect of Load Parameters

Increase in load amplitude has an adverse effect on fatigue life, whereas increase in mean load imposes an additional hardening in the materials leading to increase in fatigue life.

2.2 Effect of Neutron Irradiation

The SPF load conditions were systematically selected, through numerical simulation, to ensure identical stress conditions for each dpa. Increase in displacement damage exhibited detrimental effect on SP fatigue life. To comprehend this behavior, total displacement range and hysteresis energy accumulation rate (HEAR) at mid fatigue life was studied (Fig. 1). The ratcheting behavior is a combined effect of cyclic (due to load amplitude) and monotonic (due to mean load) deformation [2]. Here, total displacement range and HEAR represents the effect of load amplitude and mean load respectively. HEAR shows an increasing trend with increase in irradiation damage. On the other hand, no such trend was observed for total displacement range. This shows that the prime reason behind the material failure is ductility exhaustion.

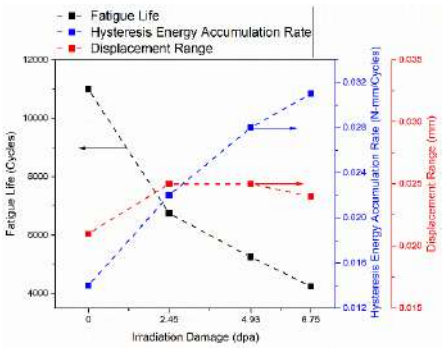

Fig.1. The effect of irradiation damage on fatigue life, HEAR and displacement range.

ACKNOWLEDGEMENT

Authors gratefully thank the support rendered by colleagues of Post Irradiation Examination Division of IGCAR during the course of the work.

REFERENCES

[1]. S. Arunkumar, Overview of small punch test, Metal. Mater. Int. 26 (6) (2020) 719–738.
[2]. A. V. Pandey et al, Development of a novel approach to correlate small punch fatigue with uniaxial ratcheting fatigue, International Journal of Fatigue, 190 (2025) 108585.

Fabrication of Components with Integrated Cladding for Harsh Environments through Casting

Tumula Tirumala and Ajay Kumar*
Department of Mechanical Engineering, Indian Institute of Technology Tirupati (A.P.) India-517619
*Email: drajaykumarp@iittp.ac.in

Stainless steel (SS) coatings/claddings over aluminium alloys (AA) substrates have been practiced through friction surfacing, thermal and cold gas spraying, laser coating, and diffusion bonding. In this work, 304-grade SS is reverse-cladded to an LM25 AA through die-casting using a surface-prepared sheet insert. The clad-substrate interface was characterized micrographically and compositionally through optical and electronic microscopic techniques. Micrographs revealed that reverse cladding was achieved successfully by forming an intermetallic zone (IMZ). The IMZ contains four intermetallic layers (IMLs) of varying thickness with 6.42 ± 2.04 µm near the central region. Electron probe microanalysis showed **Fe_3(Al,** Si**)**, **Fe_3(Si,** Al**)**, **Fe (Al,** Si**)**, and **$Fe_3Al_{15}Si_2$** are the associated phases with four IMLs from the SS to AA side, respectively.

The present work explores the development of bimetallic materials designed for extreme environmental conditions through reverse cladding. Combining the superior corrosion resistance of cladded material with the low-cost and high-toughness base metals, the resulting composite achieves enhanced durability and performance. Reverse cladding ensures optimal bonding, improved thermal stability, and resistance to mechanical wear, making it suitable for applications in aggressive industrial environments. The process involves controlled material deposition, ensuring precise microstructural integrity and metallurgical compatibility. This innovative approach offers a cost-effective and sustainable solution for infrastructure, marine, and energy sector applications in harsh conditions.

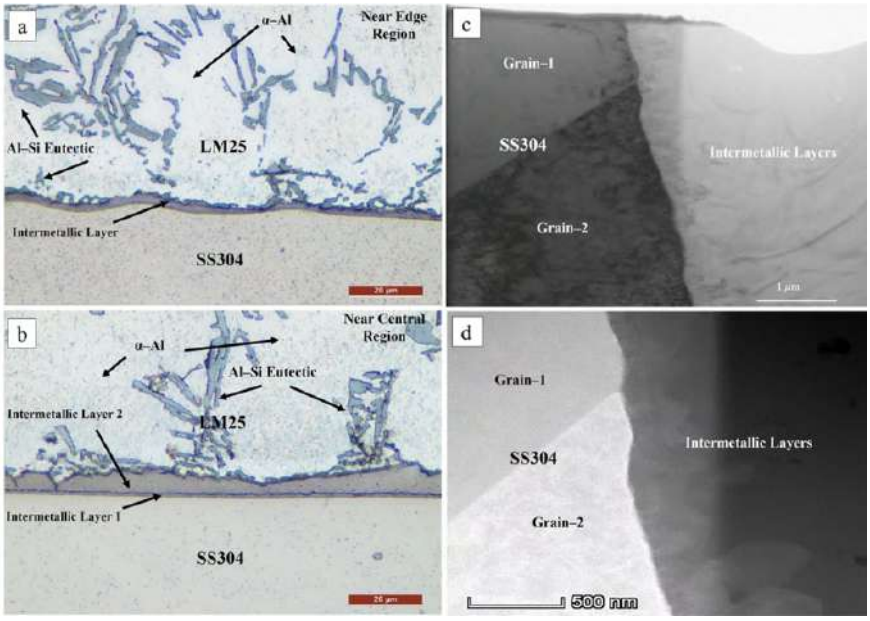

Fig. 1: Micrographs of cladding interface near-edge and central regions – a-b) optical micrographs, c-d) TEM bright field and high-angle annular dark field images of the SS/IMLs interface, respectively.

Development of an experimental setup for low-temperature ion irradiations

S. Chinnathambi

A multifunctional ion-irradiation system capable of irradiation at low temperatures and defect recovery studies has been developed at the 1.7 MV tandetron beamline. This setup comprises (a) beam-defining slits, (b) a locally designed water-cooled Faraday cup for measuring beam flux, and (c) a low-temperature sample holder for conducting irradiations at 10K. The sample holder utilizes a closed-cycle refrigerator (CCR) to maintain temperature stability at ±0.5K. The system's tilt table design allows for quick sample exchanges. The presentation will highlight all the indigenous advancements included in the system.